



UNIVERSITAT
POLITÈCNICA
DE VALÈNCIA

DOCTORAL THESIS

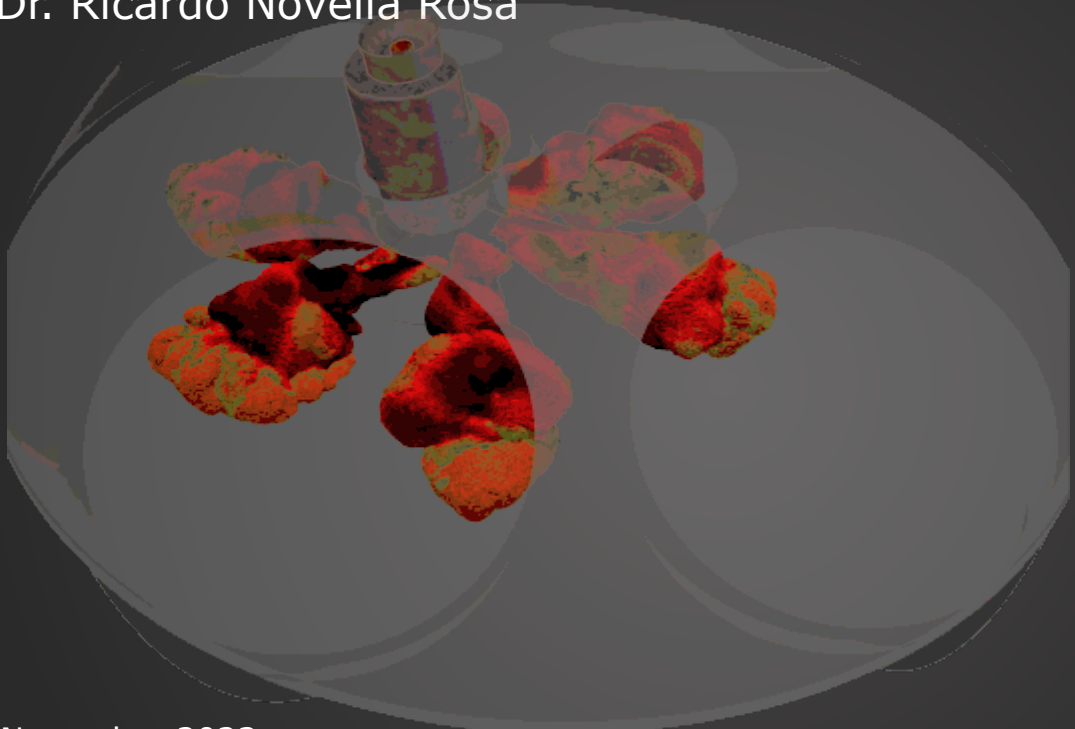
IMPLEMENTATION AND ANALYSIS OF THE PRE-CHAMBER IGNITION CONCEPT IN A SI ENGINE FOR PASSENGER CAR APPLICATIONS

PRESENTED BY

Pablo José Martínez Hernández

SUPERVISED BY

Dr. Ricardo Novella Rosa



November 2023

DEPARTAMENTO DE MÁQUINAS Y MOTORES TÉRMICOS

UNIVERSITAT POLITÈCNICA DE VALÈNCIA
DEPARTAMENTO DE MÁQUINAS Y MOTORES TÉRMICOS

DOCTORAL THESIS

**IMPLEMENTATION AND ANALYSIS OF THE
PRE-CHAMBER IGNITION CONCEPT IN A SI ENGINE
FOR PASSENGER CAR APPLICATIONS**



PRESENTED BY

D. Pablo José Martínez Hernández

SUPERVISED BY

Dr. D. Ricardo Novella Rosa

FOR THE DEGREE OF

Doctor of Philosophy

NOVEMBER 2023

DOCTORAL THESIS

“Implementation and analysis of the pre-chamber ignition concept in
a SI engine for passenger car applications”

Presented by: D. Pablo José Martínez Hernández
Supervised by: Dr. D. Ricardo Novella Rosa

THESIS EXAMINERS

Dr. D. Dario Di Maio
Dr. D. Angelo Onorati
Dr. Dña. Maria del Carmen Mata

DEFENSE COMITEE

Chairman: Dr. D. Raúl Payri Marín
Secretary: Dr. Dña. María de los Reyes García Contreras
Member: Dr. D. Dario Di Maio

Valencia, November 2023

Para Batgopi y Sofia

Abstract

The global greenhouse gas emissions increase since the start of the Industrial Revolution has become a serious hazard to human life. In addition to power generation and industry, transportation, with the rise in the total vehicle number in the last decades, is one of the main contributors to this exponential increase of global warming-causing gases. In fact, cities such as Barcelona or Madrid, among many others, are imposing traffic restrictions to mitigate this situation. However, mankind is still on time to reverse this negative tendency and fix the environmental issue for the upcoming generations.

The main goal of the present Thesis focuses on the study, implementation and analysis of the passive pre-chamber ignition concept in a near-future light-duty passenger car application. To be more specific, the investigation addresses the physical phenomena involving the combustion process when pre-chamber ignition system is used in a spark-ignition engine. Then, some strategies to improve thermal efficiency while employing this concept are applied. Finally, with all the knowledge gathered, basic guidelines for a pre-chamber pre-design are presented.

The first approach to the concept consists of its direct implementation in the engine, obtaining experimental results in three different operating conditions in terms of engine load and speed. Furthermore, different pre-chamber geometries are also evaluated. Although its direct implementation is relatively straightforward by exchanging the spark plug, understanding some of the relevant phenomena related to the combustion process, such as gas exchange or jet-tip penetration, is extremely difficult without the support of computational tools. This is the main reason supporting the use of 1D numerical tools in the present Thesis, since with proper modeling based on experimental data, further knowledge can be obtained in those situations where experimental evaluations are not feasible. These 1D tools have the benefits of their low computational cost and their ability to provide reasonably good results in a short period of time.

In terms of thermal efficiency, two different strategies, such as the increase of lambda or the increase of the exhaust gas re-circulation rate, are adopted to extend further the benefits of the passive pre-chamber ignition system. However, the physical application limits of both strategies are reached, and a series of possibilities are proposed to expand these limits and increase thermal efficiency.

Finally, with all the experimental and numerical results, some guidelines are suggested to design a pre-chamber that takes advantage of the benefits, increasing thermal efficiency compared with the conventional spark ignition and the current passive pre-chamber concepts.

Resumen

El aumento global de las emisiones de gases de efecto invernadero desde el inicio de la Revolución Industrial se ha convertido en un grave peligro para la vida humana. Además de la generación de energía y la industria, el transporte, con el aumento del número total de vehículos en las últimas décadas, es uno de los principales responsables de este incremento exponencial de los gases causantes del calentamiento global. De hecho, ciudades como Barcelona o Madrid, entre muchas otras, están imponiendo restricciones al tráfico para mitigar esta situación. Sin embargo, la humanidad aún está a tiempo de invertir esta tendencia negativa y solucionar el problema medioambiental para las generaciones futuras.

El objetivo principal de la presente Tesis se centra en el estudio, implementación y análisis del concepto de encendido por precámara pasiva para su aplicación en la próxima generación de vehículos automóviles. Más específicamente, esta investigación aborda los fenómenos físicos que intervienen en el proceso de combustión cuando se utiliza el sistema de encendido por precámara en un motor de encendido provocado. A continuación, se aplican algunas estrategias para mejorar el rendimiento térmico que se obtiene operando con este concepto. Finalmente, a partir del conocimiento generado, se presentan unas directrices básicas para el prediseño de este tipo de precámaras.

La primera aproximación al concepto consiste en su implementación directa en el motor, obteniendo resultados experimentales en tres condiciones de funcionamiento diferentes en términos de carga y régimen de giro del motor. Además, también se evalúan diferentes geometrías de precámara. Aunque su implementación directa es relativamente sencilla mediante la sustitución de la bujía, la comprensión de ciertos fenómenos relevantes relacionados con la combustión, como el intercambio de gases o la penetración de los chorros, es extremadamente difícil sin el apoyo de herramientas computacionales. Esta es la principal razón que justifica el uso de herramientas

numéricas 1D en la presente Tesis, ya que con un modelado adecuado basado en datos experimentales, se puede obtener información relevante en aquellas situaciones en las que no es factible generarla experimentalmente. Estas herramientas 1D tienen las ventajas de su bajo coste computacional y su capacidad de proporcionar resultados en poco tiempo.

En cuanto al rendimiento térmico, se adoptan dos estrategias diferentes, como el aumento de λ o el aumento de la tasa de recirculación de los gases de escape, para incrementar aún más las ventajas del sistema de encendido por precámara pasiva. Sin embargo, se alcanzan los límites físicos de aplicación de ambas estrategias y se proponen una serie de posibilidades para ampliar estos límites y aumentar el rendimiento térmico.

Finalmente, a partir de los resultados experimentales y numéricos, se sugieren algunas pautas para diseñar una precámara que aproveche las ventajas observadas, aumentando el rendimiento térmico en comparación con los conceptos de encendido por bujía convencional y por precámara pasiva actuales.

Resum

L'augment global de les emissions de gasos d'efecte d'hivernacle des de l'inici de la Revolució Industrial s'ha convertit en un greu perill per a la vida humana. A més de la generació d'energia i la indústria, el transport, amb l'augment del nombre total de vehicles en les últimes dècades, és un dels principals responsables d'aquest increment exponencial dels gasos causants de l'escalfament global. De fet, ciutats com Barcelona o Madrid, entre moltes altres, estan imposant restriccions al trànsit per a mitigar aquesta situació. No obstant això, la humanitat encara és a temps d'invertir aquesta tendència negativa i solucionar el problema mediambiental per a les generacions futures.

L'objectiu principal de la present Tesi se centra en l'estudi, implementació i anàlisi del concepte d'encesa per precàmera passiva per a la seua aplicació en la pròxima generació de vehicles automòbils. Més específicament, aquesta investigació aborda els fenòmens físics que intervenen en el procés de combustió quan s'utilitza el sistema d'encesa per precàmera en un motor d'encesa provocada. A continuació, s'apliquen algunes estratègies per a millorar el rendiment tèrmic que s'obté operant amb aquest concepte. Finalment, a partir del coneixement generat, es presenten unes directrius bàsiques per al predisseny d'aquesta mena de precàmeres.

La primera aproximació al concepte consisteix en la seua implementació directa en el motor, obtenint resultats experimentals en tres condicions de funcionament diferents en termes de càrrega i règim de gir del motor. A més, també s'avaluen diferents geometries de precàmera. Encara que la seua implementació directa és relativament senzilla mitjançant la substitució de la bugia, la comprensió d'uns certs fenòmens rellevants relacionats amb la combustió, com l'intercanvi de gasos o la penetració dels dolls, és extremadament difícil sense el suport d'eines computacionals. Aquesta és la principal raó que justifica l'ús d'eines numèriques 1D en la present Tesi, ja que amb un modelatge adequat basat en dades experimentals es pot obtindre infor-

mació rellevant en aquelles situacions en les quals no és factible generar-la experimentalment. Aquestes eines 1D tenen com a principal avantatge el seu baix cost computacional i la seua capacitat de proporcionar resultats en poc temps.

Quant al rendiment tèrmic, s'adopten dues estratègies diferents, com l'augment de λ o l'augment de la taxa de recirculació dels gasos d'escapament, per a incrementar encara més els avantatges del sistema d'encesa per precàmera passiva. No obstant això, s'aconsegueixen els límits físics d'aplicació de totes dues estratègies i es proposen una sèrie de possibilitats per a ampliar aquests límits i augmentar el rendiment tèrmic.

Finalment, a partir dels resultats experimentals i numèrics, se suggereixen algunes pautes per a dissenyar una precàmera que aprofite els avantatges observats, augmentant el rendiment tèrmic en comparació amb els conceptes d'encesa per bugia convencional i per precàmera passiva actuals.

List of publications

Following the work performed in the framework of this doctoral thesis and its associated projects, the following journal papers have been published:

- [1] J. Benajes, R. Novella, J. Gomez-Soriano, P. Martinez-Hernandiz, C. Libert, and M. Dabiri. “[Evaluation of the passive pre-chamber ignition concept for future high compression ratio turbocharged spark-ignition engines](#)”. *Applied Energy* 248, 2019, pp. 576–588.
- [2] J. Benajes, R. Novella, J. Gomez-Soriano, P. Martinez-Hernandiz, C. Libert, and M. Dabiri. “Performance of the passive pre-chamber ignition concept in a spark-ignition engine for passenger car applications”. In: *SIA Powertrain & Electronics*. 2019.
- [3] J. López, R. Novella, J. Gomez-Soriano, P. Martínez-Hernández, et al. “[Advantages of the unscavenged pre-chamber ignition system in turbocharged natural gas engines for automotive applications](#)”. *Energy* 218, 2021, p. 119466.
- [4] R. Novella, J. Gomez-Soriano, P. Martinez-Hernandiz, C. Libert, and F. Rampanarivo. “[Improving the performance of the passive pre-chamber ignition concept for spark-ignition engines fueled with natural gas](#)”. *Fuel* 290, 2021, p. 119971.
- [5] R. Novella, B. Pla, P. Bares, and P. J. Martinez-Hernandiz. “[Closed-Loop Combustion Control by Extremum Seeking with the Passive-Chamber Ignition Concept in SI Engines](#)”. In: *WCX SAE World Congress Experience*. SAE International, 2020.
- [6] J. García-Oliver, Y. Niki, R. Rajasegar, R. Novella, et al. “[An experimental and one-dimensional modeling analysis of turbulent gas ejection in pre-chamber engines](#)”. *Fuel* 299, 2021, p. 120861.
- [7] P. J. Martinez Hernandez, F. Di Sabatino, R. Novella, and I. Ekoto. “[A Numerical and Experimental Investigation on Different Strategies to Evaluate Heat Release Rate and Performance of a Passive Pre-Chamber Ignition System](#)”. In: *WCX SAE World Congress Experience*. SAE International, 2022.

- [8] F. D. Sabatino, P. J. Martinez-Hernandez, R. N. Rosa, and I. Ekoto. “Investigation of the effects of passive pre-chamber nozzle pattern and ignition system on engine performance and emissions”. International Journal of Engine Research 0 (0), 2022.
- [9] Investigation on the Effects of Passive Pre-Chamber Ignition System and Geometry on Engine Knock Intensity. Vol. ASME 2022 ICE Forward Conference. Internal Combustion Engine Division Fall Technical Conference. 2022.

Division of work between authors

The work leading up to this thesis was done in collaboration with other researchers. The respondent is the co-author of all papers on which this thesis is based, with author signatures being in order of seniority in the Institute. The respondent implemented the proposed methodology into the different engine set-ups, processed the results, performed the analysis and extracted the presented conclusions. Discussions were also performed in collaboration with supervisor Prof. Novella and the rest of the co-authors.

Funding acknowledgments

The respondent wishes to acknowledge the financial support received through contract FPI-S2-19-21993 of the Programa de Apoyo para la Investigación y Desarrollo (PAID) of Universitat Politècnica de València.

Parts of the work presented in this thesis have been supported by different collaborations with the research partner Sandia National Laboratories LLC, 7011 East Ave, Livermore, California, US.

Acknowledgements

I would like to express my sincere gratitude to my director Prof. Novella for his guidance, support and advice through the complete duration of this research. A gratitude that also must be extended to Prof. Payri and Prof. Desantes on behalf of CMT – Motores Térmicos and Universitat Politècnica de València for offering me the chance to become part of this research group during these five years.

Furthermore, I would like to thank Prof. Jose Manuel Pastor, Prof. Jose Maria García and Dr. Josep Gomez for their advice and help during this stage. I could not be able to finish this research without them. A special gratitude comes to Prof. Jose Manuel Pastor who was my director during my B.Sc. stage and supported me to start this new adventure.

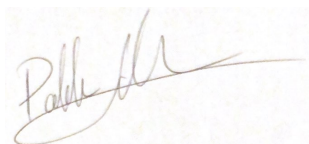
I am not forgetting all the members of Combustion-Ignition research line. I want to highlight Mr. Gabriel Alcantarilla, technician of CMT – Motores Térmicos. His work and guidance were fundamental to the attainment of the results presented in this document. Countless hours in the experimental facility with him made us good partners.

Also, I would like to thank Dr. Isaac Ekoto, Dr. Francesco Di Sabatino and all the staff of the Combustion Research Center of Sandia National Laboratories for hosting me as a visiting researcher during my stay and for all their effort to publish the work we performed together.

I want to express my affection to all the other doctoral students who shared the journey with me: Ferran, Ibrahim, Cássio, Bárbara, Johan and many others. I will never forget our special Almorsarets de española tomate in the cafeteria and our philosophical walks around the campus Ferran.

Finally, I wish to thank all my friends and family, for their unconditional support in any circumstances.

To my soulmate Batgopi, thank you for everything. After all this time... Always.



“An expert is a person who has made all the mistakes that can be made in a very narrow field.”

Neils Bohr, Copenhagen, 1885-1962

Contents

1	<i>Introduction</i>	1
1.1	Introduction	1
1.2	Thesis background and context	3
1.2.1	Air dilution	3
1.2.2	EGR dilution	4
1.3	Thesis object	5
1.4	Thesis outline	6
1.5	Conclusions	8
2	<i>Literature review</i>	11
2.1	Introduction	11
2.2	Strategies to increase thermal efficiency	11
2.2.1	Lean burn	12
2.2.2	Exhaust gas recirculation	13
2.2.3	Miller cycle	14
2.3	Pre-chamber technology	16
2.3.1	Pre-chamber applications review	16
2.3.2	Aspects of pre-chamber combustion	48
2.3.3	Pre-chamber geometry aspects	61
2.3.4	Influence of pre-chamber applications on emissions ..	65
2.4	Conclusions	68
3	<i>Tools and methodology</i>	71
3.1	Introduction	71
3.2	Experimental tools	72
3.2.1	Test bench	72
3.2.2	Engine	75
3.2.3	Pre-chamber bodies	76
3.3	Numerical tools	78

3.3.1	0D Combustion diagnosis.....	79
3.3.2	1D Wave Action model	79
3.3.3	1D Jet model	81
3.4	Methodology	82
3.4.1	Experimental activities	83
3.4.2	Numerical analysis	84
3.5	Conclusions	86
4	<i>Implementation of the concept</i>	87
4.1	Introduction	87
4.2	Implementation of the concept in stoichiometric conditions using gasoline as fuel	88
4.3	Implementation of the concept in stoichiometric conditions using compressed natural gas as fuel	96
4.4	Compatibility with millerization strategy using compressed natural gas as fuel	107
4.5	Engine maps	114
4.6	Conclusions	117
5	<i>Dilution strategies and how to improve the concept</i>	121
5.1	Introduction	121
5.2	Compatibility with air dilution	122
5.2.1	Employing gasoline as fuel	122
5.2.2	Employing natural gas as fuel.....	128
5.3	Compatibility with EGR dilution	134
5.3.1	Employing gasoline as fuel	134
5.3.2	Employing natural gas as fuel.....	142
5.4	Operation at low engine load and speed conditions	146
5.5	Engine maps	151
5.6	Conclusions	155
6	<i>Key aspects in pre-chamber design</i>	159
6.1	Introduction	159
6.2	Nozzle orientation evaluation	160
6.3	Pre-chamber volume evaluation.....	162
6.4	Internal pre-chamber combustion evaluation.....	175
6.5	Designing a wide-range optimal pre-chamber	179
6.6	Conclusions	190
7	<i>Conclusions and future investigation paths</i>	193

7.1	Introduction	193
7.2	Key aspects of the research work	193
7.3	Future investigation activities	199

<i>Bibliography</i>		201
----------------------------	--	------------

List of Figures

1.1	Surface temperature anomalies relative to 1951–1980 from surface air measurements at meteorological stations and ship and satellite SST measurements. (A) Global annual mean anomalies. (B) Temperature anomaly for the first half decade of the 21st century [12].	1
1.2	Nitrogen oxide emissions by source category in (a) the United States and (b) European Countries [14].	2
1.3	Overview of Euro 5 and Euro 6 vehicle emissions standards for the New European Driving Cycle (NEDC) [15].	3
1.4	Thesis outline covering the key aspects of each Chapter.	8
2.1	Schematic view of all pre-chamber ignition applications chronologically sorted from top to bottom including patents and SAE papers [36].	17
2.2	Internal combustion engine developed by Harry R. Ricardo featuring the first pre-chamber application [40].	18
2.3	Internal combustion engine developed by Caleb E. Summers, featuring a mechanically actuated auxiliary intake valve [42].	19
2.4	Internal combustion engine developed by Marion Mallory, including a connection between the carburetors [43].	20
2.5	Internal combustion engine developed by Albert Bagnulo, including a connection between the carburetors [44].	20
2.6	Internal combustion engine developed by William B. Barnes, featuring a large spherical pre-chamber [45].	21
2.7	Internal combustion engine developed by Neil O. Broderson [46].	22
2.8	Torch ignition precursor engine developed by N. A. Nilov [49].	22
2.9	Heintz Ram-Straticharge engine developed by Ralph M. Heintz [51].	23

2.10	Improvements in or relating to internal combustion engines by Anthony Barnard and Charles D. Brewer [53].	23
2.11	Evaluated duel-chamber spark-ignited engine by Henry K. Newhall and Ibrahim A. El-Messiri [57].	24
2.12	CVCC engine developed by Honda [58].	25
2.13	Internal combustion engine with a spherical valveless pre-chamber developed by Walter R. Brandstetter [66].	25
2.14	Internal combustion engine concepts of General Motors (a) [67], Porsche (b) [72], Ford (c) [74] and Nissan (d) [71].	26
2.15	Internal combustion engine featuring LAG ignition concept [100].	28
2.16	Jet Plume Injection and Combustion diagram concept [107].	28
2.17	Hydrogen Assisted Jet Ignition sketch [135].	30
2.18	Pulsed Jet Combustion sketch [143].	31
2.19	Auto-inflammation Piloteé par injection de Radicaux sketch [149].	33
2.20	Homogeneous Combustion Jet Ignition system sketch [153].	34
2.21	Homogeneous Combustion Jet Ignition system sketch [154].	34
2.22	Pre-chamber spark plug featuring pilot injection concept principle [155].	35
2.23	Pre-chamber 3D CAD model (a) and cross section view cut of 3D CAD model [166].	36
2.24	Turbulence Generating Pot concept sketch [170].	37
2.25	Volkswagen Prechamber Engine (a) [173], Ford Torch Ignition (b) [172] and General Motors Plasma Jet Ignition (c) [174] sketches.	38
2.26	Swirl Chamber Spark Plug pre-chamber sketch [117].	38
2.27	Horizontal pre-chamber sketch from Tokai University [178].	39
2.28	Catalytic pre-chamber concept sketch [182].	39
2.29	Functioning of BPI concept: (a) Injection event during compression stoke, (b) air-fuel mixture in the piston bowl, (c) mixture transport into the pre-chamber spark plug, (d) ignition and inflammation with flame jets [194].	40
2.30	Arrangement and orientation of pre-chamber nozzles: (a) Top view, (b) Front view, (c) Spark plug location and orientation, (d) Combustion chamber design [202].	41
2.31	Pre-chamber and main chamber assembly sketch [210].	42
2.32	Image of MAHLE Powertrain developed pre-chamber system [213].	43

2.33	Comparison of spark ignition versus Turbulent Jet Ignition combustion systems [18].	45
2.34	Exhaust lambda and fuel economy improvement over baseline SI at $\lambda = 1$ [213].	46
2.35	Varying excess air dilution crank angle resolved images of in-cylinder combustion through the quartz piston insert for both spark ignition ($\lambda = 1$, $\lambda = 1.4$, $\lambda = 1.5$) and jet ignition ($\lambda = 1.8$) combustion [221].	47
2.36	Scavenging across the pre-chamber during the intake stroke (EGR indicates the residual gas mass fraction) [234].	49
2.37	IMEP and combustion stability for pre-chamber spark timing variation operating with the TJI concept (left) [18] and in-cylinder pressure with APIR system including spark timing (right) [148]. . .	50
2.38	Variation in 0-10% burn duration for λ sweep [223].	52
2.39	Pre-chamber combustion duration indicated by pressure traces in the pre-chamber and the main chamber [228].	53
2.40	Comparison of filtered pressure traces between the conventional spark ignition system and the pre-chamber ignition system [247]. . .	54
2.41	Sketch of the two different quenching mechanisms in the turbulent jet ignition [250].	55
2.42	Comparison of combustion characteristics at constant indicated specific fuel consumption. Adapted from [71].	57
2.43	Comparison of combustion profile between passive TJI and conventional SI at 18 bar BMEP 4000 rpm [254].	57
2.44	Specific indicated fuel consumption for different air fuel ratios λ at BMEP = 0.2 MPa and $n = 2000$ rpm [194].	58
2.45	HAI WOT performance [126].	59
2.46	Comparison of the passive TJI and conventional SI over a BMEP sweep from 6 bar up to 18 bar at 4000 rpm [19].	61
2.47	Engine out emission and exhaust port temperature comparisons of jet ignition dual fuel (gasoline-propane), liquid fuel (gasoline-gasoline) and vaporized fuel (gasoline-vaporized gasoline) together with spark ignition (gasoline) combustion systems. 1500 RPM, 4.7 bar IMEPn, (main chamber fuel - pre-chamber fuel) [24].	67
3.1	Layout of the engine test cell.	73
3.2	Schematic view of the pre-chamber assembly in the engine head. . .	77

3.3	Schematic view of the pre-chamber assembly in the engine head. . .	78
3.4	Comparison of experimental and simulated in-cylinder pressure profiles.	80
3.5	Comparison of experimental and simulated intake pressure profiles.	80
3.6	Comparison of experimental and simulated exhaust pressure profiles.	80
3.7	Schematic layout of the design workflow coupling the different numerical tools.	85
4.1	Schematic view of the pre-chamber assembly in the engine head. . .	89
4.2	Pressure (left) and heat release rate (right) profiles of the high engine load and speed conditions at $\lambda = 1$ operating with gasoline for conventional ignition system (black) and both passive pre-chamber geometries (blue and red). Dashed lines correspond to 50% of combustion (CA50).	90
4.3	Comparison of combustion phasing (CA50), gross indicated efficiency, MAPO, combustion stability (COV IMEP), combustion velocity and fuel consumption for both ignition systems at high engine load and speed conditions at $\lambda = 1$ operating with gasoline.	91
4.4	Comparison of combustion efficiency and emitted NO_x for both ignition systems at high engine load and speed conditions at $\lambda = 1$ operating with gasoline.	92
4.5	Pressure (left) and heat release rate (right) profiles of the low engine load and speed conditions at $\lambda = 1$ operating with gasoline for conventional ignition system (black) and both passive pre-chamber geometries (blue and red). Dashed lines correspond to 50% of combustion (CA50).	93
4.6	Comparison of combustion phasing (CA50), gross indicated efficiency, MAPO, combustion stability (COV IMEP), combustion velocity and fuel consumption for both ignition systems at low engine load and speed conditions at $\lambda = 1$ operating with gasoline.	93
4.7	Comparison of combustion efficiency and emitted NO_x for both ignition systems at low engine load and speed conditions at $\lambda = 1$ operating with gasoline.	94
4.8	Pressure (left) and heat release rate (right) profiles of the medium engine load and speed conditions at $\lambda = 1$ operating with gasoline for conventional ignition system (black) and both passive pre-chamber geometries (blue and red). Dashed lines correspond to 50% of combustion (CA50).	94

4.9	Comparison of combustion phasing (CA50), gross indicated efficiency, MAPO, combustion stability (COV IMEP), combustion velocity and fuel consumption for both ignition systems at medium engine load and speed conditions at $\lambda = 1$ operating with gasoline.	95
4.10	Comparison of combustion efficiency and emitted NO_x for both ignition systems at medium engine load and speed conditions at $\lambda = 1$ operating with gasoline.	95
4.11	Difference in laminar flame speed for gasoline and compressed natural gas at different pressure, temperature, λ and EGR levels. . .	97
4.12	Auto-ignition delay calculated for gasoline (top) and compressed natural gas (bottom). Black lines represent the duration of combustion without knock limitation (DoC).	99
4.13	Prospective of GHG emission in 100 years using different fuels and refinement strategies.	101
4.14	Pressure (left) and heat release rate (right) profiles of the high engine load and speed conditions at $\lambda = 1$ operating with CNG for conventional ignition system (black) and both passive pre-chamber geometries (blue and red). Dashed lines correspond to 50% of combustion (CA50).	102
4.15	Comparison of combustion phasing (CA50), gross indicated efficiency, MAPO, combustion stability (COV IMEP), combustion velocity and fuel consumption for both ignition systems at high engine load and speed conditions at $\lambda = 1$ operating with CNG.	102
4.16	Comparison of combustion efficiency and emitted NO_x for both ignition systems at high engine load and speed conditions at $\lambda = 1$ operating with CNG.	103
4.17	Pressure (left) and heat release rate (right) profiles of the low engine load and speed conditions at $\lambda = 1$ operating with CNG for conventional ignition system (black) and both passive pre-chamber geometries (blue and red). Dashed lines correspond to 50% of combustion (CA50).	104
4.18	Comparison of combustion phasing (CA50), gross indicated efficiency, MAPO, combustion stability (COV IMEP), combustion velocity and fuel consumption for both ignition systems at low engine load and speed conditions at $\lambda = 1$ operating with CNG.	104

4.19	Comparison of combustion efficiency and emitted NO_x for both ignition systems at low engine load and speed conditions at $\lambda = 1$ operating with CNG.	105
4.20	Pressure (left) and heat release rate (right) profiles of the medium engine load and speed conditions at $\lambda = 1$ operating with CNG for conventional ignition system (black) and both passive pre-chamber geometries (blue and red). Dashed lines correspond to 50% of combustion (CA50).	105
4.21	Comparison of combustion phasing (CA50), gross indicated efficiency, MAPO, combustion stability (COV IMEP), combustion velocity and fuel consumption for both ignition systems at medium engine load and speed conditions at $\lambda = 1$ operating with CNG. ...	106
4.22	Comparison of combustion efficiency and emitted NO_x for both ignition systems at medium engine load and speed conditions at $\lambda = 1$ operating with CNG.	106
4.23	Pressure (left) and heat release rate (right) profiles of the high engine load and speed conditions at $\lambda = 1$ operating with CNG for conventional ignition system (black) and passive pre-chamber geometry 1 (blue). Dashed lines correspond to 50% of combustion (CA50).	108
4.24	Comparison of combustion phasing (CA50), gross indicated efficiency, MAPO, combustion stability (COV IMEP), combustion velocity and fuel consumption for both ignition systems at high engine load and speed conditions at $\lambda = 1$ operating with CNG.	108
4.25	Comparison of fuel consumption for the three evaluated implementations, gasoline (left), CNG (center) and Millerization (right) and the three different ignition systems, SI (black), pre-chamber 1 (blue) and pre-chamber 2 (red) at high engine load and speed conditions at $\lambda = 1$	109
4.26	Comparison of combustion efficiency and emitted NO_x for both ignition systems at high engine load and speed conditions at $\lambda = 1$ operating with CNG.	110
4.27	Pressure (left) and heat release rate (right) profiles of the low engine load and speed conditions at $\lambda = 1$ operating with CNG for conventional ignition system (black) and passive pre-chamber geometry 1 (blue). Dashed lines correspond to 50% of combustion (CA50).	110

4.28	Comparison of combustion phasing (CA50), gross indicated efficiency, MAPO, combustion stability (COV IMEP), combustion velocity and fuel consumption for both ignition systems at low engine load and speed conditions at $\lambda = 1$ operating with CNG.	111
4.29	Comparison of combustion efficiency and emitted NO_x for both ignition systems at low engine load and speed conditions at $\lambda = 1$ operating with CNG.	111
4.30	Pressure (left) and heat release rate (right) profiles of the medium engine load and speed conditions at $\lambda = 1$ operating with CNG for conventional ignition system (black) and passive pre-chamber geometry 1 (blue). Dashed lines correspond to 50% of combustion (CA50).	112
4.31	Comparison of combustion phasing (CA50), gross indicated efficiency, MAPO, combustion stability (COV IMEP), combustion velocity and fuel consumption for both ignition systems at medium engine load and speed conditions at $\lambda = 1$ operating with CNG.	113
4.32	Comparison of combustion efficiency and emitted NO_x for both ignition systems at medium engine load and speed conditions at $\lambda = 1$ operating with CNG.	113
4.33	Gross indicated efficiency for spark ignition system (left) and passive pre-chamber ignition system (right) colormaps of the engine map at $\lambda = 1$ operating with CNG and Miller cycle varying engine load and speed.	114
4.34	Combustion phasing for spark ignition system (left) and passive pre-chamber ignition system (right) colormaps of the engine map at $\lambda = 1$ operating with CNG and Miller cycle varying engine load and speed.	115
4.35	Combustion velocity for spark ignition system (left) and passive pre-chamber ignition system (right) colormaps of the engine map at $\lambda = 1$ operating with CNG and Miller cycle varying engine load and speed.	115
4.36	Combustion stability for spark ignition system (left) and passive pre-chamber ignition system (right) colormaps of the engine map at $\lambda = 1$ operating with CNG and Miller cycle varying engine load and speed.	116
4.37	MAPO for spark ignition system (left) and passive pre-chamber ignition system (right) colormaps of the engine map at $\lambda = 1$ operating with CNG and Miller cycle varying engine load and speed.	116

4.38	Maximum in-cylinder pressure for spark ignition system (left) and passive pre-chamber ignition system (right) colormaps of the engine map at $\lambda = 1$ operating with CNG and Miller cycle varying engine load and speed.	116
4.39	Fuel consumption for spark ignition system (left) and passive pre-chamber ignition system (right) colormaps of the engine map at $\lambda = 1$ operating with CNG and Miller cycle varying engine load and speed.	117
4.40	Combustion phasing (upper) and gross indicated efficiency (low) for the three different engine architectures: gasoline (left), CNG (center) and Millerization (right) operating at high engine load and speed conditions at $\lambda = 1$. The different ignition systems: SI (black), pre-chamber 1 (blue) and pre-chamber 2 (red).	118
5.1	Trends of air dilution in combustion phasing (CA50), gross indicated efficiency, MAPO, combustion stability (COV IMEP), combustion velocity and fuel consumption for the studied ignition systems at high engine load and speed conditions operating with gasoline. ...	123
5.2	Trends of air dilution in combustion efficiency and emitted NO_x for the studied ignition systems at high engine load and speed conditions operating with gasoline.	124
5.3	Pressure (left) and heat release rate (right) profiles of the high engine load and speed conditions at maximum λ operating with gasoline for conventional ignition system (black) and both passive pre-chamber geometries (blue and red). Dashed lines correspond to 50% of combustion (CA50).	124
5.4	Comparison of combustion phasing (CA50), combustion velocity, combustion stability and gross indicated efficiency for both ignition systems at high engine load and speed conditions for $\lambda = 1$ and maximum λ operating with gasoline.	125
5.5	Heat release rate profiles for the $\lambda = 1$ and $\lambda = 1.6$ cases.	126
5.6	Map of gross indicated efficiency at high engine load and speed conditions.	127
5.7	Expected gross indicated efficiency trend (red line) and real gross indicated efficiency obtained (black triangle).	127

5.8	Trends of air dilution in combustion phasing (CA50), gross indicated efficiency, MAPO, combustion stability (COV IMEP), combustion velocity and fuel consumption for the studied ignition systems at high engine load and speed conditions operating with CNG.	129
5.9	Trends of air dilution in combustion efficiency and emitted NO _x for the studied ignition systems at high engine load and speed conditions operating with CNG.	129
5.10	Pressure (left) and heat release rate (right) profiles of the high engine load and speed conditions at maximum λ operating with CNG for conventional ignition system (black) and both passive pre-chamber geometries (blue and red). Dashed lines correspond to 50% of combustion (CA50).	130
5.11	In-cylinder (blue) and pre-chamber (red) pressure profiles at maximum λ operating with CNG for pre-chamber 1 ($\lambda = 1.55$) and pre-chamber 2 ($\lambda = 1.45$).	131
5.12	Velocity (left) and mass flow rate (right) profiles in one hole at maximum λ operating with CNG for pre-chamber 1 ($\lambda = 1.55$) and pre-chamber 2 ($\lambda = 1.45$).	131
5.13	Trends of EGR dilution of combustion phasing (CA50), gross indicated efficiency, MAPO, combustion stability (COV IMEP), combustion velocity and fuel consumption for the studied ignition systems at high engine load and speed conditions operating with gasoline.	135
5.14	Trends of EGR dilution of combustion efficiency and emitted NO _x for the studied ignition systems at high engine load and speed conditions operating with gasoline.	136
5.15	Pressure (left) and heat release rate (right) profiles of the high engine load and speed conditions at maximum EGR operating with gasoline for conventional ignition system (black) and both passive pre-chamber geometries (blue and red). Dashed lines correspond to 50% of combustion (CA50).	136
5.16	Comparison of combustion phasing (CA50), combustion velocity, combustion stability and gross indicated efficiency for both ignition systems at high engine load and speed conditions for stoichiometric and maximum EGR operating points with gasoline.	137
5.17	Trends of EGR dilution of combustion phasing (CA50), gross indicated efficiency, MAPO, combustion stability (COV IMEP), combustion velocity and fuel consumption for the studied ignition systems at medium engine load and speed conditions operating with gasoline.	138

5.18	Trends of EGR dilution of combustion efficiency and emitted NO_x for the studied ignition systems at medium engine load and speed conditions operating with gasoline.	139
5.19	Pressure (left) and heat release rate (right) profiles of the medium engine load and speed conditions at maximum EGR operating with gasoline for conventional ignition system (black) and both passive pre-chamber geometries (blue and red). Dashed lines correspond to 50% of combustion (CA50).	139
5.20	Comparison of combustion phasing (CA50), combustion velocity, combustion stability and gross indicated efficiency for both ignition systems at medium engine load and speed conditions for stoichiometric and maximum EGR operating points with gasoline.	140
5.21	Borghetti-Peters diagram and trends observed when increasing the dilution rate with air and EGR.	141
5.22	Computed laminar flame speeds (s_L) and flame thickness (l_f) for air and EGR diluted cases.	142
5.23	Trends of EGR dilution of combustion phasing (CA50), gross indicated efficiency, MAPO, combustion stability (COV IMEP), combustion velocity and fuel consumption for the studied ignition systems at high engine load and speed conditions operating with CNG. . . .	143
5.24	Trends of EGR dilution of combustion efficiency and emitted NO_x for the studied ignition systems at high engine load and speed conditions operating with CNG.	144
5.25	Pressure (left) and heat release rate (right) profiles of the high engine load and speed conditions at maximum EGR operating with CNG for conventional ignition system (black) and both passive pre-chamber geometries (blue and red). Dashed lines correspond to 50% of combustion (CA50).	145
5.26	Comparison of combustion phasing (CA50), combustion velocity, combustion stability and gross indicated efficiency for both ignition systems at high engine load and speed conditions for stoichiometric and maximum EGR operating points with CNG.	145
5.27	Trends of EGR dilution of combustion phasing (CA50), gross indicated efficiency, MAPO, combustion stability (COV IMEP), combustion velocity and fuel consumption for the studied ignition systems at medium engine load and speed conditions operating with CNG. .	146

5.28	Trends of EGR dilution of combustion efficiency and emitted NO_x for the studied ignition systems at medium engine load and speed conditions operating with CNG.	146
5.29	Comparison of combustion phasing (CA50), gross indicated efficiency, exhaust temperature, combustion stability (COV IMEP), combustion velocity and fuel consumption for both ignition systems at low engine load and speed conditions at $\lambda = 1$ operating with gasoline.	147
5.30	Comparison of combustion phasing (CA50), gross indicated efficiency, exhaust temperature, combustion stability (COV IMEP), combustion velocity and fuel consumption for both ignition systems at low engine load and speed conditions at $\lambda = 1$ operating with CNG.	148
5.31	Comparison of combustion phasing (CA50), gross indicated efficiency, exhaust temperature, combustion stability (COV IMEP), combustion velocity and fuel consumption for both ignition systems at low engine load and speed conditions at $\lambda = 1$ operating with CNG and increased intake temperature.	150
5.32	Comparison of combustion phasing (CA50), gross indicated efficiency, exhaust temperature, combustion stability (COV IMEP), combustion velocity and fuel consumption for both ignition systems at low engine load and speed conditions at $\lambda = 1$ operating with CNG and different EGR dilution levels.	151
5.33	External EGR dilution level colormap of the engine map for pre-chamber 1 at $\lambda = 1$ operating with CNG and Miller cycle varying engine load and speed.	152
5.34	Gross indicated efficiency for passive pre-chamber ignition system without external EGR (left) and passive pre-chamber ignition system with external EGR (right) colormaps of the engine map at $\lambda = 1$ operating with CNG and Miller cycle varying engine load and speed.	152
5.35	Combustion phasing for passive pre-chamber ignition system without external EGR (left) and passive pre-chamber ignition system with external EGR (right) colormaps of the engine map at $\lambda = 1$ operating with CNG and Miller cycle varying engine load and speed.	153

5.36	Combustion velocity for passive pre-chamber ignition system without external EGR (left) and passive pre-chamber ignition system with external EGR (right) colormaps of the engine map at $\lambda = 1$ operating with CNG and Miller cycle varying engine load and speed.	153
5.37	Combustion stability for passive pre-chamber ignition system without external EGR (left) and passive pre-chamber ignition system with external EGR (right) colormaps of the engine map at $\lambda = 1$ operating with CNG and Miller cycle varying engine load and speed.	154
5.38	MAPO for passive pre-chamber ignition system without external EGR (left) and passive pre-chamber ignition system with external EGR (right) colormaps of the engine map at $\lambda = 1$ operating with CNG and Miller cycle varying engine load and speed.	154
5.39	Maximum in-cylinder pressure for passive pre-chamber ignition system without external EGR (left) and passive pre-chamber ignition system with external EGR (right) colormaps of the engine map at $\lambda = 1$ operating with CNG and Miller cycle varying engine load and speed.	155
5.40	Fuel consumption for passive pre-chamber ignition system without external EGR (left) and passive pre-chamber ignition system with external EGR (right) colormaps of the engine map at $\lambda = 1$ operating with CNG and Miller cycle varying engine load and speed.	155
6.1	Trends of combustion phasing (CA50), gross indicated efficiency, exhaust temperature, combustion stability (COV IMEP), combustion velocity and fuel consumption for the different ignition systems at low engine load and speed conditions and $\lambda = 1$	161
6.2	Trends of combustion efficiency and emitted NO_x for the different ignition systems at low engine load and speed conditions and $\lambda = 1$.	162
6.3	Trends of combustion phasing (CA50), gross indicated efficiency, exhaust temperature, combustion stability (COV IMEP), combustion velocity and fuel consumption for the different ignition systems at high engine load and speed conditions operating with EGR and $\lambda = 1$	163
6.4	Trends of combustion efficiency and emitted NO_x for the different ignition systems at high engine load and speed conditions operating with EGR and $\lambda = 1$	163
6.5	Pressure difference between main and pre-chamber (ΔP) profiles of high engine load and low engine load cases with passive pre-chamber ignition system at $\lambda = 1$ operating with CNG.	164

6.6	Jet momentum profiles and fuel mass inside pre-chamber of high engine load and low engine load cases with the passive pre-chamber ignition system at $\lambda = 1$ operating with CNG.	165
6.7	Maximum jet momentum peak map at low engine load and speed conditions at $\lambda = 1$ operating with CNG, varying pre-chamber volume and hole diameter.	167
6.8	Maximum jet momentum peak map at high engine load and speed conditions at $\lambda = 1$ operating with CNG, varying pre-chamber volume and hole diameter.	167
6.9	Jet penetration profiles of high engine load and low engine load cases with the passive pre-chamber ignition system at $\lambda = 1$ operating with CNG.	169
6.10	Map of t^* values at low engine load and speed conditions at $\lambda = 1$ operating with CNG, varying pre-chamber volume and hole diameter.	170
6.11	Map of t^* values at high engine load and speed conditions at $\lambda = 1$ operating with CNG, varying pre-chamber volume and hole diameter.	170
6.12	Jet penetration at low engine load and speed conditions at $\lambda = 1$ operating with CNG.	171
6.13	Trends of combustion phasing (CA50), gross indicated efficiency, exhaust temperature, combustion stability (COV IMEP), combustion velocity and fuel consumption for both ignition systems at low engine load and speed conditions at $\lambda = 1$ operating with CNG. ...	172
6.14	Trends of combustion efficiency and emitted NO_x for both ignition systems at low engine load and speed conditions at $\lambda = 1$ operating with CNG.	173
6.15	Trends of combustion phasing (CA50), gross indicated efficiency, MAPO, combustion stability (COV IMEP), combustion velocity and fuel consumption for both ignition systems at high engine load and speed conditions at $\lambda = 1$ operating with CNG.	174
6.16	Trends of combustion efficiency and emitted NO_x for both ignition systems at high engine load and speed conditions at $\lambda = 1$ operating with CNG.	175
6.17	Map of jet momentum peak at low engine load and speed conditions at $\lambda = 1$ operating with CNG, varying combustion start and duration.	176

6.18	Jet momentum and heat release rate profiles at low engine load and speed conditions at $\lambda = 1$ operating with CNG for baseline pre-chamber combustion profile and considered best combustion profile case.	177
6.19	Map of t^* at low engine load and speed conditions at $\lambda = 1$ operating with CNG, varying combustion start and duration.	178
6.20	Maximum jet momentum peak map at low engine load and speed conditions with enhanced combustion inside pre-chamber at $\lambda = 1$ operating with CNG, varying pre-chamber volume and hole diameter.	178
6.21	Fuel mass inside pre-chamber at start of ejection (SoE) maps for the passive pre-chamber ignition concept without EGR (left) and with EGR (right) at $\lambda = 1$ operating with CNG.	180
6.22	Maximum combustion velocity peak in the pre-chamber maps for the passive pre-chamber ignition concept without EGR (left) and with EGR (right) at $\lambda = 1$ operating with CNG.	181
6.23	Maximum jet momentum peak maps for the passive pre-chamber ignition concept without EGR (left) and with EGR (right) at $\lambda = 1$ operating with CNG.	182
6.24	Maps of t^* for the passive pre-chamber ignition concept without EGR (left) and with EGR (right) at $\lambda = 1$ operating with CNG.	183
6.25	Maps of t^* for the four extreme operating condition points modifying pre-chamber volume and cross sectional area at $\lambda = 1$ operating with EGR. Black lines represent the iso-line where t^* value of the map is obtained.	184
6.26	Iso-lines of t^* value for the extreme cases in the engine map, optimum pre-chamber geometry for each case (color squares) and selected compromise pre-chamber geometry (black star).	185
6.27	Fuel mass inside pre-chamber at start of ejection (SoE) maps for the passive pre-chamber ignition concept for pre-chamber (left) and compromise pre-chamber (right) at $\lambda = 1$ operating with CNG.	186
6.28	Maximum combustion velocity peak in the pre-chamber maps for the passive pre-chamber ignition concept for pre-chamber (left) and compromise pre-chamber (right) at $\lambda = 1$ operating with CNG.	187
6.29	Maximum jet momentum peak maps for the passive pre-chamber ignition concept for pre-chamber (left) and compromise pre-chamber (right) at $\lambda = 1$ operating with CNG.	188

6.30 T* value maps for the passive pre-chamber ignition concept for pre-chamber (left) and compromise pre-chamber (right) at $\lambda = 1$ operating with CNG. 189

6.31 Comparison of t* values at the most extreme operating conditions for baseline pre-chamber (blue), designed compromise pre-chamber (orange) and optimized pre-chamber geometry for each condition (yellow) at $\lambda = 1$ operating with CNG. 190

List of Tables

3.1	Main specifications of the gasoline fuel.	74
3.2	Main specifications of the compressed natural gas fuel.	74
3.3	Main specifications of the engine with standard Otto cycle.	75
3.4	Main specifications of the engine with Miller cycle.	76
3.5	Main specifications of the evaluated pre-chamber geometries.	77
3.6	Studied operating points.	83
4.1	Studied operating points from Section 1.2 to Section 1.5.	88
4.2	Main geometrical parameters of the studied pre-chambers.	88
4.3	Main specifications of the engine.	89
4.4	Main specifications of the gasoline.	89
4.5	Main specifications of the compressed natural gas.	96
4.6	Life cycle assessment of natural gas and gasoline E10.	100
4.7	Main specifications of the engine.	107
5.1	Studied operating points.	122
5.2	Design of experiments carried out in the 1D Wave Action model modifying combustion phasing and duration.	126
5.3	Energy balance inside the pre-chamber for PC1 and PC2 at high engine load and engine speed conditions.	133
5.4	Energy balance inside the pre-chamber for pre-chamber 1 and pre-chamber 2 at low engine load and speed conditions.	149
6.1	Studied operating points.	160
6.2	Geometrical specifications of the new manufactured versions of pre-chamber 1.	160
6.3	Design of experiments modifying pre-chamber volume and nozzle sectional area carried out in the 1D Wave Action model.	166

6.4	Geometrical specifications of the baseline pre-chamber 1 and new pre-chamber.	168
6.5	Design of experiments modifying pre-chamber combustion start and duration carried out in the 1D Wave Action model.	176
6.6	Geometrical specifications of the baseline pre-chamber 1 and compromise pre-chamber.	185

List of Symbols and Acronyms

ΔP	Pressure difference
γ	Ratio of specific heats
η	Efficiency
λ	Air to fuel ratio
APIR	Auto-Inflammation Piloté par Injection des Radicaux
aTDC	after Top Dead Centre
BC	Black carbon
BDC	Bottom Dead Centre
BMEP	Brake Mean Effective Pressure
BPI	Bowl Pre-chamber Ignition
CA10	Crank Angle for 10% of Fuel Burnt
CA1090	Crank Angle for 10-90% of Fuel Burnt or Combustion Duration
CA50	Crank Angle for 50% of Fuel Burnt
cad	Crank Angle Degree
CCV	Cycle-to-Cycle Variation
CFD	Computational Fluid Dynamics
CH ₄	Methane
CI	Compression-Ignited
CNG	Compressed Natural Gas
CO	Carbon Monoxide
CO ₂	Carbon Dioxide
COV	Coefficient of Variance
COV IMEP	Combustion Stability
C _p	Heat Capacity Constant Pressure
CR	Compression Ratio
C _v	Heat Capacity Constant Volume
CVCC	Compound Vortex Controlled Combustion
DI	Direct Injection
DoC	Duration of Combustion
DoE	Design of Experiments
DOHC	Double Overhead Camshaft
EAE	Energy Available for Ejection

EGR	Exhaust Gas Recirculation
EIVC	Early Intake Valve Closing
EVO	Exhaust Valves Opening
FSN	Filter Smoke Number
FW	Natural Gas from Food Waste
GHG	Greenhouse Gases
GHG-100	Greenhouse Gases in a 100 Year Prospect
H ₂	Hydrogen
HAJI	Hydrogen Assisted Jet Ignition
HC	Hydrocarbons
HCCI	Homogeneous Charge Compression Ignition
HCJI	Homogeneous Combustion Jet Ignition
HLHS	High Load High Speed
HLLS	High Load Low Speed
HRCI	Homogeneous Combustion Radical Ignition
HRR	Heat Release Rate
HSDI	High Speed Direct Injection
ICE	Internal Combustion Engine
IGR	Internal Gas Recirculation
IMEP	Indicated Mean Effective Pressure
ISFC	Indicated Specific Fuel Consumption
IVC	Intake Valves Closing
JPIC	Jet Plume Injection and Combustion
LAG	Lavinia Aktivatisia Gorenia
LES	Large Eddy Simulation
lf	Flame thickness
LG	Natural Gas from Landfill Gas Recovery
LHV	Lower Heating Value
LIVC	Late Intake Valve Closing
LLHS	Low Load High Speed
LLLS	Low Load Low Speed
LPG	Liquefied Petroleum Gas
lt	Integral Length Scale
MAPO	Maximum Amplitude Pressure Oscillation
MBF	Mass Burn Fraction
MBT	Maximum Brake Torque
<i>m_{egr}</i>	Mass Flow EGR
<i>m_{int}</i>	Mass Flow Intake
N ₂	Nitrogen
N ₂ O	Nitrous Oxide
NEDC	New European Driving Cycle
NG	Natural Gas
NO _x	Nitrous Oxides (NO and NO ₂)
NTC	Negative Temperature Coefficient
PC	Pre-chamber

PCCI	Premixed Charge Compression Ignition
PCFA	Premixed Charge Forced Auto-Ignition
PCI	Pre-chamber Injection
PCIS	Pre-chamber Ignition System
PFI	Port Fuel Injection
PJC	Pulsed Jet Combustion
PM	Particulate Matter
POC	Pollutants of Concern
Q	Heat
Q_{wall}	Heat Loss Through Walls
RANS	Reynolds-averaged Navier-Stokes
RCEM	Rapid Compression Expansion Machine
RON	Research Octane Number
RPM	Revolutions Per Minute
SI	Spark-Ignition
sl	Laminar Flame Speed
SoC	Start of Combustion
SoE	Start of Ejection
t^*	Time Needed for the Jet to Reach the Furthest Combustion Chamber Wall
TDC	Top Dead Centre
TGP	Turbulence Generating Pot
TJI	Turbulent Jet Injection
TKE	Turbulent Kinetic Energy
u'	Turbulence Intensity
VOC	Volatile Organic Compound
W	Work
WAM	Wave Action Model
WS	Natural Gas from Waste Sludge

CHAPTER 1

Introduction

1.1. Introduction

The exponential increase of the greenhouse gases (GHG) emissions from the last decades of the twentieth century up to present days has become into one of the most challenging concerns that mankind has ever faced [10, 11].

Global temperatures are in an ascendant line from the 80s century [12], which not only acts as a pendulum changing the maximum and the minimum temperatures, but also affects the global fauna, especially marine wildlife [13], increasing water temperature and compromising their natural habitat. In Figure 1.1 the temporal evolution of the temperature change can be observed. It is clear how from the 80s decade of last century, temperature is exponentially increasing.

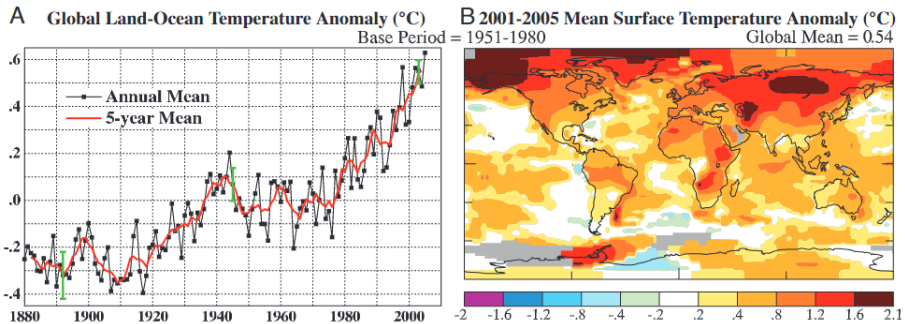


Figure 1.1: Surface temperature anomalies relative to 1951–1980 from surface air measurements at meteorological stations and ship and satellite SST measurements. (A) Global annual mean anomalies. (B) Temperature anomaly for the first half decade of the 21st century [12].

In the present context, one of the most effective ways to contain the total amount of emissions is to develop new highly efficient engines for the transportation sector. Moreover, one of the main contributors to the total amount of emitted greenhouse gases is, precisely, the transportation sector itself. Furthermore, the nitrogen oxides (NO_x) are another relevant kind of pollutant generated by this sector (see Figure 1.2) which also has a relevant impact in the human health [14].

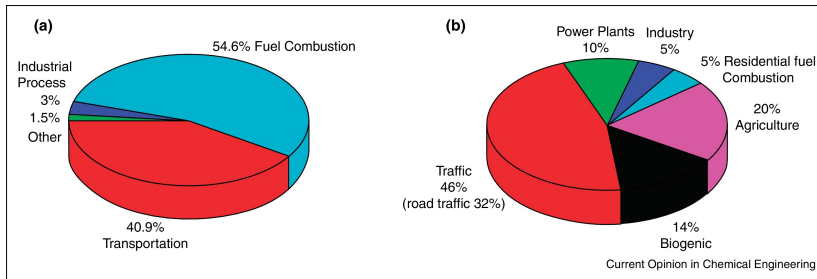


Figure 1.2: Nitrogen oxide emissions by source category in (a) the United States and (b) European Countries [14].

It is remarkable that, even the contribution of the transportation sector to the global GHG emissions is not the predominant role, there has been a high development and investigation activities since last decades to reduce the sectoral contribution.

For that purpose, public institutions such as European Union, in the seeking of reducing the environmental issues while protecting human health have been promoting new regulations (see EURO VI and future EURO VII [15, 16]). These regulations include restrictions to the greenhouse gases and nitrogen oxides generated in the combustion process, which forces the manufacturers to develop new high-efficient thermal powerplants to fulfill with the legislation. In Figure 1.3, a comparison of vehicle emission standards including GHG and NO_x was presented by Williams et al. [15]. The pollutant emissions are presented in g/km for CO, HC, NO_x and PM, while number of solid particles (PN) is presented in #/km.

Moreover, car customers are more and more aware of the environmental problems and they have started to consider the generated emissions as an aspect to decide whether to buy a car model or not. Willingness-to-pay measures of CO_2 reduction may be found in the potential car buyers [17], which highlights the awareness of the environmental problem mankind is facing.

Pollutant	Euro 5 Light-Duty		Euro 6 Light-Duty	
	Gasoline	Diesel	Gasoline	Diesel
CO	1.0	0.5	1.0	0.5
HC	0.1 ^a		0.1 ^a	
HC+NO _x		0.23		0.17
NO _x	0.06	0.18	0.06	0.08
PM	0.005 ^c	0.005	0.005 ^c	0.005
PN (#/km)		6.0 × 10 ¹¹	6.0 × 10 ¹¹ ^d	6.0 × 10 ¹¹

^a and 0.068 g/km for NMHC; ^c applicable only to DI engines, 0.0045 g/km using the PMP measurement procedure; ^d applicable only to DI engines, 6 × 10¹² #/km within the first three years of Euro 6 effective dates.

Figure 1.3: Overview of Euro 5 and Euro 6 vehicle emissions standards for the New European Driving Cycle (NEDC) [15].

As aforementioned, newly high-efficient thermal engines are being developed which will be the new standard in the light-duty applications. These engines are mainly equipped with direct fuel injection into the combustion chamber (Port Fuel Injection - PFI) and take advantage of combustion strategies to reduce fuel consumption and/or emissions.

1.2. Thesis background and context

In the present framework, it arises as mandatory the seeking of new combustion processes that are able to take advantage of the thermal efficiency increase strategies.

These strategies are focused to the reduction of the fuel consumption. By reducing the total amount of burned fuel in the combustion process, the total amount of generated pollutants decreases.

Most popular strategies nowadays are related to the lean burn concept or the diluted combustion. Key idea of these strategies is to operate with excess of air (in the lean burn) or with recirculated exhaust gases (diluted combustion).

A short introduction is presented in this Chapter, and a further discussion will be carried out in the Literature Review Chapter (see Chapter 2).

1.2.1. Air dilution

First of the mentioned strategies is the lean burn. Main aspect of this concept is the increased air fraction in the intake during the combustion process.

The excess of air has some benefits including the lower pumping losses or the reduction of specific heat ratio among others which turn into an increase of the thermal efficiency.

However there are some drawbacks that must be taken into account. Main drawback is related to the effective operating limit or dilution limit. It is not possible to keep increasing the excess of air at a certain point. When reaching this limit, combustion stability becomes compromised and partial burning starts to appear, increasing the emitted carbon monoxide (CO) and hydrocarbons (HC).

To avoid these problems, one potential solution is to increase the energy provided when initiating combustion. A higher energy release strengthens combustion stability and allows a greater amount of air excess, thus improving thermal efficiency.

Regarding NO_x formation, an increased air dilution mixture may lead to lower combustion temperatures which turn into a reduced thermal NO_x formation. Moreover, the reduced amount of fuel at these conditions may lead to an even greater NO_x prompt formation since there is less available fuel. On the other hand, richer mixtures will tend to increase the combustion temperature and the available nitrogen-containing compounds of the fuel, thus leading to an increased NO_x formation, both thermal and prompt mechanisms. This NO_x formation reduction of the lean strategy is aligned with the upcoming EURO VII regulations.

1.2.2. EGR dilution

The other commonly applied strategy is the recirculation of exhaust gases or EGR. Key aspect of this strategy is to introduce in the intake hot burned gases from previous combustion cycle.

The addition of exhaust gases has some benefits in terms of lower pumping losses, reduced specific heat ratio and reduced combustion temperature that lead to higher thermal efficiency and a reduction in the generated nitrogen oxides (NO_x).

However, as it happens with the lean burn concept, there are some drawbacks related to the use of this strategy. The most important one is the effective dilution limit. Similar to the lean burn concept, there is a maximum rate of EGR that is possible to introduce through the intake while keeping a proper combustion stability. Reaching this limit will turn into decreased combustion efficiency and higher emitted CO and HC pollutants.

And again, the potential solution to avoid this drawback is the increase of the energy released when initiating combustion process.

In this context, the application of a pre-chamber ignition system becomes a clear solution to allow the use of these kind of increasing thermal efficiency strategies since it has been reported an excellent synergy between these concepts [18, 19].

1.3. Thesis object

The purpose of the present investigation work is to further extend the available knowledge of the pre-chamber ignition system in a spark-ignition near-future passenger car engine.

In this way, it is intended to carry out a systematic investigation work that allows the identification, and the subsequent analysis, of the fundamental characteristics of the present ignition concept, which also includes key guidelines for an optimized design of the basic geometrical aspects, such as internal volume or number and diameter of nozzles.

This object was divided into separated partial tasks in order to make easier the analysis of the phenomena involving the ignition concept. These tasks are the following:

- Experimental evaluation of the pre-chamber performance: in order to perform the experimental analysis of the pre-chamber ignition concept a test plan which modifies operating parameters (such as engine load, engine speed or dilution degree among many others) was developed. The modification of such parameters ensures the study of the complete engine map. Furthermore, tests were carried out using different combustion strategies with the aim of increase the overall thermal efficiency of the engine (lean burn or diluted combustion). The test bench was set up with all needed devices to perform the measurements and assure the repeatability between tests under safe conditions.
- Analysis of the scavenging process within the pre-chamber: for completing this activity, numerical models based on wave action models were built in order to recreate the physical phenomena that occurs in both combustion chambers (pre-chamber and main combustion chamber). A complete model that simulates the experimental facility was generated and, simplified models only including both combustion chambers were created to calculate large amount of simulations with low computation costs. All of these models were validated with experimental results.

- Study of the relationship between pre-chamber combustion and hot gas ejection processes: to complete this activity, the results obtained after completing the established experimental test plan were analyzed and compared against the numerical results obtained from the previous activity. In this way, it is possible to determine the cause-effect relationships between the jet ejection process and the combustion within the pre-chamber. Furthermore, a free-jet model was built to simulate the jet penetration length into the main combustion chamber and to predict whether the jet will impact on the inner cylinder wall and the time when it will happen depending on the jet momentum flux.
- Identify the impact of the basic geometrical characteristics of the pre-chamber on the performance of the concept: all of experimental and numerical results obtained along the investigation work were analyzed for each different pre-chamber geometry, founding trends in some basic pre-chamber design parameters.

However, it should be noted that since one of the objects of the present project is to provide some guidelines for a complete pre-chamber design methodology, the different phases and objectives are iterative.

In this way, once an optimized pre-chamber has been designed after completing the different phases, this new pre-chamber should be manufactured and the complete process will be repeated to experimentally verify if the design methodology followed meets the proposed objectives and if possible, further improve the design.

1.4. Thesis outline

After giving some background context and setting the global framework where this investigation work is able to further extend the knowledge of its main object, the structure of the present document will be described, focusing on the main relevant aspects that the reader will find throughout the different Chapters.

For that purpose, a simplified sketch of the main topics covered can be found in Figure 1.4. Boxes in first column represent each Chapter which is divided the document, while boxes in second and third column represent the key idea and a brief description of what can be found respectively.

- In Chapter 1, the investigation work is presented, framing it in a specific context where the pre-chamber ignition system is a potential solution to mitigate the issues related to the large amount of emitted pollutants and, therefore meeting the standards adopted by public institutions. Also, the document is described and itemized, letting the reader a guide to navigate through the book.
- In Chapter 2, the reader can found a complete description of the most popular strategies utilized nowadays to increase the thermal efficiency of a passenger car engine. Moreover, a complete revision of the pre-chamber technology can be found in this Chapter, including not only a historical evolution and its key milestones but also a deep investigation of the main aspects of the combustion process that may be affected by the employment of such a pre-chamber system.
- Regarding Chapter 3, the experimental facilities, including a complete description of the test bench and the researched engine along with a detailed explanation of the numerical tools employed to calculate the simulations can be found. Furthermore, the details of the used fuels during the experimental phase and a complete description of the methodology followed both in the experimental and numerical activities can also be found in this Chapter.
- The Implementation of the concept Chapter 4 is the first of the three results chapters. The ignition concept is directly implemented into the engine and first results including different engine configurations and pre-chamber geometries can be found in this Chapter. Three different operating points in terms of engine load and speed (high engine load and speed, medium engine load and speed and low engine load and speed conditions) are evaluated and the application of the passive pre-chamber ignition system is evaluated in such conditions.
- In Chapter 5, the results of the application of the strategies to increase thermal efficiency combined with the passive pre-chamber ignition system are presented. Both increasing excess of air and recirculating exhaust gases into the intake are evaluated with the same engine configurations and at the same operating conditions as in the previous Chapter.
- Regarding Chapter 6, the experimental results obtained in previous chapters is used as a starting point to develop numerical activities in order to find a pre-chamber geometry able to increase the tolerance

limit of the lean burn and EGR strategies. Numerical and experimental evaluation of basic pre-chamber geometry aspects are presented and a basic design guidelines are introduced within this Chapter.

- Finally, Chapter 7 gathers the key aspects found during the completion of the present investigation work and proposes the continuation of the research activities in some different paths, highlighting main benefits and drawbacks of the use of the passive pre-chamber ignition concept.

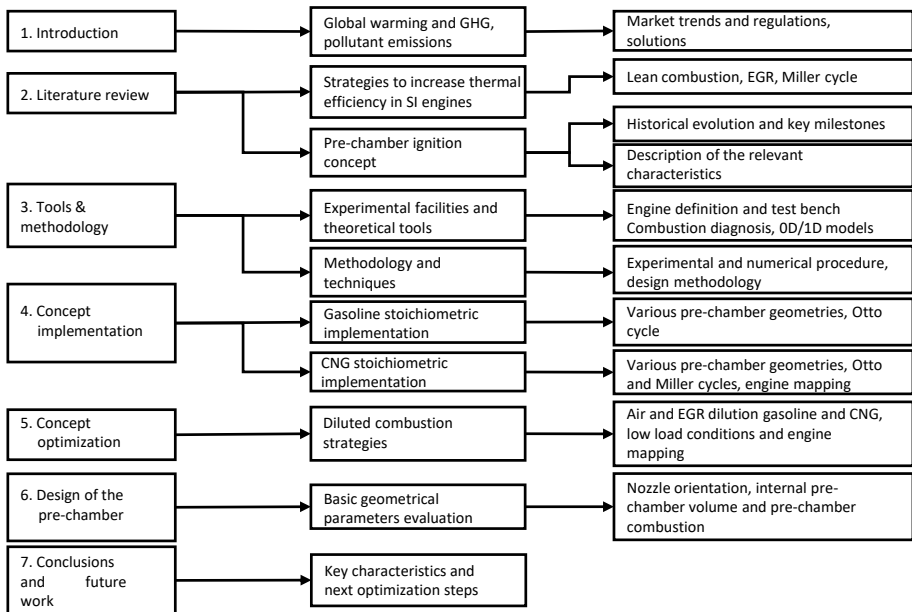


Figure 1.4: Thesis outline covering the key aspects of each Chapter.

1.5. Conclusions

In present Chapter 1, a global introduction to the environmental issues that mankind is facing, especially in terms of greenhouse gases and nitrogen oxides emissions is presented, along with some of the actions that public institutions are performing to mitigate this problem.

Also, some potential solutions to reduce the contribution to this environmental issue from the transportation sector are introduced, pointing main benefits and their respective drawbacks that avoid a direct implementation in the present kind of passenger car engines.

However, the pre-chamber ignition system has been marked as a potential solution to overcome the main drawbacks related to those thermal efficiency increase strategies by means of providing a larger amount of energy during the ignition event, which turns into a more stable combustion process and therefore, an increased dilution tolerance.

Regarding the document itself, the research work has been set up into a framework and its main objective has been divided into a series of short points in order to facilitate the fulfillment of them. Furthermore, a clear outline of how is the document organized has been included, highlighting the main aspects that are addressed in each Chapter.

Literature review

2.1. Introduction

The seek of reducing pollutant emissions in the transport operation has been identified as a critical aspect of fulfilling the upcoming regulations and reducing the carbon footprint of human activities. In the present framework, a review of the available literature arises as an essential step to frame the problem and provide a global overview of the current strategies with their main benefits and drawbacks.

The present Chapter consequently, focuses on the literature review of the most relevant strategies to increase thermal efficiency of Spark-Ignition (SI) engines and its combination with different ignition systems, especially those related with pre-chamber applications, that solve some drawbacks of these strategies.

A description of the state of the art of the increasing efficiency strategies, along with pre-chamber applications, can be found in this Chapter in order to provide the reader a better context of the main issues and findings, which are interesting to have in mind for understanding the addressed problem.

2.2. Strategies to increase thermal efficiency

Since the last decades of twentieth century the automotive sector has been focused on increasing the thermal efficiency of their produced SI engines and thus, reducing the fuel consumption. This interest of the manufacturers of transportation sector lead to the development of some concepts and technologies, such as lean burn, exhaust gas recirculation (EGR) or Miller cycle, that perfectly combine with thermal engine applications in this framework.

In this Section, a general overview of these concepts is presented, which act as theoretical introduction for the latter results of Chapter 4, Chapter 5 and Chapter 6.

2.2.1. Lean burn

Lean burn strategy consists of burning the fuel with an excess of air [20]. This is when the air-to-fuel ratio is greater than stoichiometric ($\lambda = 1$), defining λ as the division of the air-to-fuel ratio by the stoichiometric air-to-fuel ratio. This combustion strategy has some advantages compared with conventional stoichiometric combustion.

Main advantage is related to the increase of the specific heat ratio (γ) as the excess of air increases [21], which turns into an increase in thermal efficiency following the ideal Otto cycle description, showed in Equation 2.2.1 [22].

$$\eta_{th} = \frac{W}{Q} = 1 - \frac{1}{CR^{\gamma-1}} \quad (2.2.1)$$

In this Equation, CR represents the compression ratio, defined as the maximum cylinder volume divided by the clearance volume. Specific heat ratio (γ) is defined as the division of heat capacity at constant pressure by heat capacity at constant volume (C_p/C_v), also known as Mayer's relation.

Furthermore, the lean burn strategy is able to increase the thermal efficiency not only by affecting the γ parameter, but also by reducing the heat transfer losses due to the reduction of temperatures during the combustion and expansion processes and the pumping losses by tending through a minor throttling conditions operation at similar provided engine power, which further reduces the fuel consumption [23, 24]. Moreover, the control of the power output can be performed by modifying the supply of fuel to the main chamber, avoiding extra throttling losses, as it is done in Compression-Ignition (CI) engines.

In addition, as combustion occurs at lower temperatures, the formation of nitrogen oxides (NOx) is hindered, resulting in lower NOx emissions. Moreover, the emissions of CO and HC are also reduced when operating with excess of oxygen. This trend continues with increasing the excess of air, resulting in even lower nitrogen emissions with higher λ values. However, significant reductions can only be achieved when exceeding λ values over 1.4, which coincides with the lean limit operation of conventional SI engines.

At this lean limit, the normal engine operation becomes compromised with the appearance of misfire cycles due to the narrow flammability limits of most of the used fuels in transportation sector [25]. This reduced flammability limit is one of the causes of a poor combustion stability, along with the slower laminar flame speeds of lean mixtures. The slower flame speed causes partial burning and it affects the flame kernel growth and propagation issues. All of these causes lead to misfire cycles, in where no power output is obtained because the fuel has not been ignited.

Misfire cycles not only cause a substantial reduction in the obtained indicated mean effective pressure (IMEP), but also increase the emitted hydrocarbons (HC) and carbon monoxide (CO) [26]. This effect, combined with the several effectiveness reduction of the three-way catalyst at operating points far from the stoichiometric conditions make the lean burn strategy unapproachable without any kind of solution to enhance ignition, both from the efficiency and pollutant emissions points of view.

These main drawbacks joined with very restrictive pollutant regulations from public institutions, that barely forced to the universal use of the three-way catalyst, have excluded lean burn strategy from the combination of solutions that are able to fulfill these regulations during many time. However, with the development of enhancing ignition technologies, an increasing interest in this kind of strategy has been acquired.

2.2.2. Exhaust gas recirculation

Exhaust gas recirculation (EGR) is a strategy to reduce the thermal formation of nitrogen monoxide (NO) by means of increasing the total amount of exhaust gases retained in the cylinder at intake valve closing [27].

The reduction of the formation of nitrogen oxides comes from the lower oxygen content in the mixture achieved with the addition of EGR. This oxygen reduction is able to decrease the overall flame temperature thus affecting the nitrogen oxides formation. This effect can be enhanced if the EGR is previously cooled [27, 28].

Also, there is a reduction in the heat transfer losses due to the lower temperatures during the combustion and expansion processes and in the pumping work caused by the increased intake manifold pressure. These two events are the main contributors to the increase of the thermal efficiency.

However, some drawbacks related to this strategy may appear. The thermal efficiency is also affected by the combustion temperature, which may lead to an increase of the fuel consumption and the CO and HC formation. Other aspects such as the increased combustion duration or the higher combustion variability may turn into greater fuel consumption [29].

The percentage of EGR can be calculated as in Equation 2.2.2. Where \dot{m}_{EGR} is the recirculated exhaust mass flow and \dot{m}_{int} is the total intake mass flow.

$$EGR = \frac{\dot{m}_{EGR}}{\dot{m}_{int}} * 100 \quad (2.2.2)$$

Besides of the increase in thermal efficiency and the limitation in the NO formation, there is another advantage related to the EGR operation. This strategy does not require the variation of the air-to-fuel ratio, allowing the use of a three-way catalyst able to reduce, even more, the total amount of emitted pollutants, making the use of this strategy the most popular way to fulfill the previous emissions regulations. Moreover, the application of EGR can be used as a means to avoid knocking issues and it opens a path to increase compression ratio and even further, increase thermal efficiency.

However, as in lean burn strategy, it appears a tolerance limit where the benefits in terms of thermal efficiency are lost due to the increase of the cycle-to-cycle dispersion. The lower flammability limit and the reduction in the laminar flame speed are the main causes of this reduction in the combustion stability. Furthermore, the increase in the combustion duration negatively affects the obtained power, reducing the thermal efficiency. It becomes mandatory the modification of the spark triggering event timing to overcome the increase in the combustion duration and recover some of the efficiency losses.

Along with the modification of the spark timing, enhancing combustion and/or the use of ignition velocity strategy arise as a critical need to obtain most of the benefits of the EGR strategy and, if possible, extend the dilution limit to maximize its benefits.

2.2.3. Miller cycle

Miller cycle, named after its inventor R.H. Miller, is a modification of the conventional Otto cycle commonly used in SI engines [30]. This new operating cycle features an expansion ratio greater than its compression ratio. The change in the compression ratio can be performed either by an early intake valve closing (EIVC) or by a late intake valve closing (LIVC), reducing

the effective compression ratio. The engine knock issues when operating with conventional Otto cycle could be solved by the lower temperature and pressure of the mixture, either operating with EIVC or LIVC, thus opening a path for safely increasing the overall compression ratio [31, 32].

Despite this lower specific power showed at aspirated conditions when operating with Miller cycle, the lower heat transfer and pumping losses compared with conventional Otto cycle at boosted conditions are significant to take this operating cycle in consideration. In fact, the original Miller's design included a supercharger to limit the power output loss due to the shortened compression ratio [33].

Pumping losses are the main constraint of engine efficiency at low engine loads, meanwhile knocking issues limits the maximum achievable compression ratio and spark timing at high engine loads. Cleary et al. [34] proved that using a Miller cycle with EIVC was able to reduce up to a 7% of fuel consumption at low engine loads, optimizing the intake valve lift, duration and timing. Patychuk et al. [35] studied the effects of the Miller cycle with LIVC operating at high engine loads, proving a reduction on pollutant emissions. Cao et al. [33] experimentally compared both intake valve closing strategies on a highly boosted and high compression ratio direct-injection (DI) SI engine, proving a fuel economy improvement at high engine loads with LIVC and at low engine loads with both LIVC and EIVC.

The reduced temperature and pressure of the mixture not only lowers the knocking tendency of the engine, but also limits the thermal formation of NO, thus reducing the overall NO_x pollutant emissions. However, the lower temperature may lead to a negative effect on the combustion velocity. As the temperature is lower, the laminar flame speed and the flame kernel growth are affected, limiting the obtained thermal efficiency. Enhancing either turbulence or ignition can solve these kind of issues and make the application of Miller cycle a very interesting solution to increase thermal efficiency by joining it with advanced ignition systems.

In summary, the main drawback from all three evaluated strategies that are able to increase engine thermal efficiency is the lack of a reliable ignition source that, on one hand increases combustion stability, and in the other hand enhances combustion velocity, either by accelerating the laminar flame speed or by igniting in multiple sites.

2.3. Pre-chamber technology

As discussed in the previous Section 2.2, the use of an advanced ignition system that is able to increase both the combustion velocity and the combustion stability becomes imperative to take advantage of the benefits of those strategies.

In this framework, the use of a pre-chamber ignition concept arises as a potential solution to merge the application of Miller cycle with either lean burn or exhaust gas recirculation strategies and obtain their main benefits in terms of thermal efficiency increase and pollutant emissions reduction.

It is important to explain that there are two different approaches to implement a pre-chamber ignition concept. In the first approach, the pre-chamber integrates a dedicated fuel supply system within the pre-chamber volume, generally a fuel injector, which is able to control the air-to-fuel ratio inside the pre-chamber during the complete engine cycle, keeping it at suitable near to stoichiometric values. This approach is commonly known as stratified or active pre-chamber. Being this mixture control its main advantage at the price of increasing the assembly costs. On the other hand, the other approach does not include the dedicated fuel supply, so the mixture admitted within the pre-chamber has the same air-to-fuel ratio as in the main chamber, transferring the combustion properties from one chamber to the other. This approach is known as homogeneous or passive pre-chamber. Its main advantages are the lower assembly costs and the easiness to exchange between conventional spark plug and other pre-chamber geometries.

Along this Section 2.3, a general review of the evolution of pre-chamber technology is presented, focusing on the Turbulent Jet Ignition concept, since it is the subject of study of the present work, while the influence of the pre-chamber ignition concept on main combustion parameters, the effect of its geometry and emissions is discussed.

2.3.1. Pre-chamber applications review

In order to provide a logical sense to the review Section, the different pre-chamber applications will be chronologically introduced and distinguished between active (with auxiliary fueling) and passive (without auxiliary fueling) systems, focusing in those which are more relevant or have a greater impact on the evaluated technology in the present work.

Regarding the temporal evolution of this kind of technology, Elisa Toulson et al. [36], Carlos Eduardo Castilla Alvarez et al. [37] and Sipeng Zhu et al. [38] did a fantastic work summarizing many of these applications,

in where a shortened version of the present review can be found in their mentioned articles. As a brief and visual summary, the development of the pre-chamber technology, including patents and SAE articles from the very beginning applications to the present ones can be found in Figure 2.1.

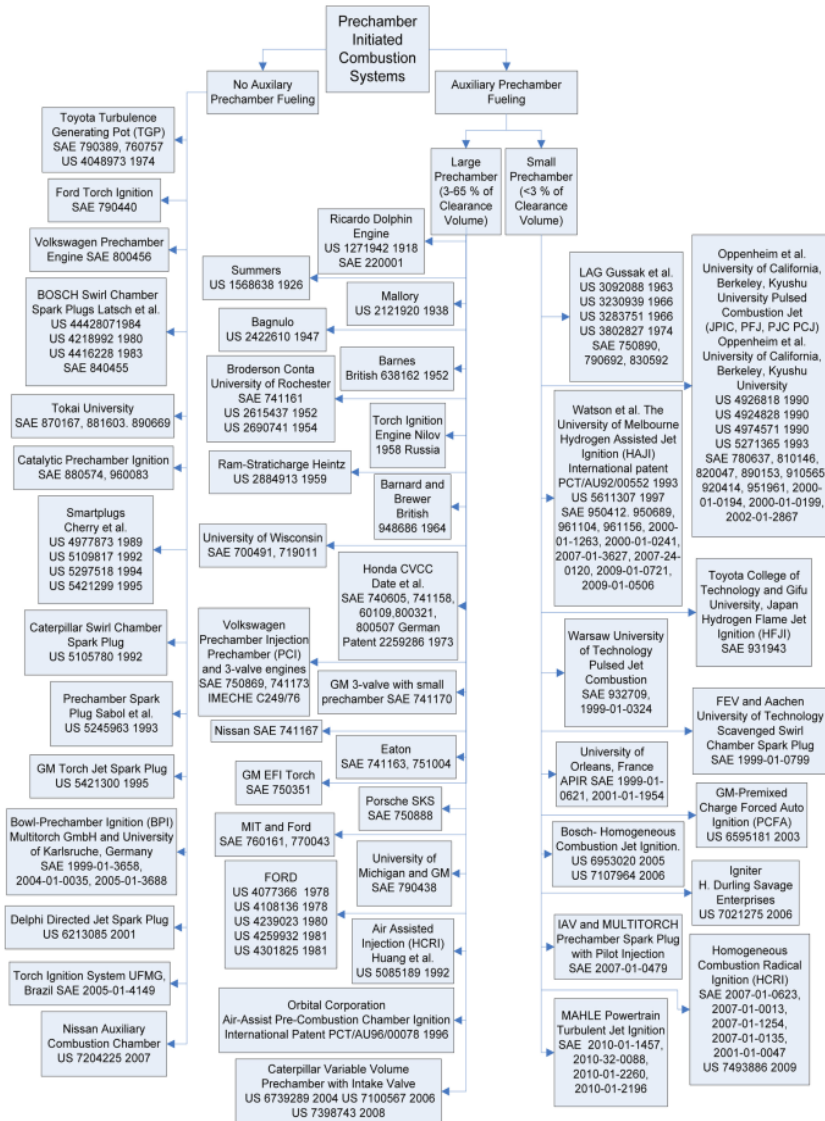


Figure 2.1: Schematic view of all pre-chamber ignition applications chronologically sorted from top to bottom including patents and SAE papers [36].

2.3.1.1. Active large pre-chamber applications

Technologies to initiate combustion by means of pre-chamber cavities in SI engines began at early stages of twentieth century. These kind of engines employed a large active pre-chamber (more than 3% of clearance volume and dedicated fuel supply). First developed application was introduced by Harry R. Ricardo [39]. This was a 2-stroke 3-valve stratified charge SI engine known as Ricardo Dolphin engine [40, 41]. A schematic view of the engine can be found in Figure 2.2.

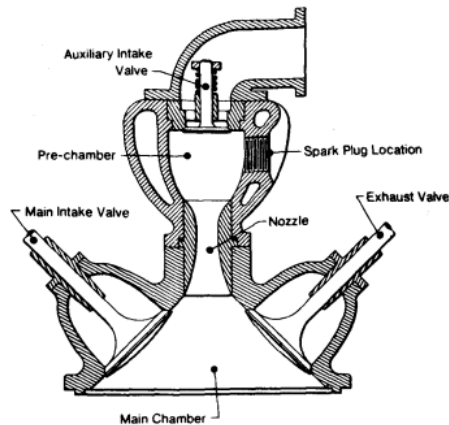


Figure 2.2: Internal combustion engine developed by Harry R. Ricardo featuring the first pre-chamber application [40].

This engine featured the use of an auxiliary intake valve actuated by means of air pressure difference in the valve head, being necessary a later opening of the main chamber intake valve in order to overcome the pneumatic force requirements. In this application, the pre-chamber was filled with a very rich air-to-fuel mixture, while on the contrary, the main chamber was filled with a very lean air-to-fuel mixture, or even, pure air. One significant characteristic was that intake manifold was not throttled, controlling the power output by varying the air-to-fuel ratio and the quantity of the supplied rich charge. The spark plug was located within the pre-chamber and it was connected to the main chamber through one nozzle. This nozzle allowed the transfer of reactive and burned gases between the chambers after ignition happened.

Ricardo reported a series of successful results but also some drawbacks. At part loads he found a lack of performance and efficiency mainly due to the pneumatic actioning of the auxiliary intake valve [40, 41].

Another early pre-chamber application in a 3-valve engine was developed and patented by Caleb E. Summers [42]. His main advance compared with Ricardo's engine was the introduction of a mechanically actuated auxiliary intake valve. A sketch of his internal combustion engine can be found in Figure 2.3.

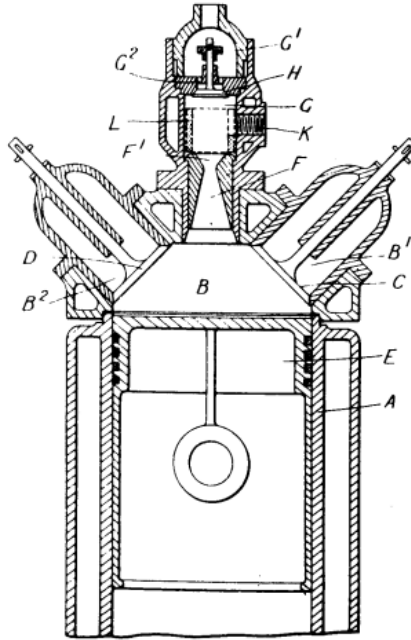


Figure 2.3: Internal combustion engine developed by Caleb E. Summers, featuring a mechanically actuated auxiliary intake valve [42].

In this application, two different carburetors were used. The auxiliary carburetor provided a rich air-to-fuel ratio mixture while the main carburetor was set to very lean conditions. Pre-chamber nozzle was designed to provide high swirl inside the pre-chamber and it was located away from the spark plug to avoid the admission of lean mixture inside the pre-chamber [40, 41].

Marion Mallory patented a pre-chamber application engine featuring two separated carburetors connected between their throttle plates [43]. Furthermore included two different spark plugs, one within the pre-chamber and another in the main combustion chamber. The nozzle was designed to be flow-restrictive in order to obtain an igniting flame for the lean mixture. In this engine, dual fuel could be implemented [40, 41]. A sketch of this engine can be found in Figure 2.4.

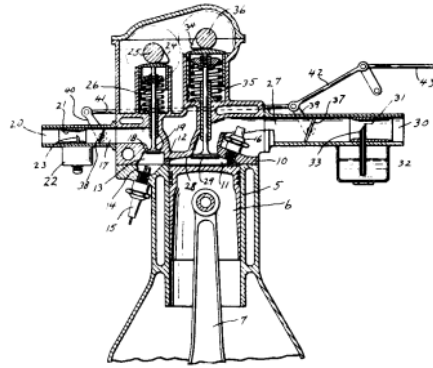


Figure 2.4: Internal combustion engine developed by Marion Mallory, including a connection between the carburetors [43].

Albert Bagnulo developed another pre-chamber application in a 3-valve stratified charge engine [41, 44]. His main development consisted in creating high swirl within the pre-chamber during compression stroke by means of the tangential location of the nozzle, thus stratifying the mixture with the centrifuge force. The sketch of his patent can be found in Figure 2.5.

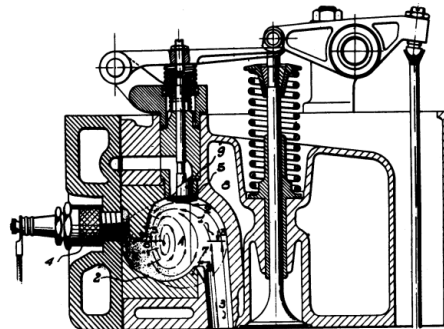


Figure 2.5: Internal combustion engine developed by Albert Bagnulo, including a connection between the carburetors [44].

William B. Barnes patented a large spherical pre-chamber application in Great Britain [45]. A very rich mixture was ignited within the pre-chamber and completely burned in the main chamber, providing an excess of air to this chamber [40, 41]. A sketch of his patent can be found in Figure 2.6.

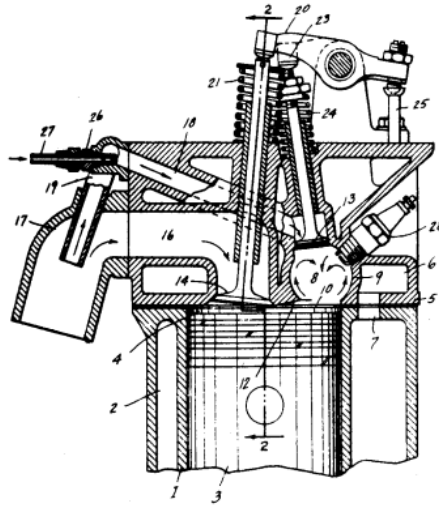


Figure 2.6: Internal combustion engine developed by William B. Barnes, featuring a large spherical pre-chamber [45].

Neil O. Broderson also developed a dual chamber engine that was able to stratify the main charge [46, 47]. His invent used a dual chamber configuration igniting a near to stoichiometric mixture in the auxiliary chamber, while only air, was introduced in the main chamber [40, 48]. The sketch of his patent can be found in Figure 2.7.

Meanwhile, in the USSR, Nilov [49] suggested an engine featuring the use of a pre-chamber remotely positioned from the main chamber, leading to a very preliminary concept of the torch ignition engine [40, 41], founding very promising results in terms of fuel consumption at low equivalence ratios [50]. This torch ignition concept will be further explained in the passive pre-chamber applications Subsection 2.3.1.3. Simple sketch of this engine can be found in Figure 2.8.

Following with the active pre-chamber applications, next development was suggested in 1959 by Ralph M. Heintz in the USA [51]. His invent featured an reentrant tube to improve the mixing inside the pre-chamber during compression stroke. Furthermore, it helped to heat the rich air-to-fuel mixture during both intake and compression strokes. His pre-chamber included several nozzles to increase the penetration of the flaming jets into the main chamber, thus improving fuel consumption and reducing emissions [40, 41, 52]. Figure 2.9 introduces a sketch of this engine.

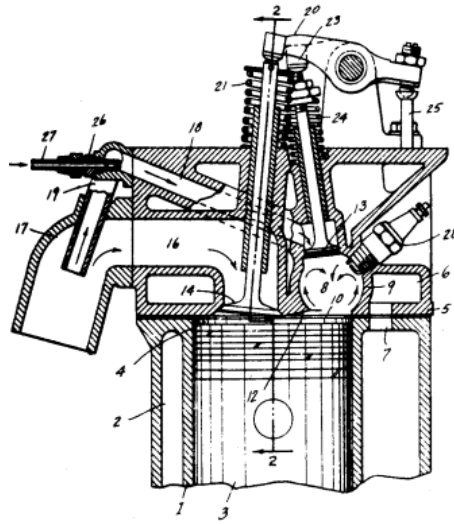


Figure 2.7: Internal combustion engine developed by Neil O. Broderson [46].

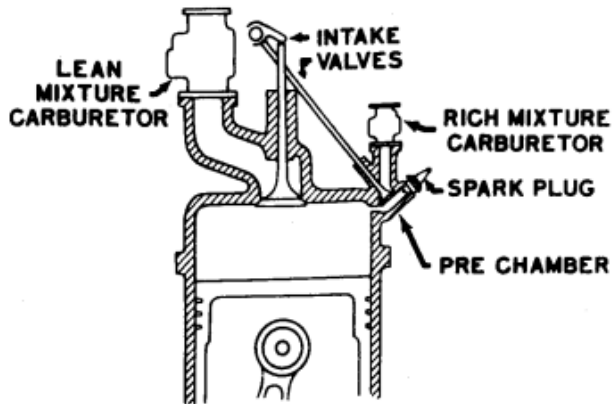


Figure 2.8: Torch ignition precursor engine developed by N. A. Nilov [49].

In the 60's decade, Anthony Barnard and Charles D. Brewer patented an improvement to the 3-valve SI engine [53]. They achieved an independent auxiliary intake valve timing, opening it only briefly during the minimal required time in order to minimize over-breathing [40, 41]. In Figure 2.10 the simplified sketch of the engine can be found.

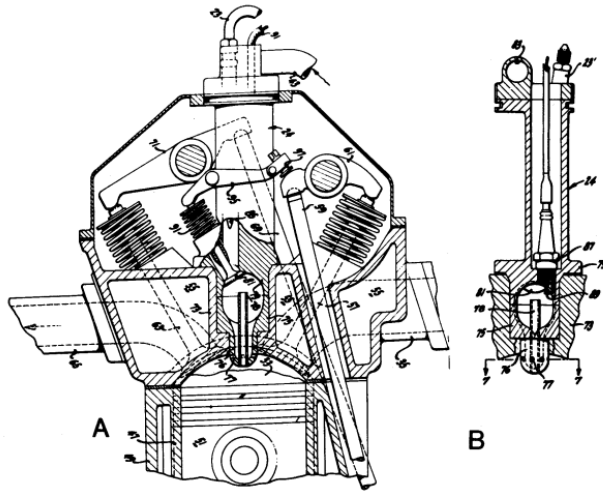


Figure 2.9: Heintz Ram-Straticharge engine developed by Ralph M. Heintz [51].

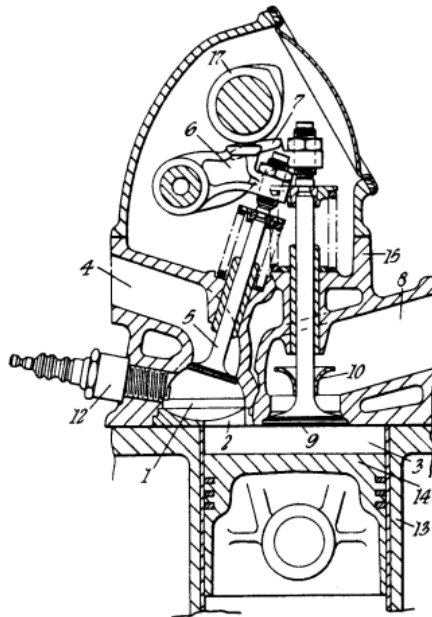


Figure 2.10: Improvements in or relating to internal combustion engines by Anthony Barnard and Charles D. Brewer [53].

Scientists from the University of Wisconsin, such as Henry K. Newhall and Ibrahim A. El-Messiri [54–56] investigated the emissions formation and a combustion process for controlling the exhaust emissions in a dual-chamber SI engine, founding that an extreme quenching of the flame may lead to a very low NO formation even at high oxygen conditions [57]. The sketch of the evaluated engine can be found in Figure 2.11.

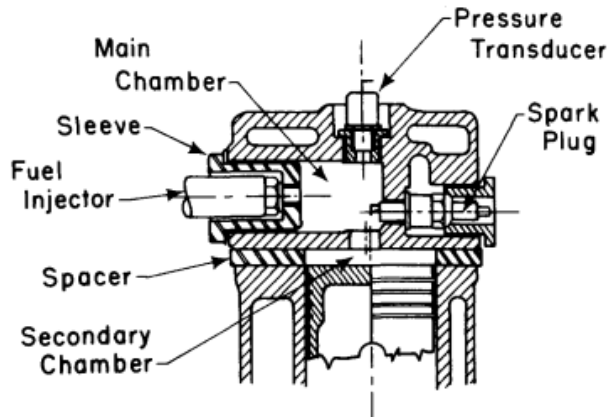


Figure 2.11: Evaluated duel-chamber spark-ignited engine by Henry K. Newhall and Ibrahim A. El-Messiri [57].

After developing more complex injection technologies, the three valve and additional carburetor engine was substituted by more modern designs featuring fuel injector systems within the pre-chamber. Moreover, the use of two separated and interconnected chambers became commonly used in this stratified kind of engines. The mixture in the second chamber can be easily ignited by means of a second dedicated spark plug. In these engines, a regular flame front is created inside the pre-chamber and it advances and exits through the orifices, reaching the main combustion chamber. The most interesting example of this new technology was the Honda Compound Vortex Controlled Combustion (CVCC) developed by Tasuke Date et al., who set new standards for these applications [58–61].

This new engine was able to fulfill the emissions standards in 1975 without the use of an after-treatment system [36, 62] and loss of fuel economy [58]. This engine presented a slow burn principle to optimize the emissions reduction, making the exhaust gases having an excess of air and temperature for further oxidation [40, 63]. A sketch of this engine can be found in Figure 2.12.

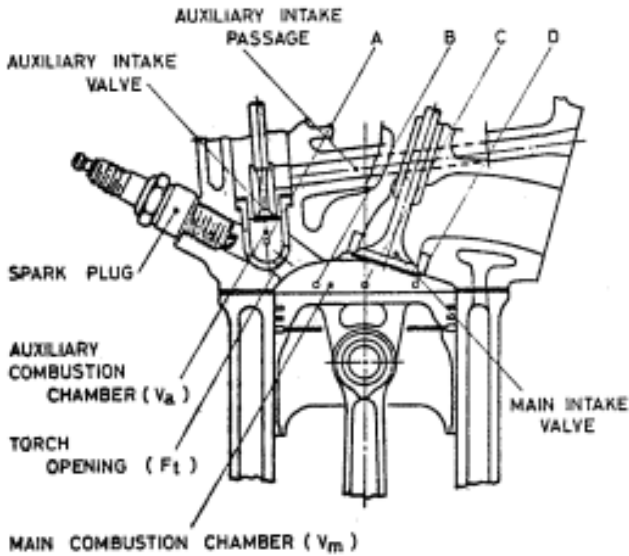


Figure 2.12: CVCC engine developed by Honda [58].

In the same 70's decade, Volkswagen group led by Walter R. Brandstetter developed a pre-chamber injection stratified charge engine (PCI), using a divided combustion chamber with a spherical valveless pre-chamber [64, 65], founding good fuel consumption and low emissions, specially when operating with lean mixtures without driving issues caused by the stratified charge in the road testing [66]. The sketch of the pre-chamber application in the engine can be found in Figure 2.13.

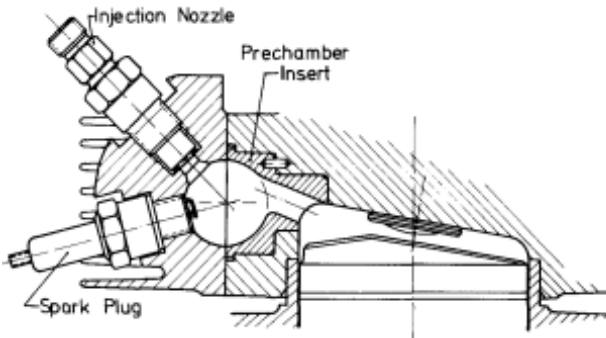


Figure 2.13: Internal combustion engine with a spherical valveless pre-chamber developed by Walter R. Brandstetter [66].

The invention of the Honda's CVCC engine led to another manufacturers, such as General Motors [67–70], Nissan [71], Porsche [72, 73] or Ford [74, 75], to explore the potential of the stratified charge using a pre-chamber application engine during this decade. The reduced emissions and the improvement in fuel economy achieved by the CVCC engine renewed the interest in these kind of applications [69, 76, 77]. In Figure 2.14 simplified sketches of the developed engines can be found.

By the end of the 70's and the early beginnings of the 80's, Lazslo Hideg and Robert P. Ernest developed and patented a pre-chamber application for rotative engines [78–80], while Aladar O. Simko developed and patented a new assembly to control the fuel in a dual chamber compression ignition engine [81, 82].

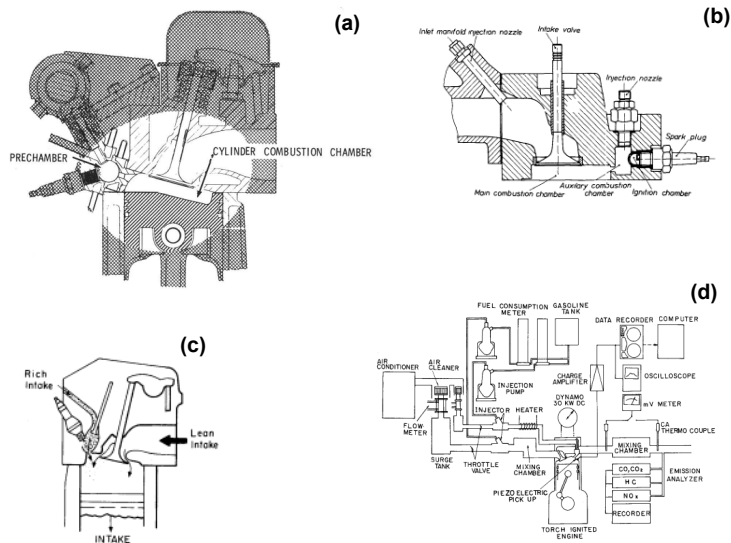


Figure 2.14: Internal combustion engine concepts of General Motors (a) [67], Porsche (b) [72], Ford (c) [74] and Nissan (d) [71].

Despite all the work performed in the development of these kind of large active pre-chamber systems, the interest in these applications decayed in the early 80's in favor of the development of small active and passive pre-chamber systems. However, some patents during the 90's and late 00's can be found. The work of Huei-Huay Huang and Rong-Fang Hong developing the Air Assisted Injection (HRCI) for a two-stroke engine [83] is notable.

Also, the development of the variable volume pre-chamber performed by Caterpillar has a remarkable impact on the progress of this technology [84–86].

2.3.1.2. Active small pre-chamber applications

The development of the large active pre-chamber applications started in the early years of the twentieth century. However, it will not be until the 60's decade when first small active pre-chamber applications (less than 3% of the clearance volume) were implemented and developed.

Nikolai Semenov developed the theory of chain reactions and studied the ignition phenomena [87–91] that served as a theoretical base for developing the jet ignition concept. Main characteristic of jet igniters is the smaller orifice diameter of the pre-chamber hole/s compared with those of the large pre-chamber clearance volume applications. This reduced diameter quickens the movement of the burning mixture when exits from the nozzle, but extinguishes the flame. Then, combustion in the main chamber is reignited by means of the active radicals species that were ejected from the pre-chamber. However, pre-chamber internal volume has to be small in order to avoid the impinging on the main chamber walls [92].

This jet ignition was firstly evaluated by Lev Abramovich Gussak [93–95], leading to the development of the Lavinia Aktivatsia Gorenia (LAG, in Russian) or Avalanche Activated Combustion (in English) [96–103]. Gussak proposed the use of a very rich mixture (λ around 0.5) in a very small separated pre-chamber (around 3% of clearance volume) to generate reactive jets chemically active. These jets contain radical species that are able to ignite the lean main chamber. Some of these species include CO, H₂, peroxides or aldehydes [104]. The result consisted in the ignition of an ultra-lean mixture (λ around 2) in the main chamber, highlighting the relevance of the active radicals in this kind of ignition concept. In Figure 2.15, a sketch of the engine utilized to evaluate this ignition concept is shown.

During the 80's and 90's, Antoni K. Oppenheim et al. in the University of Berkeley, and later Eiichi Murase et al. in the Kyushu University extensively studied and developed flame jet ignition. Their research work lead to the development of the Jet Plume Injection and Combustion (JPIC) concept [105–116]. This concept uses the pulsed jet combustor shown in Figure 2.16, which is a smaller version of a LAG application using a swirl chamber spark plug [117].

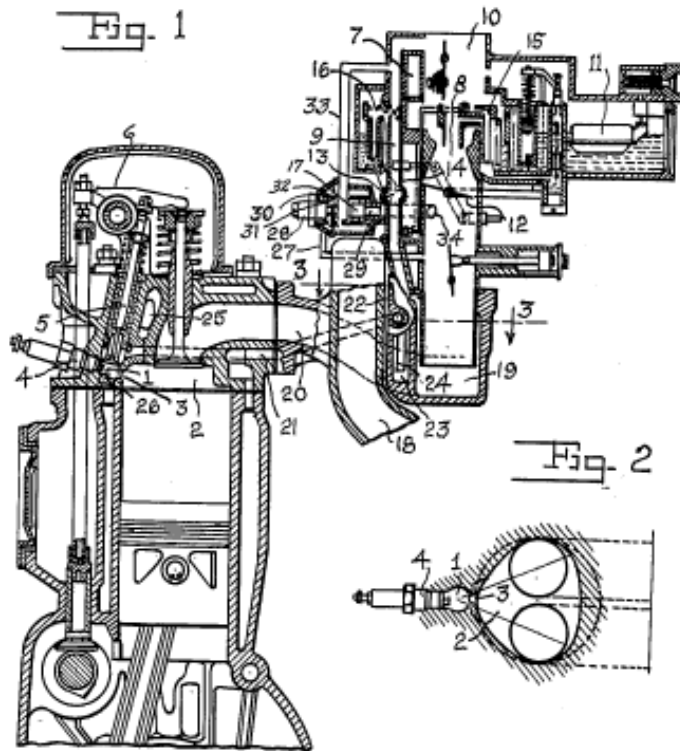


Figure 2.15: Internal combustion engine featuring LAG ignition concept [100].

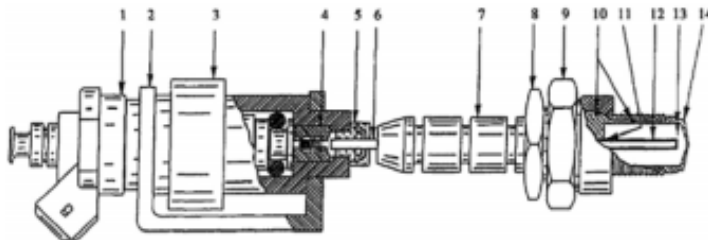


Figure 2.16: Jet Plume Injection and Combustion diagram concept [107].

The dedicated fuel injector is able to provide either fuel or a mixture of air and fuel to the pre-chamber. Then, after the injection process has finished, the rich pre-chamber mixture is ignited, increasing the resulting pressure and forcing the ejection of combustion products into main chamber, thus enhancing turbulence to the engine cylinder [118]. This flame ignition

system has some similarities to the concept developed by Shigeki Yamaguchi et al. [119], in where multiple ignition sites [120] were studied to shorten combustion duration and igniting leaner mixtures with lower flame speeds. This concept reported ignition of extreme lean mixtures with λ values up to 2.2 [121]. Moreover, the reduction of the combustion duration leads to the decrease of the heat transfer losses, increasing the maximum achieved pressure compared with conventional spark plug ignition.

Furthermore, the effect of basic pre-chamber geometrical parameters on combustion, such as volume or orifice diameter was evaluated, determining that there is a minimum orifice size that is able to ignite the lean mixture [119]. Otherwise, if the orifice diameter exceeds the limit, the resulting jet velocity is too high to ignite the mixture due to the velocity gradient [108, 109]. Moreover, as the orifice diameter becomes smaller the heat losses increase, leading to lower maximum pressure. On the contrary, the pre-chamber volume showed little impact compared with the hole diameter. In any case, enriching the air-to-fuel mixture within the pre-chamber helped to ignite leaner mixtures in the main chamber.

The development of this pre-chamber application not only led to a new jet ignition system, but also to a way of controlling the ignition timing of Homogeneous Charge Compression Ignition engines (HCCI) [122–124]. The pulsed jet flame can be used as a triggering event for auto-igniting the lean mixture in the main chamber. Those extremely lean mixtures are in λ values from 2.5 to 3.0 that are impossible to ignite by means of a conventional spark plug. Furthermore, the equivalence ratio of the mixture restricted the flame propagation from the jet as the dilution ratio is located outside the flammability limits.

Next step in the pre-chamber applications development was taken by Harry C. Watson et al. [125–134] at the University of Melbourne. The new concept was called Hydrogen Assisted Jet Ignition (HAJI). This concept uses a pre-chamber combustor to generate chemically active turbulent jets able to ignite ultra-lean mixtures in the main combustion chamber. A section view of this concept can be seen in Figure 2.17.

The HAJI normal functioning consists of injecting a small quantity of hydrogen (around 2% of the total fuel energy) near to the spark plug within the pre-chamber, in order to generate a rich mixture in the vicinity of the electrodes. As combustion inside pre-chamber advances, the resulting gas formed by burnt gases, active species and fresh mixture, travels through the pre-chamber holes, exiting at high speed rates, into the main chamber. Then, this ejected mass flow is able to ignite the ultra-lean mixture located in the

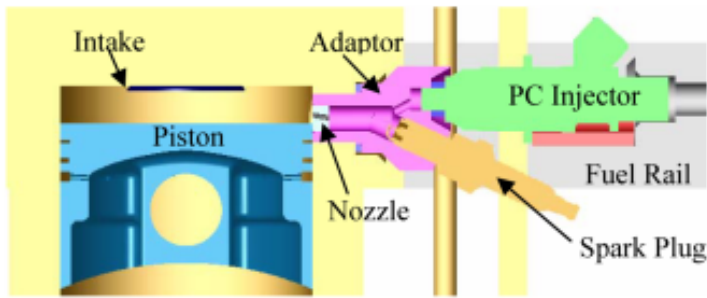


Figure 2.17: Hydrogen Assisted Jet Ignition sketch [135].

main chamber [128, 129]. The ignition is caused by means of the chemically active reactive species (mainly H and OH) along with the elevated turbulence levels induced by the jets, which turns in an overall two to three more orders of magnitude of provided energy compared with a conventional spark plug [134]. Being the jets an ignition source that solve main drawbacks of lean combustion and slow laminar flame speed fuels, broadening the operative air-to-fuel mixture ratio [130].

The main difference between HAJI concept and any other developed active pre-chamber applications resides in the extremely low internal volume of the pre-chamber (around 1% of the clearance volume) [130], featuring stable combustion process in mixtures up to $\lambda = 5$ [126]. Furthermore, the leaner combustion process achieved by means of this ignition system led to a more reduced combustion temperatures, thus reducing the NO formation and emission, also, benefits in terms of fuel consumption due to the reduced pumping losses were obtained [20, 127]. However, hydrocarbons emission becomes significant as the wall quenching of the flame is considerably increased at these lean conditions.

Following with this HAJI concept, several research works were performed modifying the utilized fuels. Zaw Kyaw et al. found that the use of gasoline within the pre-chamber restricted the maximum lean limit due to its flammability limit [131], while Elisa Toulson et al. studied the performance of alternative pre-chamber fuels such as compressed natural gas or liquefied petroleum gas, founding an extension of the lean limit of the HAJI concept [27, 132, 135–137]. Ferenc Hamori evaluated the HAJI concept in several engine load conditions, obtaining an increase in the thermal efficiency in all cases [138, 139].

Investigators of Gifu University and Toyota College of Technology in Japan studied an ignition concept similar to the HAJI system. Wakai et al. [140–142] isolated the effect on extending the lean limit by the active radicals and the turbulence generated by the jets in order to determine which had more influence on extending the lean limit. They found that turbulence has a more significant role than that of the chemically active radicals since a strong radical effect would be able to modify the reaction process and extend the lean inflammation limit but with the operating turbulence level that possibility was very low [36].

The jet ignition applied to an engine was studied by Piotr Wolański et al. [143–145] at the Warsaw Institute of Technology, developing the Pulsed Jet Combustion (PJC). In this application, the pre-chamber is located around the tip of the spark plug, having a central electrode through the rich mixture was able to flow. A simple sketch of the concept can be found in Figure 2.18. The spark triggering event happens during compression stroke and the increase in the pre-chamber forces a high pressure jet of combustion products to exit and ignite the main chamber lean mixture.

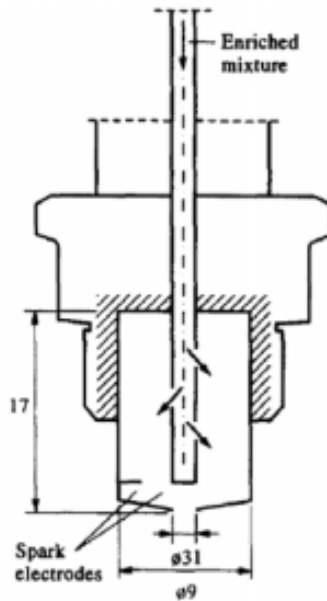


Figure 2.18: Pulsed Jet Combustion sketch [143].

Main obtained results showed a faster combustion process, higher pressure peak and rise compared to conventional spark ignition. However, as the lean ratio was closer to the stoichiometric case, less improvements were obtained when comparing with conventional spark plug system [143, 146].

A research work in scavenged swirl chamber spark plugs was performed by Hans-Jürgen Koß et al. at the Aachen University of Technology [147], following the work performed by Reinhard Latsch in the early 80's with the unscavenged swirl chamber spark plug [117]. They found that residual gases trapped inside pre-chamber of previous cycle/s reduce the effective ignition lean limit, being comparable the combustion enhancement to that obtained with a regular spark plug system near the lean limit. To avoid those issues, a methane fuel-like scavenged pre-chamber was evaluated, greatening the lean limit compared to the unscavenged swirl chamber spark plug. Being the rich stratified mixture near the electrodes the main contributor to this improvement.

In the 90's decade, a new concept was developed whose main objective was to be used as ignition system for both SI and CI engines. This system was called Auto-inflammation Piloteé par injection de Radicaux (APIR, in French), or Self Ignition Triggered by Radical Injection at the University of Orléans [146, 148, 149].

This ignition system featured very small nozzle diameter (less than 1 mm) connecting pre-chamber and main combustion chamber. These holes are able to quench the flame propagation and avoid the combustion in the jet vortex [36]. Furthermore, in order to assure a better feed of active radicals to the main chamber, the total number of holes was increased up to ten. This characteristic, in addition with the extremely narrow diameter, let a proper pressure rise to eject the jets and avoided the refilling of the pre-chamber with residual gases from main combustion chamber during the exhaust stroke [148]. Further investigation of this concept highlighted that in-cylinder aerodynamics should be lowered in order to avoid extra heat losses to the walls, thus increasing engine efficiency. Also higher knock resistance was found, letting an increase in the achievable compression ratio [149]. A simple sketch of APIR concept can be found in Figure 2.19.

During the early years of twenty-first century, Paul M. Najt et al. from General Motors [150, 151] patented a dual-mode combustion engine ignited by means of a pre-chamber system using pulsing jets. This concept was named Premixed Charge Forced Auto-Ignition (PCFA). The engine was able to run operating with an ultra-lean mixture in the main chamber. This mixture ignited rapidly forcing the ignition of the remaining unburnt fraction

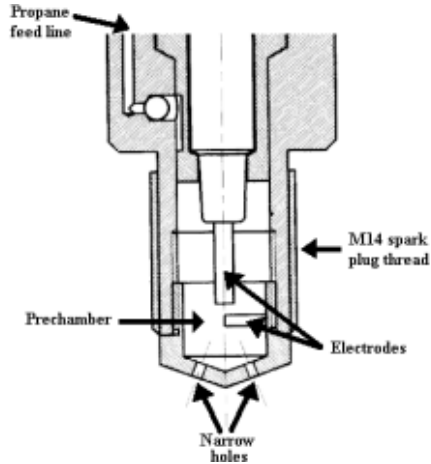


Figure 2.19: Auto-inflammation Piloteé par injection de Radicaux sketch [149].

by means of compression ignition. The main advantage associated to this concept was the possibility to operate as HCCI system even at low engine loads, with the resulting pumping losses reduction and limited NO_x emission.

Further efforts to operate with this kind of ignition systems were carried out by Aleksandar Kojic et al. from Robert Bosch GmbH [152, 153], patenting the Homogeneous Combustion Jet Ignition (HCJI) system. The key of this concept relied on the control of auto-ignition in the main chamber achieved by the timing of compression ignition within the pre-chamber. The pre-chamber counts with a sort of dedicated piston which forces the auto-ignition of pre-chamber mixture, then, the expelled hot jet gases into the main chamber force the auto-ignition of the lean mixture. A sketch of the concept can be found in Figure 2.20.

Harold E. Durling developed a new ignition concept featuring a fuel delivery system for the pre-chamber able to ignite the mixture both by means of a conventional spark plug and by means of compression ignition [36, 154]. Main idea consists in operating with conventional spark plug at high engine loads without the need of auxiliary fuel supply to the system, while compression ignition is used at low engine loads. By this way is possible to obtain the advantages of both systems. The sketch of this ignition system can be observed in Figure 2.21.

Following the work of Hans-Jürgen Koß et al. [147], more recent work to avoid some of the issues related to the poor scavenging of the pre-chamber was carried out by Reinhard Latsch et al. [155]. A pilot injection during the inlet stroke was proposed to help in evacuating the residual gases from the

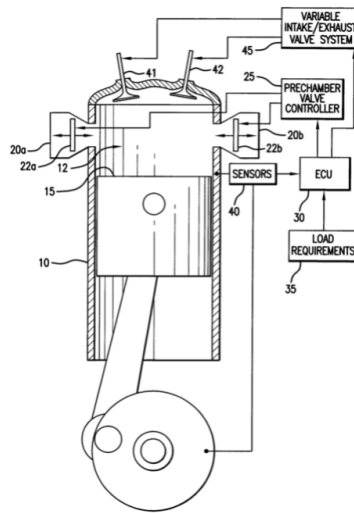


Figure 2.20: Homogeneous Combustion Jet Ignition system sketch [153].

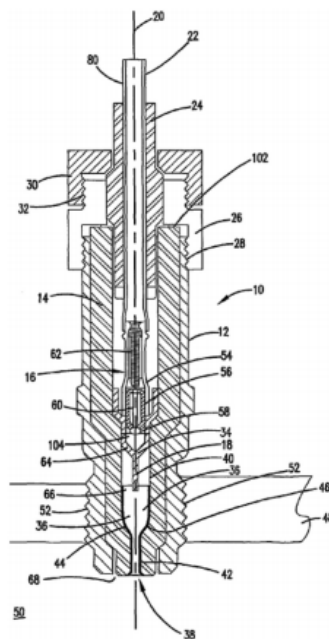


Figure 2.21: Homogeneous Combustion Jet Ignition system sketch [154].

pre-chamber. Several gaseous fuels were evaluated, founding that hydrogen was the best tested fuel to extend lean limit. A conceptual sketch of the functioning of this ignition system can be found in Figure 2.22.

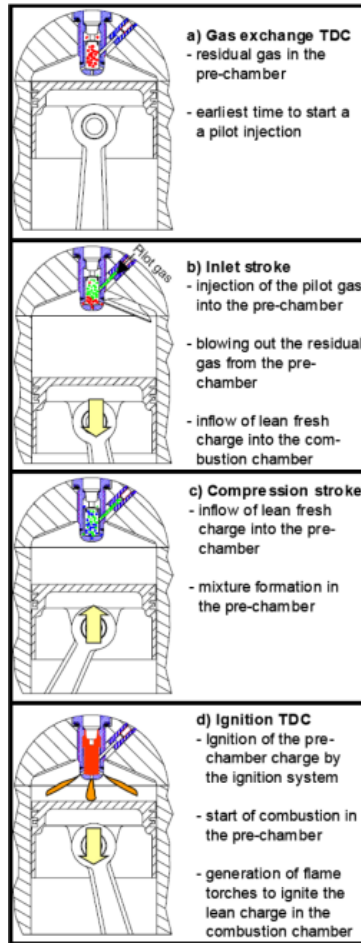


Figure 2.22: Pre-chamber spark plug featuring pilot injection concept principle [155].

David A. Blank patented and developed the Homogeneous Combustion Radical Ignition (HRCI) system [156–161]. The concept features auxiliary mini-chambers that ignite the mixture within them, then, chemically active reactive jets are expelled to the main chamber through small conducts, igniting the lean mixture. Main advantages of this system include better combustion efficiency and a decrease in the pollutant emissions.

Investigators of the Federal University of Minas Gerais in Brazil evaluated the use of a pre-chamber ignition system (PCIS) in commercial SI engines [162–167]. Main results reported from their investigation work indicate

that the pre-chamber ignition system showed effectiveness to burn lean mixtures thus extending lean limit while keeping suitable combustion stability levels [165]. The use of further fuel consumption improvement strategies was reported to even increase the benefits of using pre-chamber ignition systems [163]. The 3D CAD model of the stratified pre-chamber evaluated is presented in Figure 2.23.

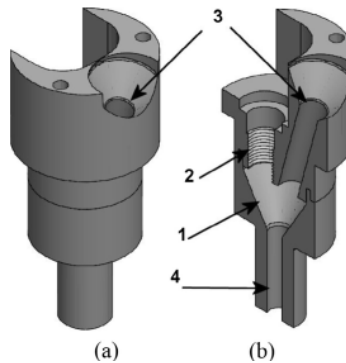


Figure 2.23: Pre-chamber 3D CAD model (a) and cross section view cut of 3D CAD model [166].

2.3.1.3. Passive pre-chamber applications

Despite the active pre-chamber applications had benefit from their popularity due to their ability to easily ignite lean mixtures, some efforts were taken to develop unscavenged pre-chamber applications. Main advantage of these systems rely on the simplicity of the concept and the low assembly cost compared to the scavenged systems.

Basic functioning of the unscavenged pre-chamber concept can be split into three different parts. First one consists of the filling of the pre-chamber, which is achieved generally by the compression stroke of the piston. The piston movement introduces the fresh mixture from the main chamber into the pre-chamber. Then, this mixture is ignited, increasing the resulting pressure within the pre-chamber and ejecting the reactive jets. Ending with the ignition of the main chamber mixture due to the reactivity of these ejected jets.

One of the first applications of this system was performed by Norihiko Nakamura et al. from Toyota Motor Company [168–170]. This Turbulence Generating Pot (TGP) torch cell concept was shown to increase the lean

operating range compared to conventional spark plug system with the benefit of removing the dedicated fuel supply to the pre-chamber. In Figure 2.24 is presented a sketch of the concept.

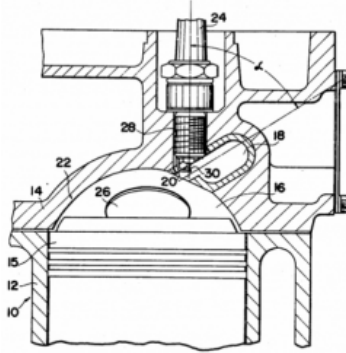


Figure 2.24: Turbulence Generating Pot concept sketch [170].

The torch cell ignition concept was also developed during the 70's decade by Ford Motor Company [171, 172], Volkswagen [173] and General Motors [174]. The basic pre-chamber geometry to maximize performance was investigated, founding the best results between 10% and 15% of the clearance volume [173], while the ignition timing was shown to be critical for obtaining suitable fuel consumption levels without emissions penalties [172]. Also it was found that jets increase the rate of combustion [174]. A sketch of these two investigated engines can be found in Figure 2.25.

Reinhard Latsch et al. from Robert Bosch GmbH developed an ignition system focusing on simplifying the LAG process by removing the auxiliary mixture supply to the pre-chamber, this ignition concept was known as Swirl Chamber Spark Plug [117, 175–177]. This ignition concept was able to achieve a faster energy conversion and better thermal efficiency at low engine loads compared with conventional spark plug system, being this pre-chamber concept able to obtain advantages in thermal engines if geometrical aspects of the pre-chamber are properly set [117]. The sketch of the evaluated pre-chamber can be found in Figure 2.26.

Investigators from the Tokai University evaluated an horizontal unscavenged pre-chamber concept during the 80's decade [178–181]. Founding that an horizontal pre-chamber orientation leads to lower engine performances in terms of break mean effective pressures compared with a "conventional" vertical orientated pre-chamber. However, for both orientations,

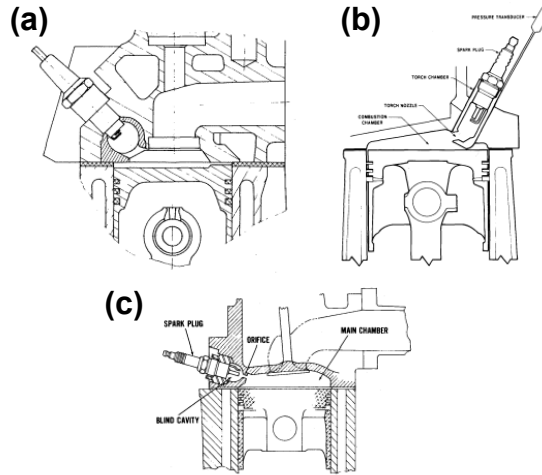


Figure 2.25: Volkswagen Prechamber Engine (a) [173], Ford Torch Ignition (b) [172] and General Motors Plasma Jet Ignition (c) [174] sketches.

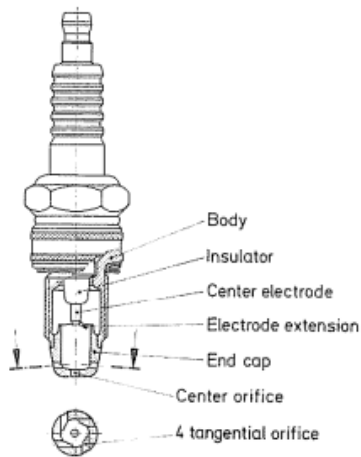


Figure 2.26: Swirl Chamber Spark Plug pre-chamber sketch [117].

pre-chamber ignition led to higher turbulence values increasing the gradient of heat release rate [178]. A simplified sketch of the horizontal evaluated pre-chamber located in the head of the engine can be found in Figure 2.27.

Another step in the unscavenged pre-chamber development was taken by Stanislaw Wojcicki et al. [182–185]. Main goal of this investigation was to analyze the effect of using a catalytic pre-chamber to ignite the mixture. The principle is based on the fact that a small amount of pre-reaction is able

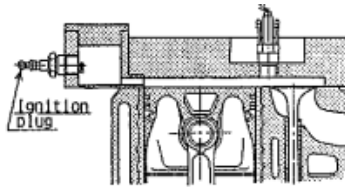


Figure 2.27: Horizontal pre-chamber sketch from Tokai University [178].

to increase mixture flame velocity and reduce ignition energy requirements [182, 184]. The application of this concept resulted in a reduction up to a 33% of the fuel consumption and an extension of the lean limit [183]. Also, the emissions of unburnt hydrocarbons and nitric oxides are lower compared with those obtained by means of a Diesel engine [183]. A sketch of the pre-chamber including the catalytic coat is presented in Figure 2.28.

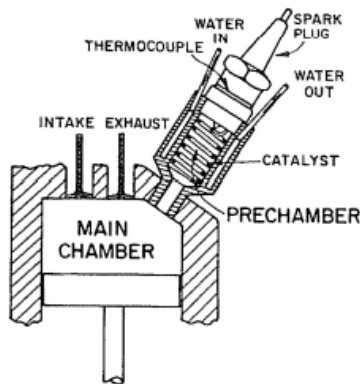


Figure 2.28: Catalytic pre-chamber concept sketch [182].

During the 90's decade, a series of patents following the unscavenged pre-chamber concept, being the most notorious the Smartplugs patents by Mark A. Cherry [186–189], the Caterpillar Swirl Chamber Spark Plug by Ronald D. Richardson [190], the Prechamber Spark Plug concept by Alexander P. Sabol et al. [191] and the General Motors Torch Jet Spark Plug by Harold E. Durling et al. [192].

Further investigation on the unscavenged swirl spark plug developed by Reinhard Latsch [117] led to the development of a new ignition system named Bowl Pre-chamber Ignition (BPI) [193–195]. In the BPI normal functioning there are two different injection events. The first one occurs during the inlet stroke, when the premixed lean mixture is injected, while

the second injection occurs during the compression stroke. This second injection only provides around 5% of the total fuel mass and it is injected towards the piston bowl, transferring mass into the pre-chamber with high turbulence flow levels [194]. This rich mixture within the pre-chamber is then, ignited and the resulting pressure difference between chambers forces the ejection of the reactive jets thus generating the inflammation of the main chamber lean mixture [193, 194]. The schematic functioning of this concept is presented in Figure 2.29.

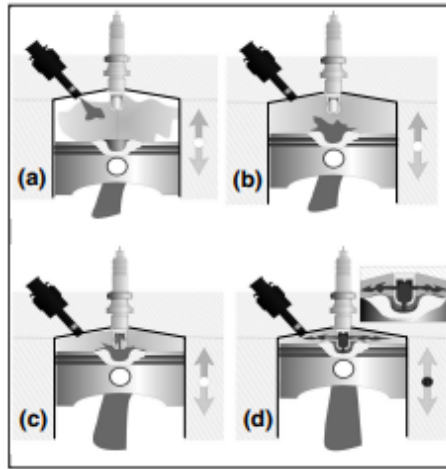


Figure 2.29: Functioning of BPI concept: (a) Injection event during compression stroke, (b) air-fuel mixture in the piston bowl, (c) mixture transport into the pre-chamber spark plug, (d) ignition and inflammation with flame jets [194].

Main results obtained with this BPI concept showed that the lean burn limit could be extended up to $\lambda = 1.7$ maintaining suitable emissions levels [194], while at part loads this concept can be joined with EGR strategy for further fuel consumption improvements [195].

In the early years of twenty-first century Harold E. Durling patented the Directed Jet Spark Plug system [196], while Masaaki Kubo patented the Nissan Auxiliary Combustion Chamber system [197].

The investigators of Federal University of Minas Gerais not only studied the active pre-chamber concept, but also worked on the unscavenged side of the pre-chamber ignition [163, 164, 198–201]. Main results obtained showed the potential of the PCIS system to reduce NO_x emissions and the improvement in fuel consumption for all evaluated driving cycles [201]. Furthermore, they found less cycle-to-cycle variation induced by the increased amount of air in the mixture and the faster combustion process led

to decreased heat transfer losses [163]. Regarding the leanest operating condition evaluated, it was possible to extend the lean limit up to $\lambda = 1.7$ reducing up to 98.4% of the NO_x emissions [200].

Meanwhile, in the University of Lund, Ashish Shah et al. investigated the pre-chamber spark plug ignition system in a heavy-duty natural gas engine [202–209]. The selected pre-chamber featured an ultra small internal volume (0.141% of the clearance volume) with four tangential nozzles and one axial nozzle. A schematic view of this pre-chamber including orientation in the cylinder head and location can be found in Figure 2.30.

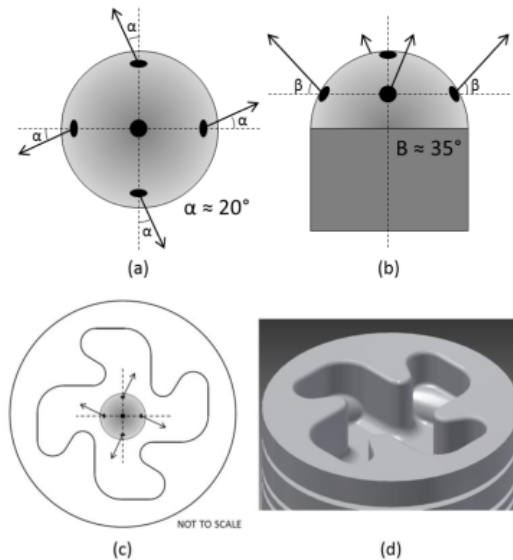


Figure 2.30: Arrangement and orientation of pre-chamber nozzles: (a) Top view, (b) Front view, (c) Spark plug location and orientation, (d) Combustion chamber design [202].

Main findings of the investigation present an increase in the lean limit operation despite the operating engine load and a potential to decrease the overall NO_x emissions [202]. Also the effect of pre-chamber volume, nozzle diameter [205] and mixture strength [204] were evaluated. Regarding internal volume there is an optimum pre-chamber volume since the heat release of the small pre-chambers is not able to sufficiently increase the pressure causing a short burst of pre-chamber ejection, but in the other hand, large pre-chamber volumes may not exhaust completely before main chamber ignition event [205]. For nozzle diameter there is also an optimum value. In this case a small nozzle diameter restricts the flow across the cham-

bers hindering the jet ejection, while a large nozzle diameter deteriorates the mixing in the main chamber [205]. In terms of air-to-fuel ratio in the pre-chamber, it was reported that increasing the richness of the mixture reduces combustion duration, benefits the ejection and reactivity of the jets and increases thermal efficiency but a cost of higher NO_x emissions [204].

More recent studies focusing on ignition of ultra-lean mixtures with hot jet ejection were developed by Sayan Biswas et al. [92, 104, 210–212]. A simple sketch of the pre-chamber assembly is presented in Figure 2.31.

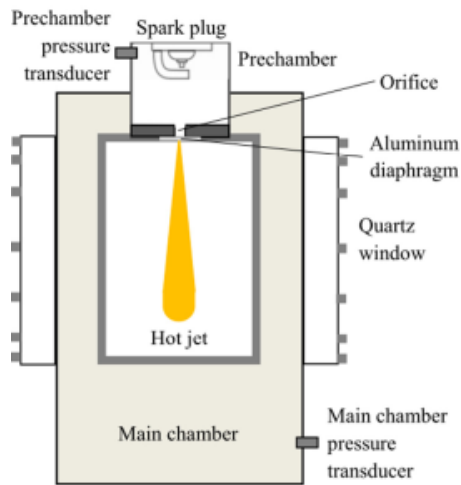


Figure 2.31: Pre-chamber and main chamber assembly sketch [210].

Main results from this investigation reported the existence of two different ignition mechanisms regarding pre-chamber ignition: jet ignition (pre-chamber flame is quenched) and flame ignition (jet contains incomplete combustion products containing flames) [210]. The first mechanism produces a jet of hot combustion products while the second mechanism produces a jet of wrinkled turbulent flames [210]. Moreover, an extension of the lean limit and higher exit temperatures were reported when using a supersonic nozzle [211].

2.3.1.4. Turbulent Jet Ignition

Among all the presented pre-chamber technologies and applications, the Turbulent Jet Ignition (TJI) concept research performed by MAHLE Powertrain [18, 213] arises as a very promising technology to extend lean limit operation and leaves the door open to combine this ignition system with other strategies for further fuel consumption improvement [19, 214].

The pre-chamber has a very small internal volume (around 2% of the clearance volume) which minimizes the hydrocarbons emissions, heat losses and the surface-to-volume ratio effects and residual gases. The pre-chamber is connected to the main chamber by a series of small orifices. These orifices benefit the flame quenching and jet penetration into the main chamber, then, lean mixture is ignited by means of the chemical, turbulent and thermal effects generated by the reactive jets in multiple locations thus increasing the combustion velocity. A dedicated fuel supply is assembled to assure a proper air-to-fuel ratio mixture in the pre-chamber and benefit the scavenge [36]. A 3D image of the pre-chamber design is presented in Figure 2.32.

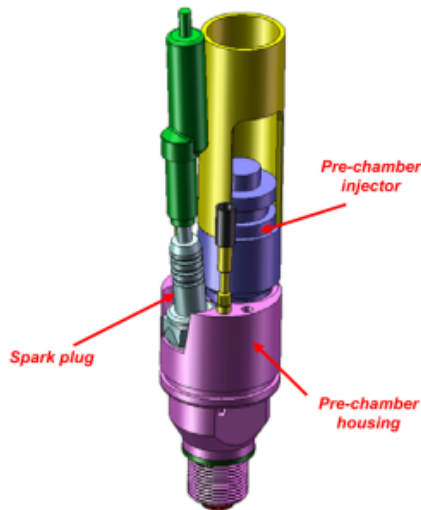


Figure 2.32: Image of MAHLE Powertrain developed pre-chamber system [213].

Deep investigation of this system was carried out by William P. Attard et al. Some studies were performed in a single cylinder engine [24, 215], in where an increase of the thermal efficiency and the potential to exceed the compression ratio when using a conventional spark plug were reported [215]. Regarding the operation at part load, the use of vaporized fuel within

the pre-chamber showed increase in the robustness of pre-chamber lean combustion process, higher pressure rates and thermal peak efficiencies, highlighting the potential of this ignition concept [24].

Furthermore, these investigators presented most of the main findings with this concept in a four cylinder engine. A brief comparison of main results in terms of stability, thermal efficiency and emissions against the air-to-fuel ratio is presented in Figure 2.33.

It is clear how this TJI concept is able to extend lean limit compared to conventional spark ignition operating with a suitable combustion stability (less than 5%) in most of the operating range [18]. The reported results show how there is an increase of the thermal efficiency in the lean region and a progressive reduction for the emitted NO_x caused mainly due to the improved combustion process, the low combustion temperature and the reduced pumping losses [18, 213]. Furthermore, improvements in terms of fuel economy were reported at low engine load and speed conditions [213]. Figure 2.34 presents the improvements at low engine load conditions.

The potential to extend knocking limit was also explored, founding an extension of the knock limit in both fueling and un-fueling of the pre-chamber operating way, which opens the door for combining this ignition concept with further strategies to improve fuel consumption [216]. Variations on the energy provided during the ignition event [217] and the flame kernel development [218] were also investigated. Main findings of these works rely on the very low necessary ignition energy (around 5 to 10 mJ) to initiate combustion. This is caused by the fact that spark discharge occupies a significant part of the internal volume of the pre-chamber [217].

Furthermore, the flame kernel development was reported to be unaffected for the variations in the ignition source. This robustness of the flame kernel development is caused because of the volume occupied of the spark discharge within the pre-chamber [218].

Different combinations of fuels in main and pre-chamber were evaluated to demonstrate the possibility to operate the concept with alternative fuels [219, 220]. Finding that Turbulent Jet Ignition reported significant lean limit extensions in any combination of liquid-vapor kind of fuel, even reaching values of $\lambda = 2$ at part load conditions, thus increasing thermal efficiency and reducing overall NO_x emissions [219].

Combustion visualization imaging in an optical engine assembly and in a rapid compression machine were recorded [221–226]. In the work performed by William P. Attard et al. [221] it was highlighted the reduction in flame propagation for lean spark ignition caused by the poor flame kernel

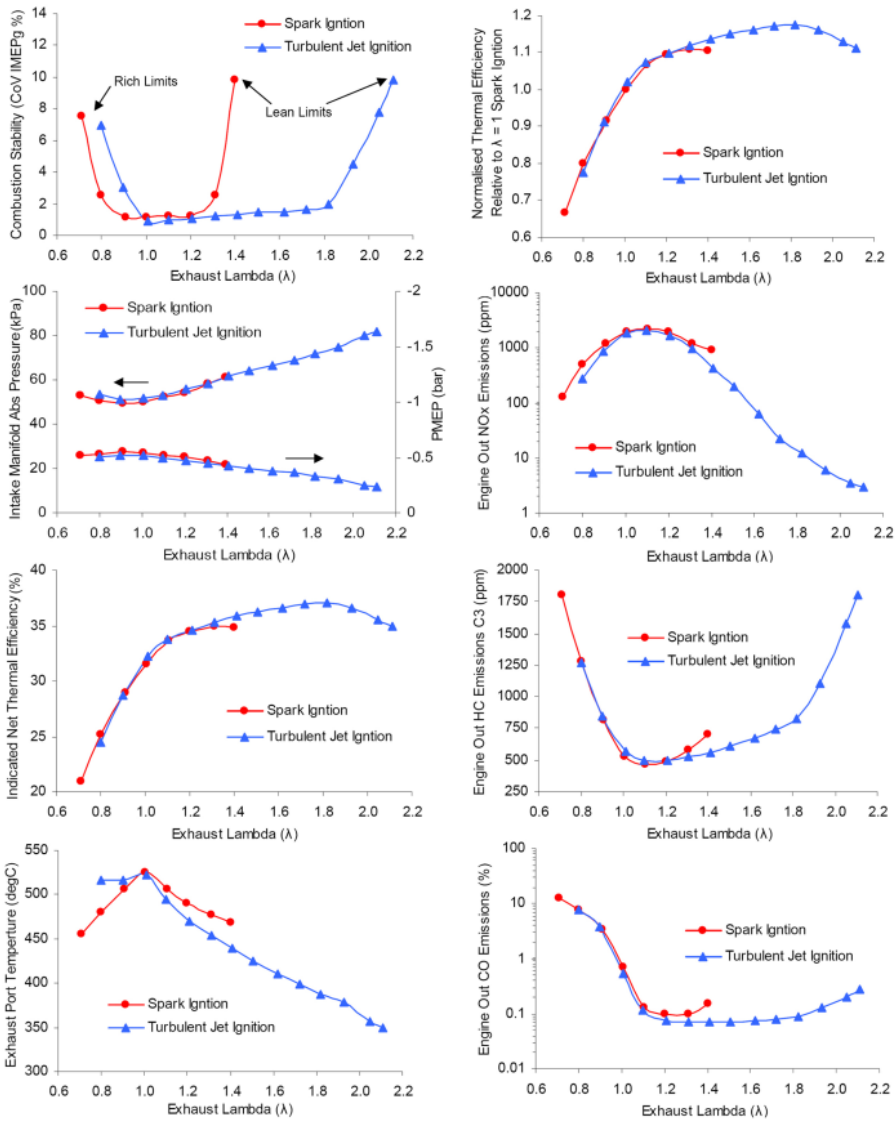


Figure 2.33: Comparison of spark ignition versus Turbulent Jet Ignition combustion systems [18].

development, but the enhanced ignition achieved with the TJI system the combustion produced visible chemiluminescence even at high lambda values up to 1.8. Combustion imaging of this study can be found in Figure 2.35. Toulson et al. [222] compared propane combustion against natural gas

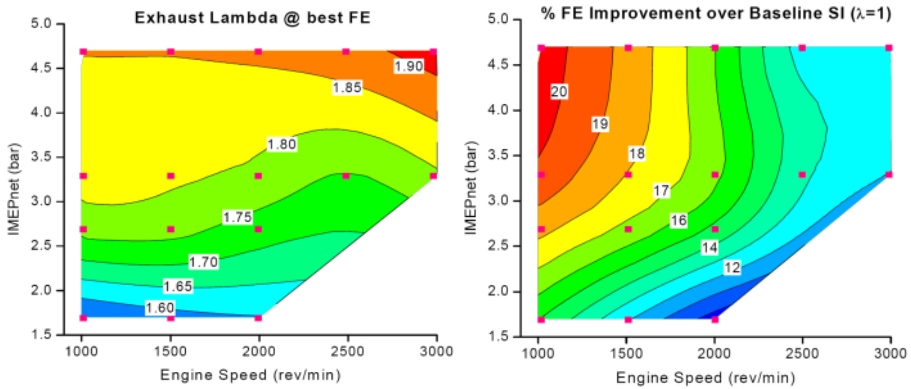


Figure 2.34: Exhaust lambda and fuel economy improvement over baseline SI at $\lambda = 1$ [213].

combustion, reporting an increase of the flame propagation for propane fuel. However, both fuels presented benefits combined with the Turbulent Jet Ignition as combustion initiator, mainly related to the increase of the lean limit and the reduction in the NO_x emissions.

Meanwhile, Gentz et al. evaluated the impact of the orifice diameter [224] or the use of iso-octane as primary fuel to overcome the limitations of the use of liquid fuel within the pre-chamber [226]. Orifice diameter had an impact on the resulting Reynolds number at stoichiometric conditions, but the leaner the mixture the less impact of diameter on the Reynolds number, so the jet does not have enough time to fully develop before reaching main chamber walls [224]. Modifying the orifice geometry also had an effect on the jet structure and fluid mechanics, inducing different auto-ignition behavior in the unburned mixture [226].

Modern studies focused on passive TJI system demonstrated the possibility to use the ignition concept in addition with Millerization or external EGR, providing enough heat flux to the exhaust to activate the after-treatment system, making it suitable for low-cost and hybrid applications [19]. Furthermore, this passive TJI system was reported to mitigate the knocking issues and achieve faster burn combustion processes and increased pressure rises [227]. Nathan Peters et al. investigated the effect of modifying lambda and pre-chamber fuel quantity to optimize the performance of the TJI [228]. It was reported that the scavenged operation of jet ignition had better combustion stability when air-to-fuel ratio within the pre-chamber was set between λ 1-1.2, however, excessively rich mixtures tended to diminish the obtained

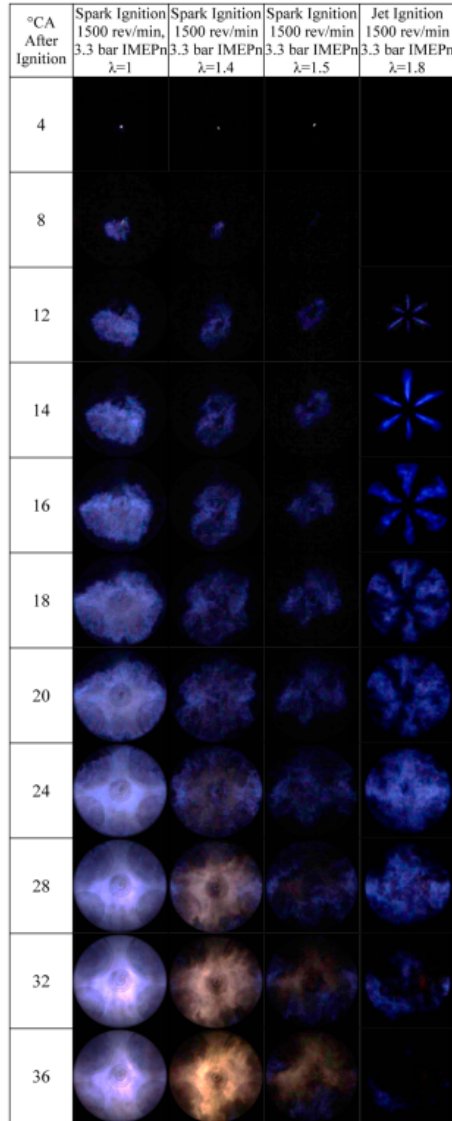


Figure 2.35: Varying excess air dilution crank angle resolved images of in-cylinder combustion through the quartz piston insert for both spark ignition ($\lambda = 1$, $\lambda = 1.4$, $\lambda = 1.5$) and jet ignition ($\lambda = 1.8$) combustion [221].

thermal efficiency, arising as a critical aspect the proper control of the mixture within the pre-chamber to obtain a suitable functioning of the system [228, 229].

Investigators from KAUST numerically evaluated different geometrical aspects of a conical shaped unscavenged pre-chamber, such as, the throat diameter, nozzle length or nozzle diameter [230], reporting that the throat diameter had the biggest impact on the pressure among the three parameters, while the nozzle length had a minor effect compared to the other ones. The nozzle diameter affected both peak pressure and residence time being a critical aspect in the design process. Also, a numerical and experimental analysis of the lean burn applying the conical shaped scavenged pre-chamber was performed by KAUST group [231]. Reported results indicate that this design features high combustion losses due to the flow restriction of the pre-chamber geometry and the excessive quenching that leads to lower reactivity of the ejected products.

Further numerical studies with advanced 3D CFD tools were performed by Bryce C. Thelen et al. [232, 233]. In their work, the location of the ignition source was modified in order to optimize the combustion process. Founding that the best location of the ignition source should be high in the pre-chamber since at this location most of the energy of the fuel can be transferred to the jets due to combustion [233].

It is clear how this ignition concept arose as a clear solution to overcome most of the problems associated with lean combustion, hence the popularity of the system. In the presented context, many researching groups have evaluated somehow or other an application of the TJI concept [38].

2.3.2. Aspects of pre-chamber combustion

As aforementioned, the use of lean burn or exhaust gas recirculation strategy requires an increment of the provided energy to ignite the mixture, in order to assure a reliable combustion process with a proper repeatability [20, 22]. The use of pre-chamber systems has demonstrated an improvement in these kind of strategies ignition [18]. Moreover, the use of a pre-chamber igniter has an inherent effect on some combustion parameters, such as the lean limit, start of combustion or flame propagation speed among many others, which will be discussed within this Section.

2.3.2.1. Pre-chamber scavenging

One of the most critical aspects of the pre-chamber ignition functioning is the pre-chamber scavenging. It is mandatory to keep a suitable stratified mixture in the vicinity of the spark plug to obtain faster flame propagation and build-

up enough pressure in the pre-chamber to assure proper jet ejection. The scavenging is driven by the pressure difference evolution between chambers and, if it is a stratified application, the fuel injection inside pre-chamber.

The evaluation of the quality of the scavenging process may only be possible with advanced 3D CFD tools. Blankmeister et al. [234] performed simulations of a passive pre-chamber application. Figure 2.36 illustrates the scavenging process during intake stroke when applying EGR with a nine nozzles pre-chamber. Exhaust pressure forces the movement of the residual gases out of the system. However, a non negligible amount of burnt gases remain into the pre-chamber volume. During intake stroke, fresh mixture comes into the system, and piston movement forces the filling of the pre-chamber, further evacuating some of the existent residual gases. Barbery et al. [235, 236] pointed that for a passive pre-chamber, the re-filling during intake stroke is quite small.

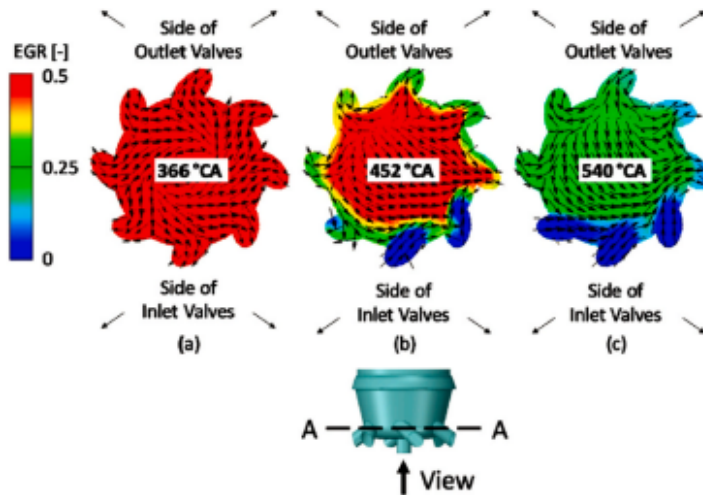


Figure 2.36: Scavenging across the pre-chamber during the intake stroke (EGR indicates the residual gas mass fraction) [234].

The total amount of residual gases after the re-filling of the pre-chamber is mainly controlled by the compression ratio rather than nozzle configuration or pre-chamber internal volume, as stated by Barbery et al. [235]. However, a proper selection of the pre-chamber basic geometry (total cross-sectional area to total internal volume) may benefit the scavenging of the pre-chamber.

Moreover, not only compression ratio affects the total amount of residual gases, the operating conditions in terms of engine load and speed play a role in this process [235].

Turbulent kinetic energy (TKE) has also an impact on the pre-chamber scavenging as suggested Desantes et al. [237] since premixed combustion is related to the turbulence field. The induced turbulence in the pre-chamber is created by the flow admitted inside the pre-chamber volume through the orifices and the auxiliary fuel supply (in active systems). In this sense, pre-chamber geometry affects the TKE and flow velocity. Blankmeister et al. [234] investigated the correlations between TKE and the pre-chamber geometry. Founding that decreasing volume or increasing nozzle diameter benefits the scavenging quality but hinders the overall TKE.

2.3.2.2. Spark timing

Including a pre-chamber has benefits in terms of combustion duration since the time to burn the total amount of fuel is reduced [40, 71, 97], thus letting the reduction in the total advance of the spark timing compared with the conventional spark ignition system. The possibility to reduce the need of the spark ignition advancement may be related to the improvement of the flame propagation speed [179].

For scavenged pre-chamber applications, Robinet et al. [148], Blank et al. [157] or Attard et al. [18] reported reductions of the spark timing compared with baseline spark plug ignition systems achieving suitable IMEP values. In Figure 2.37 the effect of the variation of spark timing operating with the TJI concept on combustion stability and IMEPn (left) and the in-cylinder pressure in an APIR application (right) is shown.

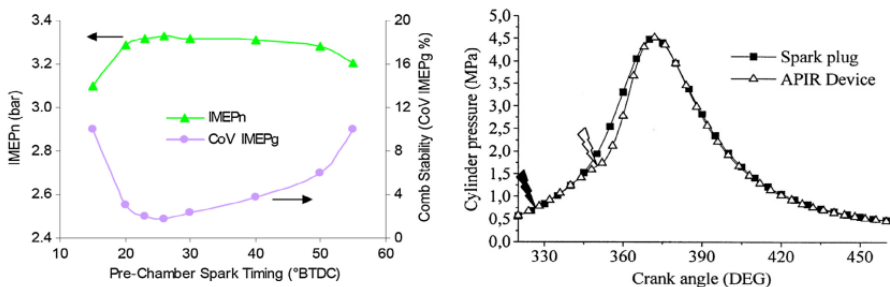


Figure 2.37: IMEP and combustion stability for pre-chamber spark timing variation operating with the TJI concept (left) [18] and in-cylinder pressure with APIR system including spark timing (right) [148].

From this Figure 2.37 it is clear how pre-chamber applications are able to delay the ignition triggering event compared with conventional spark plug. Even more, modern pre-chamber ignition systems such as TJI are not strongly affected by the modification of the spark timing, being able to operate in a wide range. Moreover, varying the spark timing may lead to a reduction in the combustion temperature affecting the resulting BMEP as Roethlisberger et al. [238] and Pischinger et al. [239] reported.

Regarding the passive pre-chamber applications, Ryu et al. [178, 179] investigated the effects of modifying the spark timing, founding that the most possible delayed spark timing occurs when the jet forms a 90 degree angle with the horizontal face of the piston.

2.3.2.3. Pre-chamber combustion

Combustion inside pre-chamber follows similar rules as a conventional combustion in an SI engine. The fresh mixture within the pre-chamber is ignited by means of a conventional spark plug, then, it follows the premixed flame propagation. However, combustion dynamics in the main chamber when igniting with jets is different from a conventional SI engine, so spark timing and thus, combustion start, should be adjusted.

However, some characteristics of pre-chambers such as the small internal volume, the high cross sectional area-to-volume ratio or the turbulence levels, are significantly different compared with a conventional premixed combustion process in SI engines [240]. In fact, the flame quenching in the walls associated with the small pre-chamber orifice diameter is notably more critical compared with a conventional SI engine since flame development occurs near the walls and flame kernel growth occupies most of pre-chamber combustion duration. Furthermore, the high area-to-volume ratio increases the overall heat transfer through the walls.

Regarding combustion start, Sakai et al. [71] defined the difference in crank angle degrees between the spark timing and the effective point where pressure rise due to combustion is detected, naming this value as ignition delay. Sakai et al. [71] and Ryu et al. [241] observed that ignition delay in engines with a pre-chamber application was around 11 crank angle degrees despite the relative air-to-fuel ratio. On the contrary, conventionally ignited engines increased the delay gradually with the increase of the air-to-fuel ratio.

Investigation in pre-chamber applications showed that combustion start is advanced compared with conventional spark ignition. Toulson et al. [27, 132] reported a start in a range around 2.5% of the mass burn fraction (MBF)

duration operating with the HAJI system. This was caused by the addition of H_2 which increased the the laminar flame speed and the presence of chemically active radicals in the jet. Regarding TJI, Attard et al. [217, 221] showed that mixtures near the stoichiometric within the pre-chamber tend to accelerate the combustion start of the system mainly by the generated active radicals. This statement in addition with the multiple ignition sites generated by the increased number of nozzles quickened the combustion process. Gentz et al. [223, 226] further investigated the TJI system in rapid compression machine and founded that the new ignition system improved the combustion start. In Figure 2.38 the burn duration comparison between conventional SI engine and TJI with different nozzle diameter is presented. Regarding unscavenged pre-chamber applications, Kettner et al. [195] pointed that BPI concept is also able to reduce the MFB duration for lean mixtures.

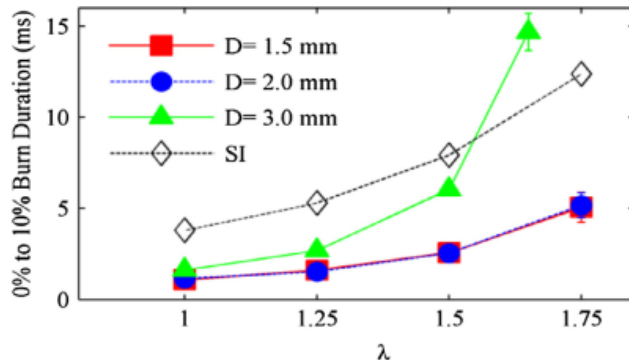


Figure 2.38: Variation in 0-10% burn duration for λ sweep [223].

Regarding the pre-chamber combustion duration, Peters et al. [228] defined it as the length of the pre-chamber pressure rising above that of the main chamber in units of crank angles [228]. In Figure 2.39 pressure traces obtained by Peters et al. of both combustion chambers.

It is remarkable that, there may happen a flow reversal after main chamber ignition due to the pressure increase. And if this refilling of the pre-chamber contains fresh mixture or intermediate combustion products, a second combustion may start within the pre-chamber, leading to a second peak in the heat release rate [230]. This was named as "reburning phase" by Distaso et al. [242, 243].

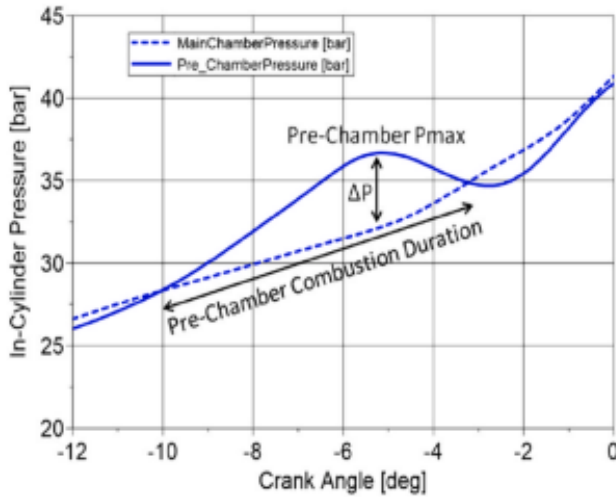


Figure 2.39: Pre-chamber combustion duration indicated by pressure traces in the pre-chamber and the main chamber [228].

2.3.2.4. Jet ejection and ignition

Once combustion process within the pre-chamber is occurring, pressure inside increases, thus forcing the movement of the combustion products, intermediate species and fresh charge mixture out of the pre-chamber through the holes into the main chamber. This process is named jet ejection. Chinathambi et al. [244] or Gentz et al. [223, 226] visualized the jet ejection process. The small cross sectional area-to-volume ratio tends to quench the flame in the orifice channel [244].

Distaso et al. [242] defined three different phases of jet ejection according to the temperature variation and the mass fraction of intermediate products. During the first phase there is an ejection of cold unburned products exiting the pre-chamber. The ejection of this mixture is related to the initial increase of pressure and the location of the spark plug, which is commonly located at the top of the pre-chamber [233]. Second phase consists of the ejection of intermediate combustion products and active radicals, which their temperature is considerably higher than those ejected during first stage. These products are the main contributors to the main chamber ignition. Finally, during third phase there is an ejection of mostly burned products and low temperature species.

Investigators such as Rajasegar et al. [245], or Gentz et al. [223, 224] performed optical research. Rajasegar et al. reported that the air-to-fuel ratio within the pre-chamber drives the formation, development and mixing of turbulent jets in the main chamber, independently of the air-to-fuel ratio of the main chamber mixture [245]. While Bunce et al. reported that the jet penetration before the ignition determines the distribution of the ignition sites [246]. Furthermore, the jet penetration is strongly related to the jet exit velocity, being directly dependent. Lower jet-exit velocities tend to reduce the jet penetration length, which may lead to fewer ignition sites and a poor combustion stability. However, an excessive jet-exit velocity can guide the jets to the cylinder walls, increasing the flame quenching. Arising the jet-exit velocity as a key aspect in the pre-chamber design.

It is remarkable that jet ejection induces a strong pressure wave into the main chamber, which it is then amplified by the main chamber combustion pressure. This pressure oscillation is notably high compared with the obtained operating with the conventional SI concept [247]. The comparison of the filtered pressure traces is shown in Figure 2.40. This pressure oscillation may come from the local fast burning of the jets, which are notably different from the pressure oscillations induced by the end-gas auto-ignition, as it was pointed by Hua et al. [248, 249].

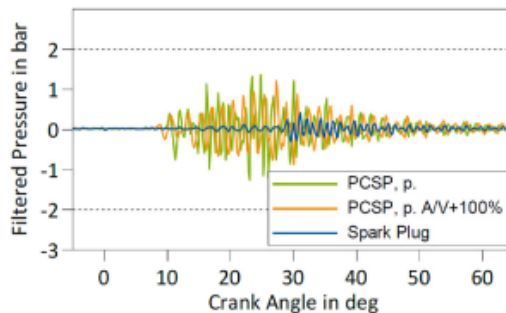


Figure 2.40: Comparison of filtered pressure traces between the conventional spark ignition system and the pre-chamber ignition system [247].

Regarding the ignition of the main chamber, the process is based on the chain reaction concept developed by Semenov [88, 89], where Gussak et al. [94, 97, 99] proposed a rich mixture to generate reactive radicals that are able to ignite very lean mixtures. The ignition of the chamber is achieved by means of chemical, thermal and turbulent effects. The chemical part is referred to the present radicals in the jets. These radicals are very re-

active and they are at high temperatures, being possible thermal triggers of the main chamber ignition event. More modern approaches such as TJI, reduce the orifice diameter so the flame front exiting of the pre-chamber is quenched, and then the main chamber mixture is reignited. Kyrattos et al. [250] pointed that there are two different mechanisms in the quenching of a turbulent jet traveling through a nozzle. First mechanism is the thermal quenching, which is conducted by the thermal loss through the walls, mainly in the orifice vicinities [251]. Second mechanism is hydrodynamic quenching, which happens once the jets have entered the main chamber and mix with the cold unburned mixture. An excessive hydrodynamic quenching may lead to the total flame extinction at extreme conditions and then, to a misfiring cycle.

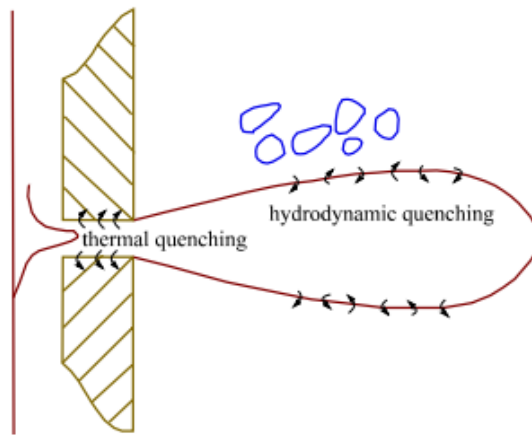


Figure 2.41: Sketch of the two different quenching mechanisms in the turbulent jet ignition [250].

Yamaguchi et al. [119] investigated the mechanisms that drive torch jet ignition in a divided chamber bomb. Modifying the nozzle diameter and chamber volume, four different ignition patterns were reported in scavenged and unscavenged pre-chamber conditions: chemical chain ignition, composite ignition, flame kernel torch ignition and flame front torch ignition. Regarding TJI ignition, recent studies carried out by Biswas et al. [92, 210, 211] used high-speed Schlieren and OH^* chemiluminescence imaging to confirm different ignition patterns according to the flame morphology and the ignition delay. The first pattern consisted of ignition with hot jets that only comprised combustion products, while the second pattern consisted in flame ignition with hot jets containing wrinkled turbulent flames and

active radicals. Also, it was found that the ignition mechanism may change between the patterns according to the variation of chamber pressure and nozzle diameter.

2.3.2.5. Main chamber flame development

As explained, the ignition in the main chamber is caused by the hot jets entrainment in multiple location. Then, the whole ejected mass is rapidly burned and the flame reaches the boundaries of the jets. After that, the flame starts its propagation outside the boundaries of the jets with a regular flame front [235, 236]. Moreover, the air-to-fuel ratio of the main chamber mixture determines the main propagation mechanism in this combustion chamber. When the air-to-fuel mixture is close to the stoichiometric conditions, the fraction of fuel mass which is firstly burned is that one ejected and contained within the turbulent jets, then, as the conditions outside the hot turbulent jets are suitable for a regular propagation, the flame propagates regularly and the amount of released energy inside the jets is small (15% of total energy) [235]. Regarding lean operation, the thermal and turbulent conditions outside jets are not as good as in the stoichiometric case, hindering flame propagation. In this case, the release energy process is mostly done within the jet boundaries [235].

Korb et al. [252] performed experimental tests with an optically accessible engine to evaluate the in-cylinder combustion process. They found that pre-chamber volume affected the development of the flame. Bigger pre-chamber volumes tend to increase the growing velocity of the flame torches, while on the other hand, small sized pre-chamber tend to reduce growth velocity of the flame torches, which the jets may be extinguished when operating at lean conditions.

2.3.2.6. Heat release rate

Heat release rate is one of the most important parameters to evaluate the performance of a combustion process. It indicates the rate at which energy stored in the fuel is liberated by the combustion process [253]. Sakai et al. analyzed the heat release rate of both torch ignited engine and a conventional engine [71]. Pointing that the heat release of a conventional engine presents somehow a bell-shaped profile, while the heat release of a pre-chamber application presents a fast increase of the heat liberation, achieving a high peak, and then a decrease after a short period of stability. Profiles of both obtained heat release rates are shown in Figure 2.42.

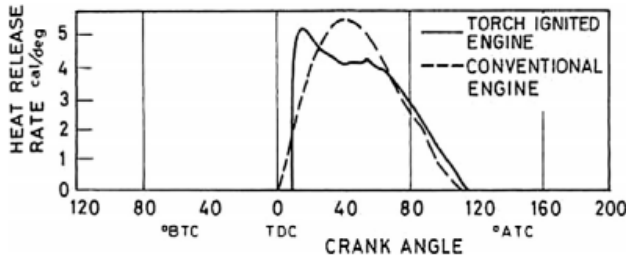


Figure 2.42: Comparison of combustion characteristics at constant indicated specific fuel consumption. Adapted from [71].

Sakai suggested that the rapid increase of the heat release and the peak value were affected by the air-to-fuel ratio in the pre-chamber mixture, being the richness of this mixture the parameter of the sharpness of this peak. The heat release rate tends to be more similar to the conventional heat release profile as the mixture becomes leaner [71]. However, not only the richness of the mixture affects the obtained profile. Parameters such as the pre-chamber internal volume, number of nozzles or their diameter also play a role in the combustion process. Bunce et al. [254] reported a 40% decrease of the total combustion duration, understood as the 10-90% MBF, using a passive TJI system. In Figure 2.43 a comparison of pressure and cumulated heat release of passive TJI and conventional SI is presented.

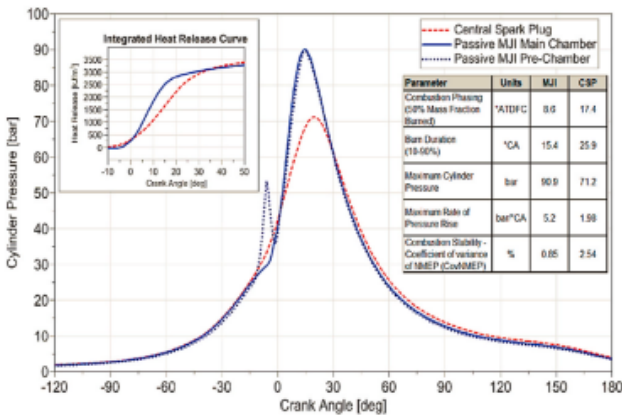


Figure 2.43: Comparison of combustion profile between passive TJI and conventional SI at 18 bar BMEP 4000 rpm [254].

The heat release curve in the main chamber may be divided into three different parts. Early stage of combustion (MBF 0-10%) includes information regarding combustion in the pre-chamber, jet ejection itself and the ignition in the main chamber [255]. In this part, pre-chamber geometry and scavenging, spark timing or auxiliary fueling (if exists) drive this combustion stage. Main stage of combustion covers 10-50% of MBF. This part is referred to combustion process after the jet ignition and is highly influenced by some jet characteristics such as the induced turbulence level and its penetration into the main chamber. Final stage of combustion covers 50-90%, where flame propagation in the main chamber is the dominator of the process.

2.3.2.7. Dilution mixture limit

One of the most important benefits of a pre-chamber ignition system is the extension of the dilution limit keeping suitable combustion stability and repeatability, thus increasing the thermal efficiency [20].

Kettner and Kuhnert et al. [194, 195] evaluated the BPI concept, founding an extension of the lean limit from $\lambda = 1.3$ to $\lambda = 1.7$. This increase in the lean operation led to lower NO_x emissions and comparable HC emission level to a conventional spark ignition engine. In Figure 2.44 the fuel consumption over the λ sweep in a BPI system is presented.

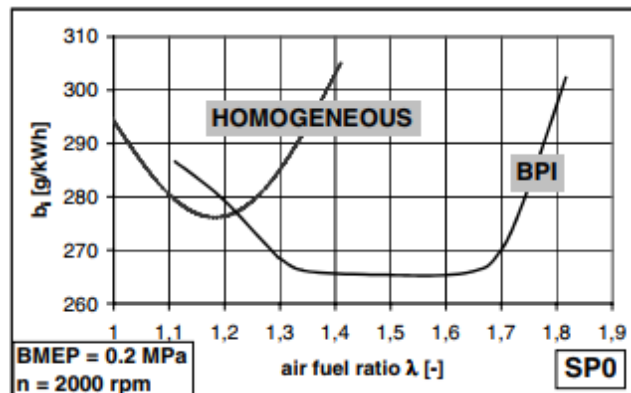


Figure 2.44: Specific indicated fuel consumption for different air fuel ratios λ at BMEP = 0.2 MPa and $n = 2000$ rpm [194].

Furthermore, for other scavenged pre-chamber applications, such as TJI, the extension of the lean limit is even greater. Attard et al. developed the TJI system [18, 213], which one of its main advantages consists of increasing the operating dilution range up to $\lambda = 2.0$ values. In an optically accessed

single cylinder engine, it was reported a visible blue chemiluminescence even at high λ values, caused by the extremely fast and very stable combustion process in the main chamber [221].

However, the leanest achieved conditions with a pre-chamber application were reached by Toulson and Lumdsen et al. when operating with the HAJI concept [126, 132]. This concept showed flammability gains in a very wide dilution operating range, even with different fuels such as compressed natural gas (CNG) or liquefied petroleum gas (LPG). Main results reported indicate that operating with hydrogen in the pre-chamber and gasoline in the main chamber allows an extension of the lean operation up to $\lambda = 2.5$ [132], while LPG and CNG in the pre-chamber extended the operation up to $\lambda = 2.35$ and $\lambda = 2.25$ respectively. This experimental analysis showed that the lean limit not only depends on the stored energy in the fuel but also on the flame propagation speed and the quantity of active radicals within the turbulent jets. Moreover, experimental analysis with single fuel feeding both chambers was carried out [137, 222], finding that lean limit was slightly reduced compared when using hydrogen in the pre-chamber and other fuel in the main chamber.

Furthermore, an operation reaching an extreme λ value of 5.0 was reported with HAJI ignition system by Lumdsen et al. [126]. Proving that a jet ignition concept is clearly able to extend the dilution limit compared with a conventional spark system and obtain benefits of this fuel consumption improvement strategy. In Figure 2.45 the performance of the HAJI system against λ is presented.

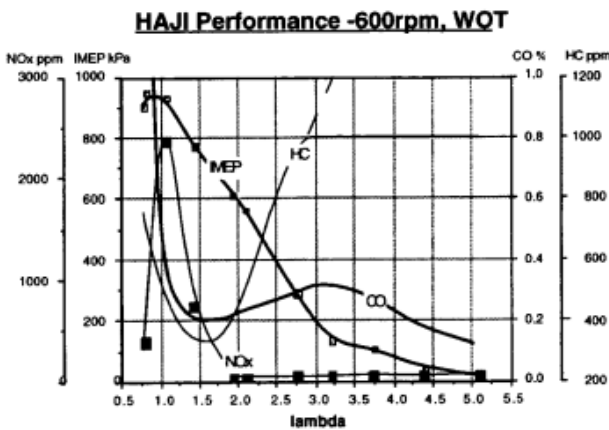


Figure 2.45: HAJI WOT performance [126].

2.3.2.8. Knocking control

Knock is the spontaneous ignition of the end-gas caused by the high temperatures and increased pressure in the combustion chamber [20, 22]. This is a non desirable effect since reduces the power output and may lead to several damage to the engine [256]. In these terms, knocking arises as a critical aspect to control, especially in long combustion processes, when the increased pressure and temperature of the combustion process benefits the auto-ignition of the end-gas charge.

The use of a pre-chamber ignition system has been demonstrated to effectively increase the combustion velocity in the main chamber by enhancing turbulence energy [257] and initiating combustion in multiple sites [18, 171]. The ejected jets tend to initiate the combustion from the outer areas of the main chamber into the central areas rather than the conventional flame development of a SI engine. These effects tend to reduce the end-gas residence time and therefore, the knocking appearance [232, 233], leading to take advantage of other thermal efficiency improvement strategies.

An evaluation of the knock limit extension for a TJI application compared with a conventional SI system was performed by Attard et al. [216]. The results of the experiments showed an effectively increase of 10 octane number requirement compared with baseline SI engine in a passive pre-chamber application at maximum brake torque conditions, while on the active side, a modest 3 octane number requirement increase was obtained. The improvement of jet reactivity and penetration led to a lower jet variability, explaining the better results of the pre-chamber applications. The reported results indicate that passive TJI is more suitable for taking advantage of the knock limit extension, not only for the reported octane number increase but also for the reduced assembly and implementation costs. Cooper et al. [19, 227] performed experimental investigations on a wide operating BMEP range with a passive TJI application in order to evaluate knock mitigation. Main results showed an improvement of combustion phasing around 9 crank angle degrees compared with conventional SI engine, avoiding the retard of the combustion phasing and the subsequently BMEP loss. Increased combustion velocity and stability were observed in the whole operating range, however, fuel improvements were only observed at highest loads. In Figure 2.46 main results of this investigation is presented.

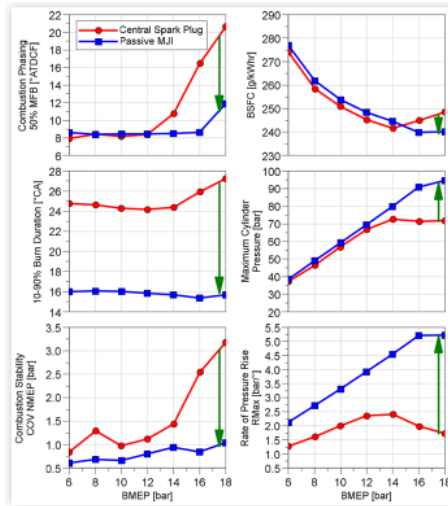


Figure 2.46: Comparison of the passive TJI and conventional SI over a BMEP sweep from 6 bar up to 18 bar at 4000 rpm [19].

2.3.3. Pre-chamber geometry aspects

The geometry of the pre-chamber in a pre-chamber ignition system plays a huge role as some aspects, such as the scavenging, the behavior of the jet ejection or main combustion characteristics, are highly dependent on the pre-chamber design.

Taking into account the rigidity of a pre-chamber system, which imposes a new fixed boundary condition, it is clear that a pre-chamber cannot be fully optimized in the whole operating engine map. Therefore, a compromise pre-chamber geometry design arises as the best solution to achieve the majority of the benefits while sacrificing some other aspects [231]. In this framework, the design of a pre-chamber application seems a very complex process where many kind of different sensitivities join in.

Some geometrical aspects that have to be highlighted are the pre-chamber internal volume, nozzle design (diameter and orientation), the location of the spark plug within the pre-chamber and the fueling strategy (for active applications).

2.3.3.1. Pre-chamber volume

The pre-chamber volume determines the total amount of available energy in the combustion process. Pre-chambers that feature larger volumes are able to increase the stored amount of mixture and thus, a greater quantity of energy can be provided in the formation of the jets and their latter ejection into the main chamber. On the other hand, a minor amount of mixture is required in pre-chambers with a smaller volume to ensure a proper combustion stability and repeatability, maintaining a suitable efficiency levels. Moreover, jet ejection process generally occurs at the end of the compression stroke, thus, a greater amount of burnt fuel within the pre-chamber does not increase the engine output power. So reducing the pre-chamber internal volume has another benefit from the thermodynamic point of view.

As it has been mentioned in the pre-chamber applications review Section 2.3.1, the volume of the pre-chamber mostly varies from 2% to 6% of the main chamber clearance volume at top dead center (TDC). As the pre-chamber is mostly located at cylinder head, its diameter is restricted, making its length the parameter to adjust the pre-chamber volume [258]. Some pre-chambers feature a narrow throat diameter which avoids the modification of the engine head to implement the pre-chamber [231]. This geometry accelerates the jet-exit velocity, however it may lead to a deterioration of the flow characteristics inside the pre-chamber.

Another aspect to have into account is the effective compression ratio of the engine. In a common pre-chamber design where the spark plug is exchanged with a pre-chamber assembly, the total volume of the pre-chamber has a direct effect on the CR, reducing the value of this parameter as the volume increases, thus leading to a decrease of the thermal efficiency. Moreover, pre-chamber internal volume may have an effect on the turbulence level inside the pre-chamber [236]. Results show that smaller pre-chamber volumes tend to increase the local turbulence inside the pre-chamber, while larger pre-chamber volumes are not as effective to transfer the turbulent energy to the vicinities of the spark plug, reducing the flame speed and hindering the performance of the pre-chamber.

2.3.3.2. Pre-chamber nozzles

The nozzle is one of the most critical aspects in the geometry selection. The nozzle quenches the flame, accelerates the intermediate products and drives them into the main chamber and distributes the ignition sites. Aspects such as pre-chamber scavenging, jet structure, jet-exit velocity or induced

turbulence are highly dependent on pre-chamber nozzle design. The nozzle design includes the selection of parameters such as orifice diameter, location, orientation or number.

In this context, the relationship between total cross-sectional area of the holes to the pre-chamber volume (A/V ratio) arises as an important parameter to characterize pre-chamber geometry since this relationship have a strong impact on residual gas fraction, turbulent kinetic energy, scavenging process or jet-exit velocity.

Regarding the scavenging process, smaller orifice diameters tend to increase pressure loss through the nozzle, thus reducing the gas exchange between chambers and avoiding the evacuation of the residual gases trapped from previous cycle. However, if the pre-chamber features larger orifice diameters it may lead to a loss of the mixture inside the pre-chamber, hindering the combustion itself and reducing the available energy to transfer to the jets [4]. In terms of flame quenching, larger orifice diameters tend to reduce the quenching of the flame compared with smaller orifice diameters [246]. However, an excessively reduced diameter may not be able to ignite the mixture in the main chamber. Finally, the jet-exit velocity is also highly affected by the selection of the orifice diameter. With smaller orifice diameters, the jet velocity tends to increase and then, increases the jet penetration length and reduces the combustion duration, making this jet-exit velocity parameter a key aspect in the nozzle design.

Moreover, the engine operating conditions have an impact on the optimal nozzle diameter. Results reported by Bunce et al. [254] showed that there is an optimum orifice area to mitigate knocking while advancing combustion phasing at high engine load conditions. Smaller orifice diameters tend to stabilize the oscillations caused by knock, mainly due to the reduced jet reactivity and the reduced mass flow. On the other hand, larger orifice diameters tend to reduce the jet-exit velocity, affecting the combustion phasing. Nevertheless, at low engine load conditions, smaller orifices are a better selection since shorter combustion duration and enhanced ignition are expected. In this framework, the selection of the orifice diameter arises as a compromise between the combustion and the scavenging processes.

The orientation of the nozzles is also a relevant aspect in the orifice design. Turbulence level inside the pre-chamber and scavenging process are strongly related to the orientation of the holes. Bolla et al. [259] analyzed the effect of the orientation of the orifices with a 3D RANS and LES numerical tools in a RCEM. Results reported indicate that the orientation of the orifices have a strong impact on turbulence intensity and fuel mass fraction in the vicinities

of the spark plug. Nozzles that provide a higher swirl create a fuel rich counter-vortex in the central axis of the spark plug and a high concentration of fuel near the electrodes of the spark plug but with low turbulence intensity. On the contrary, straight nozzles create a more turbulent mixture but with leaner ratio near the spark plug.

2.3.3.3. Spark plug design

The design of the spark plug includes the spark plug type, location, orientation and electrode gap as key parameters. The modification of the spark plug will lead to a modification of the flame kernel development and subsequently, to the modification of the combustion process within the pre-chamber [260].

Nevertheless, in small pre-chamber applications, such as TJI, the combustion development in the main chamber is less dependent on the spark plug design as long as it can be initiated by the reactive jets [218]. This effect is caused by the relatively large volume occupied by the spark discharge inside the pre-chamber [217].

Attard et al. [217] performed experimental activities modifying the provided energy by the ignition coil, from 75 to 5 mJ in an active TJI application. Main results showed that minimum required energy to initiate a stable combustion was lower than 10 mJ in a wide air dilution operating range, while reaching the operation limits required an increased energy source to assure a proper combustion process. Moreover, the ignition in the pre-chamber is not significantly affected by the spark plug energy variation, allowing extra benefits in terms of cost and service life.

2.3.3.4. Pre-chamber fuel injection strategy

As aforementioned, the active pre-chamber features an additional or auxiliary fuel injection within the pre-chamber combustion chamber, which increases the freedom degree number and opens a path for further optimizing the overall combustion process. Alternative fuels such as hydrogen [27, 137], methane [219] among other gaseous fuels are utilized in the auxiliary fuel injection.

A proper design of a gasoline injection involves advanced calculations such as the spray target, the relative air-to-fuel ratio, the mixture formation or the injection timing. In the case of active pre-chambers, the auxiliary amount of injected fuel is significantly lower compared to the main fuel injection

[261]. Moreover, conventional direct injection systems are not designed for such a small quantities of injected mass, being necessary the development of a special injector prototype for these applications [24].

Hua et al. [248] evaluated the injection timing of an auxiliary fuel injection, revealing that this timing should be set during the early stages of the compression stroke in order to assure a suitable air-fuel mixture in the pre-chamber and to avoid the fuel diffusion event from pre-chamber to main combustion chamber. However, Bunce et al. [254] found by means of advanced CFD tools that an excessive early fuel injection leads to an over-mixing within the pre-chamber mainly caused by the increased mixing time. Furthermore, injecting in early stages of the compression stroke may lead to a fuel leak through the nozzles before the spark ignition event, reducing the overall released energy. On the other hand, the fuel injection in latter phases of the compression stroke has a benefit in terms of combustion stability since it is guaranteed an suitable and ignitable mixture in the vicinities of the spark plug location. However, this strategy reduces the available time to vaporize the fuel, thus maybe reducing the quality of the process.

Not only the injection timing, but also the total amount of injected fuel plays a key role in the pre-chamber design process. This fuel amount directly affects to the pressure build-up and the combustion process within the pre-chamber. Attard et al. [220] reported that the slight enrichment of the air-to-fuel mixture within the pre-chamber benefits the formation of active radicals, thus increasing the repeatability and improving the combustion stability. However, extremely rich mixtures lead to a decrease of the combustion velocity, lower pressure build-up and a poorer jet ejection quality [262]. Furthermore, as the air-to-fuel ratio increases, the total amount of injected fuel should be increased in order to maintain a proper combustion stability in the main chamber. Experimental results performed by Peters et al. [228] supported this necessity.

2.3.4. Influence of pre-chamber applications on emissions

Since mankind is facing environmental issues related with the increase of harmful gases, the reduction, or at least the control of the emitted pollutants in the transportation sector becomes a critical aspect in the design of new applications.

All of the emitted pollutants in a SI engine are related with the combustion process. In one hand, some pollutants such as carbon monoxide (CO) or non burnt hydrocarbons (HC) arise when the combustion process is incomplete. While nitrogen oxides (NO_x) or carbon dioxide (CO_2) become more relevant in complete combustion processes.

A special pollutant is particulate matter (PM). In the evaluated kind of SI engine with a port fuel injection (PFI) strategy, such as the object of study of the present work, these emissions are not a relevant issue since the injection system provides a proper mixture homogeneity, which mostly eliminates this problem [219]. However, most of the upcoming vehicles may be equipped with a particulate filter to meet the EURO VII regulations, specially those of less than 23nm. In this regard, some authors such as Guido et al. [263, 264], have studied in detail the characterization of particulate number in natural gas fueled engines. They achieved a reduction of almost 99% of PN compared with the baseline engine by implementing different control strategies [263].

Emissions from a pre-chamber application depend on a series of factors such as the engine load, the pre-chamber geometry and configuration, the air-to-fuel ratio or the existence of an auxiliary fuel injection, among other parameters [265].

2.3.4.1. Emissions in active pre-chambers

As one of the main advantages of the active pre-chamber application is the combination of this ignition concept with the lean burn strategy, the main pollutant formation mechanisms within these kind of pre-chamber application are similar to those of that strategy.

In this way, a CO and HC emission lowering is expected at the very beginning of the lean operation. Nevertheless, the HC emissions are expected to increase when reaching ultra-lean operation ranges. In terms of NO_x , the resulting trend is opposite to the HC trend. There is a emissions increase at near-lean region operating and a decrease while increasing the dilution level.

A strong reduction of NO_x emissions even at part load was reported by Attard et al. [24]. An active pre-chamber application was evaluated between 1500-4000 rpm and 2-11 bar BMEP. A reduction of around 95% of NO_x emissions (see Figure 2.47) was expected in almost all evaluated conditions [215, 219].

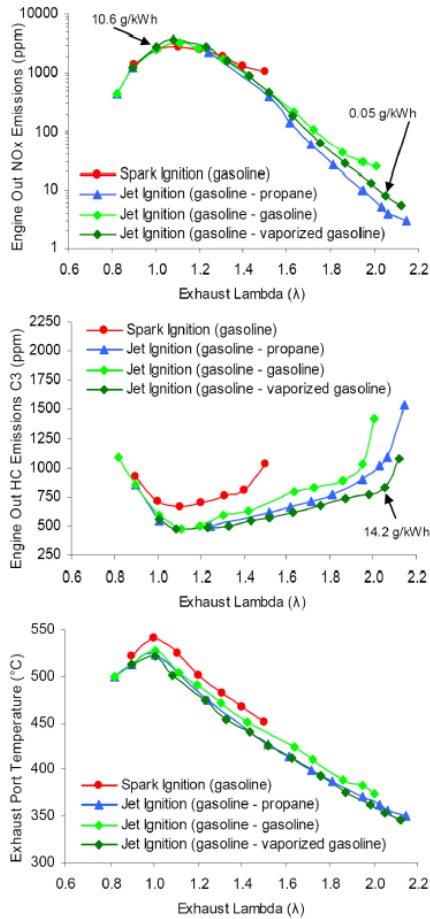


Figure 2.47: Engine out emission and exhaust port temperature comparisons of jet ignition dual fuel (gasoline-propane), liquid fuel (gasoline-gasoline) and vaporized fuel (gasoline-vaporized gasoline) together with spark ignition (gasoline) combustion systems. 1500 RPM, 4.7 bar IMEPn, (main chamber fuel - pre-chamber fuel) [24].

Continuing with NO_x pollutant, Stadler et al. [266] reported that the emissions could be lowered up to 0.2 g/kWh when operating at ultra-lean conditions ($\lambda > 2.0$). However, the remaining emitted NO_x are assumed to be related with the combustion within the main chamber.

Atis et al. [267] compared the diluted operation in a scavenged pre-chamber application between air and EGR, founding that EGR dilution is a better NO_x reducing agent at the cost of an increased HC emissions, caused

by a poorer combustion efficiency. In fact, the emissions of HC suffer a sharply increase beyond the lean limit due to the low combustion stability, which causes partial burning. This effect was also observed by Sementa et al. [268], describing how the increased HC emissions in an active pre-chamber application are related to the non-uniform behavior of the turbulent jets coming from each nozzle. Onofrio et al. [269] described how the sectional area along with the selection of operating parameters affect the trade-off between the obtained NO_x and HC and CO.

2.3.4.2. Emissions in passive pre-chambers

Stadler et al. [266] evaluated the raw emissions generated by a passive pre-chamber application with different geometrical configurations, such as the nozzle diameter, swirl angle or number of holes.

In general terms, passive pre-chamber features lower CO and HC emissions compared with an engine equipped with a conventional spark plug ignition system. This result indicates that combustion process is more efficient, leading to increased combustion completeness with a positive impact on engine efficiency.

According to some authors like Zhu et al. [38], no significant trends or differences can be found in terms of raw emissions for a passive pre-chamber application when modifying the pre-chamber configuration to maximize the thermal efficiency.

2.4. Conclusions

In this Chapter, an overview of the most relevant strategies to increase the thermal efficiency, including benefits and drawbacks has been presented. Moreover, a promising concept (pre-chamber ignition) that is able to solve these drawbacks and take advantage of the main benefits of lean burn and/or the use of Miller cycle has been introduced.

As it has been reported through many years of research activities, lean burn or diluted combustion are two strategies that can increase the overall thermal efficiency by means of higher heat specific ratio or lower pumping losses. Nevertheless, this efficiency increase cannot be infinite being the dilution limit the maximum reachable condition while keeping a suitable combustion process. When reaching this limit, the stability of the process is compromised and the power output significantly reduces due to misfire cycles.

On the other hand, Miller cycle is an effective strategy to increase the thermal efficiency by means of reducing pumping losses. However, this strategy has the main drawback of the limited compression ratio.

In this framework, the pre-chamber ignition system arises as a potential solution to overcome most of these drawbacks and thus, obtain the main benefits of these kind of strategies.

Key milestones of the pre-chamber ignition system and a complete revision of how this concept affects to combustion process, including main combustion aspects, geometrical effects and pollutant formation are presented in this Chapter.

In terms of combustion aspects, the introduction of a pre-chamber combustor requires a special attention to some processes such as the scavenging or the spark plug discharge timing in order to optimize the complete combustion process. The pre-chamber geometry, in terms of volume and hole layout (diameter, number of holes and location of them), arises as a critical aspect to take into account for an optimized combustion process, not only for the pre-chamber combustion itself, but also for the global process. Nevertheless, jet ignition has been shown to an excellent way to quicken the combustion velocity and obtain those aforementioned thermal efficiency benefits.

Regarding emissions, the stoichiometric operation of the passive pre-chamber ignition concept requires the use of a three-way catalyst to achieve the restrictive emission regulations. For an active pre-chamber application, if an ultra-lean operation ($\lambda > 2$) can be sustained, NO_x and CO emissions are significantly low, but an HC catalyst may be needed to reduce the HC emissions. On the other hand, if the ultra-lean operation is unattainable, raw NO_x and CO emissions must be reduced by means of a three-way catalyst, which significantly increases the implementation costs, making the application of this concept unapproachable.

Tools and methodology

3.1. Introduction

Main goal of this Chapter consists of introducing and discussing the main tools used in the elaboration of this work, both experimental and numerical, while explaining the methodology followed when running experimental campaigns.

Test bench facility and the different engine architectures used throughout the years to generate the experimental results are presented and explained in the different Sections of this Chapter, focusing on the main differences in terms of facilities and measuring devices. Also a description of the pre-chamber geometry and a summary of all tips used during the experimental campaigns.

Work on this chapter has been partly published in the following papers:

- Evaluation of the passive pre-chamber ignition concept for future high compression ratio turbocharged spark-ignition engines [1]
- Performance of the passive pre-chamber ignition concept in a spark-ignition engine for passenger car applications [2]
- Advantages of the unscavenged pre-chamber ignition system in turbocharged natural gas engines for automotive applications [3]
- Improving the performance of the passive pre-chamber ignition concept for spark-ignition engines fueled with natural gas [4]
- An experimental and one-dimensional modeling analysis of turbulent gas ejection in pre-chamber engine [6]

Regarding numerical tools, a description of the models, main hypotheses assumed and obtained results and the interaction between them is presented and discussed.

Explanation of the engine, test bench facilities and numerical tools can be also found in the different publications.

3.2. Experimental tools

In this Section 3.2, main experimental tools, including test bench facilities, different engine architectures used and pre-chamber tips are presented.

3.2.1. Test bench

A complete sketch of the test cell including all devices and elements used to perform the experimental activities is shown in Figure 3.1. This sketch includes both fueling systems, conventional gasoline and compressed natural gas, even when those systems did not coexisted at the same time.

Compressed air intake is controlled by an external compressor, needed to generate boost conditions and stored in a compressed air tank to avoid fluctuations of the system and/or possible backflows. Intake line counts with an air dryer, a heater to adjust air temperature and a flowmeter to measure the mass flow.

The fuel injection mode is indirect to assure a homogeneous mixture between fuel and air, and injection is performed around 140 mm before intake valves. Regarding the fueling system, the gasoline line includes an AVL 733S fuel meter to measure the mass flow and an AVL 753S fuel conditioner to maintain a proper fuel temperature during the experimental campaign. Fueling pressure is kept constant at a value around 5 bar by means of a fuel pump. The line is fed by a fuel tank of 50 liters that assures a supply for the experimental activities of the workday. Main specifications of the gasoline fuel are presented in Table 3.1.

When compressed natural gas is used to feed the system, fuel is obtained from a compressed natural gas (CNG) tank large enough to assure continuity of the experimental campaign during the workday. CNG line valves and pressure regulators to control the flow and secure the system. Fuel flow is measured with a BRONKHORST F-113AC-M50-AAD-44-V flowmeter. Pressure in CNG line is maintained at 20 bar minimum at least. Main specifications of the compressed natural gas fuel are presented in Table 3.2.

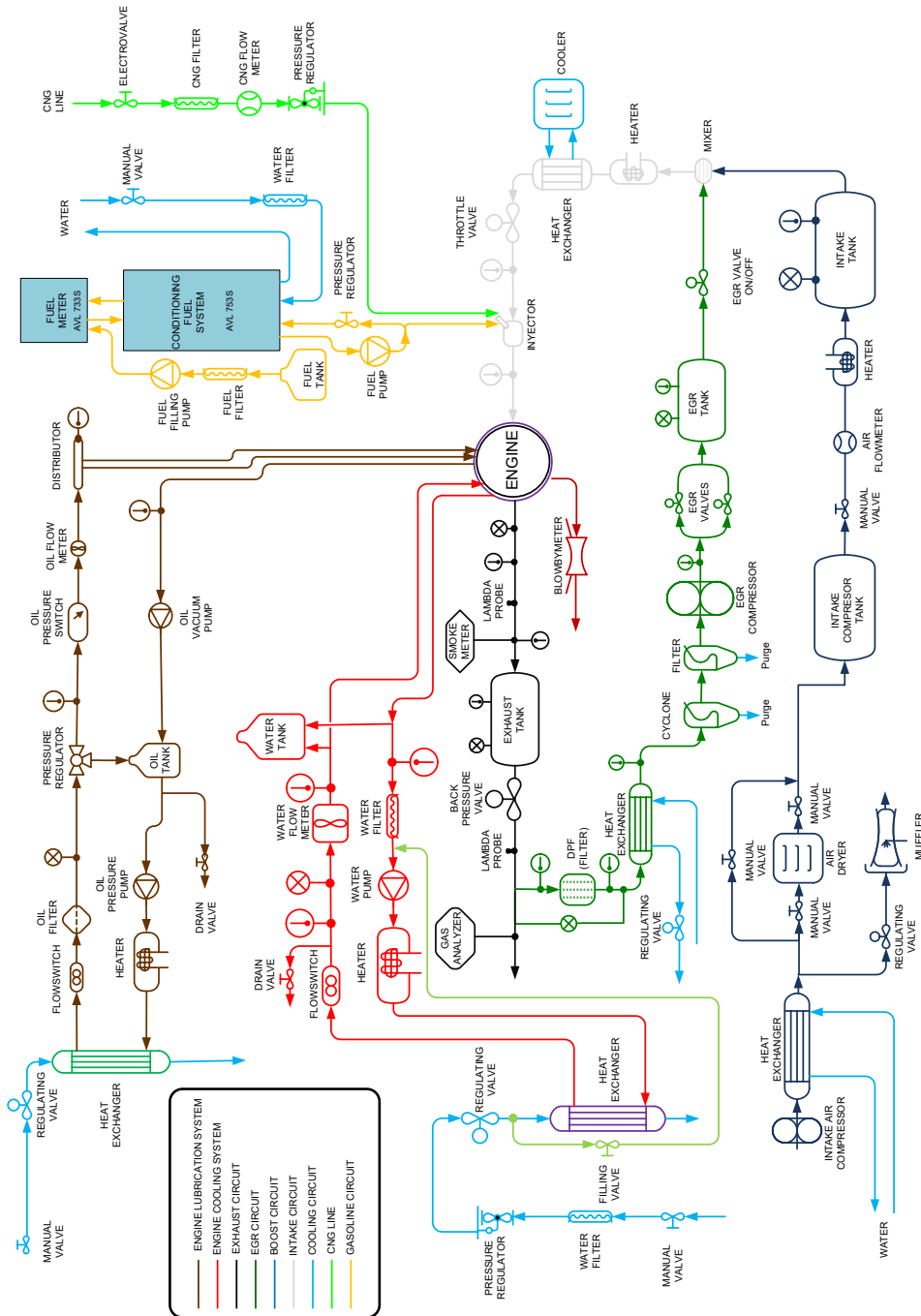


Figure 3.1: Layout of the engine test cell.

Table 3.1: Main specifications of the gasoline fuel.

Type	Gasoline RON95
H/C ratio [mol/mol]	1.761 mol/mol
O/C ratio [mol/mol]	0.0 mol/mol
Oxygen content [%]	0.0
A/F _{st} [-]	14.374
Lower Heating Value (LHV) [MJ/kg]	42.793
Density (15°C) [kg/m ³]	843.8
Kinematic viscosity (40°C) [cSt]	2.47
Reduced formula (C _x H _y O _z)	7.594 (x) - 13.376 (y) - 0.0 (z)

Table 3.2: Main specifications of the compressed natural gas fuel.

Type	CNG RON120
H/C ratio [mol/mol]	3.84 mol/mol
O/C ratio [mol/mol]	0.0 mol/mol
Oxygen content [%]	0.0
A/F _{st} [-]	16.72
Lower Heating Value (LHV) [MJ/kg]	48.931
Density (15°C) [kg/m ³]	5
Kinematic viscosity (40°C) [cSt]	18.72
Reduced formula (C _x H _y O _z)	1.077 (x) - 4.137 (y) - 0.0 (z)

The air-to-fuel ratio is measured by the assembled lambda sensors along the exhaust line and by the exhaust gas analyzer HORIBA MEXA 7100 DEGR. Regarding the pollutant emissions, an AVL 415 Smokemeter and the same exhaust gas analyzer HORIBA MEXA 7100 DEGR are installed to measure the pollutants coming from engine operation. The exhaust settling chamber is located in the exhaust line, and is needed to assure proper temperature for the gas analyzer measurements. HORIBA analyzer is able to track O₂, CO, CO₂, HC, NO_x and EGR rate measurements, while the AVL 415 Smokemeter traces soot emissions by the filter smoke number (FSN). Regarding the exhaust backpressure, it is controlled by means of a throttle valve located after the exhaust settling.

To provide the different EGR levels for the experimental campaign with diluted conditions a low pressure EGR system is assembled in the exhaust line after the exhaust settling and before the gas analyzer. Exhaust gas goes through an after-treatment system that includes particulate filters and a cyclone filter. Then, EGR is pumped by a dedicated compressor and stored in an EGR settling to avoid fluctuation of the mass flow. The desired EGR

level is achieved by means of valves and regulators controlling the total amount of EGR flow that is being added to the intake, even at highly boosted conditions.

In order to evaluate the average air-to-fuel ratio, the fresh air mass flow rate is divided by the injected fuel mass flow rate. Instantaneous intake and exhaust pressure, and in-cylinder pressure, are measured by means of piezoresistive and piezoelectric sensors, which their high frequency signals are sampled in a 0.2 cad resolution.

Oil circuit was designed to keep a constant oil pressure, assuring a proper lubrication process during all experimental campaign. For that purpose, this circuit has two pumps that are able to drive the oil through the system. Oil filter remove possible waste generated in the operation and the heater and heat exchanger keep oil temperature in reasonable values. Regarding water circuit, temperature and pressure is severely controlled and systems that require refrigeration are connected to the cooling system. This system is completely independent from the engine, avoiding possible safety issues.

3.2.2. Engine

The selected engine in the present work corresponds to a 4-stroke single-cylinder light-duty engine, which is a smaller version of a 4-stroke turbocharged spark ignition engine that will be available in the market in a close future.

Along the duration of different experimental campaigns carried out using the present engine, its architecture had suffered some modifications to adequate it to the necessities of the testing campaign. In this way, the very first version of the engine was operated with gasoline (RON95) and the standard Otto functioning cycle. Its main specifications at that moment of the campaign can be found in Table 3.3.

Table 3.3: Main specifications of the engine with standard Otto cycle.

Engine	4-stroke SI
Number of cylinders [-]	1
Displacement [cm ³]	404
Bore – Stroke [mm]	80.0 – 80.5
Compression ratio (geometric) [-]	13.4:1
Valvetrain [-]	DOHC
Number of valves/cylinder [-]	2 intake and 2 exhaust
Fuel injection system [-]	PFI (P _{max} 6 bar)
Kind of cycle [-]	Standard

The second evaluated version of the engine during experimental campaign had its functioning cycle as the Miller one. This cycle is able to reduce pumping losses and thus, increase the global performance of the engine. The compression ratio could be increased up to 15.4 in order to take advantage of this concept. This compression ratio value of 15.4 was calculated to match similar conditions of those obtained at PMS when operating with the conventional Otto cycle and compression ratio of 13.4. Main specifications of the engine during this part of the experimental campaign can be found in Table 3.4.

Table 3.4: Main specifications of the engine with Miller cycle.

Engine	4-stroke SI
Number of cylinders [-]	1
Displacement [cm ³]	404
Bore – Stroke [mm]	80.0 – 80.5
Compression ratio (geometric) [-]	15.4:1
Valvetrain [-]	DOHC
Number of valves/cylinder [-]	2 intake and 2 exhaust
Fuel injection system [-]	PFI (P _{max} 6 bar)
Kind of cycle [-]	Miller

Despite being some differences between functioning cycles, the engine shared same valvetrain system during the whole experimental campaigns. In this way, the cylinder head had four valves with double-overhead camshafts, which allow an improving of the cylinder scavenging and filling processes. Also, the regular Gasoline Direct Injection fuel supply concept was switched to a Port Fuel Injection concept. The new injection system was assembled at 140 mm from the intake manifold in order to assure a proper homogeneity of the air-to-fuel mixture. In the case of the valve overlap, it was removed for both cycles to avoid short-circuit losses.

Regarding fuel supply system, it is independent from the chosen engine architecture. In this way, half of the experimental campaign with Miller cycle uses gasoline as fuel, while the other half uses compressed natural gas.

3.2.3. Pre-chamber bodies

The implementation of different pre-chamber bodies can be directly performed as the conventional spark plug and the pre-chamber assembly share the same housing and location in the head engine. In this way, the exchange

between inductive spark plug ignition and pre-chamber concept, including the different pre-chamber bodies, can be done easily, reducing the time, and thus the cost, of the experimental activities.

A couple of schematic views of the engine and the pre-chamber housing are presented in Figure 3.2 and Figure 3.3, highlighting the location of the pre-chamber housing on the cylinder head.

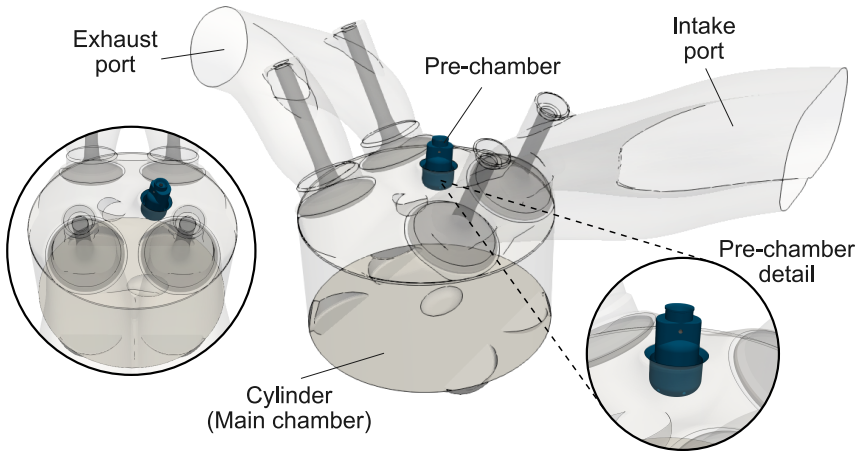


Figure 3.2: Schematic view of the pre-chamber assembly in the engine head.

In Table 3.5 main specifications of all evaluated pre-chamber geometries during the present work are shown. Note that not all of them are evaluated in all Chapters, but similar Tables including only the evaluated geometries in the corresponding Chapter will be included.

Table 3.5: Main specifications of the evaluated pre-chamber geometries.

	Tip 1 (PC 1)	Tip 2 (PC 2)	Tip 1b (PC 1b)	Tip 1c (PC 1c)	Tip new (PC new)	Tip comp (PC comp)
Volume [mm ³]	600	350	600	600	950	2000
Number of holes [-]	6	6	6	6	6	6
Hole diameter [mm]	0.7	0.7	0.7	0.7	0.7	0.95
Hole tang. angle [°]	7.5	7.5	12.5	0	7.5	7.5

The pre-chamber geometry is cylindrical with a total of 6 also cylindrical holes for all the evaluated tips, while total volume, hole diameter and hole tangential angle vary depending on the evaluated tip. For purposes of the

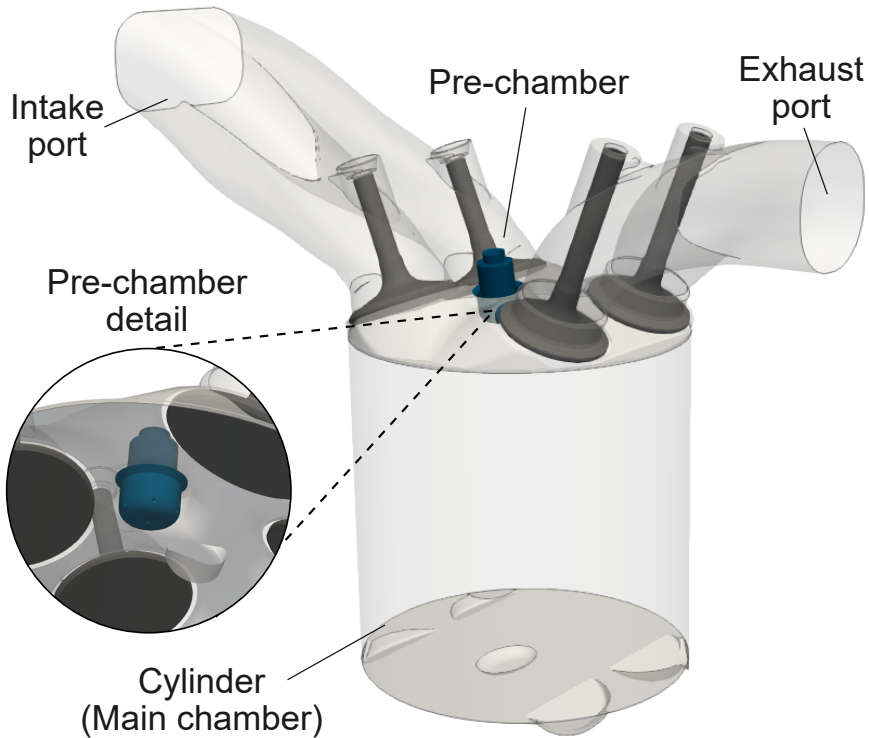


Figure 3.3: Schematic view of the pre-chamber assembly in the engine head.

present work, no special geometries are needed. However, more complex geometries with enhanced turbulence inside the pre-chamber will benefit the concept itself.

3.3. Numerical tools

In this Section 3.3, numerical tools, including combustion diagnosis, 1D Wave Action model and 1D Jet model are presented. Focusing on the relationship between the different models and the outputs generated by each one.

3.3.1. OD Combustion diagnosis

A complete in-house OD combustion diagnosis model [270, 271] was used to evaluate the global performance of the combustion process. This model was able to compute the heat release rate (HRR) from pressure signal, and then, obtain most relevant parameters related to the combustion process. These parameters included, among many others, indicated gross mean effective pressure (IMEP), start of combustion (SoC), combustion phasing (CA50) and duration (CA1090), maximum pressure and pressure gradient, combustion stability and cylinder mean gas temperature.

Results from this combustion diagnosis tool were used both to evaluate experimentally the performance of the concept and as inputs for the 1D numerical tools. In the methodology Section 3.4, deeper explanation of how were these three models joined can be found.

3.3.2. 1D Wave Action model

The second numerical tool utilized during the present work was the 1D Wave Action model. This numerical tool frames within a commercial software (GT-Suite) commonly used in the automotive industry.

The main model counted with a series of submodels that were able to simulate all parts of the test bench facility, the engine itself and the pre-chamber, including main relevant sections such as intake, exhaust or EGR line. Also, dedicated submodels to evaluate jet momentum, fuel mass inside the pre-chamber at combustion start or transferred energy were included. The model was validated against experimental results in several combinations of engine load and speed conditions. The calibration was performed by setting the air mass flow and the total injected fuel, then, some parameters such as heat release settings, discharge coefficients or heat transfer losses were modified until matching the simulated pressure profile to the experimentally obtained profile. In-cylinder, intake and exhaust pressure profiles for experimental and simulated cases can be found in Figure 3.4, Figure 3.5 and Figure 3.6 respectively, proving the model was able to accurately reproduce the experimental trends, making it suitable for further analysis.

Main chamber and pre-chamber were connected by a series of pipes and holes simulating the pre-chamber nozzles. The pre-chamber was simulated as a non-moving piston, making the model able to reproduce the evolution of pressure in both chambers and the exchange of mass and energy between them, based on the heat release evolution. Since there was no dedicated

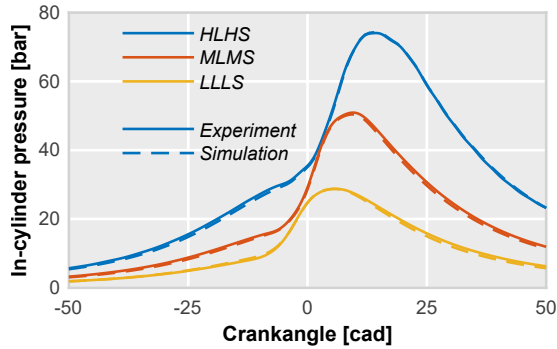


Figure 3.4: Comparison of experimental and simulated in-cylinder pressure profiles.

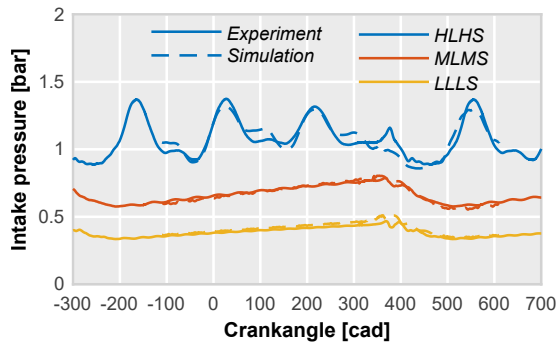


Figure 3.5: Comparison of experimental and simulated intake pressure profiles.

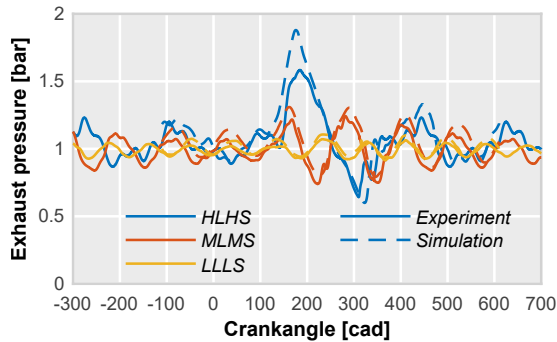


Figure 3.6: Comparison of experimental and simulated exhaust pressure profiles.

pressure transducer within the pre-chamber, the heat release evolution inside it was only imposed by means of a regular Wiebe function, which

was modeled by setting its combustion phasing (CA50) related to the spark triggering event and its duration (CA1090) to a suitable values depending on the global air-to-fuel conditions. Gas velocity and mass flow were recorded in one of the nozzles of the pre-chamber in order to obtain the resulting jet momentum flux and velocity profiles. This jet momentum flux and mass flow rate were used as inputs in the 1D Jet model. As this is a simple 1D model, the evolution of the gases in both chambers was simulated as a perfect and homogeneous mixture whose evolution was dependent on the combustion process evolution. Moreover, the resulting ejected jets in this model were a mixture of unburned gases (air and fuel), and products resulting from combustion process, such as CO, CO₂, H₂O or N₂.

Intake, exhaust and EGR lines were modeled as a series of pipes representing the different tubes of each line. The butterfly valve was simulated by means of an actuator that modified the diameter of the pipe in where it was installed in the intake. The fuel injector was included in the model in the last pipe of the intake. Also the compressor and the actuators of the EGR line were included in the exhaust line.

However, for extended geometry analysis, this complete model featured times around 2 hours for a single simulation, making it unapproachable to generate design of experiments in where several simulations will be performed. To solve this problem, a simplified model was developed. This simple model only included the chambers and the relevant parameters calculations, such as the jet momentum flux or the mass fuel inside the pre-chamber. This model focused on the closed part of the engine cycle (from IVC to EVO), where ignition, combustion inside the pre-chamber and ejection processes occur. In this model, calibration was made by setting the pressure and temperature at intake valve closing, and then, modifying similar parameters of heat transfer and losses and discharge coefficient as in the complete model. Regarding the mixture, mass fractions of air and fuel were set to match the overall air-to-fuel ratio, including products of combustion process to simulate, if needed, the evaluated amount of EGR.

3.3.3. 1D Jet model

The third numerical tool utilized in the present work was a 1D Jet model, similar to the one used in the different published articles [4, 6]. As explained in the other documents, this 1D Jet model was adapted from an actual model, whose main applications involved Diesel-like sprays [272–274]. Nevertheless, this tool was modified in order to simulate gaseous jets from a pre-chamber application. Main results obtained with this tool

included the jet penetration length profile and the time needed for the jet to reach the further wall, referred as t^* . These modifications were presented in the document [6], but for clarification purposes, the main hypotheses assumed are listed here:

- Only the turbulent mixing of hot ejected pre-chamber gases with the mixture in the main chamber was considered.
- Free-jet propagation was accounted for, omitting the interactions between piston-bowl surface and hot turbulent jets.
- Main inputs of this 1D model were the temporal evolution of jet momentum flux and mass flow through one of the pre-chamber nozzles. These inputs were obtained by means of the 1D Wave Action model.
- Also, main chamber pressure and density were obtained from the 1D Wave Action model. These inputs were the boundary conditions of the 1D Jet model simulations.
- The pre-chamber gaseous jets were modeled as a gas stream coming from the pre-chamber nozzles into the main combustion chamber. This main chamber was filled with a perfectly mixed air and fuel mixture, assuming a low Mach approach and an ideal gas equation of state.
- The pre-chamber gaseous jets were assumed to be a stream of high temperature fluid (around 1500K) that were ejected into a lower temperature region (around 700K). For simplification purposes, the mixture composition at the exit of the simulated pre-chamber nozzle and temperature were considered independent from the time.
- The radial cone angle was set at 25° for all simulations. This was made to accommodation purposes of the initial part of the ejection process. This part may be difficult to simulate, especially in these kind of 1D tools, where the uncertainties of the very first steps of the flow ejection might not be properly simulated.

3.4. Methodology

In this Section 3.4, the procedure followed to carry out the activities, both experimental and numerical, is presented.

3.4.1. Experimental activities

The three main operating condition points studied in the actual work were chosen because they compromise the performance of the pre-chamber system in different ways. The mid-to-high engine load (12.8 bar IMEP) and speed point (4500 rpm) compromises the scavenging and filling of the pre-chamber, which arises as a critical aspect in the passive pre-chamber ignition system. Assuring a proper gas exchange between chambers is mandatory for the application of this ignition concept. Furthermore, the impact of the passive pre-chamber system in terms of knocking tendency was evaluated, but staying i the safety side was mandatory in any case. The low engine load (2.85 bar IMEP) and speed (1350 rpm) operating point was selected due to the limitation of the available fuel mass inside the pre-chamber, compromising the functioning of the concept itself and the activation of the exhaust after-treatment. The medium engine load (6.8 bar IMEP) and speed (2000 rpm) point was selected as representative of the average engine use in passenger car applications. During all experimental campaigns, a series of 250 cycles were recorded in order to achieve a consistent average and dispersion results. In Table 3.6 the three operating points are summarized.

Table 3.6: Studied operating points.

Parameter	OP1	OP2	OP3
Engine speed [rpm]	4500	1350	2000
Gross IMEP [bar]	12.8	2.85	6.8

Experimental activities of Chapter 4 consisted of evaluating the three operating points comparing the resulting performances when switching from conventional spark ignition to passive pre-chamber system. Two different pre-chamber geometries were tested, which their internal volume and total hole area were modified but keeping similar area-to-volume ratio. The target IMEP was obtained by sweeping the the spark timing until achieving the maximum brake torque (MBT) at stoichiometric conditions without any EGR addition operating with the conventional spark ignition system. The total amount of fuel and air were obtained to match the targeted IMEP, and then, for the operation with pre-chamber system, these values were kept constant. This methodology was repeated for all engine architectures in order to assure similar amount of energy during the campaign.

Regarding Chapter 5, several experimental activities were carried out modifying the spark timing or increasing the dilution ratio, both by air and EGR. In the case of air dilution only the mid-to-high engine load and speed point (OP1) was evaluated, while the EGR dilution campaign was performed for the three operating points. As a reference, MBT at stoichiometric conditions in each engine architecture was the same as in the previous implementation chapter. The total amount of fuel and air were kept constant during all sweeps. The air dilution ratio was increased in steps of 0.2 until reaching the dilution limit (defined as the point where cycle-to-cycle variability was unacceptable). The EGR dilution ratio was increased in steps of 5% until reaching the dilution limit. In both cases, the spark timing was moved until achieving the MBT at the desired dilution ratio. For the low engine load and speed point a spark timing sweep was also performed modifying the start of the ignition triggering event in steps of 2 cad. This evaluation was combined with two different strategies to increase the exhaust temperature compared with the one obtained with the conventional spark ignition system. First strategy was to increase the intake temperature, while second strategy consisted in diluting the mixture with external EGR.

Regarding the engine maps presented in these two Chapters, similar methodology was followed as in the evaluation of a single operating point from Chapter 4. The gross IMEP was reached with the conventional spark ignition system and the total amount of provided energy by the fuel was kept constant when switching to passive pre-chamber ignition system.

In Chapter 6, similar spark timing and EGR dilution sweeps as in previous Chapter 5 were performed. Again, the total amount of fuel and air was obtained for the stoichiometric case of conventional spark ignition system and kept constant in all cases of each sweep.

3.4.2. Numerical analysis

Two different methodologies were followed during the numerical activities. The first methodology had a quantitative analysis approach of the most relevant parameters in the passive pre-chamber operation. A direct implementation of the experimental results obtained with the OD combustion diagnosis tool in the 1D Wave Action model was performed to obtain numerical results that are impossible to experimentally measure, such as the jet momentum flux or the fuel mass inside pre-chamber at the onset of combustion. The complete model was used to obtain numerical results with

this approach. This kind of analysis allows to broaden the knowledge of the concept, and thus, to establish relationships between parameters and set some designing paths.

The second methodology had a qualitative analysis approach. Similar pressure, temperature at IVC, main chamber heat release rate or fuel mass among other parameters were kept constant as the first approach. In this case, the simplified model was used to carry out the numerical activities. This methodology was used to carry out several simulations modifying some basic geometrical aspects of the pre-chamber, such as internal volume, hole diameter or number of holes. Also this approach was taken to modify the combustion process inside the pre-chamber to heat release profiles that were not able to reach them experimentally. Start of combustion or duration were modified with this approach.

3.4.2.1. Design methodology

The combination of the simplified 1D Wave Action model and the 1D Jet model led to the development of a basic geometrical pre-chamber parameters design methodology that showed an improve of the performance of the passive pre-chamber ignition concept. Main hypothesis assumed in the present workflow was that reducing the time that the jet needed to reach the further wall (t^*) will turn into a better sweep of the main chamber, and then, an increase of combustion velocity, which could lead to further dilution limits, increasing the overall performance. In Figure 3.7 the workflow developed for designing new pre-chamber geometries is presented.

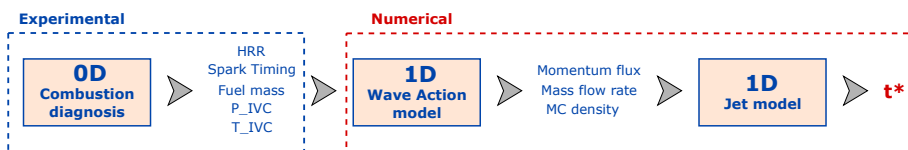


Figure 3.7: Schematic layout of the design workflow coupling the different numerical tools.

Main experimental results, such as heat release rate, fuel mass or pressure and temperature at IVC coming from the 0D combustion diagnosis tool were used as inputs into the 1D Wave Action model. In this first 1D tool, a series of simulations modifying the basic pre-chamber geometry (pre-chamber internal volume and total hole area) were performed. The experimental input parameters were kept constant for all simulations at the same conditions. Main results of the design matrix, including jet momentum flux and mass

flow rate from one of the holes, were used as inputs to the 1D Jet model. These two parameters mainly govern the ejection process. The t^* values are obtained from the 1D Jet model using the different jet momentum fluxes and mass flow rates from the previous 1D Wave Action model. The lower t^* value the better combination of internal pre-chamber volume and total hole area in terms of main chamber sweep. However, this methodology can not only be used to modify pre-chamber volume. Any relevant aspect or parameter that influences the jet momentum flux can be studied within this framework. Main advantage of this design methodology is that the t^* parameter can be used as a benchmark of the pre-chamber performance despite its geometry and/or operating conditions.

3.5. Conclusions

In this Chapter, main experimental and computational tools used during the development of the present work have been presented. Main goal was to introduce and present the links between them, highlighting the connexion and the workflow followed to fulfill the objectives.

Test bench facility was completely described, including all circuits and subsystems. The two different engine architectures evaluated were presented and summarized, focusing on the main differences, especially when switching the type of fuel, and main specifications of the fuels were introduced. Also, pre-chamber geometries evaluated during the present work are summarized.

The three different numerical tools were presented and described, highlighting the main outputs of each one and the relationship between these different tools. It was shown how the outputs obtained from each model can be used as inputs to the other one.

Methodology to obtain results, both experimental and numerical, with each tool, was presented. Main procedure in the experimental campaign was to keep the same amount of provided energy by the fuel, modifying the amount of air, EGR or the ignition system.

A design methodology from the experimental-numerical workflow was developed. Using the results of each tool as inputs for the next one in the workflow a basic pre-chamber design methodology was created, allowing to increase the pre-chamber performance by optimizing the benchmark t^* parameter.

Implementation of the concept

4.1. Introduction

The objective of this Chapter is to implement and discuss the passive pre-chamber concept in a 4-stroke spark-timing single-cylinder turbocharged engine able to reproduce the performance of the upcoming set of passenger car engines. The easiness to switch between ignition concepts and the potential to increase the performance of the engine makes this ignition system a very interesting solution in mid-term internal combustion engines.

This implementation was carried out using both calibrated gasoline as fuel (Research Octane Number 98) and calibrated compressed natural gas (Research Octane Number 120), their main characteristics are presented in Table 4.4 and Table 4.5. Furthermore, the implementation of the concept was done in two different engine architectures, with different compression ratios and thermodynamic cycles. The aim of exploring different engine architectures lies in a further comprehension of the performance of this ignition concept. The characteristics of the engine are presented in Table 4.3 and Table 4.7.

Work on this chapter has been partly published in the following papers:

- Evaluation of the passive pre-chamber ignition concept for future high compression ratio turbocharged spark-ignition engines [1]
- Performance of the passive pre-chamber ignition concept in a spark-ignition engine for passenger car applications [2]
- Advantages of the unscavenged pre-chamber ignition system in turbocharged natural gas engines for automotive applications [3]

The main operating conditions points studied in this chapter can be found in the present Table 4.1. These points are studied from Section 4.2 to Section 4.4, while in the Section 4.5 several points of the engine map were selected and evaluated to have a better understanding of the global issues of the concept. The main geometrical parameters of the studied pre-chambers are shown in Table 4.2.

Table 4.1: Studied operating points from Section 1.2 to Section 1.5.

Parameter	OP1	OP2	OP3
Engine speed [rpm]	4500	1350	2000
IMEPg [bar]	12.8	2.85	6.8

Table 4.2: Main geometrical parameters of the studied pre-chambers.

	Pre-chamber 1 (PC 1)	Pre-chamber 2 (PC 2)
Volume [mm ³]	600	350
Hole diameter [mm]	0.7	0.7
Number of holes [-]	6	4

Main results of this experimental stage were presented in the Articles [1] and [3] and in the International Conference [2].

4.2. Implementation of the concept in stoichiometric conditions using gasoline as fuel

Direct implementation can be directly performed since the spark of the conventional ignition concept and the pre-chamber and spark assembly of the TJI concept share the same housing in the head engine. In Figure 4.1 an schematic view of the assembly of the concept can be seen. This architecture allows a fast and easy exchange between concepts and/or different pre-chambers, which reduces the time needed to perform the experimental activities.

The engine characteristics where this first implementation was carried out is presented in Table 4.3. While the main characteristics of the gasoline fuel can be seen in Table 4.4. A detailed explanation of the engine architecture can be found in Chapter 3 and in the presented Articles [1–3].

4.2. Implementation of the concept in stoichiometric conditions using gasoline as fuel | 89

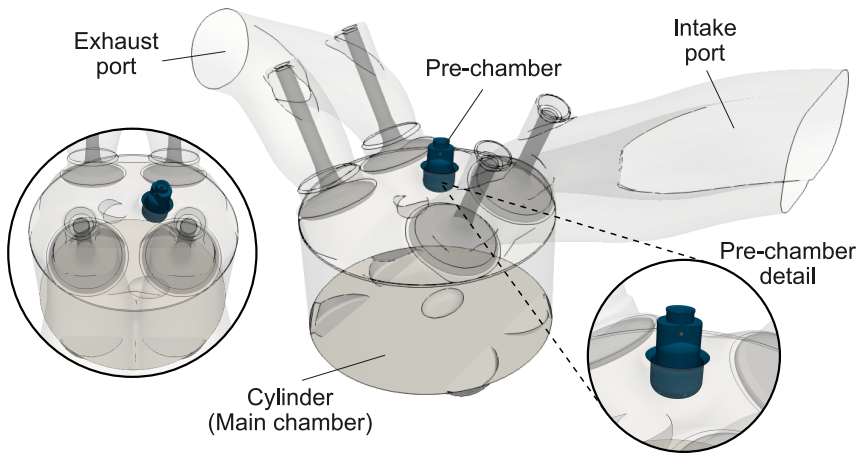


Figure 4.1: Schematic view of the pre-chamber assembly in the engine head.

Table 4.3: Main specifications of the engine.

Engine	4-stroke SI
Number of cylinders [-]	1
Displacement [cm ³]	404
Bore – Stroke [mm]	80.0 – 80.5
Compression ratio (geometric) [-]	13.4:1
Valvetrain [-]	DOHC
Number of valves/cylinder [-]	2 intake and 2 exhaust
Fuel injection system [-]	PFI (P _{max} 6 bar)

Table 4.4: Main specifications of the gasoline.

Type	Gasoline RON95
H/C ratio [mol/mol]	1.761 mol/mol
O/C ratio [mol/mol]	0.0 mol/mol
Oxygen content [%]	0.0
A/F _{st} [-]	14.374
Lower Heating Value (LHV) [MJ/kg]	42.793
Density (15°C) [kg/m ³]	843.8
Kinematic viscosity (40°C) [cSt]	2.47
Reduced formula (C _x H _y O _z)	7.594 (x) - 13.376 (y) - 0.0 (z)

The first selected operating point to implement this ignition concept corresponds to the combination of high engine speed and medium-to-high engine load (12.8 bar gross IMEP at 4500 rpm). The main reasons to operate in

these conditions are, on one hand that the filling of the pre-chamber is compromised when operating in a high speed regime and, on the other hand, that a high engine load increases the risk of operating in knocking conditions, which causes a delay in the ignition time to assure a safe operation.

Results of the pressure and heat release rate profiles comparison between conventional ignition system and pre-chamber ignition system can be found in Figure 4.2. Dark colors are the results of the average pressure and release rate profile, while in light colors the average dispersion is presented. As mentioned in Chapter 3, for the average calculation, a series of 250 cycles were recorded.

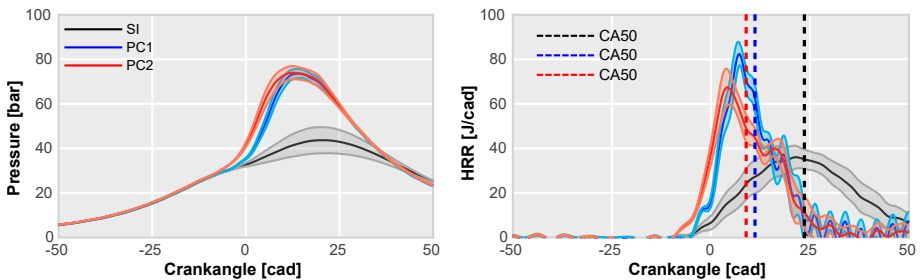


Figure 4.2: Pressure (left) and heat release rate (right) profiles of the high engine load and speed conditions at $\lambda = 1$ operating with gasoline for conventional ignition system (black) and both passive pre-chamber geometries (blue and red). Dashed lines correspond to 50% of combustion (CA50).

From this figure, it can be seen that the direct implementation of the concept shows an increase in the heat release ratio for the pre-chamber cases, leading to a significant reduction in the combustion duration (up to 2 times lower). This increase in the combustion velocity allows to improve the combustion phasing which turns into an increase of the gross indicated efficiency by means of advancing the spark timing up to values that optimize combustion phasing. This improvement is explained because the combustion phasing of the conventional ignition system cannot be properly set since knocking issues related to this operating point force to shift the combustion towards the expansion stroke to assure a safe operation, causing a decrease in the gross indicated efficiency.

Conventional spark ignition system shows a clearly delayed combustion phasing compared to the passive pre-chamber concept combustion phasing. Results of this operating point are presented in Figure 4.3, where a comparison of combustion phasing, combustion velocity, combustion efficiency and gross indicated efficiency for both ignition systems can be seen.

4.2. Implementation of the concept in stoichiometric conditions using gasoline as fuel | 91

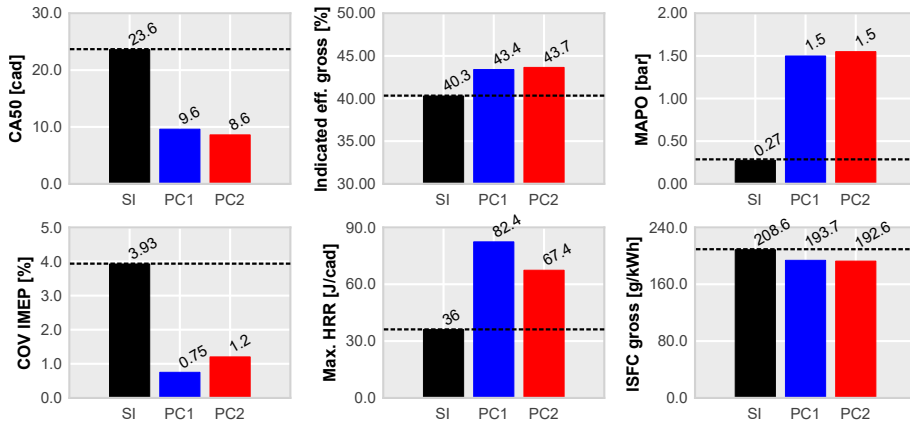


Figure 4.3: Comparison of combustion phasing (CA50), gross indicated efficiency, MAPO, combustion stability (COV IMEP), combustion velocity and fuel consumption for both ignition systems at high engine load and speed conditions at $\lambda = 1$ operating with gasoline.

Results confirm that direct operation of the passive pre-chamber ignition system in stoichiometric conditions increase the performance of the engine at this operation point even with different pre-chamber geometries. This is caused by the fast combustion velocity that allows an advance in the combustion phasing. This better phasing in addition to a high combustion stability achieved by the passive pre-chamber concept turns into an increase of around 3 percentage points in the gross indicated efficiency, also observable in the fuel consumption. This decrease of the combustion dispersion is related to the consistency of the ignition source that ignites the main chamber. As there are no propagation issues at these operating conditions, a proper flame development and combustion are achieved within the pre-chamber, then, the ejected jets full of reactive species are able to ignite the mixture in the main chamber acting each of them as different ignition sources which increases this combustion stability.

Regarding the knocking levels, it is seen that the engine is strictly compromised at these operating conditions, however for the new ignition system, a proper functioning is achieved. MAPO is increased due to the combustion velocity increase of the passive pre-chamber system, which increases pressure and temperature of the end-gas, promoting the auto-ignition. Combustion stability improves because of the increased surface and volume provided by the passive pre-chamber system for the ignition process, thus reducing the impact of local conditions during the start of the combustion process,

such as in the case of conventional spark plug system. The acceptable limit for the MAPO result strongly depends on the engine architecture and the ignition source, therefore, it is considered that is a better practice to index the relative MAPO values when operating with the conventional spark plug system. Anyway, the experimental campaign was carried out in agreement with the maximum and minimum values provided in the literature and always working in the safety side of the mechanical integrity of the engine.

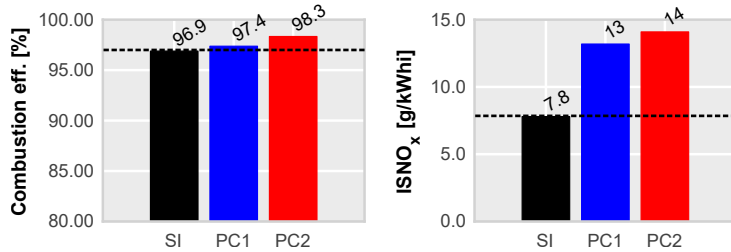


Figure 4.4: Comparison of combustion efficiency and emitted NO_x for both ignition systems at high engine load and speed conditions at $\lambda = 1$ operating with gasoline.

Regarding the emitted pollutants, in Figure 4.4, a comparison of the combustion efficiency (CO and HC emissions) and NO_x is presented. In terms of combustion efficiency, it is seen an increase of this efficiency for the passive pre-chamber ignition system. Less unburned HC and CO are present in the emissions, together with an increase of NO_x emissions.

Continuing with the second selected operating condition, it is a combination of a low engine load (2.85 bar IMEP gross) and low engine speed (1350 rpm). This operating point was selected due to the limited fuel mass in the pre-chamber at the start of combustion, which can compromise the viability of the concept itself. Results of the pressure and heat release rate are presented in Figure 4.5.

In this case, the pressure differences between concepts have been reduced, however pre-chamber 1 keeps a higher maximum pressure compared with the spark ignition system. This limited pressure difference is caused by the reduced fuel mass of the operating point compared to the high engine load point. This effect is also observable in the release rate profile. Pre-chamber 1 profile is faster than conventional spark ignition profile, but the maximum peak is considerably lower compared to the high engine load case.

Main results of the implementation of the concept when operating at low engine load and speed conditions are shown in Figure 4.6. Same parameters as in the previous results are analyzed. Combustion phasing (CA50), velocity

4.2. Implementation of the concept in stoichiometric conditions using gasoline as fuel | 93

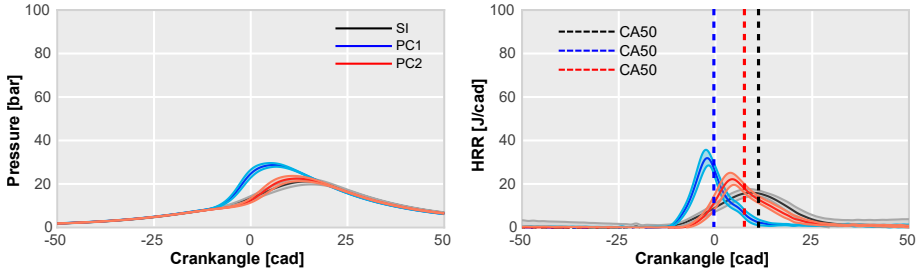


Figure 4.5: Pressure (left) and heat release rate (right) profiles of the low engine load and speed conditions at $\lambda = 1$ operating with gasoline for conventional ignition system (black) and both passive pre-chamber geometries (blue and red). Dashed lines correspond to 50% of combustion (CA50).

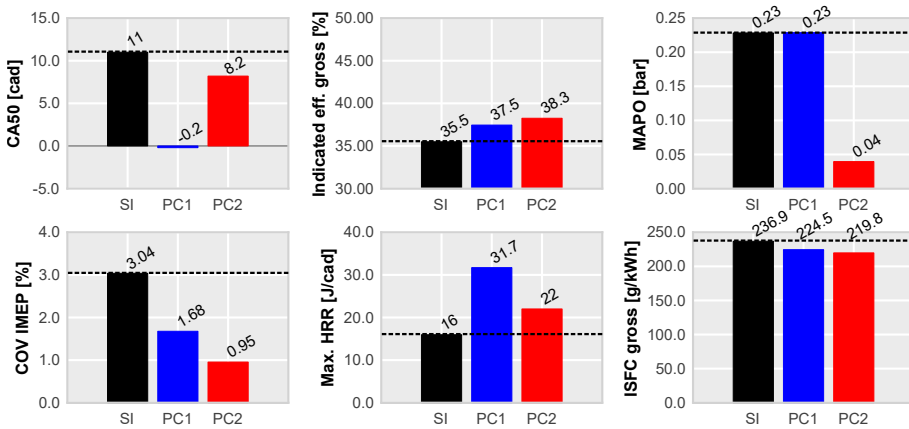


Figure 4.6: Comparison of combustion phasing (CA50), gross indicated efficiency, MAPO, combustion stability (COV IMEP), combustion velocity and fuel consumption for both ignition systems at low engine load and speed conditions at $\lambda = 1$ operating with gasoline.

and stability keep the same trends as in the high engine load case, so the combustion generated by the pre-chamber system is faster, more advanced and more stable than that of the conventional system. This causes an increase in the gross indicated efficiency, however this increase is slightly lower than the increase of the high engine load case. Regarding knocking issues, as the engine load is decreased, there is no need to delay the combustion start of the conventional system.

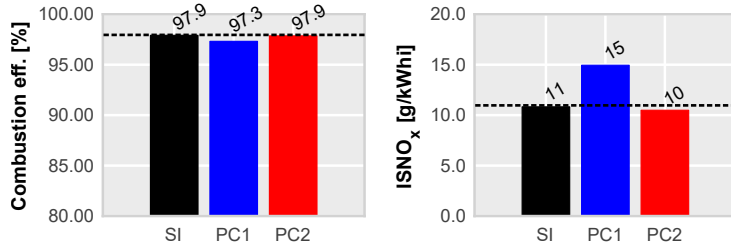


Figure 4.7: Comparison of combustion efficiency and emitted NO_x for both ignition systems at low engine load and speed conditions at $\lambda = 1$ operating with gasoline.

Regarding pollutants in this operating point, results of main emissions are shown in Figure 4.7. The combustion efficiency is kept at similar values in both systems, while the NO_x emissions are similar to the high engine load case.

The final operating studied point is a combination of medium engine load and speed, which is in between the two previous points. This point was chosen to confirm the observed trends in the previous points.

Pressure and release rate profiles of this operating point are presented in Figure 4.8. These profiles are higher compared to the low engine load case, as a result of the increase of the fuel mass. It is remarkable that pre-chamber 1 has the faster combustion profile no matter the engine load. The reason probably lies in the internal geometry of the pre-chamber and the turbulence generated inside, that accelerates the combustion velocity.

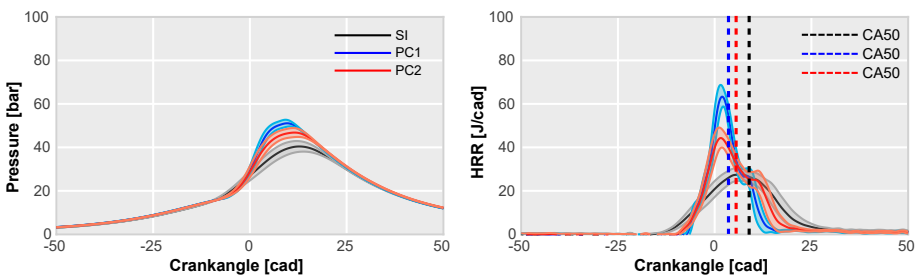


Figure 4.8: Pressure (left) and heat release rate (right) profiles of the medium engine load and speed conditions at $\lambda = 1$ operating with gasoline for conventional ignition system (black) and both passive pre-chamber geometries (blue and red). Dashed lines correspond to 50% of combustion (CA50).

4.2. Implementation of the concept in stoichiometric conditions using gasoline as fuel | 95

Main combustion parameters are shown in Figure 4.9. These results are consistent with the previous results. There is a combustion phasing advance and an increase in the combustion velocity. Results keep showing an increased indicated efficiency, however this increase is lower than that observed at the high engine load case. MAPO levels are a bit higher compared to the low engine load case but insufficient to reach knocking conditions and force a delay in the combustion onset.

In terms of pollutants, the results are presented in Figure 4.10. Combustion efficiency is slightly higher for the pre-chamber ignition system, reducing the CO and the unburned HC emissions, and as in previous results, while NO_x emissions also consistently increase.

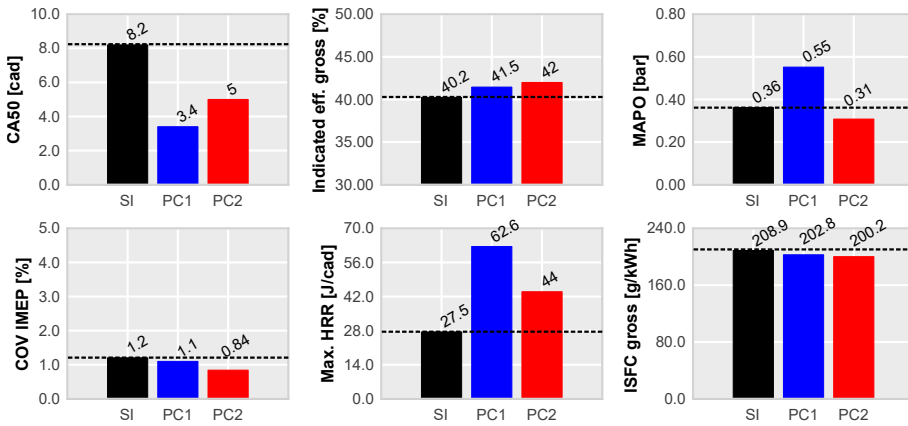


Figure 4.9: Comparison of combustion phasing (CA50), gross indicated efficiency, MAPO, combustion stability (COV IMEP), combustion velocity and fuel consumption for both ignition systems at medium engine load and speed conditions at $\lambda = 1$ operating with gasoline.

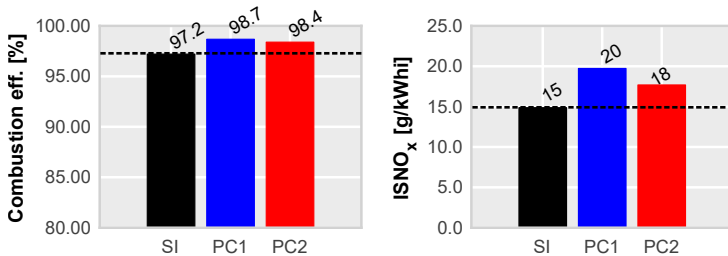


Figure 4.10: Comparison of combustion efficiency and emitted NO_x for both ignition systems at medium engine load and speed conditions at $\lambda = 1$ operating with gasoline.

In summary, these promising results encourage the evaluation of the compatibility of this passive pre-chamber ignition system with other strategies targeting the increase of the overall thermal efficiency, such as the air dilution (lean burn) or the addition of external EGR. Furthermore, the use of a fuel with a reduced CO₂ emissions compared with conventional gasoline, such as compressed natural gas (CNG), is a very promising investigation pathway.

4.3. Implementation of the concept in stoichiometric conditions using compressed natural gas as fuel

After the first implementation and analysis of this ignition concept, next step consisted of evaluating this new concept using compressed natural gas (CNG) as a fuel keeping the same engine architecture as in previous Section 4.2. Main characteristics of this fuel are presented in the Table 4.5, recovered from previous Chapter. The operating condition points were kept the same in order to have a direct comparison between fuels.

Table 4.5: Main specifications of the compressed natural gas.

Type	CNG RON120
H/C ratio [mol/mol]	3.84 mol/mol
O/C ratio [mol/mol]	0.0 mol/mol
Oxygen content [%]	0.0
A/F _{st} [-]	16.72
Lower Heating Value (LHV) [MJ/kg]	48.931
Density (15°C) [kg/m ³]	5
Reduced formula (C _x H _y O _z)	1.077 (x) - 4.137 (y) - 0.0 (z)

However there are some implications of switching the kind of fuel that must be taken into account before analyzing the new ignition system. One of the main differences between both types of fuels is related to the thermochemical properties of the mixture, including the auto-ignition delay or laminar flame speed properties, which have been proven to be critical parameters for the combustion process. Deep investigation about this topic has been presented in the article [3].

As a first step, a modeling work to evaluate the impact in the laminar speed of the flame was done. Maintaining the same IMEP gross target and the same gross indicated efficiency the required air flow rates for each fuel were estimated. Taking an stoichiometric air-to-fuel ratio (A/F_{stoich}) of the gasoline of 14.374 and a value of natural gas of 16.72, and lower heating values

4.3. Implementation of the concept in stoichiometric conditions using compressed natural gas as fuel | 97

of 42.793 MJ/kg for gasoline and 48.931 MJ/kg for CNG, the resulting increment of air flow rate when operating with natural gas of around 2-3%, turning in a similar increase in terms of intake pressure.

If this increase of the intake pressure is assumed as negligible, the calculation of the sensitivity of both fuels to the laminar flame speed can be calculated by means of a 1D flame speed model [275]. Intake temperature, intake pressure, λ and EGR were modified and the results are shown in Figure 4.11, where the difference between the laminar flame speeds of both fuels is plotted. The two fixed variables in each plot were estimated from the experimental data at the spark timing of the high engine load and speed operating point.

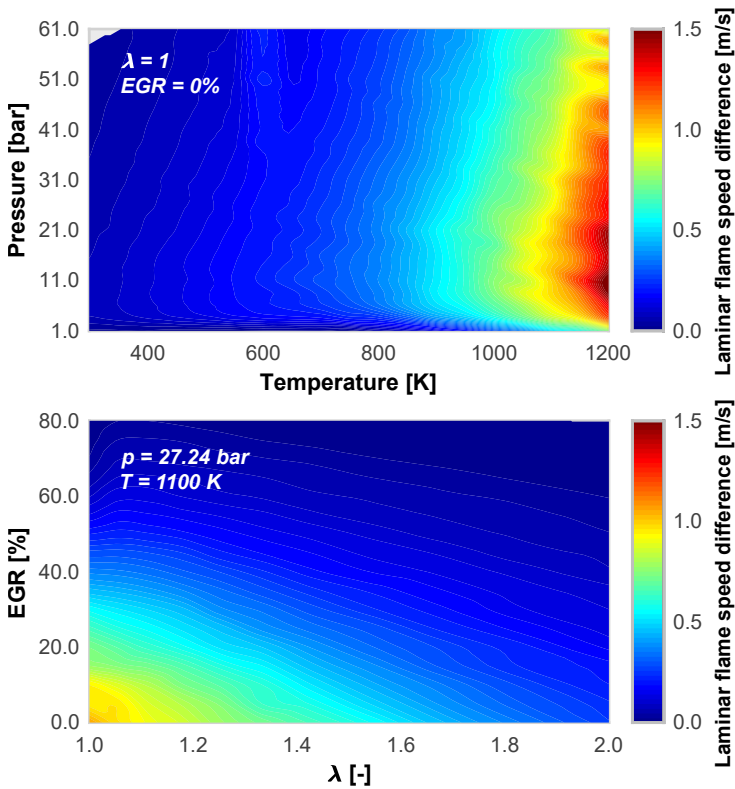


Figure 4.11: Difference in laminar flame speed for gasoline and compressed natural gas at different pressure, temperature, λ and EGR levels.

In this Figure 4.11 a difference between speeds is plotted, a negative value indicates that the flame speed of the natural gas is higher than the gasoline flame speed. However, as there is no negative value below 0, the flame speed

of the gasoline is kept always in values higher than those of the natural gas. Analyzing the top graph reveals that an increase in the pressure has small effect in flame speed, while it is also seen that increasing temperatures tend to rise the gap between both fuels. Regarding the sensitivity to λ and EGR, similar trends are observed: an increase in the dilution ratio reduces the gap between both fuels.

From these results, it is clear that compressed natural gas fuel is worse in terms of laminar flame speed compared to gasoline fuel in the whole range considered. However, if an increase of the turbulent flame speed through turbulence enhancement is achieved and the heat release rate is kept constant, there are some important benefits in terms of auto-ignition delay. In Figure 4.12 the auto-ignition delay is plotted against temperature and air dilution ratio. In this map, the high engine load and speed operating point is represented and its knock tendency is studied when operating with both types of fuel. A representative duration of combustion (DoC) without knock limitation (obtained from the experimental database) is plotted as a black line, while the high load/speed operation condition is pointed in the map. In this case, the pressure considered coincides with the value at which the 50% of the fuel is burned (CA50). This value should be representative of the average pressure inside the chamber at the potential onset of the end-gas knock. In this case, the negative temperature coefficient (NTC) region is observed when operating with gasoline like fuel, while it is not observed in the natural gas map. This coefficient is associated with a cool flame process [276, 277]. As it can be seen, the auto-ignition delay operating with CNG increases almost three orders of magnitude, thus hindering the end-gas knock onset. In this way, a suitable combustion phasing can be reached, avoiding possible knock issues.

The application of compressed natural gas has some drawbacks in terms of laminar flame speeds characteristics that must be kept in mind during the engine design, however, there is a clear benefit in terms of auto-ignition delay that confirms the interest of natural gas implementation in SI engines.

Besides this basic thermochemical aspects study, there has been carried out a life cycle analysis has been carried out using the GREET software developed by Argonne National Laboratories [278] in order to estimate the global impact on the GHG emission when switching to compressed natural gas fuel.

This software provides an overview of the main pollutant emissions generated in the whole production, transportation and compression process of different fuels. In this case, the European mix of renewable natural gas

4.3. Implementation of the concept in stoichiometric conditions using compressed natural gas as fuel | 99

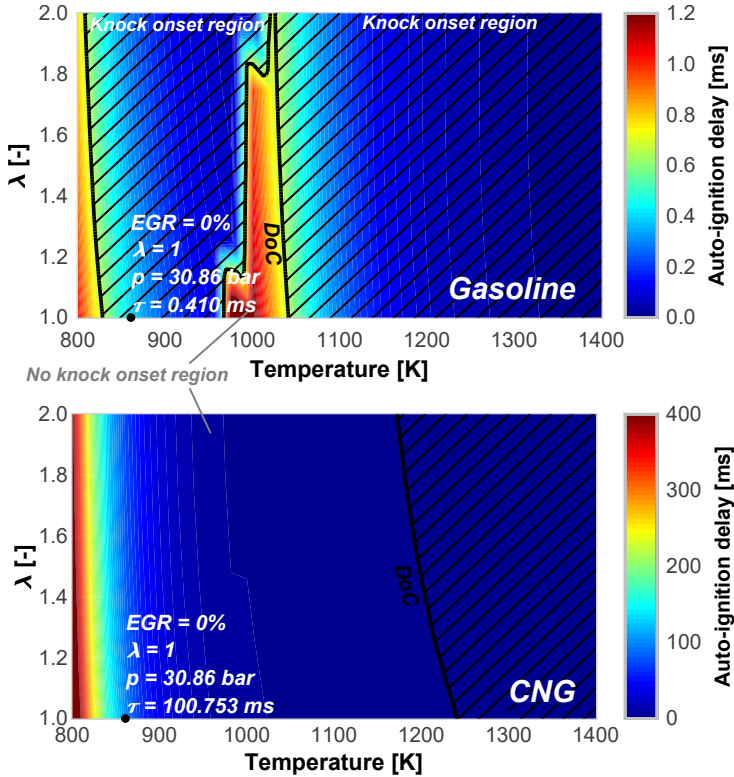


Figure 4.12: Auto-ignition delay calculated for gasoline (top) and compressed natural gas (bottom). Black lines represent the duration of combustion without knock limitation (DoC).

production [279] is considered being a combination of food waste (74%), landfill gas (17%) and waste sludge (9%) processes. The life cycle assessment shown in Table 4.6, shows a comparison of the pollutant emissions between conventional natural gas (NG), natural gas coming from food waste (FW), natural gas coming from landfill gas recovery (LG), natural gas coming from waste sludge (WS) and gasoline with 10% of ethanol. The composition of de natural gas is compatible with a compressed natural gas refined from different renewable sources.

The different emissions considered are carbon dioxide (CO_2), volatil organic compound (VOC), carbon monoxide (CO), nitrogen oxides (NO_x), particulate matter (PM), sulfur oxides (SO_x), methane (CH_4), nitrous oxide (N_2O), black carbon (BC), pollutants of concern (POC) and the overall greenhouse gases in a 100 year prospect (GHG-100).

Table 4.6: Life cycle assessment of natural gas and gasoline E10.

	Emissions (kg per MJ of fuel)				
	Well to Use				
	NG	FW	LG	WS	Petrol E10
CO ₂	7.88E-3	3.54E-2	-5.51E-2	-5.27E-2	1.78E-2
VOC	1.05E-5	-3.21E-5	-2.61E-5	-1.10E-4	2.80E-5
CO	3.51E-5	-2.40E-5	-3.63E-5	-1.24E-4	1.68E-5
NO _x	4.28E-5	-7.82E-6	-9.23E-6	-1.57E-4	3.25E-5
PM ₁₀	1.54E-6	-5.02E-6	-4.08E-6	-4.52E-5	3.68E-6
PM _{2.5}	7.69E-7	-4.89E-6	-4.77E-6	-3.06E-5	2.32E-6
SO _x	1.49E-5	-6.73E-5	3.80E-6	-1.05E-3	1.48E-5
CH ₄	2.43E-4	-5.27E-3	3.73E-4	-7.12E-4	1.09E-4
N ₂ O	1.53E-6	-5.77E-6	-1.08E-6	-2.31E-5	2.40E-6
BC	1.72E-7	-3.64E-6	-5.36E-6	-6.66E-6	3.43E-7
POC	2.46E-7	6.06E-7	2.11E-7	-1.74E-6	5.74E-7
GHG-100	1.57E-2	-1.24E-1	-4.43E-2	-8.07E-2	2.18E-2

Results of the life cycle assessment present a reduction on the GHG emission when switching from a gasoline fuel to a natural gas fuel. Furthermore, using natural gas coming from renewable sources decreases the values below zero, which indicates that the GHG present in the atmosphere are consumed and reduced as time goes by. Using natural gas from these kind of sources will help to stabilize and control the climate change [280]. Focusing on the most relevant pollutants for CNG engines (CO₂, NO_x and CH₄), there is a significant reduction of pollutants for the renewable gas sources. Waste sludge is the most clean source since it presents a reduction for all pollutants, while food waste and landfill gas also present a significant overall reduction, but some pollutants are still positive, which means that further pollutant reduction strategies should be included.

However, the adoption of CNG instead of gasoline-like fuels is not the only possibility to advance in the decarbonization path. Nowadays, applications like Battery Electric Vehicles (BEV) or Hybrid Electric Vehicles (HEV), along with the usage of biofuels are different possibilities to help in this global goal. In fact, these kind of alternative fuels, might play a crucial role in the transition to electrical fleets, as the implementation of a biofuel may not require excessive engine or hardware modifications in a vehicle.

An overview of the GHG emission in the next 100 years is presented in Figure 4.13 for the different fuels and refinement strategies considered so far. The overall GHG-100 recovery using an European mix for the natural gas production is -1.07E-1 kg/MJ, which means that using compressed natural

4.3. Implementation of the concept in stoichiometric conditions using compressed natural gas as fuel | 101

gas from renewable sources will reduce the GHG in the atmosphere if the fuel consumption of the engine is maintained when switching the fuel. Thus, the interest of developing new combustion strategies that help to reduce the fuel consumption when using renewable-based source fuels is clear and they will enable the future application of these new technologies.

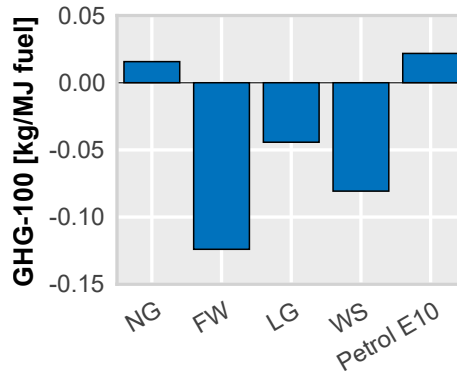


Figure 4.13: Prospective of GHG emission in 100 years using different fuels and refinement strategies.

As it has been proven, employing CNG as a fuel in SI engines, does not have only benefit in terms of thermochemical properties, but also in terms of emissions. Is a clear investigation pathway in the short and medium term for the automotive industry. Continuing with the implementation of this new ignition concept, the same three operating points have been studied using CNG as fuel.

Pressure and heat release rate profiles from this operating point can be seen in Figure 4.14. The average profiles are presented in dark colors and the standard deviations are presented in light colors. As the Research Octane Number of the CNG fuel is higher than that of the gasoline, the combustion phasing restriction related to the knocking appearance in the conventional ignition system is not present anymore.

Avoiding knocking issues allows to advance the combustion phasing of the conventional spark ignition system increasing the resulting pressure. Regarding the combustion velocity, a reduction of the combustion duration is kept for this passive pre-chamber ignition concept, however the difference between concepts decreases.

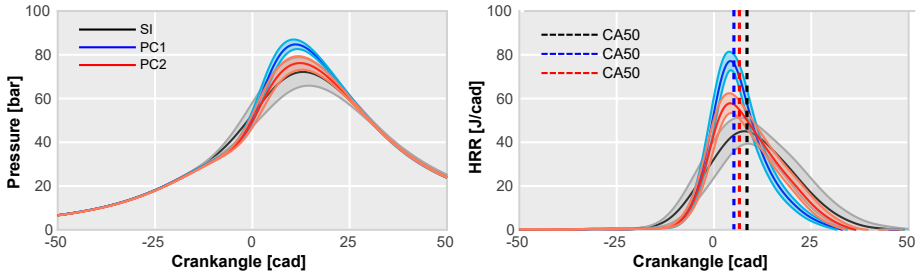


Figure 4.14: Pressure (left) and heat release rate (right) profiles of the high engine load and speed conditions at $\lambda = 1$ operating with CNG for conventional ignition system (black) and both passive pre-chamber geometries (blue and red). Dashed lines correspond to 50% of combustion (CA50).

Focusing on the gross indicated efficiency, it is clear that the lack of the knocking restrictions limits the advantages of the passive pre-chamber ignition concept. In Figure 4.15, a comparison of the combustion phasing, gross indicated efficiency, combustion stability combustion velocity, knocking and fuel consumption for both ignition systems is presented.

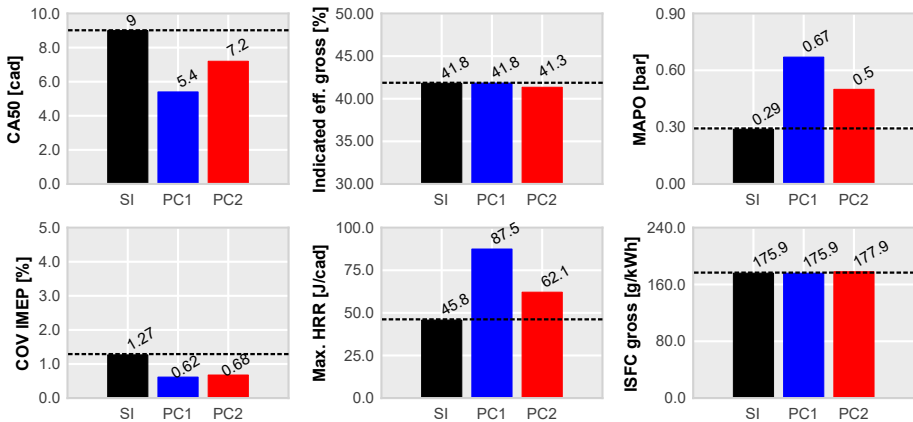


Figure 4.15: Comparison of combustion phasing (CA50), gross indicated efficiency, MAPO, combustion stability (COV IMEP), combustion velocity and fuel consumption for both ignition systems at high engine load and speed conditions at $\lambda = 1$ operating with CNG.

The increase of efficiency observed with the gasoline fuel is not present with this high ON fuel at this operating point, even, a lack of performance compared with conventional spark ignition system is observed for pre-chamber 2. The increased combustion velocity does not help to improve the efficiency as

4.3. Implementation of the concept in stoichiometric conditions using compressed natural gas as fuel | 103

long as the combustion phasing is properly set. Furthermore, the combustion stability achieved by both ignition systems is quite similar, reducing the possibilities of the passive pre-chamber concept to have a better performance. However, taking into account the fuel consumption, there is a clear gain when operating with CNG, even with the reduced efficiency levels compared to the same point when operating with gasoline (a decrease of around 3% of the total efficiency is related to a decrease of around 9% of fuel consumption), caused by the higher energy content (greater lower heating value) of this fuel.

In terms of emitted pollutants there is a reduction in NO_x compared to the gasoline fuel emissions, however there is a reduction of the combustion efficiency, which increases the CO and the unburned HC.

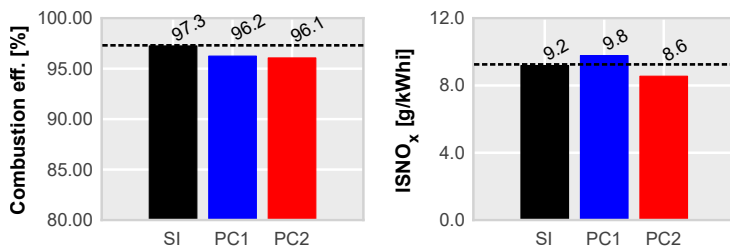


Figure 4.16: Comparison of combustion efficiency and emitted NO_x for both ignition systems at high engine load and speed conditions at $\lambda = 1$ operating with CNG.

Continuing with the low engine load and speed point, the profiles of the in-cylinder pressure and the heat release rate are shown in Figure 4.17. Pressure profiles are very similar since the reduced amount of fuel of this operating point avoids observing significant pressure differences, also the heat release rate profiles are very similar. Only the pre-chamber 1 profile keeps the trend of the higher engine load point with an increased maximum heat release rate peak.

Main combustion parameters resulting from the implementation at these conditions are shown in Figure 4.18. It is clear how the efficiency levels are reduced as long as the engine load decreases, even if the combustion phasing, velocity and stability are kept at suitable values. This decrease of performance is related to the longer combustion process and the increased heat transfer. The fuel consumption levels are similar to those of gasoline at these operating conditions, so if the mix sources to refine the CNG consist of renewable sources there will be also a benefit in terms of GHG emissions.

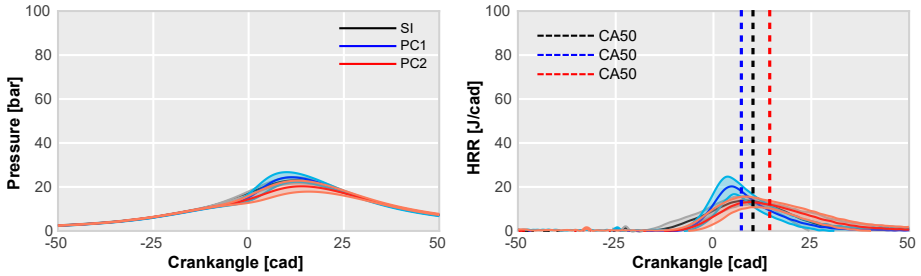


Figure 4.17: Pressure (left) and heat release rate (right) profiles of the low engine load and speed conditions at $\lambda = 1$ operating with CNG for conventional ignition system (black) and both passive pre-chamber geometries (blue and red). Dashed lines correspond to 50% of combustion (CA50).

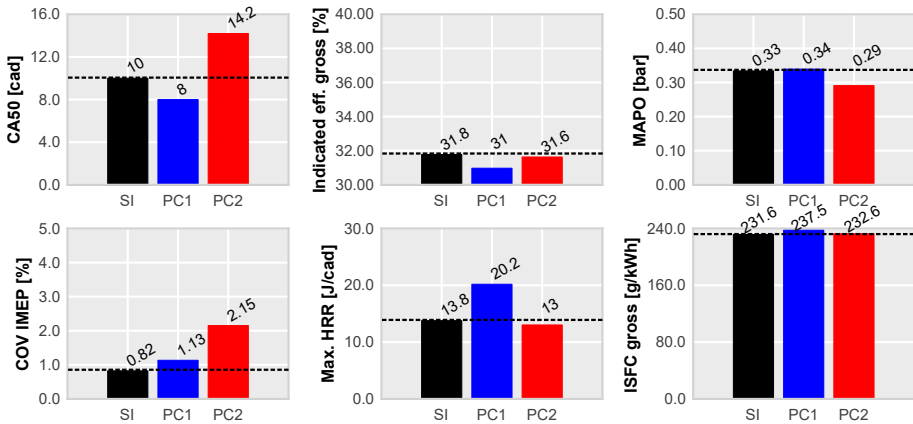


Figure 4.18: Comparison of combustion phasing (CA50), gross indicated efficiency, MAPO, combustion stability (COV IMEP), combustion velocity and fuel consumption for both ignition systems at low engine load and speed conditions at $\lambda = 1$ operating with CNG.

In terms of emissions, Figure 4.19 shows the comparison between concepts. According to the results, reduced levels of NO_x are achieved, but again, the related combustion efficiency is lower for the new ignition system.

Finally, the profiles of the medium engine load and speed point are presented in Figure 4.20. There is an increment of the obtained in-cylinder pressure due to the increased fuel mass, however it is not enough to achieve significant differences between concepts. Regarding the heat release profile, pre-chambers show an increased velocity peak and reduced duration, letting a delay in the combustion start compared to conventional spark timing. However, despite this increase of the combustion velocity and a similar

4.3. Implementation of the concept in stoichiometric conditions using compressed natural gas as fuel | 105

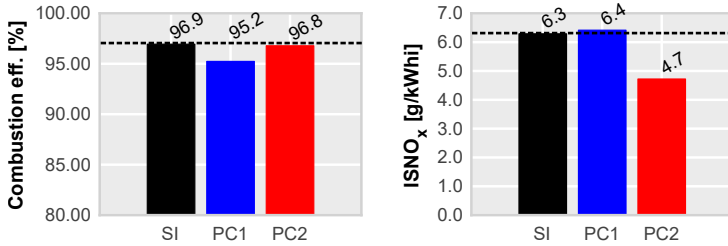


Figure 4.19: Comparison of combustion efficiency and emitted NO_x for both ignition systems at low engine load and speed conditions at $\lambda = 1$ operating with CNG.

combustion phasing, results of the gross indicated efficiency in Figure 4.21 indicate that conventional ignition system still has the best performance with this engine architecture. Fuel consumption levels are again decreased compared to the gasoline levels.

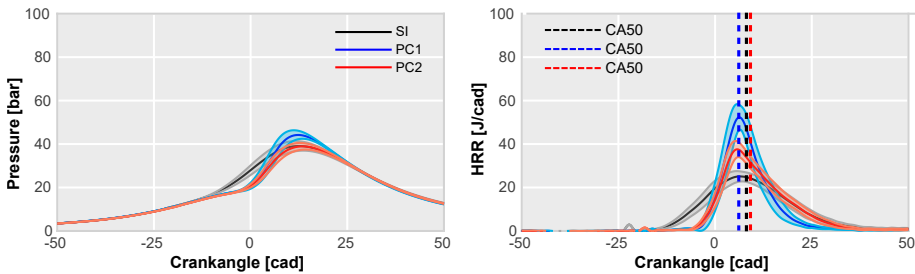


Figure 4.20: Pressure (left) and heat release rate (right) profiles of the medium engine load and speed conditions at $\lambda = 1$ operating with CNG for conventional ignition system (black) and both passive pre-chamber geometries (blue and red). Dashed lines correspond to 50% of combustion (CA50).

Also, similar trends of the emitted pollutants are achieved at these operating conditions. Figure 4.22 shows the combustion efficiency and NO_x emissions levels. Results are quite similar to the results of the other operating points.

The operation with CNG keeping the same engine architecture as in the previous Section 4.2 has shown that CNG has some benefits related to the increase of the auto-ignition delay and the decrease of the fuel consumption, achieving similar levels of efficiency than those of the conventional ignition system at medium and high engine load conditions. Making a brief comparison, the decrease of the fuel consumption is around a 10% at the high engine load and speed conditions, while it is around 12% for the medium

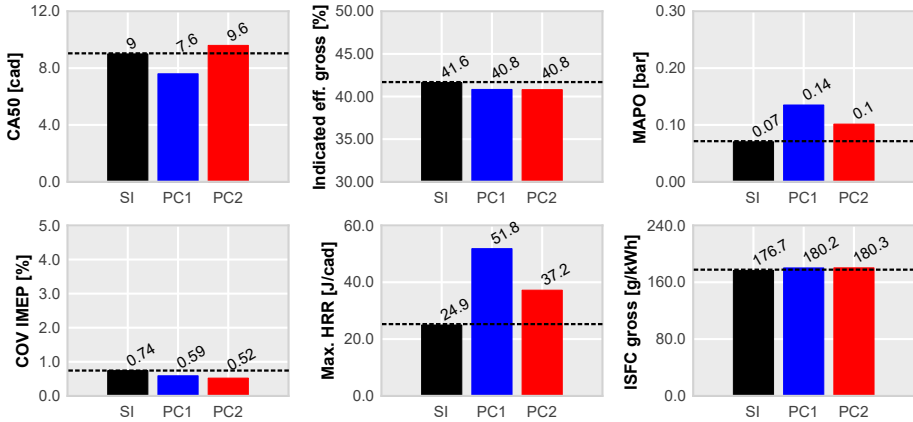


Figure 4.21: Comparison of combustion phasing (CA50), gross indicated efficiency, MAPO, combustion stability (COV IMEP), combustion velocity and fuel consumption for both ignition systems at medium engine load and speed conditions at $\lambda = 1$ operating with CNG.

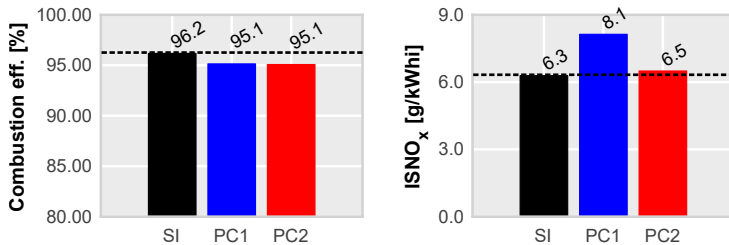


Figure 4.22: Comparison of combustion efficiency and emitted NO_x for both ignition systems at medium engine load and speed conditions at $\lambda = 1$ operating with CNG.

engine load and speed. Regarding the low engine load and speed conditions, the transition to a gaseous fuel turns into an increase around 5% of the indicated fuel consumption. In terms of auto-ignition delay, the operation with the gaseous fuel increases the residence time of the end-gas up to 3 orders of magnitude, which completely removes the combustion phasing limitation of the gasoline fuel when operating with the conventional spark ignition system.

This leads to a decrease of the overall GHG emissions, and this benefit can be further improved if the mix to generate the natural gas is mostly formed by renewable sources. On the other hand, to get the advantages of this

ignition concept, the in-cylinder pressure must be increased until reaching knocking conditions, both by increasing the engine load or by increasing the compression ratio.

So the next step could consist of a combination of the increase of the compression ratio with a Miller strategy to have the benefits of the ignition concept with the benefits of using natural gas as a fuel.

Since the performance of pre-chamber 2 is compromised compared to the pre-chamber 1 at high engine load and speed conditions, further analysis will be carried out comparing conventional spark ignition against pre-chamber 1. The main cause is that it has been proved that increasing the engine load tends to increase the performance of this new ignition system, and pre-chamber 1 has been proved to have a better operation at those conditions.

4.4. Compatibility with millerization strategy using compressed natural gas as fuel

With the purpose of increasing the in-cylinder pressure, a modification of the engine architecture was carried out by implementing the Miller cycle and increasing the compression ratio until 15.4. Main benefit of the implementation of this cycle is the reduced pumping losses associated to its operation. Main characteristics of the engine architecture are presented in Table 4.7. Same fuel was kept from the previous Section 4.3.

Table 4.7: Main specifications of the engine.

Engine	4-stroke SI
Number of cylinders [-]	1
Displacement [cm ³]	404
Bore – Stroke [mm]	80.0 – 80.5
Compression ratio (geometric) [-]	15.4:1
Valvetrain [-]	DOHC
Number of valves/cylinder [-]	2 intake and 2 exhaust
Fuel injection system [-]	PFI (P_{max} 6 bar)

In this step, the implementation of the concept in this new engine architecture was done. Results of the first operating point (high engine load and speed) of the in-cylinder pressure profile and heat release rate for the conventional spark ignition system and the passive pre-chamber ignition system is presented in Figure 4.23.

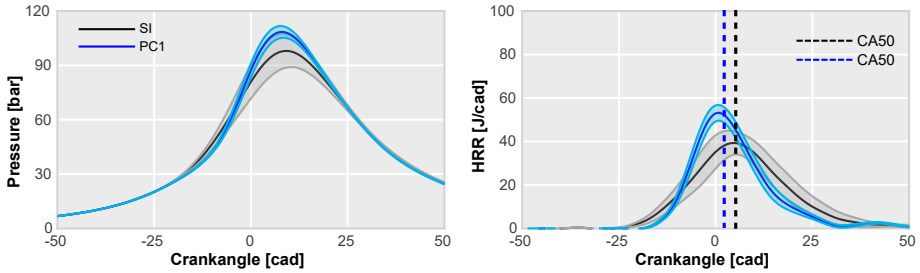


Figure 4.23: Pressure (left) and heat release rate (right) profiles of the high engine load and speed conditions at $\lambda = 1$ operating with CNG for conventional ignition system (black) and passive pre-chamber geometry 1 (blue). Dashed lines correspond to 50% of combustion (CA50).

Results show how the combustion velocity for pre-chamber system is still higher than spark system, however, the difference of combustion velocities between both ignition systems has been reduced compared with previous results in Figure 4.2 and Figure 4.14. Regarding the in-cylinder pressure, as the CNG is a fuel with a high knocking resistance, the increase of the maximum pressure is not enough to achieve knocking conditions, which limits the advantages of the passive pre-chamber ignition system.

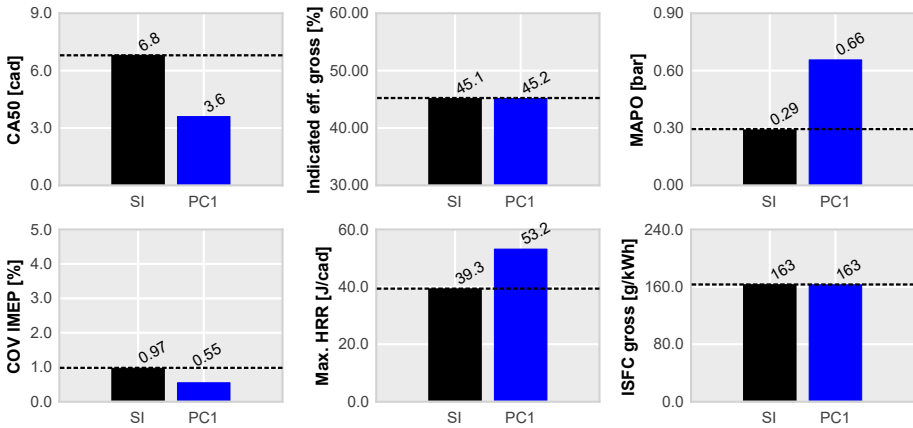


Figure 4.24: Comparison of combustion phasing (CA50), gross indicated efficiency, MAPO, combustion stability (COV IMEP), combustion velocity and fuel consumption for both ignition systems at high engine load and speed conditions at $\lambda = 1$ operating with CNG.

4.4. Compatibility with millerization strategy using compressed natural gas as fuel | 109

The results in terms of gross indicated efficiency, combustion phasing, stability, combustion velocity, knocking and fuel consumption are presented in Figure 4.24. Gross indicated efficiency levels are similar, there is no clear advantage in passive pre-chamber ignition system at these conditions, however it has been increased compared with the previous architecture operating with natural gas. Combustion stability and phasing parameters are also quite similar, so the reduction of combustion velocity difference between concepts when operating with Miller cycle may be caused by the advanced IVC, which hinders the scavenge process in the pre-chamber and increases the residual gas fraction at the start of combustion, reducing the laminar flame speed and thus, the overall combustion velocity.

For better understanding the operation of the three implementations, the results of the fuel consumption for these cases when operating at high engine load and speed conditions at $\lambda = 1$ are presented in Figure 4.25. Left plot corresponds with the results of the gasoline implementation (Section 4.2), center plot corresponds with the results of the CNG implementation (Section 4.3) and right plot corresponds with the implementation of Miller cycle and CNG (Section 4.4). Black bars represent the fuel consumption of conventional spark ignition (SI), blue bars correspond with the fuel consumption provided by pre-chamber 1 (PC1) and red bars correspond with the fuel consumption provided by pre-chamber 2 (PC2). It is clear how there is an increase of the indicated efficiency as the CR increases and the engine handles with higher in-cylinder pressures. However, the difference between the conventional spark ignition and the passive pre-chamber ignition systems is being reduced, as long as the limitation of the spark timing due to the end-gas knock restriction is removed.

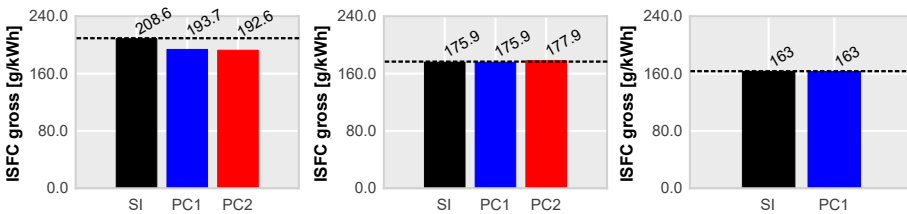


Figure 4.25: Comparison of fuel consumption for the three evaluated implementations, gasoline (left), CNG (center) and Millerization (right) and the three different ignition systems, SI (black), pre-chamber 1 (blue) and pre-chamber 2 (red) at high engine load and speed conditions at $\lambda = 1$.

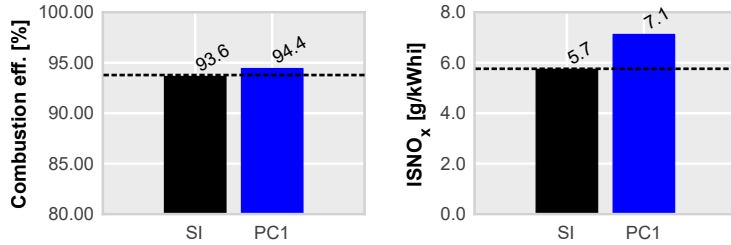


Figure 4.26: Comparison of combustion efficiency and emitted NO_x for both ignition systems at high engine load and speed conditions at $\lambda = 1$ operating with CNG.

Regarding the pollutants, main results are presented in Figure 4.26. Combustion efficiency shows slightly lower values than those of the standard cycle, which indicates a higher CO and HC emissions. In terms of NO_x there is an increment for the pre-chamber system compared to conventional system, however these values are also lower than those of the obtained in the standard cycle.

The second studied point corresponds to the combination of low engine load and speed. At these conditions, results of in-cylinder pressure and heat release rate profiles are presented in Figure 4.27. It is clear that pre-chamber system accelerates the combustion even at these low engine conditions, however the velocity difference is not enough to assure a increase of the maximum pressure, resulting in similar pressure profiles. Furthermore, these profiles are also similar to the profiles obtained in the previous Section 4.3 operating with the standard cycle.

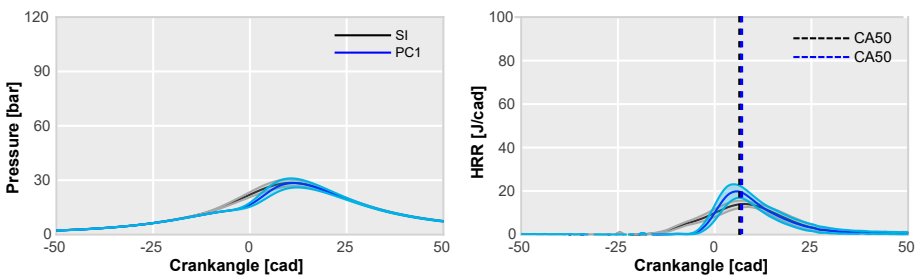


Figure 4.27: Pressure (left) and heat release rate (right) profiles of the low engine load and speed conditions at $\lambda = 1$ operating with CNG for conventional ignition system (black) and passive pre-chamber geometry 1 (blue). Dashed lines correspond to 50% of combustion (CA50).

4.4. Compatibility with millerization strategy using compressed natural gas as fuel | 111

Main results of the implementation at these conditions appear in Figure 4.28. Results show a decrease of the gross indicated efficiency for the passive pre-chamber ignition compared to the conventional spark ignition system. The main cause of this decrease is the reduced achieved pressure due to the reduced fuel mass, since the combustion phasing and stability levels are similar and there is an increment of the combustion velocity for the pre-chamber system.

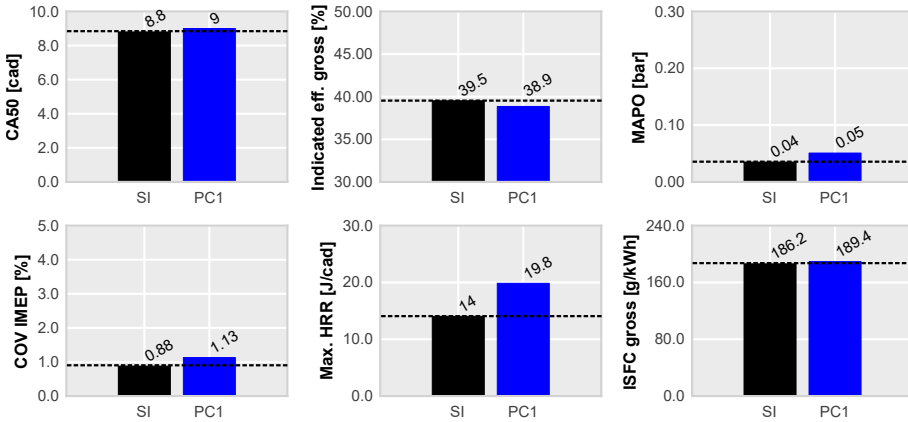


Figure 4.28: Comparison of combustion phasing (CA50), gross indicated efficiency, MAPO, combustion stability (COV IMEP), combustion velocity and fuel consumption for both ignition systems at low engine load and speed conditions at $\lambda = 1$ operating with CNG.

In terms of pollutants at these conditions, shown in Figure 4.29, the same trend is observed as in the previous operating point.

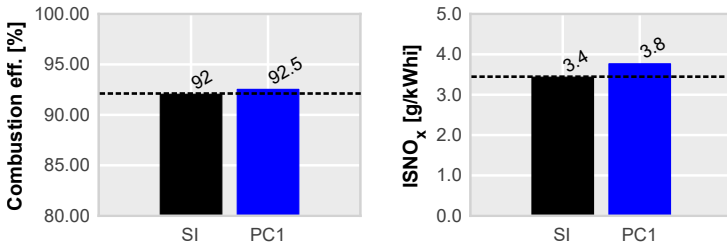


Figure 4.29: Comparison of combustion efficiency and emitted NO_x for both ignition systems at low engine load and speed conditions at $\lambda = 1$ operating with CNG.

Pressure and heat release profiles for the medium engine load and speed point are presented in Figure 4.30. As the engine load increases profiles for both pressure and heat release of the pre-chamber system tend to increase the difference between concepts. In this way, the pressure and combustion velocity maximum peaks are higher than those in the low engine load conditions, however this is still not enough to overcome the gross indicated efficiency of the conventional spark ignition system.

Main combustion parameters of the operation at medium engine load and speed are presented in Figure 4.31. As it was mentioned before, the gross indicated efficiency of the new ignition system is not higher as the conventional system, even when there is an advanced combustion phasing and a proper combustion velocity of the new concept. This is caused by the insufficient in-cylinder pressure, which is not enough to take advantage of the benefits of this concept. Gross indicated efficiency of low and medium engine loads of the pre-chamber system are lower than efficiency of the spark system, while at high engine load these efficiencies are similar.

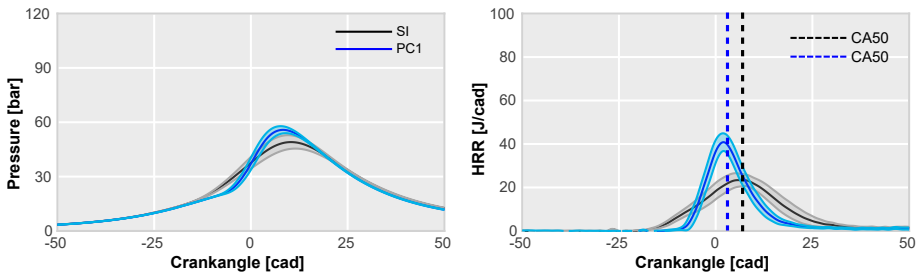


Figure 4.30: Pressure (left) and heat release rate (right) profiles of the medium engine load and speed conditions at $\lambda = 1$ operating with CNG for conventional ignition system (black) and passive pre-chamber geometry 1 (blue). Dashed lines correspond to 50% of combustion (CA50).

Main results of emitted pollutants at these conditions are shown in Figure 4.32, where there is a reduced combustion efficiency of the pre-chamber system, causing a decrease in the combustion temperature and a reduced NO_x emissions. This reduction of the combustion efficiency may be related to the decrease of the exhaust tailpipe temperatures, which for the conventional spark ignition system is around 560 Celsius degrees and for passive pre-chamber system is around 520 Celsius degrees.

In summary, employing a gaseous-like fuel, or any other kind of fuel, which its Research Octane Number avoids reaching knocking conditions negatively affects the performance of this ignition concept. This lack of per-

4.4. Compatibility with millerization strategy using compressed natural gas as fuel | 113

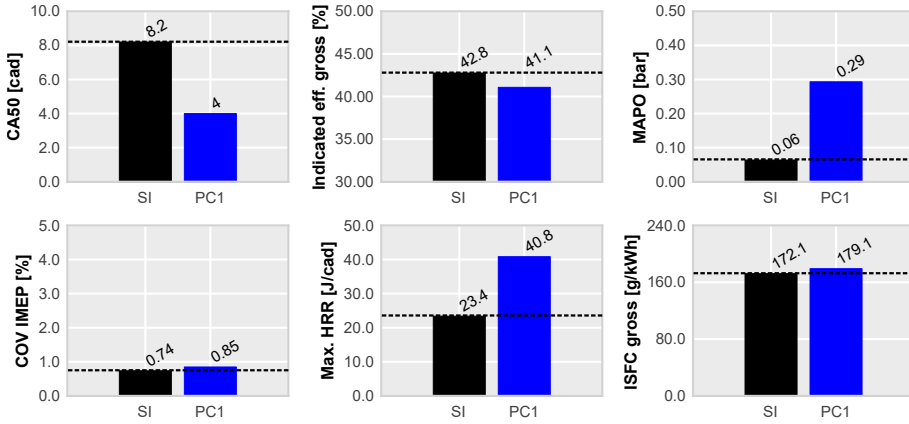


Figure 4.31: Comparison of combustion phasing (CA50), gross indicated efficiency, MAPO, combustion stability (COV IMEP), combustion velocity and fuel consumption for both ignition systems at medium engine load and speed conditions at $\lambda = 1$ operating with CNG.

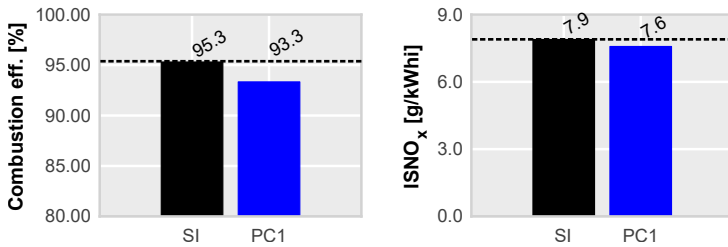


Figure 4.32: Comparison of combustion efficiency and emitted NO_x for both ignition systems at medium engine load and speed conditions at $\lambda = 1$ operating with CNG.

formance seems to be unaffected by different operation cycles, highlighting that reaching knocking conditions in the conventional spark ignition system is a critical aspect to obtain performance benefits when switching to the pre-chamber ignition concept. If this new ignition system is intended to be operated with a gaseous fuel, a key design parameter of the engine must be the maximum in-cylinder pressure achieved. As it has been proved by the different efficiencies obtained in the different engine loads, increasing the resulting in-cylinder pressure helps to increase the pre-chamber system efficiency.

4.5. Engine maps

To have a better overview of the concept, a complete engine map was measured. The engine architecture is the same as in the Section 4.4, keeping the compressed natural gas as fuel. A full comparison of both ignition concepts is shown in the present section.

Gross indicated efficiency for both ignition systems is presented in Figure 4.33. Results show that there are no significant benefits in employing passive pre-chamber ignition concept at these conditions. Best performance is achieved at high engine loads and speed, where efficiency reaches similar values as conventional spark system. In the remaining conditions, the lack of efficiency is caused by the increased heat transfer losses, specially at low/medium engine load and low/medium engine speed. Furthermore, when operating at low-end torque conditions (high engine load and low engine speed), there is a reduction of performance of the pre-chamber concept caused by the impossibility of a proper combustion phasing.

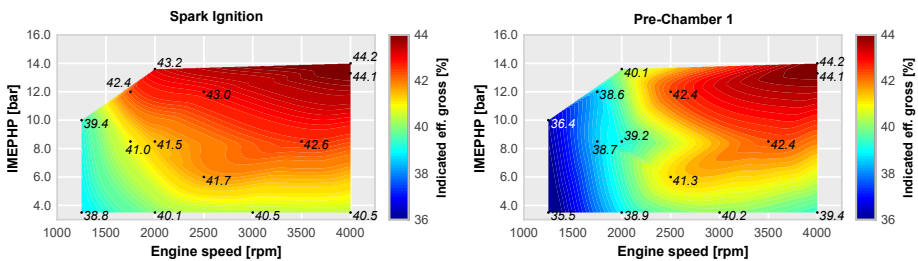


Figure 4.33: Gross indicated efficiency for spark ignition system (left) and passive pre-chamber ignition system (right) colormaps of the engine map at $\lambda = 1$ operating with CNG and Miller cycle varying engine load and speed.

Combustion phasing is shown in Figure 4.34, it is clear how in low-end torque area for the pre-chamber system, the combustion phasing is not well set, even reaching negative values, which mean that the 50% of combustion occurs before reaching the TDC, leading to a decrease of efficiency. These combustion phasing results are mainly caused due to the fast combustion occurring at those operating conditions. It is also remarkable that, at low engine load and high speed, combustion phasing is quite pushed away from the optimum values. In Figure 4.35, the combustion velocity is presented for both ignition systems. The combustion velocity reached at low-end torque conditions is almost the double as the combustion velocity reached

where maximum efficiency is obtained. The fast combustion and the high dispersion of this operating condition makes unable to delay the combustion and increase the overall efficiency.

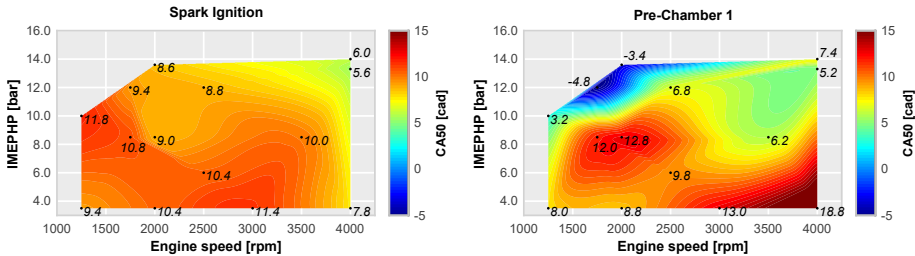


Figure 4.34: Combustion phasing for spark ignition system (left) and passive pre-chamber ignition system (right) colormaps of the engine map at $\lambda = 1$ operating with CNG and Miller cycle varying engine load and speed.

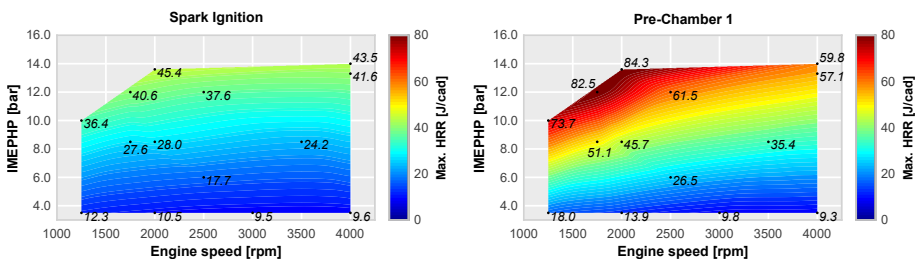


Figure 4.35: Combustion velocity for spark ignition system (left) and passive pre-chamber ignition system (right) colormaps of the engine map at $\lambda = 1$ operating with CNG and Miller cycle varying engine load and speed.

As mentioned before, at low-end torque conditions there exists a high dispersion compared with the rest of the engine map. These results are shown in Figure 4.36. At low-end torque conditions the combustion stability is compromised, while in the rest of the engine map, it is kept at lower values. In terms of knocking, MAPO colormap presented in Figure 4.37, these low-end torque conditions present the highest knocking issues. For this engine configuration, the conventional spark ignition system is not affected by knocking in any condition, so the potential advantages of switching to passive pre-chamber ignition concept are limited. This effect can also be seen in the combustion phasing colormap, since spark system is not compromised, results of both systems are quite similar, except for the low-end torque conditions.

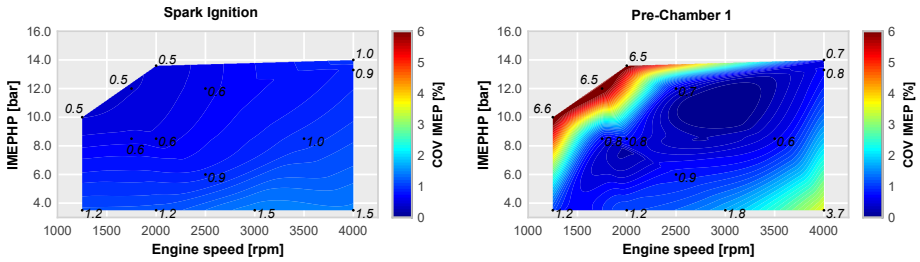


Figure 4.36: Combustion stability for spark ignition system (left) and passive pre-chamber ignition system (right) colormaps of the engine map at $\lambda = 1$ operating with CNG and Miller cycle varying engine load and speed.

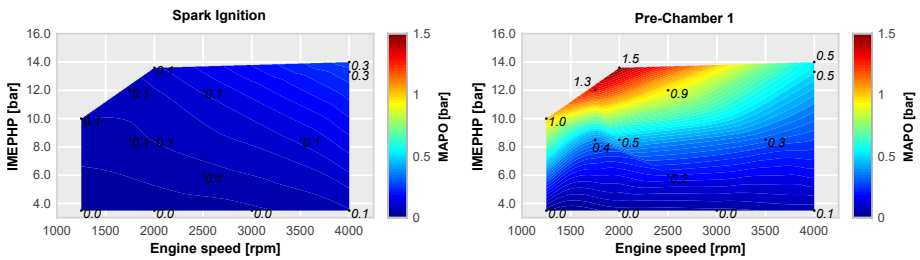


Figure 4.37: MAPO for spark ignition system (left) and passive pre-chamber ignition system (right) colormaps of the engine map at $\lambda = 1$ operating with CNG and Miller cycle varying engine load and speed.

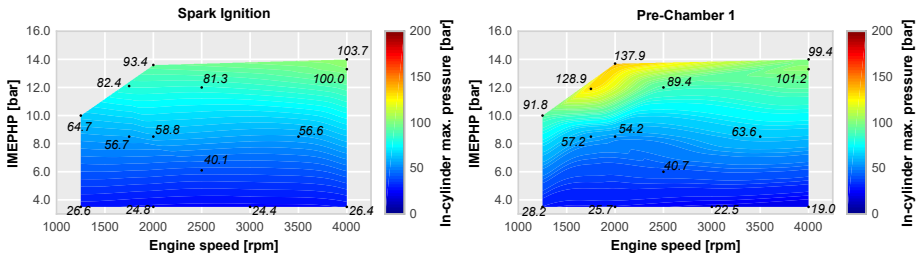


Figure 4.38: Maximum in-cylinder pressure for spark ignition system (left) and passive pre-chamber ignition system (right) colormaps of the engine map at $\lambda = 1$ operating with CNG and Miller cycle varying engine load and speed.

In terms of in-cylinder pressure, there are no significant differences between concepts. In Figure 4.38 values of the maximum pressure achieved are presented. As there is no need to delay the combustion, maximum pressures of both ignition systems are similar. However, as the combustion is faster in the low-end torque region, there is an increase of the pressure in that region for the pre-chamber ignition concept. Regarding the fuel consump-

tion, presented in Figure 4.39, there is a clear increase of consumption for the passive pre-chamber ignition concept at low engine speed conditions. This increase in the consumption may be caused by the increase of the heat losses. As the engine speed decreases, the heat transfer through the walls increases, which leads a higher heat losses.

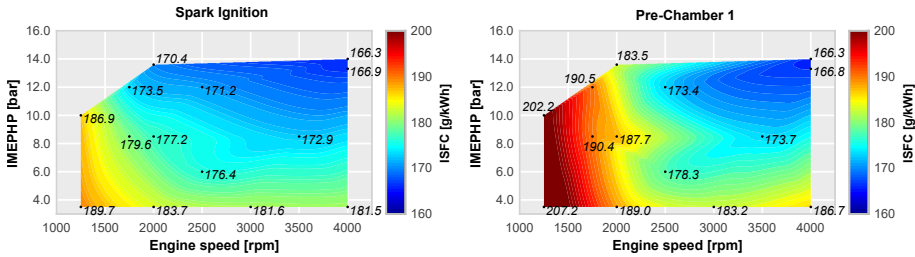


Figure 4.39: Fuel consumption for spark ignition system (left) and passive pre-chamber ignition system (right) colormaps of the engine map at $\lambda = 1$ operating with CNG and Miller cycle varying engine load and speed.

In summary, when operating with this engine architecture and this kind of fuel, the main advantages of the use of this new passive pre-chamber ignition system are limited. Efficiencies are quite similar to those obtained with the conventional spark system, except in the low engine speed region, where the heat transfer losses are higher. Regarding to the low-end torque region, the efficiency obtained with the pre-chamber ignition system is reduced due to the fast combustion and the combustion instability due to the knocking conditions, these issues avoid a good combustion phasing and thus, diminishing the efficiency levels.

4.6. Conclusions

In this chapter, the implementation of the passive pre-chamber ignition concept has been presented. The aim was to understand how performs this new system in the near-future passenger car applications, focusing on the relevant parameters of the combustion.

The performance of this ignition system has been evaluated in two different engine architectures employing two different kinds of fuel. Results revealed that the performance of the engine can be improved when switching to passive pre-chamber ignition concept if the combustion phasing is strongly limited by knock.

Knock limits the performance of the conventional ignition system because it forces to push away the combustion from the TDC in order to assure a safe functioning, when switching to passive pre-chamber ignition concept, the increase in the combustion velocity allows to burn the charge fastly and avoid the end-gas knock, letting an advance in the combustion phasing and thus, increasing the efficiency.

However, this increase in the efficiency is obtained only when the conventional system operates in knocking conditions. If the fuel is changed to a more knocking resistant one, such as compressed natural gas, main advantage of pre-chamber system is lost. As there is no need to delay the combustion phasing, similar efficiency levels are obtained for both ignition systems. To obtain advantage of the new system, an increase in the maximum in-cylinder pressure must be achieved.

To illustrate this conclusion, Figure 4.40 gathers the combustion phasing and gross indicated efficiency of the three evaluated cases at the high engine load and speed conditions, which is the most restrictive case. The upper row presents the different values of the combustion phasing obtained for each ignition system while the lower row presents the different gross indicated efficiencies. Left plots correspond with the implementation with gasoline fuel, center plots with the CNG fuel implementation and right plots with CNG fuel and Miller cycle.

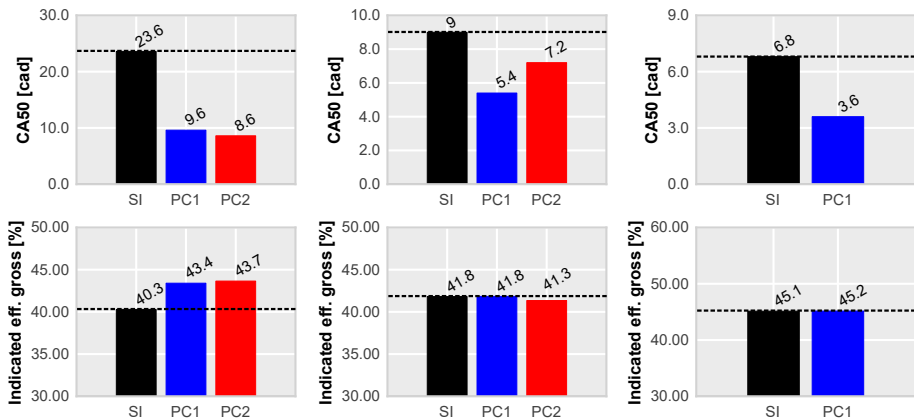


Figure 4.40: Combustion phasing (upper) and gross indicated efficiency (low) for the three different engine architectures: gasoline (left), CNG (center) and Millerization (right) operating at high engine load and speed conditions at $\lambda = 1$. The different ignition systems: SI (black), pre-chamber 1 (blue) and pre-chamber 2 (red).

The increase of the compression ratio and switch to Miller cycle did not improve the obtained performance as long as the compressed natural gas was kept as operating fuel. Results with this new architecture show similarities with the previous engine architecture, because the increase of the pressure was not enough to reach knocking conditions when employing conventional ignition system. Once again, to obtain a clear benefit from the passive pre-chamber ignition system, a strong increase in the cylinder pressure is mandatory.

The operation at low-end torque has been revealed as a risky operating condition with the passive pre-chamber ignition system. The fast combustion and the instability avoids a proper combustion phasing, leading to complete the 50% of the combustion before the TDC. Furthermore, the operation at low engine speeds revealed that the increase of the heat losses increase the consumption of the engine.

In view of the previous results, one of the main applications that could obtain the benefits from the direct application of this ignition system is as the thermal engine of hybrid car applications. Since the operating point to generate the electric supply of the batteries will be kept constant, it can be selected to take advantage of the passive pre-chamber ignition system. Also, in a bigger scale, this concept can be implemented in power plants, such as cogeneration plants, to generate electricity.

Dilution strategies and how to improve the concept

5.1. Introduction

This chapter is focused on evaluating dilution strategies and understanding their limits, both with air and external EGR, combined with the passive pre-chamber ignition concept. Lean burn strategy is a fashionable way to improve the indicated efficiency of SI engines by means of reducing pumping losses and heat transfer through the walls while increasing the specific heat ratio (in the case of diluting with air). However the main drawback of these strategies is the worsening of the combustion characteristics which compromises the ignition of the charge. In this framework seems reasonable to use the passive pre-chamber ignition concept to try to overcome such issue.

Work on this chapter has been partly published in the following papers:

- Evaluation of the passive pre-chamber ignition concept for future high compression ratio turbocharged spark-ignition engines [1]
- Performance of the passive pre-chamber ignition concept in a spark-ignition engine for passenger car applications [2]
- Improving the performance of the passive pre-chamber ignition concept for spark-ignition engines fueled with natural gas [4]
- Analysis and improvement of the passive pre-chamber ignition concept in a spark-ignition turbocharged engine fueled with CNG - P05

As in the previous Chapter 4, the evaluation was carried out using both calibrated gasoline as fuel (Research Octane Number 98) and calibrated compressed natural gas (Research Octane Number 120), which their main characteristics are presented in Table 4.4 and Table 4.5. Evaluation of both air and EGR dilution was carried out with the standard engine architecture, which its main characteristics are presented in Table 3.3, while the engine maps were obtained with the second engine architecture, employing Miller cycle. In Table 3.4.

Main operating conditions are similar to those presented in previous chapter, however a dilution sweep was carried out to evaluate the performance of the engine with this ignition system. These points are presented in Table 5.1. Regarding Section 5.5, several points of the engine map were selected and evaluated to have a better understanding of the global issues of the concept. The main geometrical parameters of the studied pre-chambers are the same as the previous shown in Table 3.5. Main results of this experimental stage were presented in the Articles [1, 3, 4].

Table 5.1: Studied operating points.

Parameter	OP1	OP2	OP3
Engine speed [rpm]	4500	1350	2000
Engine load [bar]	12.8	2.85	6.8

5.2. Compatibility with air dilution

5.2.1. Employing gasoline as fuel

Diluting with air was the first strategy investigated to increase the engine efficiency. Firstly, a calibrated gasoline, which its main characteristics can be seen in Table 4.4, was used. The easiness of boosting the intake pressure makes the air dilution a very promising strategy to reduce the fuel consumption and an interesting point to start the evaluation of this lean burn strategy.

In this way, first results of the trends obtained when increasing the air dilution are shown in Figure 5.1. This evaluation was performed at high engine load and speed conditions (OP1 of the Table 5.1) since this operating point is the most favorable point where main advantages can be seen, as it was described in previous Chapter 4.

In this figure black line corresponds with the trend of conventional spark ignition system and blue and red lines correspond with the trends of the new ignition concept (pre-chamber 1 and pre-chamber 2 respectively). First look at the results highlights that this strategy effectively increases the gross indicated efficiency in the whole operating range, almost until the maximum dilution limit is reached. For pre-chamber 2 this limit is around $\lambda = 1.6$ while for pre-chamber 1 this limit is slightly higher. Conventional system shows a reduced operating range compared with pre-chamber system.

Regarding the rest of the combustion parameters, it is clear how this pre-chamber concept is able to maintain a good combustion phasing all over the operating range. This, joined with an increased combustion velocity and the ability of this ignition system to avoid end-gas knock turns into the higher efficiency, despite the high combustion dispersion of passive pre-chamber ignition concept.

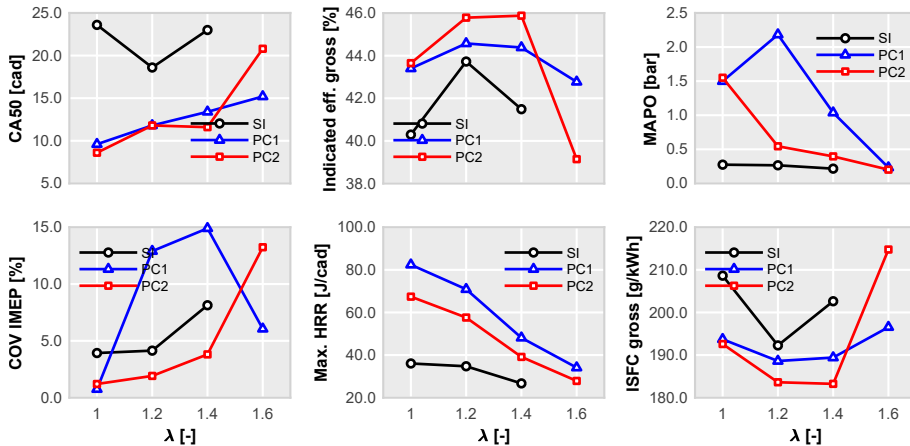


Figure 5.1: Trends of air dilution in combustion phasing (CA50), gross indicated efficiency, MAPO, combustion stability (COV IMEP), combustion velocity and fuel consumption for the studied ignition systems at high engine load and speed conditions operating with gasoline.

In terms of pollutants emissions results can be seen in Figure 5.2, a good combustion efficiency is observed in the whole operating range, but the efficiency for pre-chamber 1 system is lower compared to the other two systems. NO_x trends of the passive pre-chamber ignition concept are compared with the obtained when employing the conventional spark system. However, the reduction achieved at high diluted conditions is not enough to overcome the use of an after-treatment system, making this passive pre-chamber system, at least at these conditions, not suitable for this strategy.

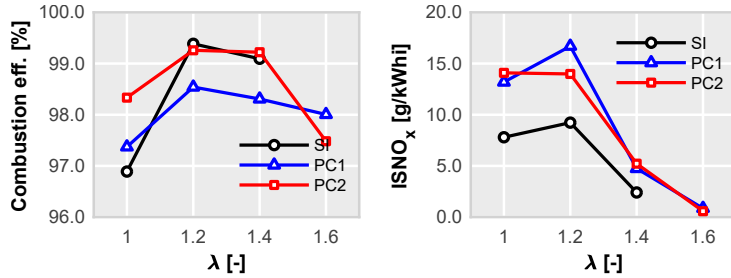


Figure 5.2: Trends of air dilution in combustion efficiency and emitted NO_x for the studied ignition systems at high engine load and speed conditions operating with gasoline.

Comparing the pressure and heat release rate profiles of the stoichiometric case (in Figure 4.2, from the previous Chapter 4) and the most diluted case (in Figure 5.3), shows that the difference between heat release rate profiles of the ignition systems have been reduced. In this figure black lines correspond with the conventional spark ignition system while blue and red lines are related with the passive pre-chamber ignition system. Also, as in the profiles of previous chapter, light color areas represent the standard deviation and dashed lines the time when combustion has completed the 50% of its process.

As an effect of the lean burn strategy, increasing the dilution ratio reduces the combustion velocity and evens out the different profiles, leading to a similar pressure profiles and a reduction of the obtained gross indicated efficiency at the maximum dilution levels. This reduction is caused by the worse combustion phasing, the lower combustion velocity and the increased cycle-to-cycle variability.

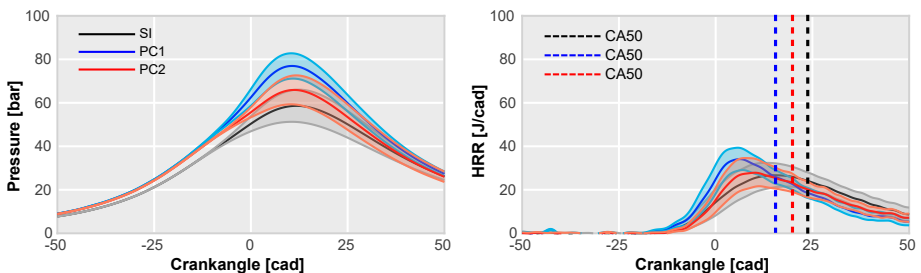


Figure 5.3: Pressure (left) and heat release rate (right) profiles of the high engine load and speed conditions at maximum λ operating with gasoline for conventional ignition system (black) and both passive pre-chamber geometries (blue and red). Dashed lines correspond to 50% of combustion (CA50).

In Figure 5.4 a brief comparison of the mentioned parameters are presented at the stoichiometric and maximum measured dilution points. Black bars correspond with the conventional spark ignition system, blue bars correspond with pre-chamber 1 and red bars correspond with pre-chamber 2.

It is seen how there is a reduction of the gross indicated efficiency for the pre-chamber system. As stated before this reduction may be led by the poor combustion phasing, the reduced combustion velocity or the higher instability, known drawbacks of the lean burn strategy.

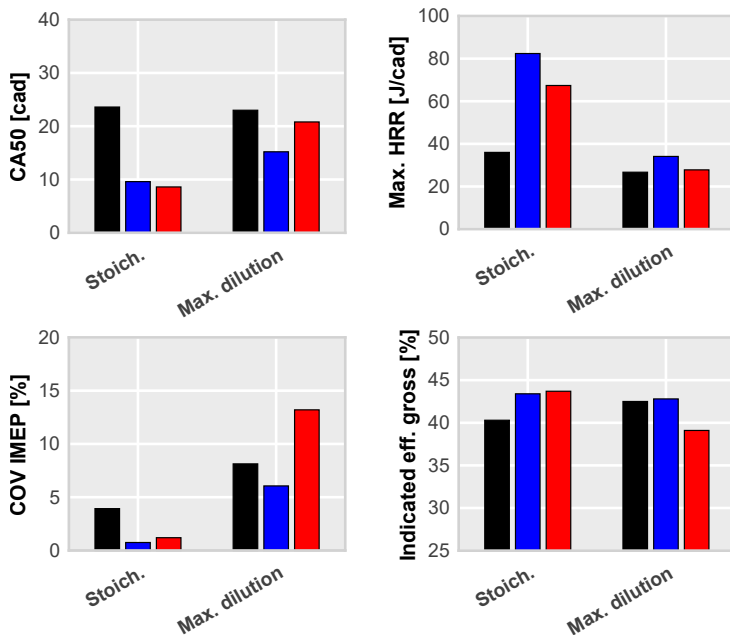


Figure 5.4: Comparison of combustion phasing (CA50), combustion velocity, combustion stability and gross indicated efficiency for both ignition systems at high engine load and speed conditions for $\lambda = 1$ and maximum λ operating with gasoline.

To have a better knowledge of this situation and discover the prevalent parameters, a simple study using a 1D Wave Action model was carried out. In this study, the combustion phasing (through combustion start) and combustion duration are evaluated. Pressure profiles for the stoichiometric and maximum diluted cases of pre-chamber 1 ignition system are used as inputs, changing their start and combustion duration. These combustion profiles are presented in Figure 5.5. Blue line is the average-cycle of the stoichiometric case and red line is the average-cycle of most diluted case.

Profile for the stoichiometric case is sharper and shorter compared with the profile of the diluted case, which is smoother and its duration is noticeably increased.

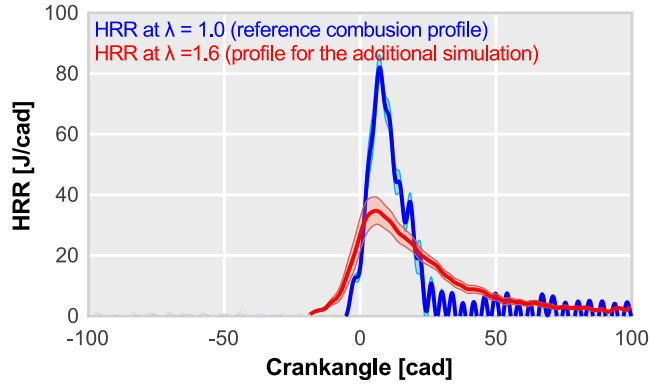


Figure 5.5: Heat release rate profiles for the $\lambda = 1$ and $\lambda = 1.6$ cases.

The design of experiments is detailed in Table 5.2, containing maximum, minimum and number of levels of the combustion start (through combustion phasing) and combustion duration (multiplying the original value by a factor). Original combustion starts at -5 cad ATDC and takes 30 cad to complete the combustion process. In this DOE, combustion start was varied from -10.4 to 10.4 cad ATDC while combustion duration was multiplied by a factor from 0.8 to 3.0.

Table 5.2: Design of experiments carried out in the 1D Wave Action model modifying combustion phasing and duration.

	Min. value	Max. value	# levels
Combustion phasing [cad]	-10.4	10.4	5
Combustion duration factor [-]	0.8	3.0	12

Results of this design of experiments are presented in Figure 5.6. Gross indicated efficiency trends show that between combustion phasing and duration, the combustion phasing is the dominant parameter. As the combustion phasing is pushed away from the TDC the gross indicated efficiency decreases, while the duration of the combustion has less effect since similar efficiencies are obtained when keeping the same phasing.

Points in the map represent the experimental results of the gross indicated efficiency in terms of combustion phasing and duration for the different diluted conditions. Despite the high increase in combustion duration between the most extreme cases (from 15 cad to 45 cad), as the combustion phasing is not so compromised the decline in indicated efficiency is reduced.

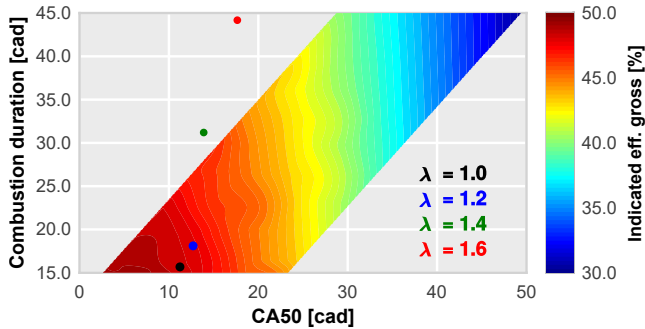


Figure 5.6: Map of gross indicated efficiency at high engine load and speed conditions.

These results are significant and, going in depth, if the stoichiometric combustion profile can be kept constant in the whole dilution range, through turbulent enhancement or a better pre-chamber geometry, there will be expected an increase in the gross indicated efficiency. To confirm this reasoning, a simple calculation in the 1D Wave Action model was performed. Heat release profile of the stoichiometric case was forced to be constant while the air dilution was increased.

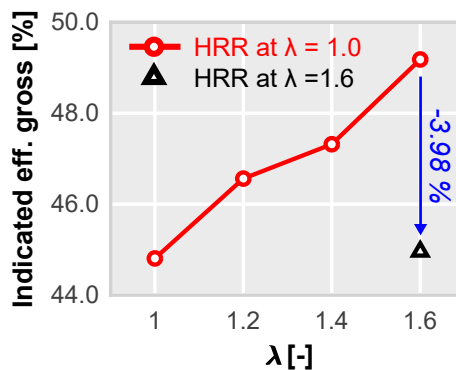


Figure 5.7: Expected gross indicated efficiency trend (red line) and real gross indicated efficiency obtained (black triangle).

The efficiency trend obtained is presented in Figure 5.7. Red line represents the variation of gross indicated efficiency when increasing the dilution ratio and keeping the same heat release rate profile as the stoichiometric case, while black triangle is the experimental gross indicated efficiency measured at $\lambda = 1.6$. Results show that keeping a suitable heat release rate profile (short combustion duration and a proper combustion phasing) is mandatory to increase the efficiency.

5.2.2. Employing natural gas as fuel

Second part of the air dilution evaluation consisted of increasing the air dilution when operating with natural gas, which its properties can be found in Table 4.5. Same considerations of the thermo-chemical properties of the fuel as in the implementation section (Section 4.3) of the previous Chapter 4 are taken into account.

As it was described in previous Chapter, the higher auto-ignition delay offered by the natural gas fuel helps to avoid reaching knocking conditions when operating with the conventional spark ignition system. In this situation, a reduction of the gap between concepts is expected in terms of gross indicated efficiency. Results of combustion phasing, velocity, stability, indicated efficiency, knocking and fuel consumption are plotted for the different dilution ratios measured when using natural gas are shown in Figure 5.8.

Gross indicated efficiency levels are similar for the three different ignition systems as expected, however pre-chamber ignition offers a slightly higher values until the maximum dilution limit is reached. This increase of the efficiency may come from the higher combustion velocity since combustion phasing levels are quite similar between concepts. Once the maximum dilution is reached, the lack of performance comes from the extreme combustion deterioration and instability (COV IMEP levels of almost a 80% for pre-chamber 1). Also, as the natural gas has a increased resistance to knocking, MAPO levels have lowered compared with those obtained when using gasoline, not reaching the knocking limit and letting the conventional spark system to be properly tuned.

Looking at the pollutant trends in Figure 5.9, combustion efficiency trends are similar for the three ignition systems, until the dilution limit is reached. At that point appear that misfiring cycles that notably reduce combustion efficiency and increase the combustion instability. In terms of NO_x , there is an increase of emitted pollutant at $\lambda = 1.2$ due to the combination of

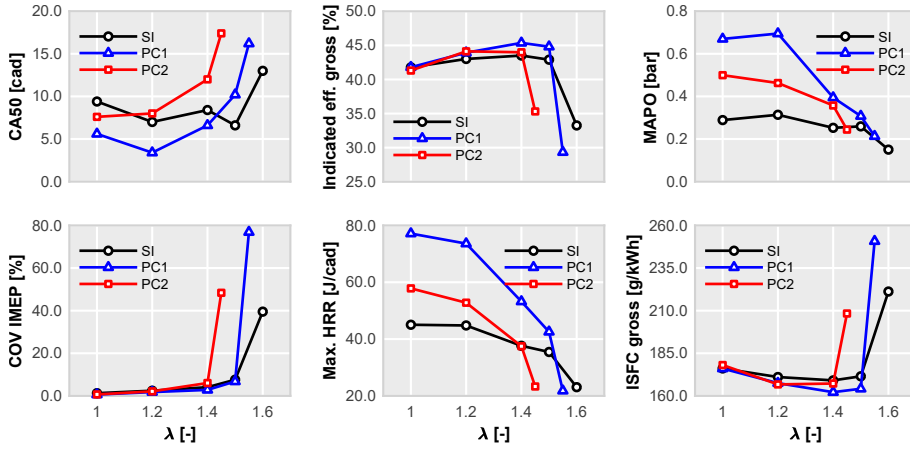


Figure 5.8: Trends of air dilution in combustion phasing (CA50), gross indicated efficiency, MAPO, combustion stability (COV IMEP), combustion velocity and fuel consumption for the studied ignition systems at high engine load and speed conditions operating with CNG.

excess of oxygen and combustion temperature. The same result as in the gasoline trends is observed, the emitted NO_x decreases as long as the dilution increases but is not enough to overcome the use of an after-treatment system.

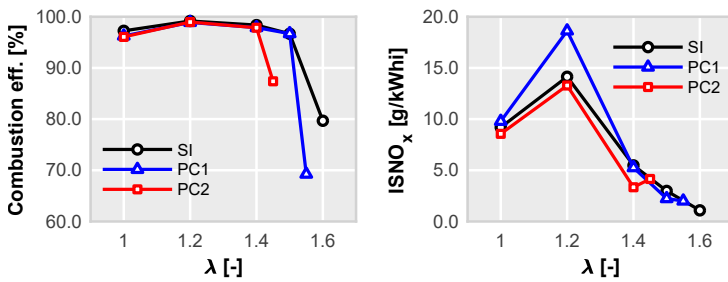


Figure 5.9: Trends of air dilution in combustion efficiency and emitted NO_x for the studied ignition systems at high engine load and speed conditions operating with CNG.

A comparison of pressure and heat release rate profiles of stoichiometric and maximum dilution conditions is shown in Figure 5.10. As in previous figures, solid lines represent the cycle-averaged profile while light colors represent the standard deviation. Dashed lines represent the combustion phasing (CA50). At stoichiometric conditions combustion phasing is properly

set due to the highest knocking resistance of the compressed natural gas. When increasing the dilution, combustion phasing is delayed due to the lower combustion velocity and it is pushed away from the TDC.

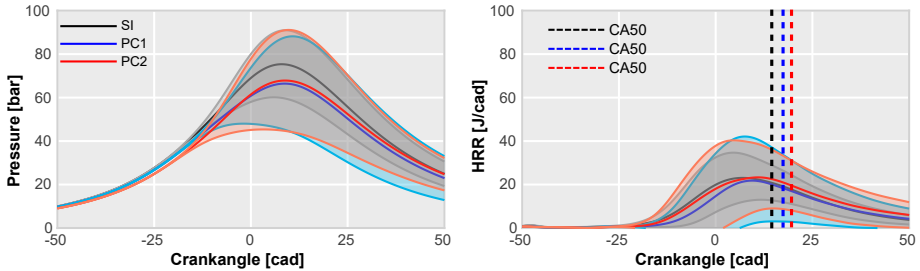


Figure 5.10: Pressure (left) and heat release rate (right) profiles of the high engine load and speed conditions at maximum λ operating with CNG for conventional ignition system (black) and both passive pre-chamber geometries (blue and red). Dashed lines correspond to 50% of combustion (CA50).

These results are compatible with those obtained when operating with gasoline fuel. Heat release rate profiles are balanced, leading to similar pressure profiles. However, having similar pressure and heat release rate profiles does not lead to similar maximum dilution levels (maximum dilution ratio for pre-chamber 1 is $\lambda = 1.55$, while for pre-chamber 2 is $\lambda = 1.45$). This is particularly relevant between the two different pre-chamber systems.

In order to determine the possible causes of the different performance between pre-chambers, simulations with the 1D Wave Action model were carried out for the passive pre-chamber configurations at the most diluted conditions. The key idea is to analyze different causes and approve or refuse them depending on results and knowledge provided by this 1D Wave Action model.

One explanation could lie in the performance of the jets. Several authors [136, 210, 232, 237, 281, 282] have investigated the jets features (velocity, penetration, entrainment...) and their implications on combustion. Hence, taking advantage of this 1D Wave Action model, a study of the jet dynamics was performed.

First of all, the main chamber and pre-chamber pressure profiles are presented in Figure 5.11 as a first step to analyze the performance of the turbulent jets. In this figure, the red profile, which corresponds with the pressure profile inside the pre-chamber, shows a secondary bump located around -25 CAD. This pressure perturbation is related to the PC combustion that forces the ejection of hot gas into the main chamber and its subsequent

ignition. Comparing the two different pre-chamber profiles, there is no substantial differences among them, maintaining the maximum pressure difference between both chambers (Δp).

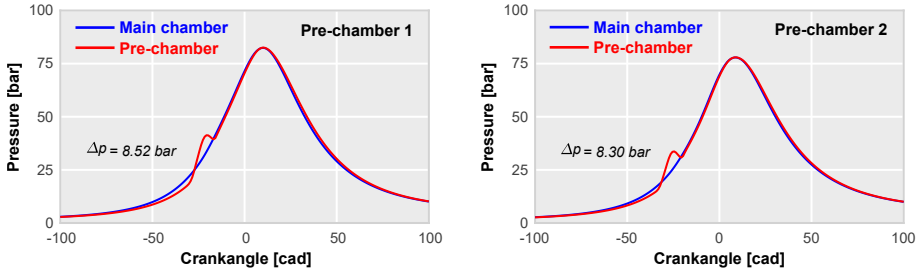


Figure 5.11: In-cylinder (blue) and pre-chamber (red) pressure profiles at maximum λ operating with CNG for pre-chamber 1 ($\lambda = 1.55$) and pre-chamber 2 ($\lambda = 1.45$).

As the pre-chambers were designed to keep similar hole diameter and ratio between the total gas exchange area and pre-chamber volume (PC1 = 3.9 m^{-1} and PC2 = 4.4 m^{-1}), it is reasonable to think that these little differences in the behavior of pre-chambers are explained by their design itself (see Figure 3.2 and Table 4.2). As a result, the instantaneous velocity and mass flow rate through a given orifice of the pre-chamber should be also similar.

This is confirmed in Figure 5.12 in which the temporal evolution of both parameters is plotted for the two pre-chamber configurations. The bulk temperature of the jets also plays a relevant role in the main chamber ignition. However, the variation of bulk temperature between both chambers is not representative, being around 2000 K in both cases.

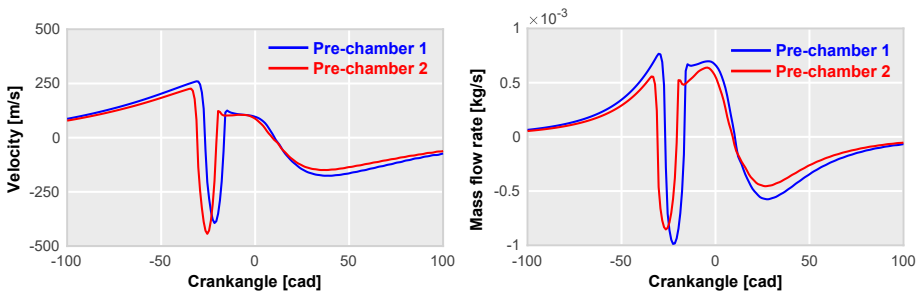


Figure 5.12: Velocity (left) and mass flow rate (right) profiles in one hole at maximum λ operating with CNG for pre-chamber 1 ($\lambda = 1.55$) and pre-chamber 2 ($\lambda = 1.45$).

In view of these results, it can be expected that the root cause of the different tolerance to dilution between both pre-chambers does not lie on the jet properties.

However, even these pre-chambers were designed to keep similar area to volume ratios, another possible explanation could be the distinct pre-chamber volumes, leading a lack of the energy available for the main chamber ignition. Hence, an energy balance inside the pre-chamber during the ejection process was performed to compare the levels of energy available for igniting the main chamber.

The total amount of energy depends on the total amount of fuel available within the pre-chamber at the start of ejection. It is remarkable that the start of ejection may be different between points and/or pre-chambers depending on the spark timing used to achieve MBT conditions. In this way, delaying the spark timing increases the available energy as the piston movement forces more mixture mass to enter in the pre-chamber. The energy can be split in different parts, such as, the energy transferred to the jet (hereinafter referred as Energy Available for Ejection, EAE), unburned fuel inside the pre-chamber volume at the end of ejection process (referred as Unburned), heat loss through the walls (referred as Q_{wall}) and fuel mass loss through orifices due to pressure increase inside the pre-chamber (the ejection in inert conditions, referred as Inert). First one of the different parts in which total energy has been divided is the effective energy to generate the hot jet in reactive conditions, which is the source of the ignition in the main chamber.

This 1D model provides outcomes that help to estimate all of the energy losses. However there are two considerations that must be taken into account when analyzing the results. The first one is the assumption by the 1D model of a perfect mixing during combustion. This means that combustion products are being evacuated from the very first moment that combustion starts, which causes a minimization of the inert mixture ejection (Inert). The second one, the 1D model requires a combustion rate profile in both chambers because it does not have a predictive combustion model. In the case of combustion profile in main chamber, it was obtained directly from experimental activity through combustion diagnosis [270, 271]. While combustion profile inside the pre-chamber was calibrated to obtain a 99% of burned fuel at the end of ejection process. In this way, the total amount of unburned fuel (Unburned) is low by its definition.

These two hypotheses are consistent with some results provided by more advanced numerical methods (3D Computational Fluid Dynamics) which consider geometrical effects, such as the location of the electrodes at the

top of the pre-chamber. Regarding the pre-chamber volume, as it is quite small compared with the global displaced volume, it ensures that almost all mixture is consumed when flow between both chambers is inverted. Besides the proximity of the walls and the enhanced turbulence inside the pre-chamber distort the flame front while directing combustion products to a given hole by following a preferential path. Thereby, this process can be considered, somehow, in between a perfect mixing and a perfect scavenge process. In this way, the assumption of a perfect mixing process can be considered as the best possible situation, since the amount of ejected inert flow is minimum, letting to perform a qualitative analysis of the energy share available for igniting the main chamber.

Hence, an energy balance at these high engine load and speed conditions was carried out. Main results of this study are presented in Table 5.3. The analysis with the stoichiometric cases are included to quantify the reduction of available energy due to the spark timing advance as the dilution ratio increases, and thus, the extension of combustion duration. The calculated values are normalized to their corresponding stoichiometric test.

In a first sight, 'Unburned' and 'Inert' contributions to the energy balance are negligible due to the aforementioned hypotheses. Furthermore, heat transfer through the walls ' Q_{wall} ' is significantly low since the ejection process finishes in few milliseconds. Thus, the EAE can be considered proportional to the total energy available within the pre-chamber at the spark timing. As piston movement forces the gases to enter into the pre-chamber, the total amount of fuel increases. For instance, total energy available inside PC1 decreases almost 40% when the spark timing is advanced from -18 (stoichiometric case) to -32 (maximum dilution case).

Table 5.3: Energy balance inside the pre-chamber for PC1 and PC2 at high engine load and engine speed conditions.

		EAE	Q_{wall}	Unburned	Inert	Σ
PC1	Stoich.	0.918	0.003	0.002	0.077	1.000
	Max. λ	0.585	0.002	0.003	0.000	0.590
PC2	Stoich.	0.950	0.005	0.000	0.045	1.000
	Max. λ	0.580	0.003	0.002	0.028	0.613

Since the energy provided by any of both pre-chamber configurations exceeds by far the energy provided by a conventional spark plug (70 mJ), it can be expected that the earlier ignition issues of passive pre-chamber concept are not due to the amount of energy available in the pre-chamber.

In a conventional SI combustion, the heat release rate depends on the flame propagation velocity, the amount of fuel per unit volume and the flame surface. With the hypothesis that flame velocity and the charge density are comparable at a particular λ value (which seems reasonable as the thermochemical properties of the fluid are similar at a particular engine load and speed condition), increasing the number of ignition locations must lead to an increase of the initial flame surface and, thus, a greater heat release rate is expected. Passive pre-chamber ignition takes advantage of this principle in the main chamber: each turbulent jet is able to ignite the charge in the main chamber at a given location.

This trend can be observed in Figure 5.8. In this Figure, maximum heat release rate at $\lambda = 1$ increases with the number of pre-chamber holes. Looking deeply into the maximum heat release values, the ratio between both pre-chamber combustion velocity and pre-chamber number of holes coincides, in a value around 1.5. If the main cause of this efficiency drop is related with the number of pre-chamber holes, this value around 1.5 should be maintained in the whole operating range. However, this relationship is only maintained as long as the cycle-to-cycle variability is kept in low values (this is at low dilution ratios, from 0% to 40%). When cycle-to-cycle variability rises, the relationship is broken, being this cycle-to-cycle variability the main constraint to maintain, or even improve, efficiency levels at high dilution ratios (>50%).

It is therefore reasonable to conclude that the pre-chamber design is key aspect when optimizing the passive pre-chamber ignition concept for a particular condition of λ value. The internal fluid dynamics pattern of the pre-chamber must be smoothed to reduce the turbulence variability in the spark plug region, thereby decreasing cycle-to-cycle variability.

5.3. Compatibility with EGR dilution

5.3.1. Employing gasoline as fuel

Evaluation with external EGR followed the same approach as the evaluation with air dilution. The addition of cooled EGR is a very promising strategy to reduce the fuel consumption while reducing the emitted NO_x . Firstly the ignition concept was evaluated using gasoline as fuel at high engine load and speed conditions. Main properties of the fuel can be found in Table 4.4.

In Figure 5.13 results of main combustion parameters are shown for the EGR evaluation at high engine load and speed conditions. Black line corresponds with the conventional ignition concept while blue and red lines correspond with the passive pre-chamber ignition concept (pre-chamber 1 and 2 respectively). It is observed how the indicated efficiency is greater for the pre-chamber cases at these conditions in the whole operating range until the dilution limit is reached. This is mainly caused by the better combustion phasing and the increased combustion velocity provided by the pre-chamber ignition system.

When reaching this dilution limit, similar issues as described when diluting with air happen. Combustion stability is highly compromised, leading to misfiring cycles and a significant decrease of the gross indicated efficiency. The dilution limit of pre-chamber 1 operation was not included due to severe dispersion, in which only one out of four cycles fired, causing a extremely high CoV IMEP factor, however this limit is reached around 22% of EGR.

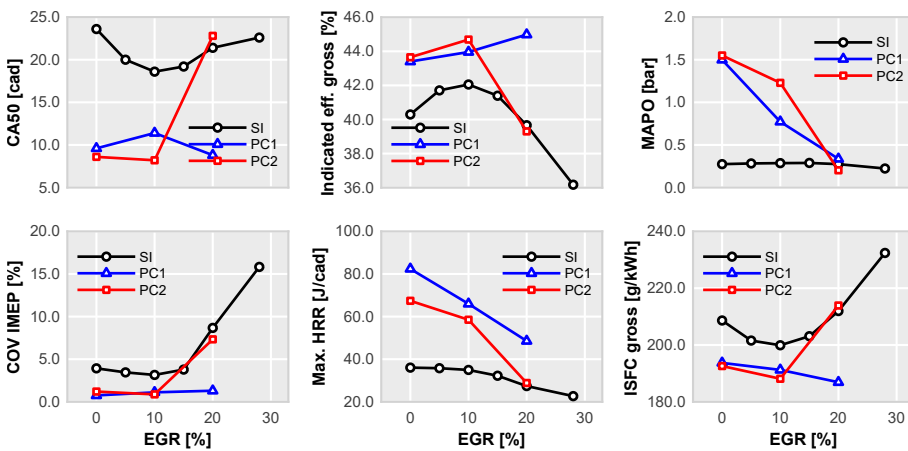


Figure 5.13: Trends of EGR dilution of combustion phasing (CA50), gross indicated efficiency, MAPo, combustion stability (COV IMEP), combustion velocity and fuel consumption for the studied ignition systems at high engine load and speed conditions operating with gasoline.

Regarding pollutant emissions, presented in Figure 5.14, NO_x decreases as effect of increasing the external EGR and the combustion efficiency is kept at similar values for all three cases.

The pressure and heat release rate profiles of the three ignition systems at maximum dilution measured conditions are included in Figure 5.15. Increasing the dilution ratio, the sharpened heat release rate profile becomes smoother and longer. Red profile, corresponding with pre-chamber 2 is now

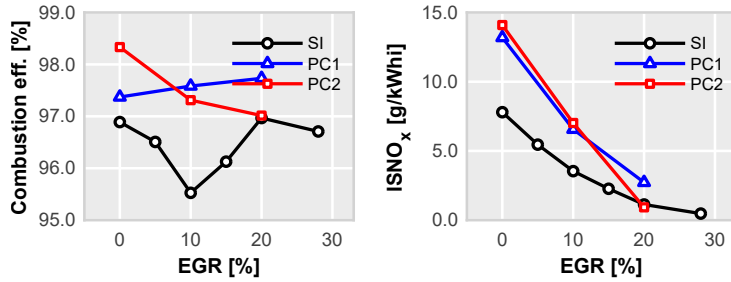


Figure 5.14: Trends of EGR dilution of combustion efficiency and emitted NO_x for the studied ignition systems at high engine load and speed conditions operating with gasoline.

quite similar to that obtained with conventional spark system, and thus, main benefits of the passive pre-chamber operation are lost at these conditions. Pre-chamber 1 offers some benefits compared with the conventional spark system until the dilution limit is reached. However, compared to pre-chamber 2, the main results at the effective maximum dilution limit tend to be quite similar between them.

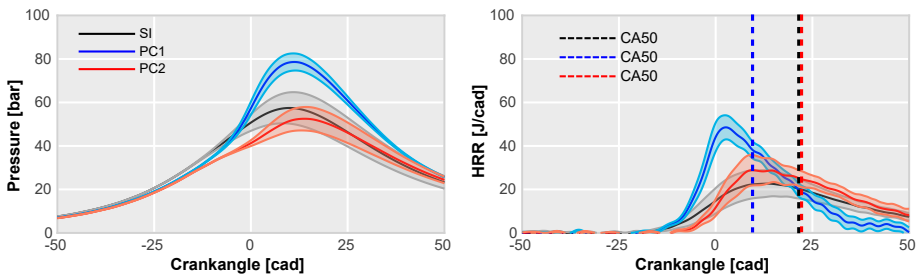


Figure 5.15: Pressure (left) and heat release rate (right) profiles of the high engine load and speed conditions at maximum EGR operating with gasoline for conventional ignition system (black) and both passive pre-chamber geometries (blue and red). Dashed lines correspond to 50% of combustion (CA50).

Figure 5.16 shows a quick overview of the most relevant combustion parameters. At the maximum dilution ratio, the "quality" of the combustion decreases, suffering of a reduction in the gross indicated efficiency, however if this critical situation is not reached, the faster combustion process and better combustion phasing, together with the increase in the heat specific ratio, help to increase the overall efficiency, as pre-chamber 1 results show. Furthermore

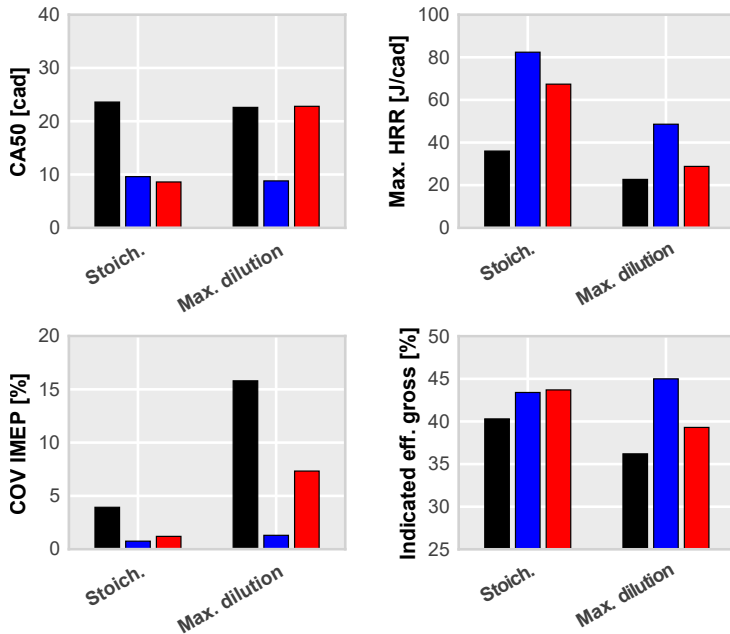


Figure 5.16: Comparison of combustion phasing (CA50), combustion velocity, combustion stability and gross indicated efficiency for both ignition systems at high engine load and speed conditions for stoichiometric and maximum EGR operating points with gasoline.

it is seen how, again, the most critical parameter is the combustion phasing, since pre-chamber 1 generates the fastest combustion process in all cases but pre-chamber 2 shows slightly better efficiency in some cases.

The next operating point corresponds with a combination of medium engine load and speed (6.8 bar IMEP at 2000 RPM). At these conditions the proper operation with external EGR becomes more compromised, there is an early increased combustion instability as the EGR dilution increases. The tolerance to EGR becomes more critical compared with the operation at high engine load. These results can be seen in Figure 5.17.

As the increased instability pushes the combustion phasing towards the expansion stroke the gross indicated efficiency suffers an important drop for the passive pre-chamber ignition system, specially pronounced at those dilution ranges where the operation at high engine load was not so compromised. This effect is more evident as the combustion velocity decreases, avoiding the bit recovery of the combustion phasing. It is also remarkable

that the operation at maximum diluted conditions, in both engine loads, is comparable with a "go-no-go" system, since the efficiency is suddenly limited in around 1-3% EGR.

As expected, lowering the engine load affects the knocking tendency of the operating condition. Without a combustion phasing restriction, the spark ignition system is able to set the combustion in optimal values (CA50 is around 25 cad in the previous conditions while now it is around 10 cad), resulting in a reduction of the optimization gap of the passive pre-chamber ignition system. This is clearly seen in the gross indicated efficiency trends at early dilution conditions, in where there is little or even there is not efficiency gain for pre-chamber concept.

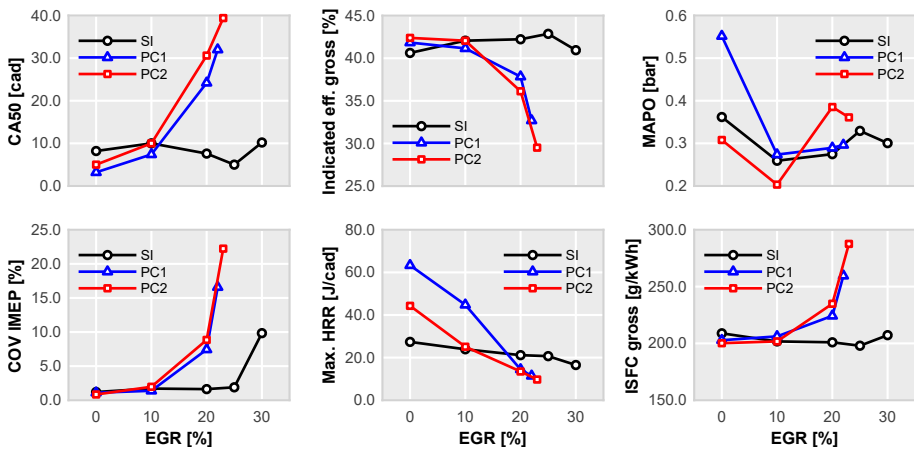


Figure 5.17: Trends of EGR dilution of combustion phasing (CA50), gross indicated efficiency, MAPO, combustion stability (COV IMEP), combustion velocity and fuel consumption for the studied ignition systems at medium engine load and speed conditions operating with gasoline.

Results of the emitted pollutants are presented in Figure 5.18. Combustion efficiency trends are quite similar for the three different ignition systems, however it is seen how suffers a remarkable decrease when reaching the dilution limit. This effect is related to the high combustion dispersion. Regarding the emitted NO_x , the effect of increasing EGR can be observed, reducing the overall emissions as the dilution increases.

Pressure and heat release rate profiles of the three different ignition systems at maximum diluted conditions are presented in Figure 5.19. In these cases, the reduction of the available fuel due to the lower engine load negatively affects the performance of the passive pre-chamber ignition concept, as it has been proven in the previous Section 5.2. The combination of the

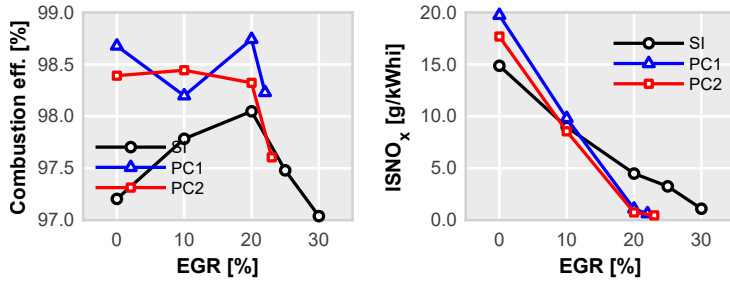


Figure 5.18: Trends of EGR dilution of combustion efficiency and emitted NO_x for the studied ignition systems at medium engine load and speed conditions operating with gasoline.

external EGR with a lower availability of fuel to ignite the main chamber makes the maximum heat release rate to decrease, pushing the combustion phasing towards the expansion stroke and avoiding pre-chambers to reach the conventional ignition system maximum pressure.

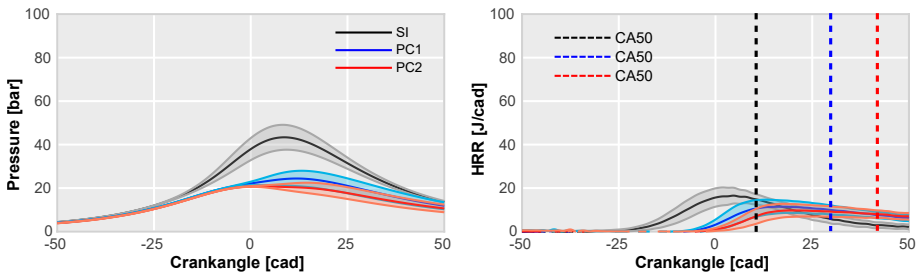


Figure 5.19: Pressure (left) and heat release rate (right) profiles of the medium engine load and speed conditions at maximum EGR operating with gasoline for conventional ignition system (black) and both passive pre-chamber geometries (blue and red). Dashed lines correspond to 50% of combustion (CA50).

Focusing on the relevant combustion parameters, Figure 5.20, shows a comparison of the combustion phasing, velocity and stability and gross indicated efficiency between the stoichiometric and the maximum diluted conditions. The lack of performance is quite critical for the passive pre-chamber ignition system. This is caused due to the aforementioned lack of available fuel to properly initiate the combustion at the main chamber and the increased dispersion caused by the lean burn strategy.

The addition of EGR is specially critical when employing the passive pre-chamber ignition system. In this case, the external EGR is added to the internal EGR that was not properly scavenged, increasing the effective EGR

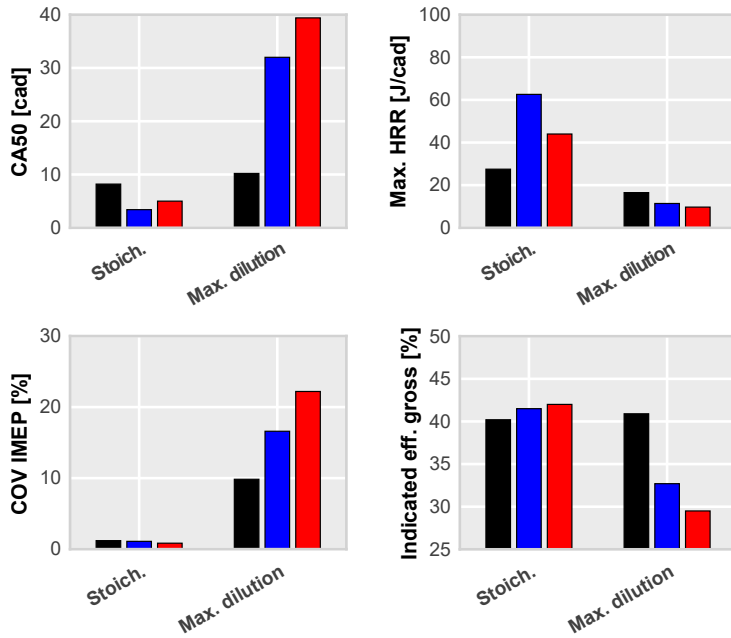


Figure 5.20: Comparison of combustion phasing (CA50), combustion velocity, combustion stability and gross indicated efficiency for both ignition systems at medium engine load and speed conditions for stoichiometric and maximum EGR operating points with gasoline.

dilution ratio. This may be one of the causes to the lower dilution tolerance of EGR compared when diluting with fresh air. For example, in the high engine load and speed case, pre-chamber 1 shows around 40% less of tolerance when diluting with EGR than with fresh air.

Making the assumption that integral length scale (l_t) and turbulence intensity (u') are constant along the whole dilution operating range, the evolution in the flame regime diagram can be calculated. This diagram is also called Borghi-Peters Diagram [283, 284]. This hypothesis can be considered since the engine hardware and the operating engine speed are kept constant.

Moderate Reynolds numbers ($10 < Re < 100$) and Karlovitz numbers close, or even, below to 1 are the parameters that define a typical flame in conventional spark-ignition engines [285, 286]. These kind of flames are framed in the corrugated flamelets regime. The flame structure is

modified by the turbulent field, as in the literature of premixed flames theory [287], can be found that the entire reactive-diffusive flame structure (l_f) is embedded within eddies of Kolmogorov scale size.

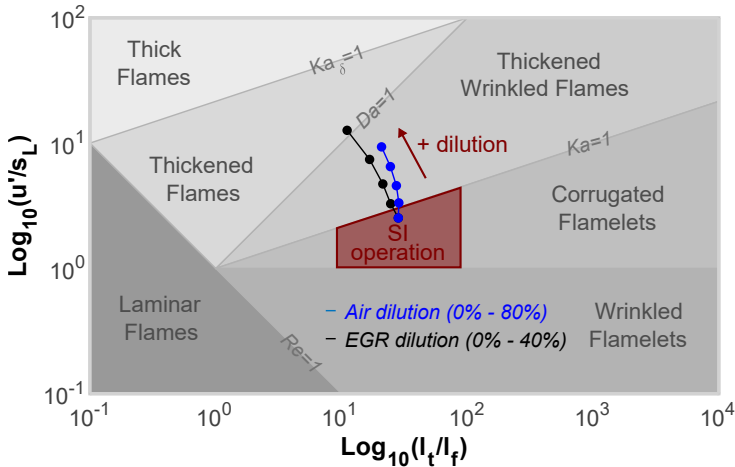


Figure 5.21: Borghi-Peters diagram and trends observed when increasing the dilution rate with air and EGR.

In Figure 5.21, a Borghi-Peters diagram is presented, highlighting the region where conventional SI engines operate. The evolution of the flame features according to the dilution ratio is shown in blue and black lines, for air and EGR dilution respectively. In these trends, the reference turbulence values u' and l_f were chosen arbitrary in order to focus the reference conditions (0% of dilution) inside the SI operation regime, while the laminar flame features, such as laminar flame speed (s_L) and flame thickness (l_f), were calculated by the premixed laminar flame-speed model included in the commercial software CONVERGE [275]. This code simulates an ideal case set-up to measure flame speed in a channel with a fixed cross-sectional area keeping the pressure constant. In this case, four different air cases ranging from 0% to 80% and four additional cases ranged between 0% and 40% for EGR dilutions were calculated. Despite these are not exact calculations, this method allows to qualitative clarify what is the path traveled by the flame when increasing the dilution levels.

Results of this study, presented in Figure 5.21, show how the flame features are moved towards the thickened flame, no matter the kind of dilution method. In this new region, the size of the eddies becomes smaller than the flame thickness, letting a penetration into the diffusive flame structure and enlarging the front flame thickness whereas decreasing its laminar speed.

This effect is presented in Figure 5.22. All simulated laminar flame speeds and thickness are plotted depending on their dilution degree. However, as it is observed in Figure 5.21, the effect of EGR dilution is more marked since the flame reaches more unstable regimes (closer to $Ka_\delta = 1$ where the eddies can even penetrate into the reaction flame structure) with lower dilution rates. This behaviour can be explained by both the flame thickness enlargement and the laminar flame speed reduction observed in Figure 5.22 when considering EGR to increase the engine efficiency.

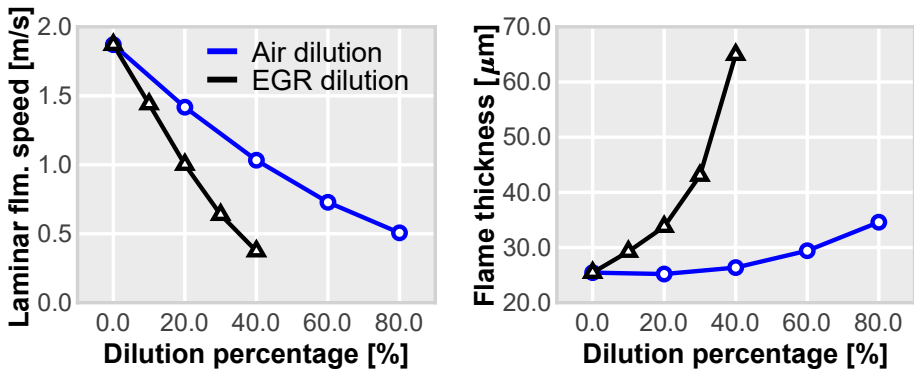


Figure 5.22: Computed laminar flame speeds (s_L) and flame thickness (l_f) for air and EGR diluted cases.

5.3.2. Employing natural gas as fuel

As in the previous Section 5.2, the second part of the external EGR strategy consisted in the evaluation of the compatibility when employing compressed natural gas as fuel. Fuel properties are the same used in the other natural gas subsection, which its main properties can be found in Table 4.5.

Since the engine architecture is kept constant, same issues regarding the higher knocking resistance feature of the natural gas are expected to happen. Thus, slightly gains, or even a lack, of performance compared with conventional spark ignition system is expected when combining an EGR dilution strategy with compressed natural gas at these particular conditions.

First operating point corresponds with the combination of high engine load and speed conditions (12.8 bar and 4500 rpm). Main trends when increasing the dilution ratio are presented in Figure 5.23. Black line corresponds with conventional spark ignition as reference, while blue and red lines correspond with passive pre-chamber ignition system, pre-chamber 1 and pre-chamber 2 respectively.

Results of gross indicated efficiency fit with the previous prediction. Along the whole operating range, passive pre-chamber system is only able to reach the spark ignition concept efficiency, and, when reaching the dilution limit, their efficiency suffers a high drop, furthermore, this limit is found earlier than the spark ignition system limit. In this case, the maximum dilution limit of pre-chamber 1 was not measured due to safety issues, however, it is around 1-3% EGR beyond the last measured point. The rest of combustion parameters are in line with the previous obtained results. Higher combustion velocity and proper combustion phasing for both ignition concepts that turn in a similar operation until the dispersion becomes critical.

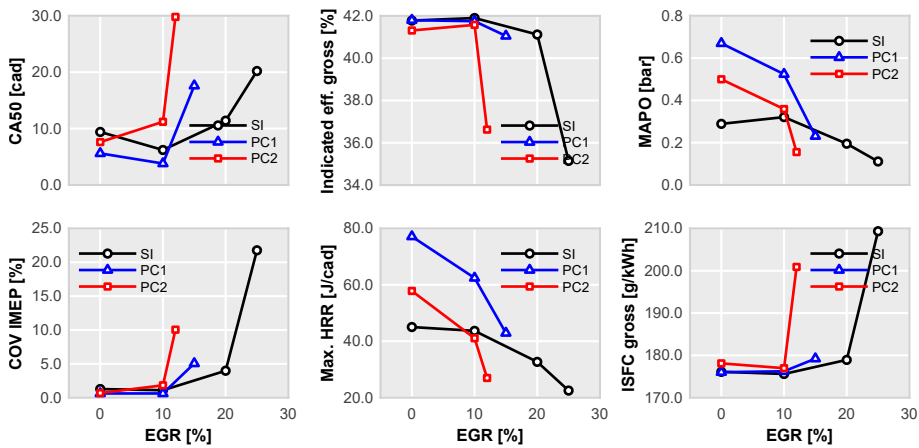


Figure 5.23: Trends of EGR dilution of combustion phasing (CA50), gross indicated efficiency, MAPO, combustion stability (COV IMEP), combustion velocity and fuel consumption for the studied ignition systems at high engine load and speed conditions operating with CNG.

Comparing with previous results with gasoline fuel, it is evident that passive pre-chamber system has suffered a reduction of the gross indicated efficiency. The efficiency gain is lost mainly due to the good combustion phasing achieved by the conventional spark ignition since there are no knocking limitations. In this sense, as long as the conventional system is not compromised, the passive pre-chamber system will be only able to match the spark-ignition system efficiency. This main idea is observed in both fuels at operating conditions that do not compromise the combustion phasing, even with both dilution strategies.

Regarding pollutants emissions, the emitted NO_x decrease as the dilution ratio increases, while both systems keep a suitable combustion efficiency.

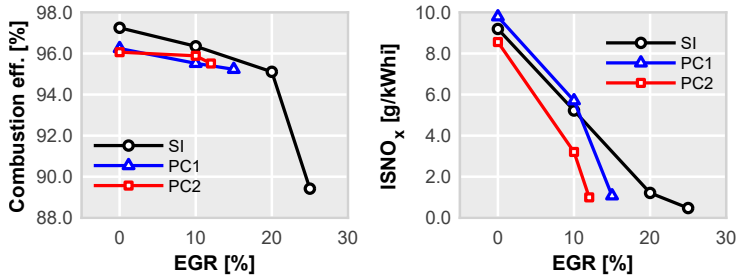


Figure 5.24: Trends of EGR dilution of combustion efficiency and emitted NO_x for the studied ignition systems at high engine load and speed conditions operating with CNG.

Pressure and heat release rate profiles, and the comparison between stoichiometric and maximum dilution ratios are shown in Figure 5.25 and Figure 5.26 respectively.

Comparing the results with the gasoline previous results at the same conditions, it is evident that the passive pre-chamber ignition operates similarly. Increasing the dilution ratio reduces the maximum combustion velocity peak and enlarges the duration, this causes a delay on the combustion phasing leading to a reduced maximum pressure.

However, despite the benefits that bring EGR dilution strategy, there are no gains in terms of indicated efficiency as long as combustion is well phased in the whole operating range. Again, caused by the higher knocking resistance of the compressed natural gas. In order to obtain improvements when using this alternative ignition concept, either increasing the dilution ratio achieved by pre-chamber system or a higher compression ratio that forces the conventional system to operate out of its optimal range is needed.

Regarding the operation at medium engine load, similar results as those obtained at high engine load are expected, since lower loads tend to be more knocking friendly, and this has been proved a must condition to obtain clear benefits of this passive pre-chamber system. Main results are presented in Figure 5.27, while pollutants emissions trends are presented in Figure 5.28.

As expected, main results are even worse than those obtained at high engine load conditions. Operation of passive pre-chamber is limited by the earlier stability drop, leading to a reduced maximum dilution limit compared with conventional spark system. Also, the combustion phasing of spark ignition system is well set along the operating range, leading to obtaining a good performance.

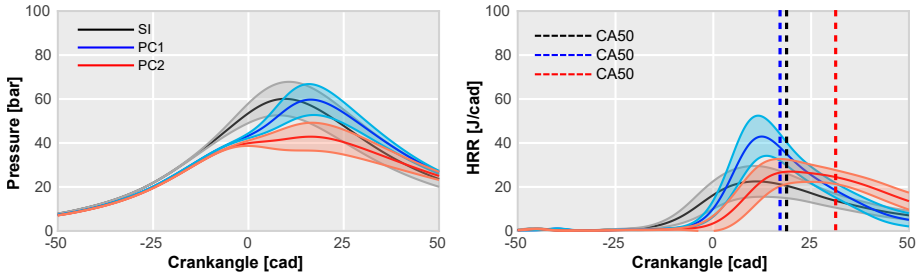


Figure 5.25: Pressure (left) and heat release rate (right) profiles of the high engine load and speed conditions at maximum EGR operating with CNG for conventional ignition system (black) and both passive pre-chamber geometries (blue and red). Dashed lines correspond to 50% of combustion (CA50).

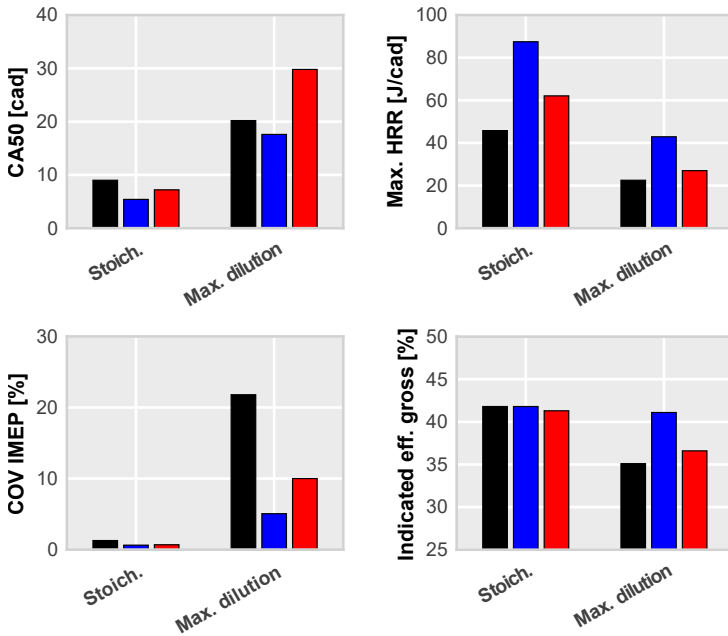


Figure 5.26: Comparison of combustion phasing (CA50), combustion velocity, combustion stability and gross indicated efficiency for both ignition systems at high engine load and speed conditions for stoichiometric and maximum EGR operating points with CNG.

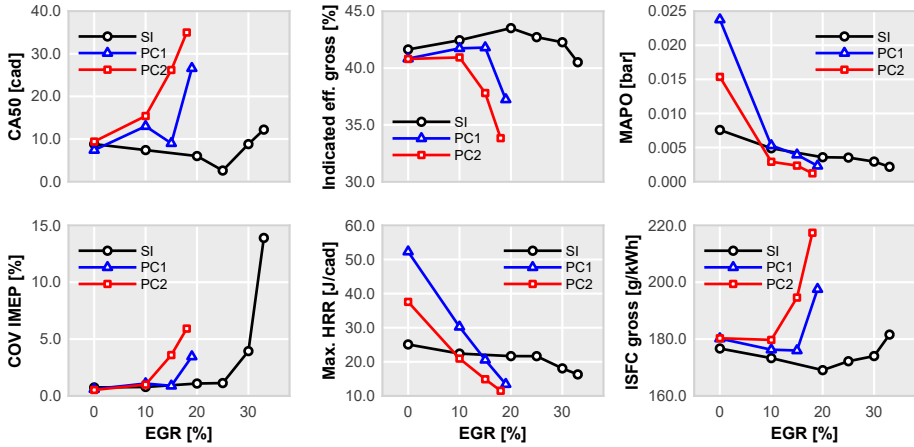


Figure 5.27: Trends of EGR dilution of combustion phasing (CA50), gross indicated efficiency, MAPO, combustion stability (COV IMEP), combustion velocity and fuel consumption for the studied ignition systems at medium engine load and speed conditions operating with CNG.

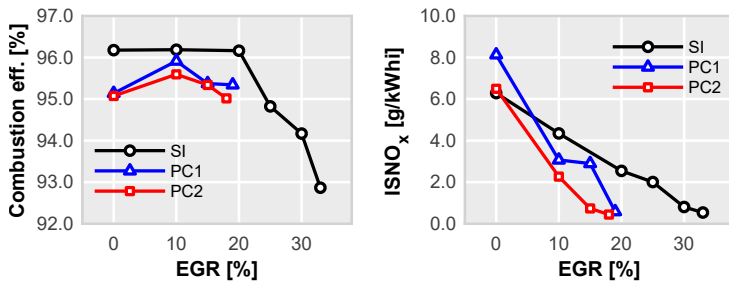


Figure 5.28: Trends of EGR dilution of combustion efficiency and emitted NO_x for the studied ignition systems at medium engine load and speed conditions operating with CNG.

5.4. Operation at low engine load and speed conditions

It is well-known that one of the most critical aspects of the passive pre-chamber ignition system is the operation at low engine loads and speeds. The exhaust heating capability of this concept is compromised due to the fastest combustion process and the high combustion dispersion at delayed spark timings.

In this section, the ability of the two studied pre-chamber definitions to achieve a proper exhaust tailpipe temperature is evaluated, and two different strategies to increase this output are proposed and analyzed. The operating condition is presented in Table 5.1, specifically OP3, which corresponds with the low engine load and speed conditions (2.8 bar and 1350 RPM).

Main results when operating with gasoline are presented in Figure 5.29. Here the combustion was delayed in steps of 2 cad until the combustion dispersion was unacceptable in the case of pre-chamber tests. Black line corresponds with conventional spark ignition system, blue line with pre-chamber 1 and red line with pre-chamber 2. These results highlight the main problems associated to the pre-chamber ignition system when delaying the combustion.

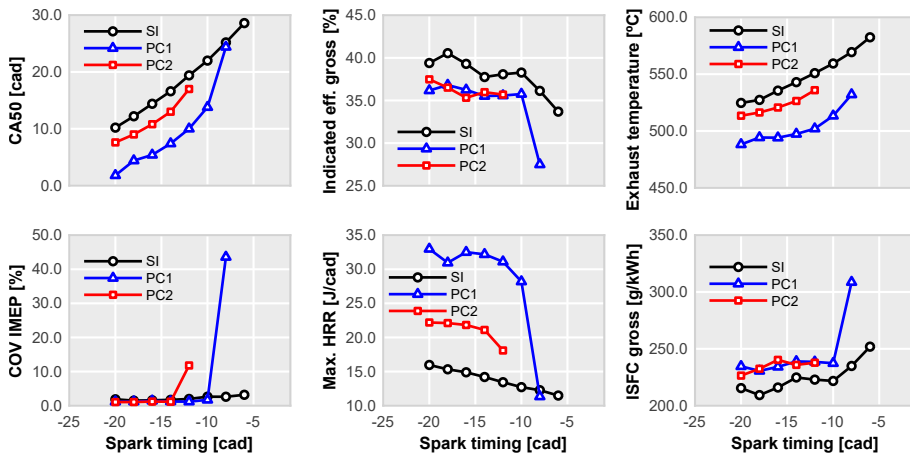


Figure 5.29: Comparison of combustion phasing (CA50), gross indicated efficiency, exhaust temperature, combustion stability (COV IMEP), combustion velocity and fuel consumption for both ignition systems at low engine load and speed conditions at $\lambda = 1$ operating with gasoline.

The maximum combustion velocity is higher for pre-chamber concept in the whole operating range, even more than double for pre-chamber 1 compared with conventional spark system. This high velocity avoids a long combustion duration which is suitable to increase the exhaust temperature. Due to this increased velocity, appears a higher relative heat loss that reduces the obtained gross indicated efficiency. Also, it is important that the operation of passive pre-chamber suffers a high stability drop at a given spark timing, reducing the effective operating range and limiting the obtained exhaust temperature.

Same testing campaign was carried out using compressed natural gas as fuel. Main results of this evaluation are presented in Figure 5.30. As in previous figure, black line is the conventional spark trend while blue and red lines correspond with pre-chamber concept trends (pre-chamber 1 and pre-chamber 2 respectively).

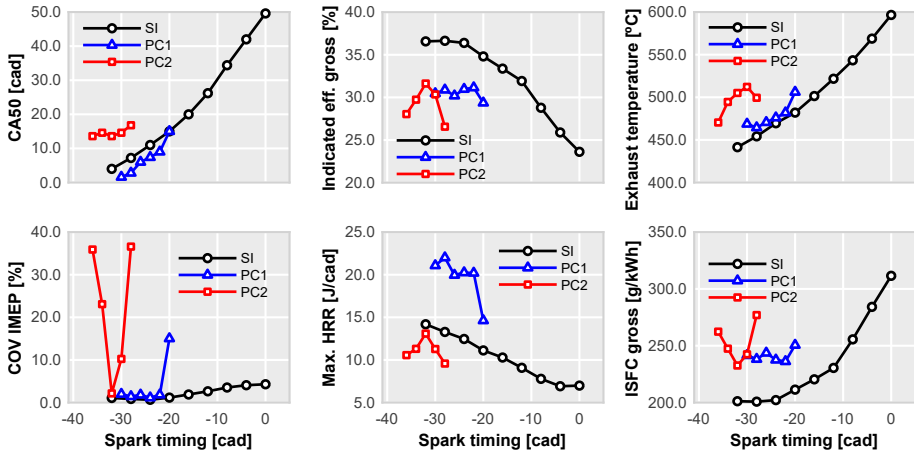


Figure 5.30: Comparison of combustion phasing (CA50), gross indicated efficiency, exhaust temperature, combustion stability (COV IMEP), combustion velocity and fuel consumption for both ignition systems at low engine load and speed conditions at $\lambda = 1$ operating with CNG.

These results are in line with those obtained with gasoline fuel. There is a stable combustion for pre-chamber 1 until the stability drop appears, then it becomes impossible a proper operation, leading to a significant decrease of performance earlier than the required spark timing delay to obtain a proper temperature in the exhaust pipeline. In case of pre-chamber 2, the operating range is extremely narrow, and its proper operation at these conditions is almost impossible.

Here, the same issue with the fast combustion is observed. For pre-chamber concept, the fast combustion achieved lead to a decrease of indicated efficiency due to the higher heat loss. Comparing pre-chamber 1 with the SI, as the operation with CNG is not limited by the knocking issues, the main benefit of utilizing a pre-chamber is lost, then, as this system adds an extra element (the pre-chamber itself), there are greater heat losses, worsen by the low engine speed of this operating condition. In case of pre-chamber 2, despite its combustion velocity is similar to the conventional spark system, the worse combustion phasing leads to the decreased efficiency loss.

An energy balance inside the pre-chamber was carried out to dig deeper into the root cause of the lack of operating range for pre-chamber 2 configuration compared with pre-chamber 1 configuration. Results of this balance can be found in Table 5.4. A comparison of energy available within the pre-chamber and its distribution between both pre-chambers is presented. Results are normalized to pre-chamber 1 values.

This table shows how pre-chamber 1 configuration is able to increase the available energy for jets generation (up to a 70%). This difference can be explained by the increased pre-chamber volume. As pre-chamber 1 has a larger volume, the total fuel amount stored during pre-chamber filling is greater than the obtained with pre-chamber 2, leading to a increase in the pre-chamber performance.

Table 5.4: Energy balance inside the pre-chamber for pre-chamber 1 and pre-chamber 2 at low engine load and speed conditions.

	EAE	Q_{wall}	Unburned	Inert	Σ
PC1	0.714	0.003	0.010	0.273	1.000
PC2	0.408	0.003	0.007	0.172	0.590

In order to increase the obtained exhaust temperature when operating with passive pre-chamber ignition system, two different strategies have been evaluated, employing compressed natural gas as fuel. First strategy consists of increasing the intake temperature up to 70°C. As this air flow temperature is increased, the overall temperature in the whole process is expected to increase, leading to a proper exhaust tailpipe temperature and also better conditions to promote stable combustion even at delayed spark timings. During the evaluation of these two strategies, pre-chamber configuration 2 has been excluded from the experimental campaign because of its poor performance and narrow operating range.

Results of first strategy can be found in Figure 5.31. Black and blue lines correspond with conventional spark ignition concept, standard and increased temperature respectively, while red and green lines correspond with passive pre-chamber system. In this case, intake temperature was intentionally increased up to 70°C in both ignition concepts.

With this strategy, exhaust temperature is slightly increased, however, due to its narrow spark timing operating range, the maximum attainable value is limited. On the other hand, an increase in the gross indicated efficiency

is obtained until the dispersion is unacceptable. This greater efficiency in reaches similar levels than those obtained with conventional spark ignition at 70°C.

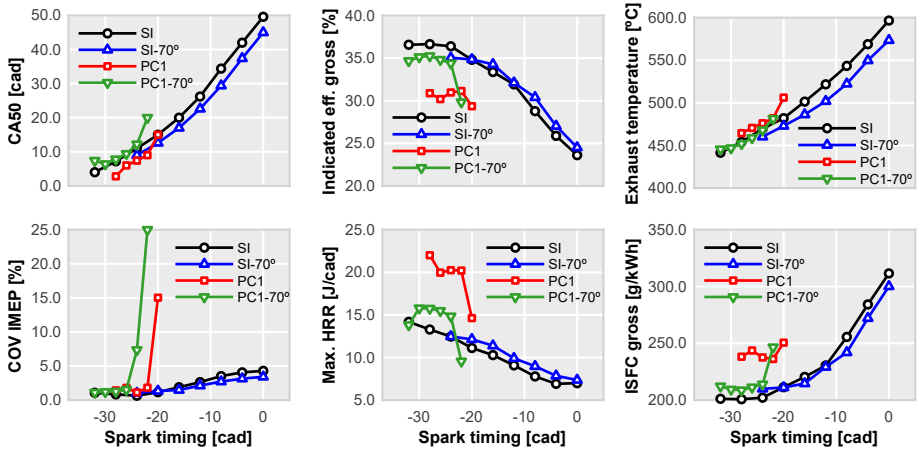


Figure 5.31: Comparison of combustion phasing (CA50), gross indicated efficiency, exhaust temperature, combustion stability (COV IMEP), combustion velocity and fuel consumption for both ignition systems at low engine load and speed conditions at $\lambda = 1$ operating with CNG and increased intake temperature.

Second studied strategy consisted of diluting with external EGR. Diluting increases the combustion duration by reducing the combustion peak velocity, which delays the combustion process towards the expansion stroke increasing the temperature in the exhaust tailpipe. Dilution ratio was increased in steps of 5% until the dispersion system was unacceptable.

Main results of this strategy can be found in Figure 5.32. Black, blue and red lines correspond with conventional spark ignition trends at the different dilution limits, while green, orange and purple lines correspond with passive pre-chamber system. Same combustion outputs are studied as in previous approach. In this case, there is a clear benefit in terms of exhaust temperature as the dilution ratio is increased for the pre-chamber ignition system.

This increase of exhaust temperature is related to the reduction of combustion velocity and the subsequent delay of combustion phasing. As CA50 is pushed away from TDC the resultant exhaust temperature increases. However is still not enough to assure a proper heat flux that activates the after-treatment system. It is remarkable that operation with 10% EGR slightly

increases the indicated efficiency by reducing the pumping losses and heat transfer while it is able also to increase the obtained temperature around 50 degrees.

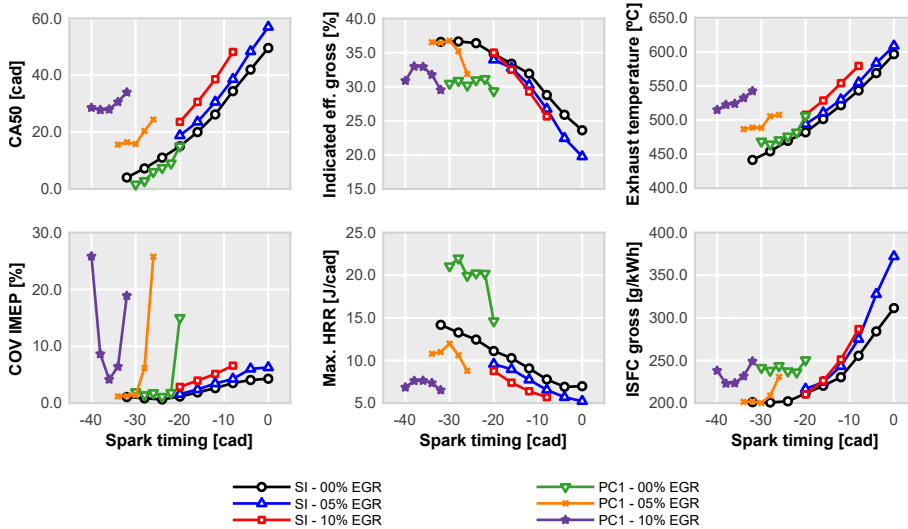


Figure 5.32: Comparison of combustion phasing (CA50), gross indicated efficiency, exhaust temperature, combustion stability (COV IMEP), combustion velocity and fuel consumption for both ignition systems at low engine load and speed conditions at $\lambda = 1$ operating with CNG and different EGR dilution levels.

5.5. Engine maps

As dilution strategy arises as a promising solution to increase performance of passive pre-chamber ignition concept in different combinations of engine load and speed, the complete engine map, as in previous Chapter 4, was measured. In this case, a comparison between passive pre-chamber system with and without external EGR is performed. This comparison was made with pre-chamber configuration 1, since it has shown suitable performance in the different studied operating points.

The different dilution levels measured are shown in Figure 5.33. These dilution ratios optimize the performance of passive pre-chamber ignition system. The dilution value was obtained increasing the external EGR until combustion dispersion was unacceptable or indicated efficiency started to

decrease. Higher engine speeds tend to decrease the maximum dilution ratio due to the shortest cycle time, while on the contrary, lower engine speeds are able to operate with higher diluted conditions.

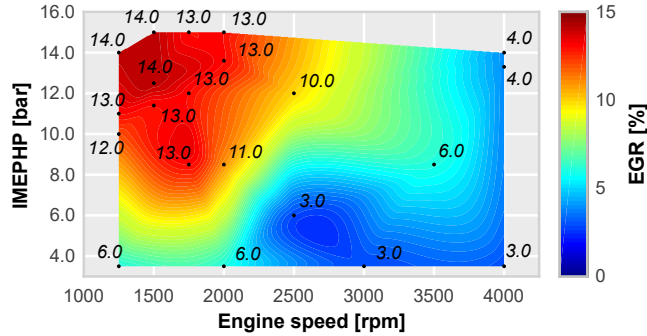


Figure 5.33: External EGR dilution level colormap of the engine map for pre-chamber 1 at $\lambda = 1$ operating with CNG and Miller cycle varying engine load and speed.

The first and more important result obtained when adding external EGR is that the effective operating range in the engine map increased. Low-end torque area now can be reached, and the operation is no longer compromised. Results of gross indicated efficiency with and without EGR can be seen in Figure 5.34.

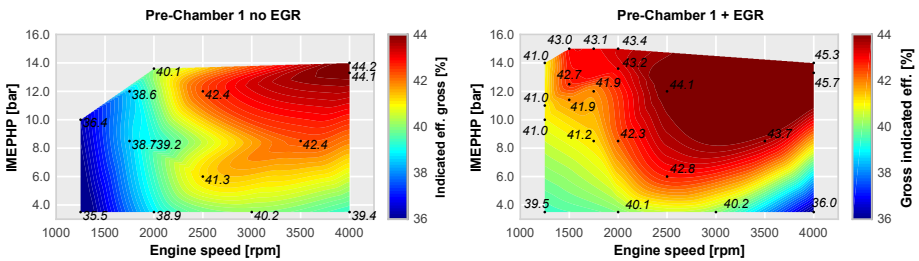


Figure 5.34: Gross indicated efficiency for passive pre-chamber ignition system without external EGR (left) and passive pre-chamber ignition system with external EGR (right) colormaps of the engine map at $\lambda = 1$ operating with CNG and Miller cycle varying engine load and speed.

Adding EGR increases the overall gross indicated efficiency in the whole engine map except in the low engine load and high speed area. The increase in efficiency is related to the lower pumping losses achieved by this strategy, specially at low and medium engine speeds (the point 10 bar at 1250 RPM

increases its efficiency from 36.4 to 41.0). On the contrary, low engine loads and high speed suffer a decrease in their performance, mostly caused by the higher instability and the bad combustion phasing.

Results of combustion phasing (CA50) and combustion velocity are presented in Figure 5.35 and Figure 5.36 respectively. The combustion phasing issue at low-end torque region is solved with the addition of external EGR. Now, combustion phasing is not set earlier than TDC, allowing to measure points with higher engine load. The better combustion phasing achieved is caused by the EGR effect of lowering the combustion velocity. This combustion velocity has been reduced in the whole engine map. These beneficial effects have the drawback at high engine speed in where combustion phasing is even worsened.

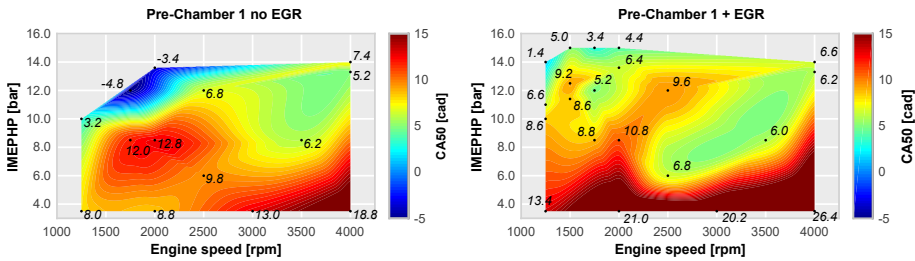


Figure 5.35: Combustion phasing for passive pre-chamber ignition system without external EGR (left) and passive pre-chamber ignition system with external EGR (right) colormaps of the engine map at $\lambda = 1$ operating with CNG and Miller cycle varying engine load and speed.

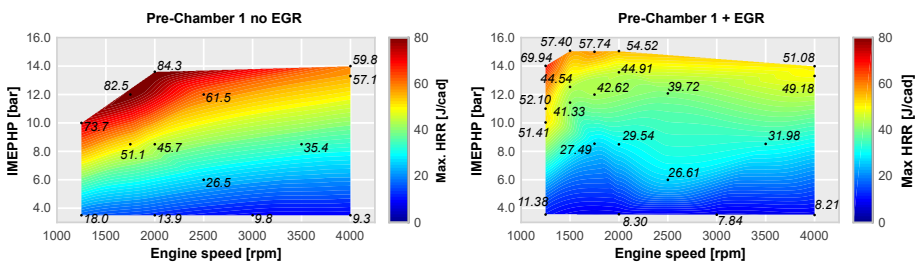


Figure 5.36: Combustion velocity for passive pre-chamber ignition system without external EGR (left) and passive pre-chamber ignition system with external EGR (right) colormaps of the engine map at $\lambda = 1$ operating with CNG and Miller cycle varying engine load and speed.

Combustion stability results are presented in Figure 5.37. As explained before with the combustion phasing results, the stability increases in the low-end torque region due to the slower combustion process achieved by the addition of external EGR. However, in terms of high engine speed and low engine loads, the lower combustion velocity has a harmful effect on combustion stability, negatively affecting the efficiency.

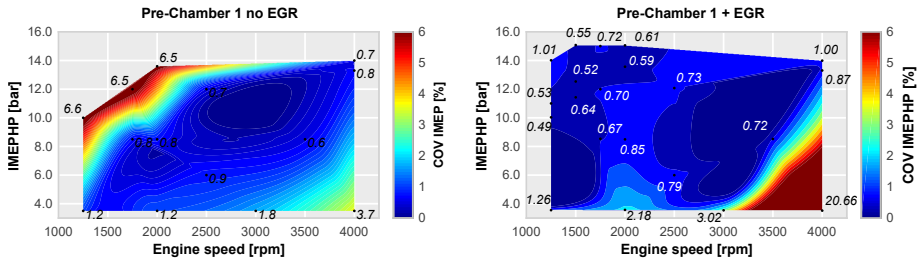


Figure 5.37: Combustion stability for passive pre-chamber ignition system without external EGR (left) and passive pre-chamber ignition system with external EGR (right) colormaps of the engine map at $\lambda = 1$ operating with CNG and Miller cycle varying engine load and speed.

Regarding the knocking tendency of the concept, as long as the combustion duration is increased, knocking is no longer an issue, even at high engine loads. In Figure 5.38, maximum amplitude of pressure oscillation is shown, and, in the most critical area, values showing a clear knock tendency have disappeared.

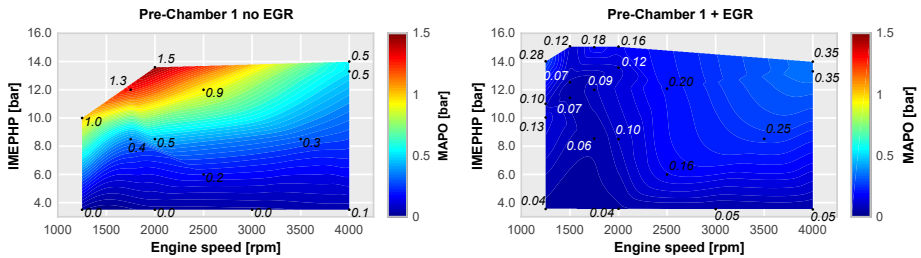


Figure 5.38: MAPO for passive pre-chamber ignition system without external EGR (left) and passive pre-chamber ignition system with external EGR (right) colormaps of the engine map at $\lambda = 1$ operating with CNG and Miller cycle varying engine load and speed.

Maximum in-cylinder pressure and fuel consumption are presented in Figure 5.39 and Figure 5.40. Maximum pressure is decreased for each point as the combustion duration increases with the addition of EGR. However,

maximum values reached remain quite similar between the addition or not of EGR. These maximum values, around 130 bar, are located in the low-end torque for both cases. Regarding fuel consumption, it is a related parameter of indicated efficiency. Best fuel consumptions are found in areas where efficiency is high.

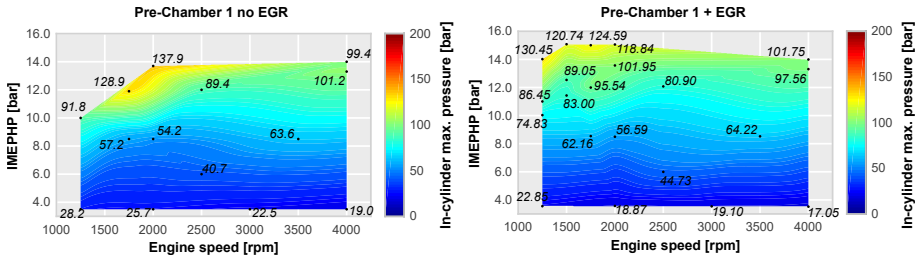


Figure 5.39: Maximum in-cylinder pressure for passive pre-chamber ignition system without external EGR (left) and passive pre-chamber ignition system with external EGR (right) colormaps of the engine map at $\lambda = 1$ operating with CNG and Miller cycle varying engine load and speed.

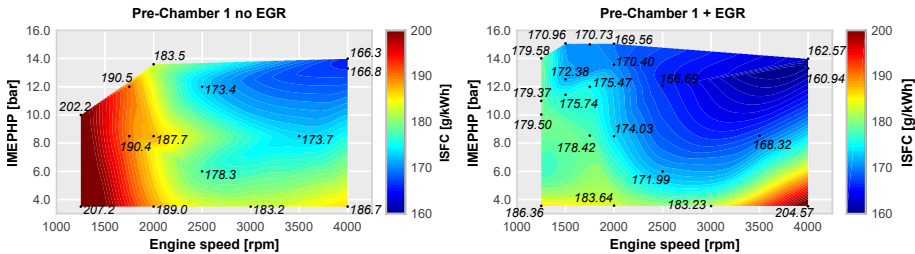


Figure 5.40: Fuel consumption for passive pre-chamber ignition system without external EGR (left) and passive pre-chamber ignition system with external EGR (right) colormaps of the engine map at $\lambda = 1$ operating with CNG and Miller cycle varying engine load and speed.

5.6. Conclusions

In this Chapter, evaluation of lean burn strategy, both by air dilution and external EGR dilution, has been evaluated with conventional spark ignition and passive pre-chamber ignition systems. Also the compatibility of passive pre-chamber ignition concept with after-treatment devices, the three-way catalyst, is analyzed, focusing on the exhaust heating ability of the concept.

Air dilution evaluation showed an increase in the operating range for passive pre-chamber ignition compared with conventional spark ignition system when operating with gasoline. Also, the indicated gross efficiency is increased in the whole range until the dilution limit is reached due to the best combustion phasing of the pre-chamber system. In the limit, the obtained heat release profiles are quite similar between them, avoiding the advantage related to the passive pre-chamber ignition concept. Also it has been proved that combustion phasing is a prevalent parameter when seeking an increase in the indicated efficiency.

This increase of performance is no longer obtained when switching to compressed natural gas fuel since conventional spark system is able to achieve a proper combustion phasing, limiting and reducing the operative range and the efficiency gap between concepts. The difference in terms of maximum dilution ratio between pre-chambers can be explained by their design. A proper pre-chamber definition is able to extend the maximum dilution ratio.

Similar results are obtained if lean burn strategy relies on adding external EGR. When conventional spark ignition is restricted by knocking, passive pre-chamber arises as a solution to advance combustion phasing and increase indicated efficiency. However, if the combustion phasing is not restricted, both by reduced engine load or by the higher ignition delay of the fuel, the gap between efficiencies is reduced. Furthermore, the operating range when diluting with EGR is shorter for passive pre-chamber system. This is caused by the difficult of a proper scavenging process inside the pre-chamber, adding the external EGR with the IGR of previous cycle.

Regarding the operation at low engine load and speed, where the exhaust temperature is compromised, passive pre-chamber ignition system has shown difficulties to achieve a proper heat flow in the exhaust tailpipe. This is one of the most critical aspects of this ignition system, since compromises the control of pollutant emissions. Two different strategies were evaluated to increase temperature in the exhaust line. Increasing the intake temperature and the addition of external EGR. Both strategies were not able to achieve enough temperature. However, the addition of EGR showed a remarkable increase of temperature keeping similar efficiency without EGR.

When evaluating lean burn strategy in a complete engine map clear benefits are obtained in the whole operating range, specially in the low-end torque region. In this area, a good combustion phasing is only achieved if passive pre-chamber is operated with EGR, otherwise the combustion phasing is

set earlier than the TDC. This is caused by the longer combustion duration. Main drawbacks appear at low engine loads and high speed, when the cycle takes less time and the scavenging is even more compromised.

To sum up with, the pre-chamber design arises as a key parameter to assure a proper performance of this concept. Optimized pre-chamber geometries are able to operate with higher dilution ratios, which turns into performance benefits in the different studied engine loads.

Key aspects in pre-chamber design

6.1. Introduction

This Chapter evaluates different pre-chamber parameters and how they affect the global performance of the concept. Experimental and simulation campaigns are carried out to highlight the key parameters that enhance combustion process within the pre-chamber. Then, this knowledge is merged and a brand-new pre-chamber definition with a compromise geometry arises as solution to increase overall performance of the concept, combined with a diluted combustion strategy, in the whole engine map.

Despite previous Chapters investigated the performance of this concept using two different types of fuel and two engine architectures, this Chapter focuses on compressed natural gas fuel and Miller architecture. Main characteristics can be found in Table 4.5 and Table 4.7 respectively. The idea behind choosing this particular configuration relies on obtaining higher efficiency when the passive pre-chamber system does not provide clear benefits in any of the operating conditions compared with the conventional spark ignition system, in order to highlight design improvements.

Operating conditions are similar to those studied in previous Chapters, however, the extreme conditions in terms of engine load and speed are deeper analyzed since they are the most restrictive limitations of the concept. Table 6.1 includes the studied points.

Work on this chapter has been partly published in the following papers:

- Improving the performance of the passive pre-chamber ignition concept for spark-ignition engines fueled with natural gas [4]

Table 6.1: Studied operating points.

Parameter	OP1	OP2
Engine speed [rpm]	4500	1350
Engine load [bar]	12.8	2.85

6.2. Nozzle orientation evaluation

First studied geometrical parameter is nozzle tangential angle. Because of 1D tools have geometrical limitations, two new pre-chambers, which are based on the pre-chamber 1 definition, with different tangential angles were manufactured and evaluated. In Table 6.2 main specifications of these pre-chambers are presented. One pre-chamber has an increased tangential angle compared with the baseline while the other one has their nozzles with a complete radial orientation.

Table 6.2: Geometrical specifications of the new manufactured versions of pre-chamber 1.

	Pre-chamber 1		
	(PC1)	(PC1b)	(PC1c)
Volume [mm ³]	600	600	600
Hole diameter [mm]	0.7	0.7	0.7
Number of holes [-]	6	6	6
Hole tangential angle [degrees]	7.5	12.5	0

Main goal of this Section consists of obtaining advantages in terms of wider operating range at low engine load conditions and/or an increased dilution tolerance at high engine load conditions. For that purpose, a spark timing sweep was performed at low engine load and speed conditions. Results of the experimental campaign at low engine load are presented in Figure 6.1.

Black line is baseline spark ignition system, which is presented as reference to compare with passive pre-chamber concept. Blue line corresponds with baseline pre-chamber 1 and red and green lines represent the trends of version b and c of pre-chamber 1 respectively. Most remarkable result is that there are three levels of combustion stability which correspond with the three different tangential angles. In this way, pre-chamber performance is scaled with their respective combustion stability.

Increasing the tangential angle of the pre-chamber nozzles tends to increase the swirl level within pre-chamber, stabilizing the combustion process. This increased stability affects also the combustion velocity and phasing.

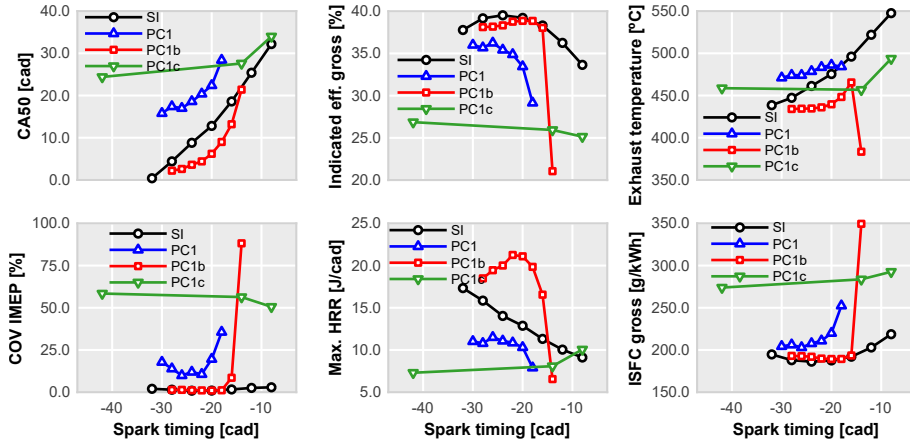


Figure 6.1: Trends of combustion phasing (CA50), gross indicated efficiency, exhaust temperature, combustion stability (COV IMEP), combustion velocity and fuel consumption for the different ignition systems at low engine load and speed conditions and $\lambda = 1$.

Higher swirl level enhances combustion velocity at low engine loads and speeds, pushing the combustion phasing towards the TDC. Despite pre-chamber 1 has a more retarded combustion phasing, it is not able to heat up the exhaust tailpipe enough to activate after-treatment systems. This situation is even worse for the other configurations since, either by the fast combustion or misfire cycles, their exhaust temperature is lower.

Pre-chamber 1b is the most stable configuration among the three studied geometries. Even it operates at the same level as conventional spark ignition until the stability drop. However, pre-chamber 1c, which its nozzles are fully radial, has only three measured points due to its extremely high dispersion in the whole operating range. In fact, this instability conditioned the measurements due to its extremely retarded phasing.

Main pollutants emissions are presented in Figure 6.2. As it is expected, best combustion efficiency is obtained for pre-chamber 1b, which is the most stable pre-chamber configuration, while pre-chamber 1c has a very poor efficiency due to its extreme dispersion. In terms of NO_x , its emissions are reduced retarding the combustion onset.

Evaluation of EGR dilution tolerance was also performed with this set of pre-chambers at high engine load and speed conditions. Main results of this experiment are shown in Figure 6.3. As in previous Figures, black

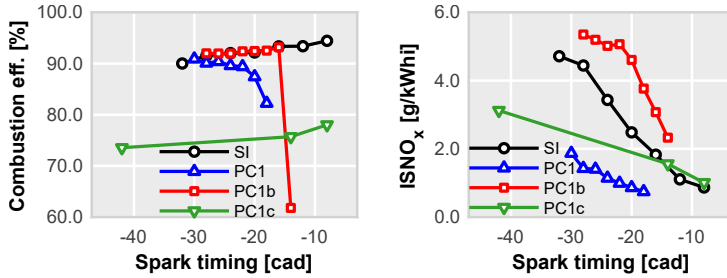


Figure 6.2: Trends of combustion efficiency and emitted NO_x for the different ignition systems at low engine load and speed conditions and $\lambda = 1$.

line and blue line are the baseline trends (spark ignition and passive pre-chamber respectively), while red and green represent the trends of the new pre-chamber versions b and c.

At these conditions indicated efficiency does not show a constant trend in terms of swirl level. Radial nozzles pre-chamber and more tangential nozzles pre-chamber are quite similar in terms of combustion stability, phasing and velocity, while baseline pre-chamber 1 shows a slightly increased maximum dilution tolerance. This higher maximum dilution tolerance is obtained due to the faster combustion process and a higher combustion stability.

In these terms, increasing swirl level helps to increase combustion stability at non diluted conditions, while it shows an optimum value that increases the EGR tolerance level.

Main pollutant emission trends are presented in Figure 6.4. Combustion efficiency and NO_x follow the expected trends. Combustion efficiency and NO_x decrease as long as dilution ratio increases, independently of nozzle orientation.

6.3. Pre-chamber volume evaluation

In this Section, the pre-chamber volume is evaluated by means of 1D simulations and a later experimental campaign that verifies the main hypotheses considered. A new pre-chamber configuration will be developed and compared against baseline pre-chamber 1.

In previous Chapters the significance of pre-chamber volume has been highlighted as some assumptions regarding dilution tolerance or fuel mass inside pre-chamber at different engine load conditions were accepted. Pre-chamber configurations with higher internal volume showed better performance compared with those pre-chambers with small volumes.

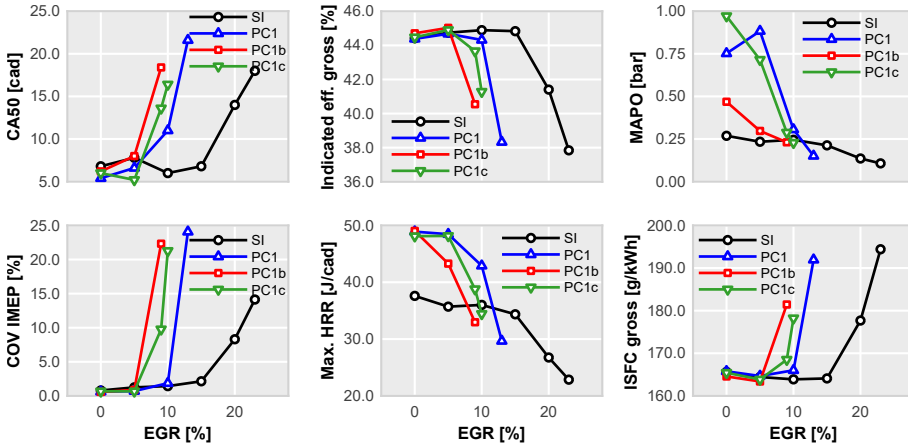


Figure 6.3: Trends of combustion phasing (CA50), gross indicated efficiency, exhaust temperature, combustion stability (COV IMEP), combustion velocity and fuel consumption for the different ignition systems at high engine load and speed conditions operating with EGR and $\lambda = 1$.

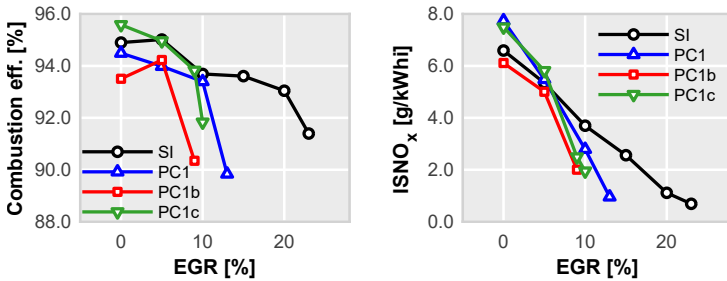


Figure 6.4: Trends of combustion efficiency and emitted NO_x for the different ignition systems at high engine load and speed conditions operating with EGR and $\lambda = 1$.

To start with this evaluation, first step consists of analyzing the effect of different engine loads and the impact of fuel mass inside pre-chamber on pressure difference between main chamber and pre-chamber (ΔP). This evaluation is carried out with pre-chamber 1 baseline configuration (see Table 6.2). Jet momentum is mostly driven by this pressure difference, and it can be considered as a key designing parameter since jet momentum is related to the ability of the jet to advance from discharge hole to main combustion chamber, initiating the combustion process in multiple sites.

Pressure difference profiles between chambers of a high engine load case and a low engine load case are presented in Figure 6.5. Evolution of ΔP can be divided into four different stages: filling, ejection, backflow re-filling and emptying. Note that this ΔP stages analysis correspond with the high engine load case, since the higher peaks of its profile let a better understanding of the process. Positive values correspond with higher pressure in the pre-chamber.

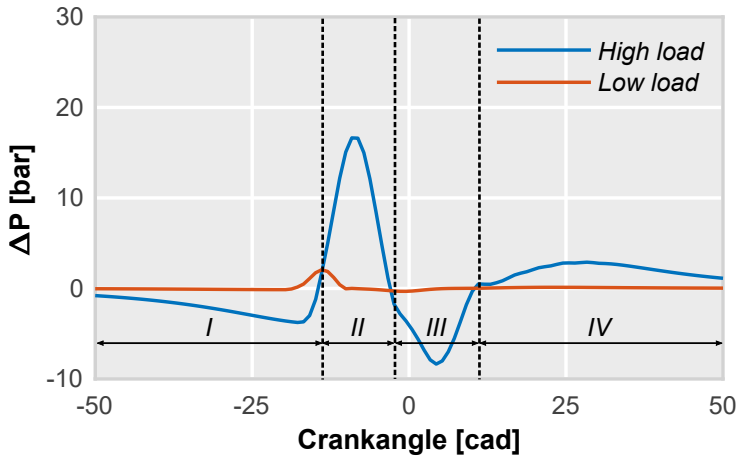


Figure 6.5: Pressure difference between main and pre-chamber (ΔP) profiles of high engine load and low engine load cases with passive pre-chamber ignition system at $\lambda = 1$ operating with CNG.

During first stage (I), the piston movement forces the filling of the pre-chamber. The engine is running in its compression stroke and this is one of the most critical stages for a proper operation, since it determines the total amount of fuel that pre-chamber is able to store within. Higher engine loads and bigger pre-chambers tend to increase the total amount of fuel.

Second stage corresponds with ejection process (II). During this stage, combustion starts inside pre-chamber, leading to an increase of the pre-chamber pressure. This increased pressure forces the jets to enter into the main chamber and initiate combustion in there. Combustion process inside pre-chamber seems a key parameter to optimize when designing pre-chambers, since it handles the quality of ejected jets.

Once ejection process has started, combustion in the main chamber starts, increasing its pressure and making way to the third stage, backflow re-filling (III). Pressure in the main chamber increases and once it has overcome

pressure of pre-chamber, it forces a re-filling of pre-chamber. However, this time pre-chamber is filled mainly with residual gases coming from combustion.

Finally, fourth stage (IV) corresponds with the emptying of pre-chamber. This stage is dominated by the exhaust stroke, forcing the residual gases of the pre-chamber to exit and scavenge the volume. It is remarkable that this is a very sensitive process, since a good scavenge of pre-chamber volume will turn into greater amount of fresh air-fuel mixture in the next cycle and a better performance.

Results of jet momentum profile and fuel mass at combustion onset inside pre-chamber of the studied cases are presented in Figure 6.6. It can be seen that jet momentum is strongly affected by fuel mass inside pre-chamber at start of combustion, achieving the high engine load case ejection peak (II) values up to 7 times higher than of the low engine load case. Again, the evaluation of the four stages is carried out at the high engine load case. Despite all different stages have positive jet momentum values, direction of the flow is similar for stages I and III (entering to pre-chamber) but different for stages II and IV (exiting from pre-chamber).

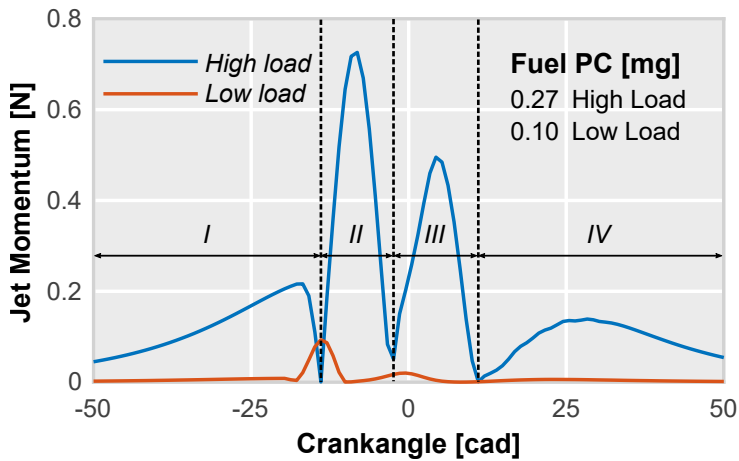


Figure 6.6: Jet momentum profiles and fuel mass inside pre-chamber of high engine load and low engine load cases with the passive pre-chamber ignition system at $\lambda = 1$ operating with CNG.

As it has been highlighted, the increment of fuel mass inside the pre-chamber at the start of combustion will turn into higher jet momentum values and a better sweeping of the main chamber. Increasing pre-chamber volume arises as one solution that follows this path to increase performance of the concept.

To evaluate the impact of pre-chamber volume and nozzles diameter, a study in the 1D Wave Action model was carried out. Start of combustion and its duration were fixed to reference values (-16 cad ATDC and 12 cad respectively) in order to isolate the effects of geometrical variations. Pre-chamber volume was varied from 400 mm³ to 1000 mm³ in steps of 50 mm³, while hole diameter was varied from 0.4 mm to 1.6 mm in steps of 0.1 mm. Main parameters of this study are summarized in Table 6.3.

Table 6.3: Design of experiments modifying pre-chamber volume and nozzle sectional area carried out in the 1D Wave Action model.

		Min. value	Max. value	# levels
DOE	Volume [mm ³]	400	1000	13
	Hole diameter [mm]	0.4	1.6	13
	SoC _{PC} [cad ATDC]	-16	-16	1
	Comb. duration [cad]	12	12	1

Jet momentum results coming from this evaluation at low engine load and speed conditions are presented in Figure 6.7. To isolate the effect of varying the number of holes, the hole diameter parameter was converted into cross sectional area of all holes. These results show a clear trend towards increasing pre-chamber volume as long as hole area is kept constant. Maximum jet momentum peak increases due to the higher amount of fuel mass stored at start of combustion inside pre-chamber (baseline fuel mass at low engine load is 0.10 mg and its momentum peak is 0.068 N while for a 950 mm³ pre-chamber fuel mass is increased up to 0.17 mg and momentum peak up to 0.104 N).

Optimum value of cross sectional area can be found only if the pre-chamber volume is fixed, however, two general considerations can be obtained. For smaller diameters pressure drop is high, compromising the amount of fuel inside pre-chamber. On the other hand, if the hole diameter is too large, combustion process is not able to increase pre-chamber pressure and assure a proper jet ejection process, hindering main chamber sweep and ignition of the charge.

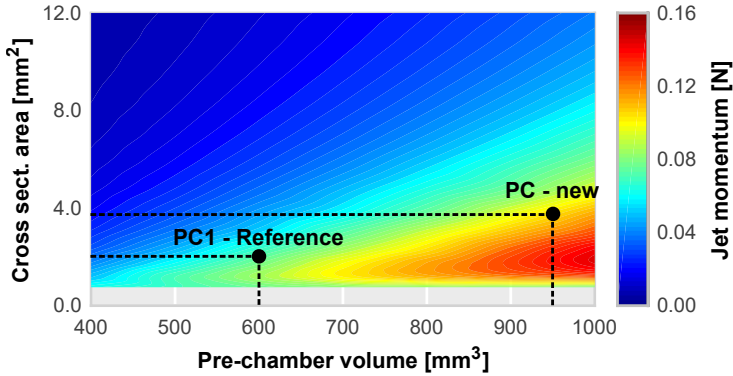


Figure 6.7: Maximum jet momentum peak map at low engine load and speed conditions at $\lambda = 1$ operating with CNG, varying pre-chamber volume and hole diameter.

Same approach was made for the other considered operating point, keeping the same parameters as in previous study. Results of jet momentum peak for the simulations at high engine load and speed are presented in Figure 6.8. Similar trend for pre-chamber volume is observed at high engine load conditions. Bigger pre-chambers show an increased jet momentum peak due to the higher mass fuel amount stored when combustion starts, which leads to an increase of available energy for generating the hot reactive jets. However, maximum jet momentum peak values are around ten times greater for high engine load case than low engine load case, which indicates that designing requirements are less restrictive for high engine load cases.

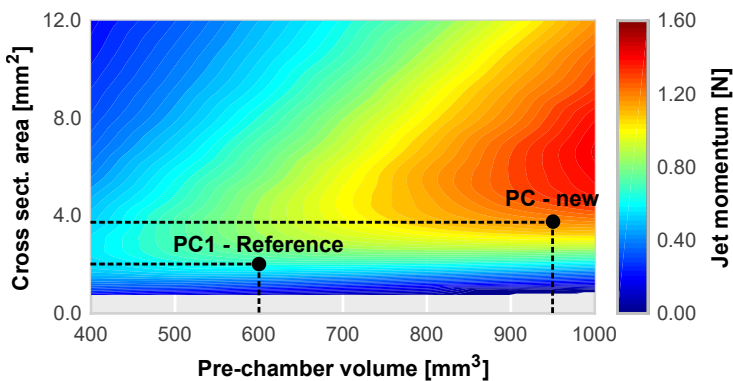


Figure 6.8: Maximum jet momentum peak map at high engine load and speed conditions at $\lambda = 1$ operating with CNG, varying pre-chamber volume and hole diameter.

In view of these results, a new pre-chamber configuration was selected (PC - new) and pointed in both momentum peak maps. This new pre-chamber is a compromise solution between both operating conditions, with an increased volume and a greater cross sectional area. As this new pre-chamber is bigger than baseline more amount of mass fuel will be stored at start of combustion, increasing the energy available to generate the jets and thus, it is intended to have a better global performance of the concept by increasing the jets surface that initiate combustion in main chamber. Main geometrical characteristics of this pre-chamber can be found in Table 6.4.

Table 6.4: Geometrical specifications of the baseline pre-chamber 1 and new pre-chamber.

	(PC1)	(PC new)
Volume [mm ³]	600	950
Hole diameter [mm]	0.7	0.9
Number of holes [-]	6	6
Hole tangential angle [degrees]	7.5	7.5

Next step in current study consisted of evaluating how the jet momentum affects the jet penetration. For that purpose a 1D jet model was used to evaluate the transient penetration of a free jet, using some parameters such as mass flow rate, jet momentum profile, nozzle diameter and main thermodynamic conditions downstream in the main chamber. This model calculates, among other parameters, jet penetration according to time, then, the intersection of jet penetration with the furthest wall distance give the time that takes the jet to reach the furthest wall. This parameter was called t^* .

To illustrate this parameter, jet penetration for pre-chamber 1 at high engine load and low engine load is plotted in Figure 6.9. Blue line is jet penetration of high engine load case while orange line is jet penetration of low engine load case. Black dashed line represents the distance to the furthest wall from nozzle exit.

Intersection of jet penetration profiles with this wall distance give the time that jet takes to reach that wall. For the high engine load case this time is shorter due to the greater jet momentum peak achieved by the extra fuel mass. These results are in line with the previous maps, since low engine load case has the largest time, being the main constraint of the concept.

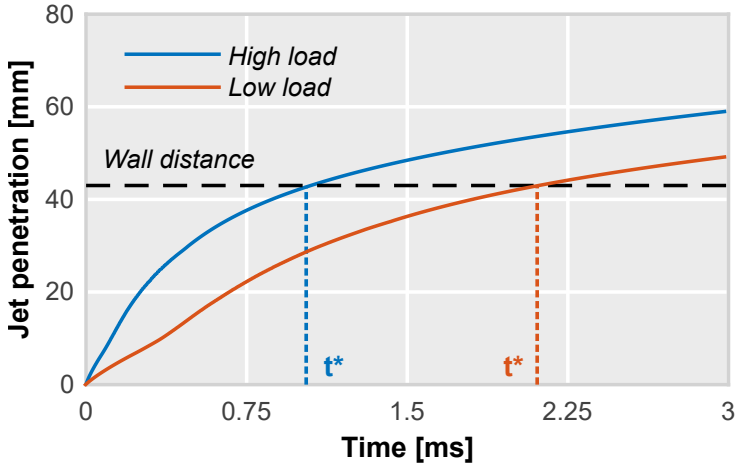


Figure 6.9: Jet penetration profiles of high engine load and low engine load cases with the passive pre-chamber ignition system at $\lambda = 1$ operating with CNG.

Greater jet momentum peaks result in a faster jet penetration, producing larger reaction surfaces that ignite the main chamber in less time. In this way, t^* becomes a clear indicator of the global performance of a pre-chamber, being a suitable benchmark for characterizing its operation.

In this way, using the results coming from the 1D Wave Action model, values of t^* have been calculated in the same range, varying pre-chamber volume (from 400 mm^3 to 1000 mm^3) and hole diameter (from 0.4 mm to 1.6 mm). Calculations were stopped at the threshold limit of 3 milliseconds, since performance of the concept is very compromised with t^* values greater than that value. Results of the fully study at low engine load conditions are presented in Figure 6.10.

Results show how jet momentum and jet penetration are related between them. The higher the jet momentum peak the lower the time to reach the wall. This fact gives, in a certain way, consistency to the applied methodology and shows coherence between the two 1D models. Increasing pre-chamber volume turns into greater jet momentum and thus, lower t^* .

Bluer regions of the map are those where better jet performance is expected, and again, the new selected pre-chamber configuration (PC - new) is located in a better position in this map, reducing the expected t^* from around 2 ms to 1.5 - 1.6 ms.

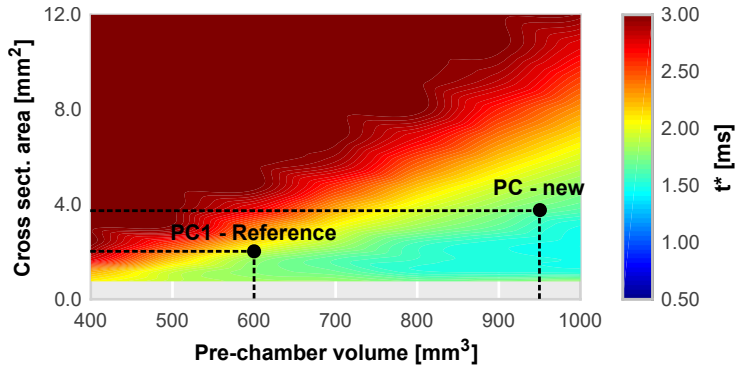


Figure 6.10: Map of t^* values at low engine load and speed conditions at $\lambda = 1$ operating with CNG, varying pre-chamber volume and hole diameter.

The same study was carried out for the other engine load. Results of t^* values at high engine load and speed conditions are presented in Figure 6.11. At these conditions, values of t^* are highly decreased in almost all map (from 2 ms at low engine load to 0.7 - 0.9 ms at high engine load). This effect is related to the higher stored energy and the ability to generate proper reactive jets. Looking at the most favorable area, the reduction is even more noticeable, reducing t^* up to 0.5 ms.

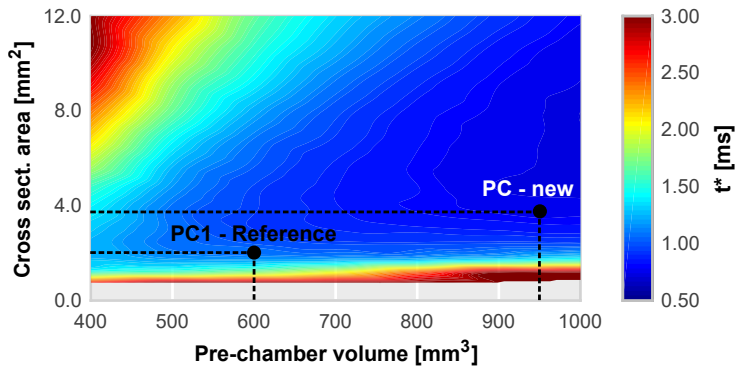


Figure 6.11: Map of t^* values at high engine load and speed conditions at $\lambda = 1$ operating with CNG, varying pre-chamber volume and hole diameter.

Again, the nozzle hole diameter has to be carefully selected, since optimal values are not the same for different engine loads. To assure a suitable performance in most of conditions, this diameter should be pushed through optimal values at lower loads due to the most restrictive conditions when the fuel mass is compromised.

Jet penetrations of baseline pre-chamber and the new selected pre-chamber at low engine load are plotted in Figure 6.12. Black line represents the distance to the furthest wall. Increasing jet momentum by means of a bigger pre-chamber volume turns into a faster jet penetration. This fast penetration is achieved by larger reaction surfaces for igniting the main chamber in less time.

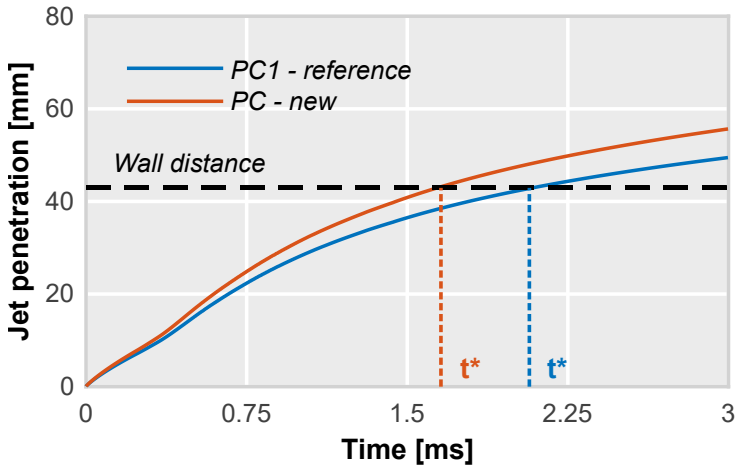


Figure 6.12: Jet penetration at low engine load and speed conditions at $\lambda = 1$ operating with CNG.

To validate the whole numerical methodology, this new pre-chamber was manufactured and experimentally evaluated in both engine load conditions. As in previous Section 6.2, main goal is to obtain a wider operating range at low engine load conditions and an increased maximum dilution tolerance at high engine load conditions.

Main results at low engine load conditions are presented in Figure 6.13. Black line represents the trend of conventional spark ignition system as reference. While blue and red lines represent trends of passive pre-chamber ignition system (blue is the baseline pre-chamber and red is the new designed pre-chamber). As it was expected, new pre-chamber configuration extends operating range compared with baseline pre-chamber, however this extension is not enough to overcome the exhaust temperature drawback.

Despite the temperature issue, the new pre-chamber provides an increase in indicated efficiency in the whole operating range compared with baseline pre-chamber, but quite far from the efficiency exhibited by conventional spark ignition system. This increase is mainly caused by the enhanced combustion phasing (CA50) achieved by the faster combustion velocity of

the new pre-chamber. This velocity is higher because of the greater amount of fuel stored at combustion start, providing higher energy and a better main chamber sweep.

These results validate the numerical approach followed in this Section since the expected increase of performance is related with the greater amount of stored fuel due to the bigger pre-chamber volume.

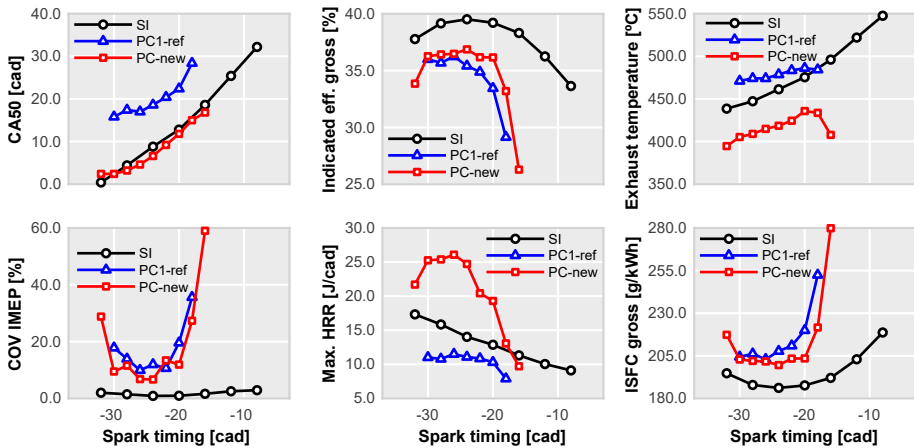


Figure 6.13: Trends of combustion phasing (CA50), gross indicated efficiency, exhaust temperature, combustion stability (COV IMEP), combustion velocity and fuel consumption for both ignition systems at low engine load and speed conditions at $\lambda = 1$ operating with CNG.

The advanced combustion phasing seems the main cause of the lack of exhaust temperature achieved by the new pre-chamber, as it advances the combustion process to the TDC. While swirl level inside the pre-chamber seems to be the main constraint to obtain higher combustion stability and thus, a better performance.

Regarding the selection of the nozzle diameter, some considerations should be taken into account. For instance, larger nozzle diameters benefit the fuel entrance into the pre-chamber, however, when the combustion within the pre-chamber starts, the associated increase of pressure is limited due to the escape of fresh mixture through these greater nozzles, causing lower jet momentum flux and thus shorter jet penetration.

On the other hand, smaller nozzle diameters benefit the pressurization of the pre-chamber and thus, lead to an increase of the jet momentum flux, generating a better jet penetration and sweeping of the main chamber. However, as the nozzle diameter is reduced, the scavenge process of the pre-chamber is compromised.

In terms of temperature, it is directly linked to this scavenge process. As a great amount of fresh mixture is burnt within the pre-chamber, greater temperatures can be achieved, leading to higher amounts of NO_x that can be emitted.

Comparing Figure 6.1 and Figure 6.13 suggests that the combination of tangential nozzle angle and bigger pre-chamber volumes, with the proper hole diameter selection, seems the right path to optimize the concept in terms of compatibility with late spark timing, at least, in these low engine loads conditions.

Regarding pollutant emissions, main trends are presented in Figure 6.14. Combustion efficiency levels are quite similar between concepts, until the dispersion starts to affect normal performance. In terms of NO_x, levels are in general higher for the new (bigger) pre-chamber due to the fastest combustion, which results in higher pressures and local temperatures, leading to that increase of emissions compared with baseline pre-chamber.

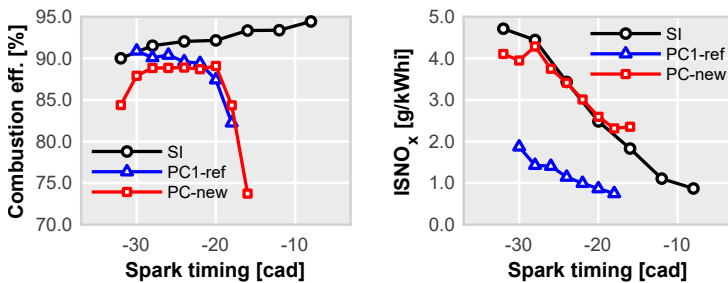


Figure 6.14: Trends of combustion efficiency and emitted NO_x for both ignition systems at low engine load and speed conditions at $\lambda = 1$ operating with CNG.

Next step consisted of evaluating the EGR dilution tolerance at high engine load conditions. EGR dilution was increased in steps of 5% until the combustion stability was unacceptable. Main results are presented in Figure 6.15, and as in the other Figures, black line represent conventional spark ignition trend, for reference, while blue and red represent passive pre-chamber trends.

It is seen how the new bigger pre-chamber is able, not only to extend the maximum dilution tolerance but also to offer a better efficiency in the whole operating range, compared with baseline pre-chamber. The stability drop suffered when combining diluted combustion with passive pre-chamber appears later. However, this extension is not enough to reach the dilution tolerance of the conventional spark ignition system.

The increase of indicated efficiency comes, as at lower engine loads, from the better combustion phasing achieved by the faster combustion velocity and a good combustion stability. Once the stability suffers a drop, the combustion phasing is pushed away from TDC, mainly by the cycles that are not burning well, leading to the decrease of efficiency. Knocking tendency of bigger pre-chambers is increased by the greater amount of fuel, leading to higher peaks in the heat release rate profile, but as long as dilution increases, knocking tends to reduce.

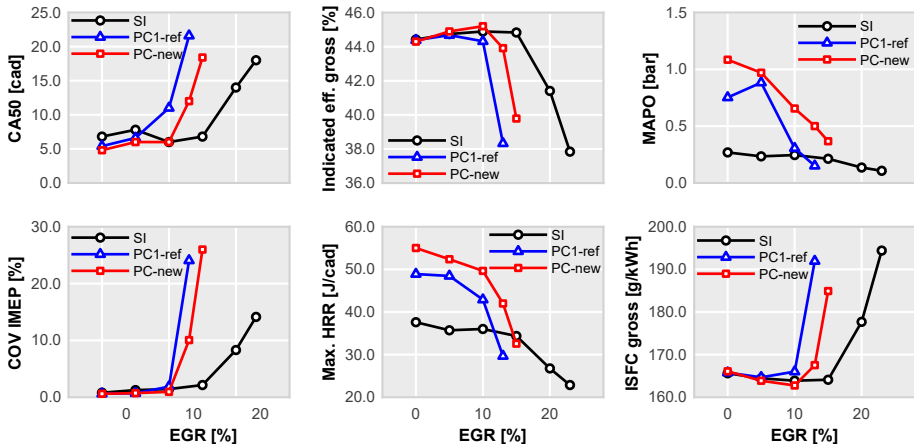


Figure 6.15: Trends of combustion phasing (CA50), gross indicated efficiency, MAPO, combustion stability (COV IMEP), combustion velocity and fuel consumption for both ignition systems at high engine load and speed conditions at $\lambda = 1$ operating with CNG.

The comparison of these results with previous nozzle angle results in Figure 6.3 shows that an increased pre-chamber volume benefits the maximum dilution tolerance, while the angle of the nozzle holes does not play such an active role as pre-chamber volume does. In these terms, the maximum dilution ratio is more dependent on scavenging and filling processes than the variation of swirl level. Even, an excessive value of tangential angle can lead to inefficiencies in the scavenging process near the spark plug location [236] and then, to a effective reduced dilution ratio.

This effect represents an important issue since, with this kind of passive pre-chamber configuration, the spark plug is located at the top of the volume, where the majority of residual gases from the previous cycle are located. Nevertheless, as Figure 6.3 shows, there exists an optimum value that in-

increases the maximum dilution tolerance, with an slightly better combustion phasing while keeping good efficiency levels. However, this increase is not enough to reach conventional spark efficiencies.

Analyzing pollutant emissions, Figure 6.16 presents the trends of combustion efficiency and NO_x . Combustion efficiencies are similar between concepts and different pre-chamber configurations, but it is remarkable that the efficiency drop of bigger pre-chamber appears later compared with baseline pre-chamber. Regarding NO_x emissions, expected trends with increasing dilution ratio are obtained.

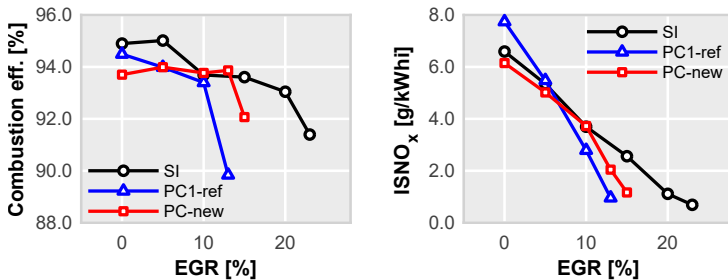


Figure 6.16: Trends of combustion efficiency and emitted NO_x for both ignition systems at high engine load and speed conditions at $\lambda = 1$ operating with CNG.

6.4. Internal pre-chamber combustion evaluation

Present Section focuses on evaluating how the combustion inside the pre-chamber affects the quality of generated reactive jets. For that purpose, 1D Wave Action model and 1D Jet model were also employed and a similar study as in previous Section was carried out.

However, as the 1D Wave Action model does not include a predictive combustion model, combustion parameters such as combustion onset or its duration, must be pre-defined. In this way, a design of experiments varying those parameters was performed, keeping the same pre-chamber volume and hole nozzle diameter in the whole studio (these parameters are the baseline pre-chamber 1 volume and diameter), in order to isolate the effects of the combustion profile.

In Table 6.5 a summary of the main parameters of this study are presented. Start of combustion inside pre-chamber was varied from -20 cad ATDC to -10 cad ATDC, while its duration was modified from 8 cad to 20 cad, both

increased in steps of 1 cad. These ranges are quite representative of these type of pre-combustions. Pre-chamber volume was set to 600 mm^3 and hole diameter to 0.7 mm.

Table 6.5: Design of experiments modifying pre-chamber combustion start and duration carried out in the 1D Wave Action model.

		Min. value	Max. value	# levels
DOE	Volume [mm^3]	600	600	1
	Hole diameter [mm]	0.7	0.7	1
	SoC _{PC} [cad ATDC]	-20	-10	11
	Comb. duration [cad]	8	20	13

Main results of this study in terms of maximum jet momentum peak at low engine load conditions are presented in Figure 6.17. Two main trends arise from these results. First one is related with combustion onset. As later fires the combustion inside pre-chamber higher jet momentum peaks are obtained. This is caused due to the extra-filling of pre-chamber by the compression stroke that increases the available energy to generate jets. This effect can be equated to increasing pre-chamber volume.

The second trend is related to combustion duration. As combustion velocity increases, the obtained ΔP also increases and subsequently, greater jet momentum peaks are obtained. Combining these two trends confirms how the ideal case should be an instantaneous combustion firing in the surroundings of the TDC, which will obtain the higher jet momentum peaks due to the great ΔP obtained and the extra amount of fuel.

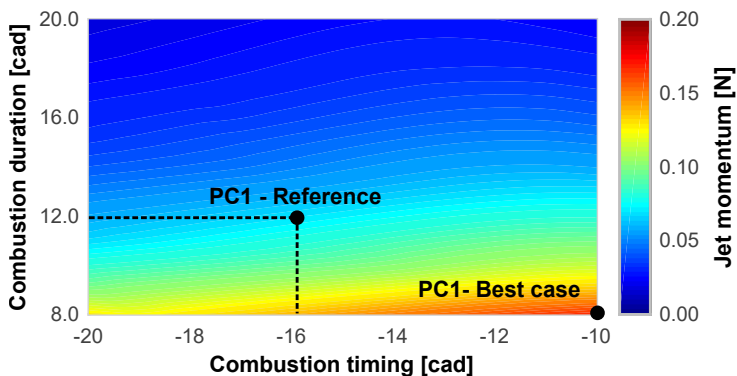


Figure 6.17: Map of jet momentum peak at low engine load and speed conditions at $\lambda = 1$ operating with CNG, varying combustion start and duration.

To illustrate the effect of a more suitable combustion inside pre-chamber, simulated heat release rate profiles and obtained jet momentum profiles of baseline case and best case are presented in Figure 6.18. The faster and later combustion profile turns into a sharper jet momentum profile, leading to an improved performance of the jets and thus, of the global concept.

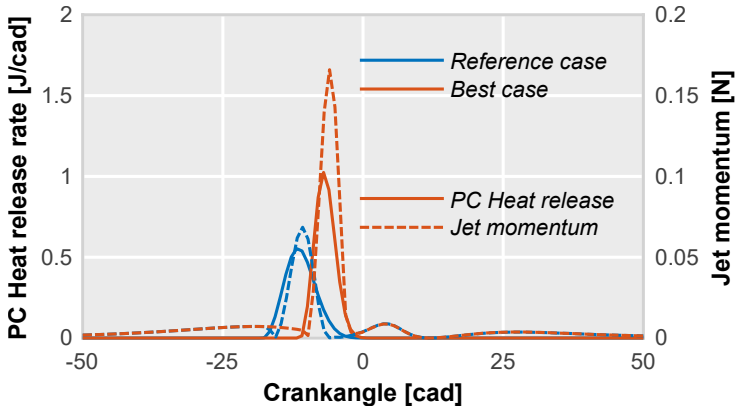


Figure 6.18: Jet momentum and heat release rate profiles at low engine load and speed conditions at $\lambda = 1$ operating with CNG for baseline pre-chamber combustion profile and considered best combustion profile case.

Jet momentum results were translated into the benchmark parameter t^* by means of the 1D Jet model. These results are presented in Figure 6.19. As in the pre-chamber volume evaluation, bluer regions indicate improvement in terms of concept performance. In this case, best combustion case is in these bluer regions of the map, highlighting how the numerical methodology works not only with different geometrical configurations but also with different combustion laws.

This is a really remarkable aspect since it indicates that this design methodology offers suitable results for the basic geometrical and combustion parameters when designing a pre-chamber. This approach can be taken as a first filter when generating a pre-chamber geometry.

Same jet momentum peak evaluation was carried out varying pre-chamber volume and hole diameter but, in this case, combustion inside pre-chamber was set to the best combustion law case previously mentioned (combustion start was set at -10 cad ATDC and combustion duration was set to 8 cad). Results of this study are shown in Figure 6.20.

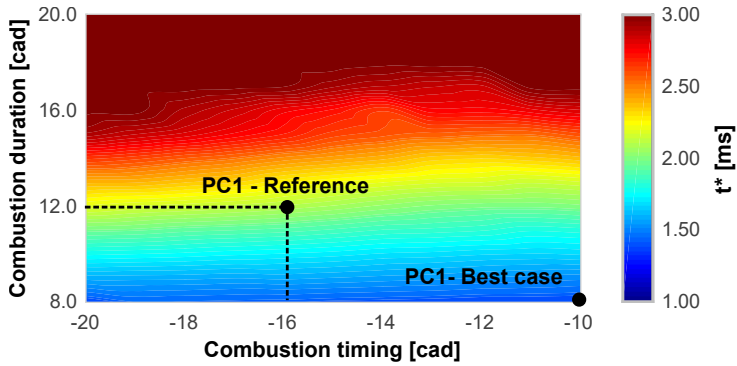


Figure 6.19: Map of t^* at low engine load and speed conditions at $\lambda = 1$ operating with CNG, varying combustion start and duration.

It is seen how the maximum jet momentum peak increases with this fast combustion law in the whole map. In this case, the axis were kept constant to better identify the performance increase when comparing with previous results in Figure 6.17.

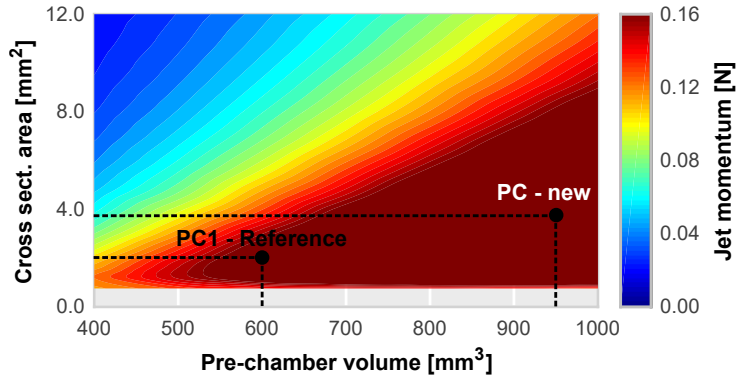


Figure 6.20: Maximum jet momentum peak map at low engine load and speed conditions with enhanced combustion inside pre-chamber at $\lambda = 1$ operating with CNG, varying pre-chamber volume and hole diameter.

From this study can be concluded that combustion inside the pre-chamber is a key aspect when designing a suitable pre-chamber geometry. If the combustion law considerably changes at different operating conditions, then the output jet momentum, and thus the t^* will change accordingly.

This is very important when defining a pre-chamber geometry at the most critical situation. If the combustion deteriorates and takes longer or do not behaves as expected, the jet momentum peak and t^* maps will no longer be adequate, and they will need be corrected and changed.

6.5. Designing a wide-range optimal pre-chamber

In the previous Chapter 5, the effect of adding external EGR was evaluated when employing passive pre-chamber ignition system. This evaluation was carried out in the whole engine map, comparing main combustion parameters and analyzing the difference between diluting or not.

However, that evaluation was only focused on what happened in the main chamber since there is not enough room to insert a dedicated pressure transducer inside the pre-chamber. In the present Section, addition of external EGR and its effects inside the pre-chamber are evaluated by means of the 1D numerical tools used in the design process. As the combination of them has been proved a good methodology to proper design and increase pre-chamber performance, it is accepted that obtained trends of combustion parameters inside pre-chamber agree with the reality of the concept.

One of the parameters that has a remarkable effect on the concept performance is the fuel mass inside pre-chamber. In Figure 6.21 the total amount of fuel when combustion starts is presented, for the map with (left) and without (right) the addition of external EGR.

The main result is that addition of external EGR hinders the storing of fuel inside the pre-chamber. Comparing values of same operating points show that fuel mass slightly decreases in the EGR cases. This effect leads to a decrease in the concept performance, despite the addition of EGR expands the operative engine map range.

Comparing the maximum combustion velocity between the two maps in Figure 6.22 the addition of EGR has the expected impact. Increasing dilution ratio lowers the combustion velocity peak, enlarging the overall combustion duration. Analyzing the obtained values at high engine load and speed (14 bar IMEP gross at 4000 RPM) the fuel mass and the combustion velocity have decreased from 0.25 mg and 1.64 J/cad respectively to 0.22 mg and 1.32 J/cad.

It may seem that these differences are negligible, however, as the total pre-chamber volume is around 2-3% of the main chamber volume, every small difference can lead to a decrease of jets performance and thus, to a series of misfiring cycles that compromises the applicability of the concept.

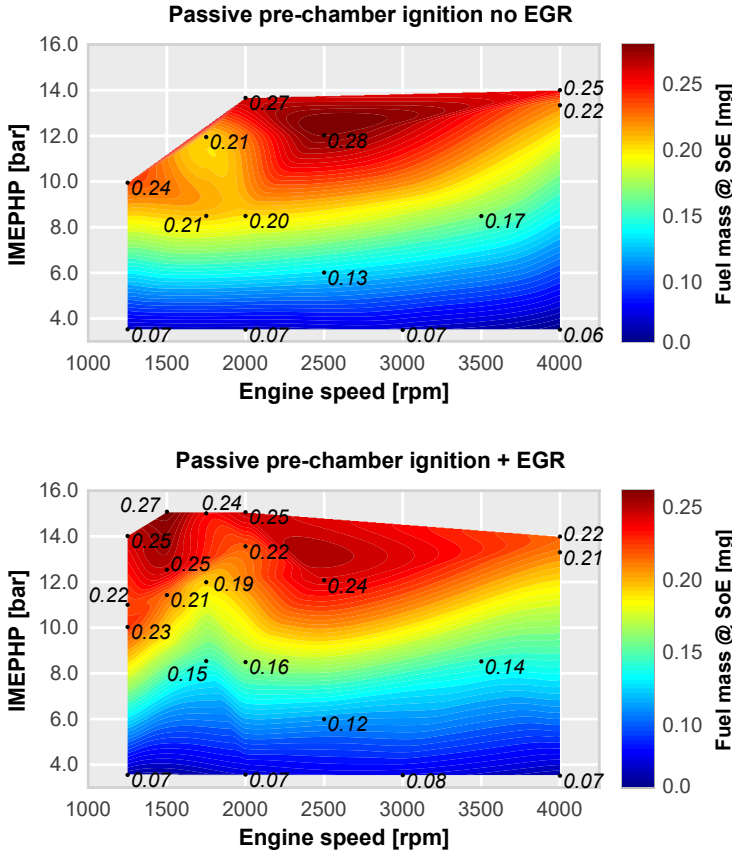


Figure 6.21: Fuel mass inside pre-chamber at start of ejection (SoE) maps for the passive pre-chamber ignition concept without EGR (left) and with EGR (right) at $\lambda = 1$ operating with CNG.

Following with this discussion, pre-chamber performance is managed by the aforementioned jet momentum peak and t^* parameters. First of these parameters is presented in Figure 6.23. As it was expected, due to the fuel mass loss and the decrease of combustion velocity, the maximum jet momentum peak is notably reduced in the whole engine map. This situation is specially critical at lower engine speeds, where this value is even halved. For the points in the low-end torque region, the jet momentum peak is notably low, which will lead to longer penetration times and poor performance.

Results of translating jet momentum peak into t^* values by means of 1D Jet model are presented in Figure 6.24. Results of t^* match the previous jet momentum peak results. In lower engine speed regions the t^* increases,

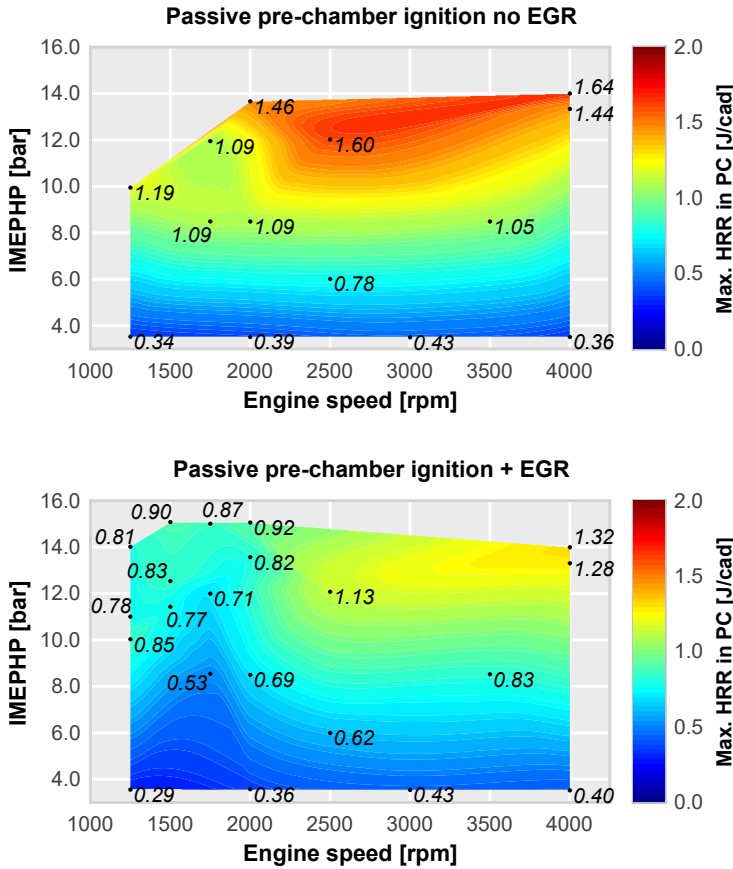


Figure 6.22: Maximum combustion velocity peak in the pre-chamber maps for the passive pre-chamber ignition concept without EGR (left) and with EGR (right) at $\lambda = 1$ operating with CNG.

independently of the operating engine load. In the low-end torque cases, the calculation was stopped at the threshold value of 3 ms since this is a quite long time that turns in a poor concept performance.

The comparison of t^* results with previous fuel mass and combustion velocity results shows that the prevalent aspect to obtain suitable t^* times is the combustion profile inside pre-chamber. Fuel mass is increased for the high engine loads however, their t^* values are higher compared with other points at similar engine load but operating at higher speeds.

As it has been highlighted the concept performance is very dependent on the operating condition, thus it might be reasonable to think that a pre-chamber definition designed to operate at a given conditions will not be

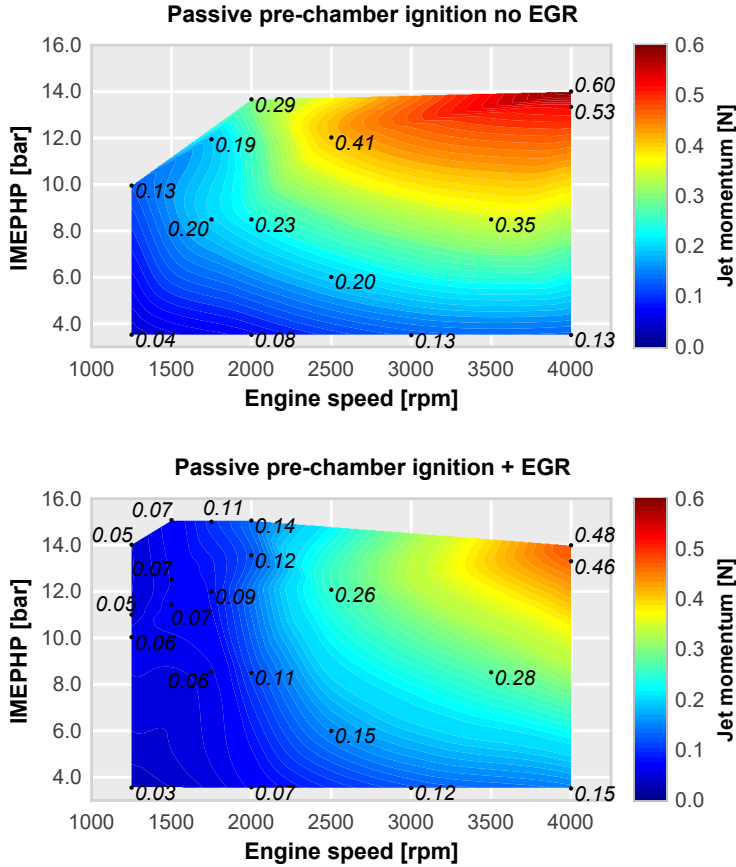


Figure 6.23: Maximum jet momentum peak maps for the passive pre-chamber ignition concept without EGR (left) and with EGR (right) at $\lambda = 1$ operating with CNG.

able to properly operate in others. This conclusion agrees with the idea that fixed boundary conditions with their fixed geometry (the pre-chamber itself) does not have the flexibility to operate optimally in each combination of engine load and speed.

This drawback can be avoided by implementing a dedicated fuel injector within the pre-chamber, thus stratificating the charge near the spark plug. However, this solution changes the concept itself, transforming the passive pre-chamber into an active pre-chamber concept, which gets out of the scope of present analysis.

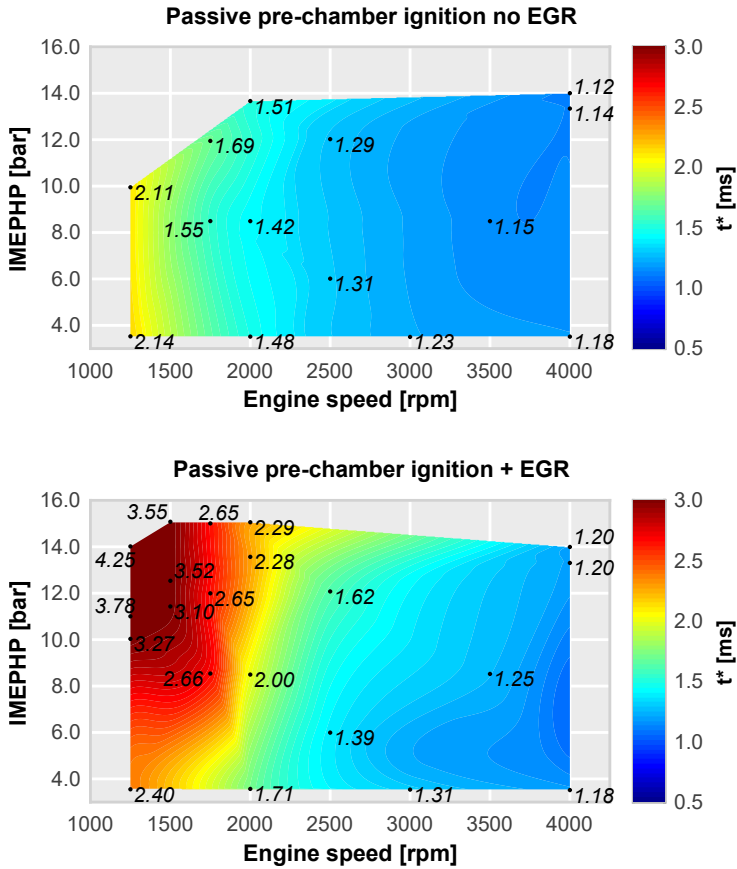


Figure 6.24: Maps of t^* for the passive pre-chamber ignition concept without EGR (left) and with EGR (right) at $\lambda = 1$ operating with CNG.

In this way, an alternative solution to increase the concept efficiency in different operating points may pass through an optimal geometry design that minimizes the t^* time in the majority of the engine map. To achieve this target, evaluation of different combinations of pre-chamber volume and hole diameter in the most extreme operating condition points (the combination of the most higher and lower engine load and speed) were evaluated in both 1D models.

The resulting maps of t^* values are presented in Figure 6.25. On the upper row, the cases with high engine load are plotted while the lower engine load cases are presented in the bottom row. In terms of engine speed, the slower cases are on the left while the faster cases are presented on the right column.

In all maps the black line represents the iso-line in where the same t^* value is found for each combination of pre-chamber volume and hole area. Black square indicates the combination of these two geometrical parameters that minimizes t^* time.

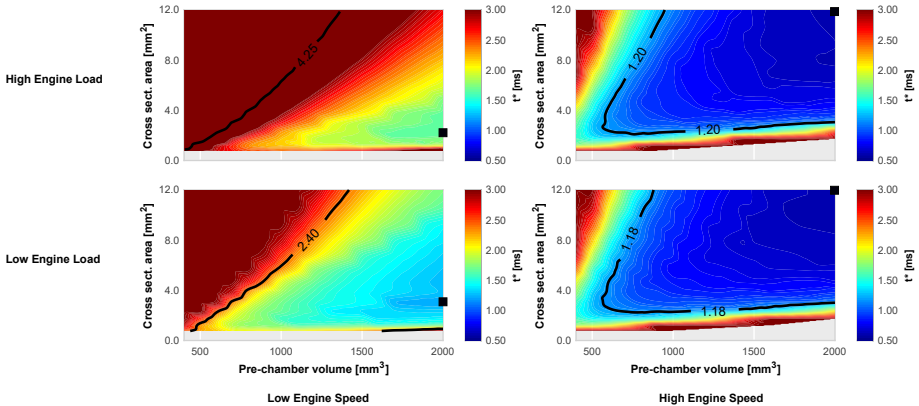


Figure 6.25: Maps of t^* for the four extreme operating condition points modifying pre-chamber volume and cross sectional area at $\lambda = 1$ operating with EGR. Black lines represent the iso-line where t^* value of the map is obtained.

Main conclusion obtained from these maps is that bigger pre-chamber tend to increase the performance of the concept at extreme conditions. Thus, it may seem reasonable to think that these type of geometries will also increase performance at the non so restrictive conditions.

In terms of nozzle hole diameter the optimum value tends to increase as the same time as the engine speed does. So, for the lower engine speed cases the best option is a small sectional area. On the contrary, for the faster cases, the optimum area is increased.

For better understanding the situation, the best geometry of each extreme condition and the iso-line of t^* are presented in Figure 6.26. Region on the left or under the line of each case represents a combination of pre-chamber volume and hole area that hinders the obtained t^* , so the combination of pre-chamber volume and hole area of a compromise pre-chamber should be located in a region in where it reduces the t^* of each case.

Since engine speed seems the main constraint to obtain reduced t^* values, it is reasonable to select a combination that further improves the concept in these situations, rather than in the faster cases since their t^* is quite low. In this way, a compromise pre-chamber was selected (the combination

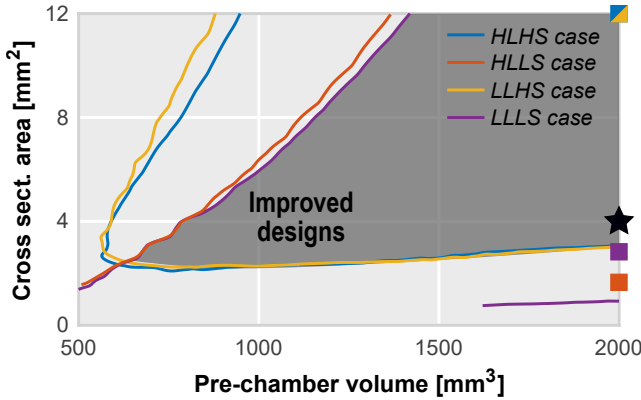


Figure 6.26: Iso-lines of t^* value for the extreme cases in the engine map, optimum pre-chamber geometry for each case (color squares) and selected compromise pre-chamber geometry (black star).

represented as a black star) and it is intended to improve the concept in all cases, but specially in those with lower engine speed. Main geometrical parameters of this pre-chamber are presented in Table 6.6.

Table 6.6: Geometrical specifications of the baseline pre-chamber 1 and compromise pre-chamber.

	(PC1)	(PC comp)
Volume [mm ³]	600	2000
Hole diameter [mm]	0.7	0.95
Number of holes [-]	6	6
Hole tangential angle [degrees]	7.5	7.5

For this new pre-chamber, similar analysis with both 1D models has been carried out to compare with baseline pre-chamber. Results of fuel mass inside pre-chamber at start of combustion are presented in Figure 6.27.

Fuel mass is notably increased in every condition due to the higher pre-chamber volume, which its minimum values are comparable with maximum values of baseline pre-chamber (around 0.20 mg in the worst cases, while 0.27 mg in the best baseline case). Note that the scale has been adapted to new pre-chamber values in order to see differences between points.

In terms of combustion velocity inside pre-chamber, Figure 6.28, differences are also noticeable. New pre-chamber geometry is able to double, and even more, the combustion velocity. This result combined with previous

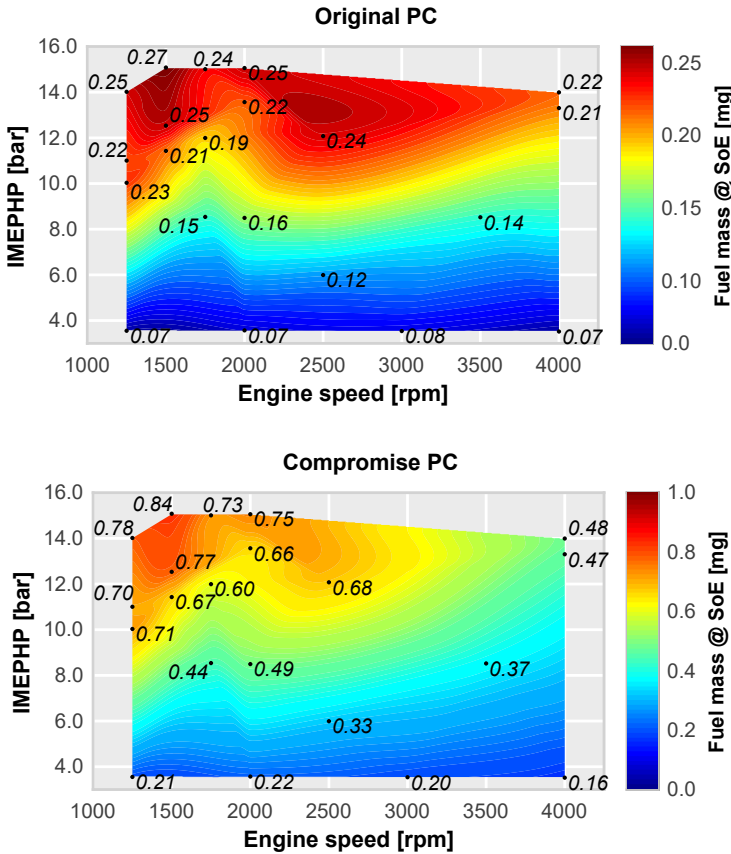


Figure 6.27: Fuel mass inside pre-chamber at start of ejection (SoE) maps for the passive pre-chamber ignition concept for pre-chamber (left) and compromise pre-chamber (right) at $\lambda = 1$ operating with CNG.

fuel mass results will turn into a remarkable increase of pre-chamber performance, as it was discussed when comparing baseline results with and without external EGR.

These maps show how the trends between the two different pre-chamber geometries are similar, with better results for the new compromise pre-chamber, indicating again that this design methodology works properly and is able to provide reliable trends.

Analyzing jets performance, in Figure 6.29 maximum jet momentum peak is presented for both pre-chambers. As fuel mass and, specially, combustion inside pre-chamber, are increased for the new compromise geometry, the maximum jet momentum peak increases in the whole map. The greatest

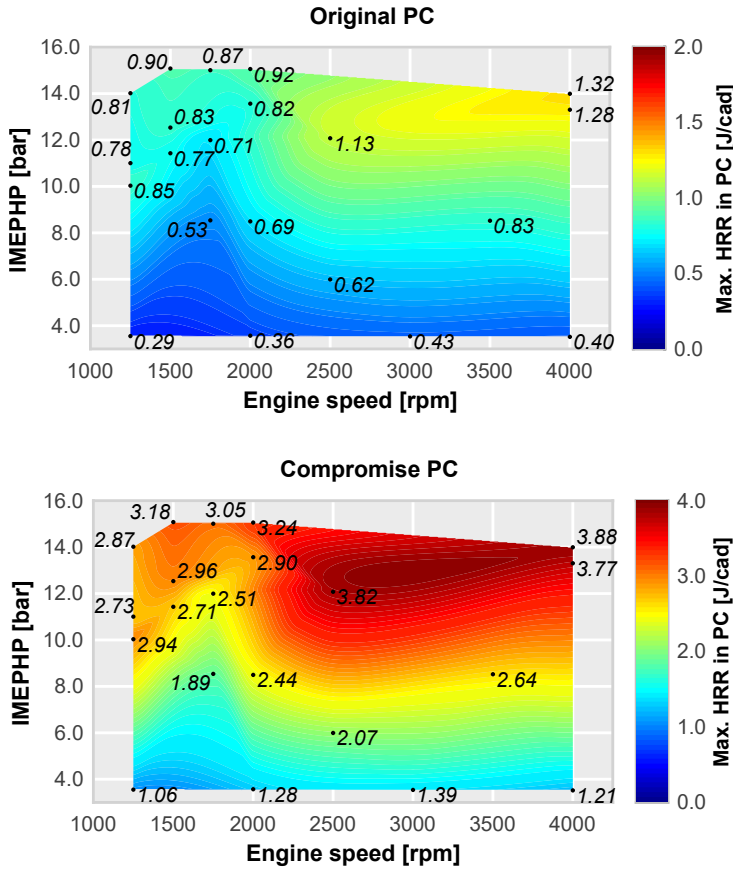


Figure 6.28: Maximum combustion velocity peak in the pre-chamber maps for the passive pre-chamber ignition concept for pre-chamber (left) and compromise pre-chamber (right) at $\lambda = 1$ operating with CNG.

increase is achieved at low-end torque (values around 0.07 N to 0.30 N) while jet momentum peak at region with better performance operating with baseline pre-chamber is almost doubled.

This increase of performance is related mostly with the faster combustion rates inside pre-chamber, as it was discussed before. Burning a greater amount of fuel in the same or even, less time, benefits the pressurization of pre-chamber, increasing difference between main and pre-chamber pressure. Translating these jet momentum peaks into t^* values results in Figure 6.30.

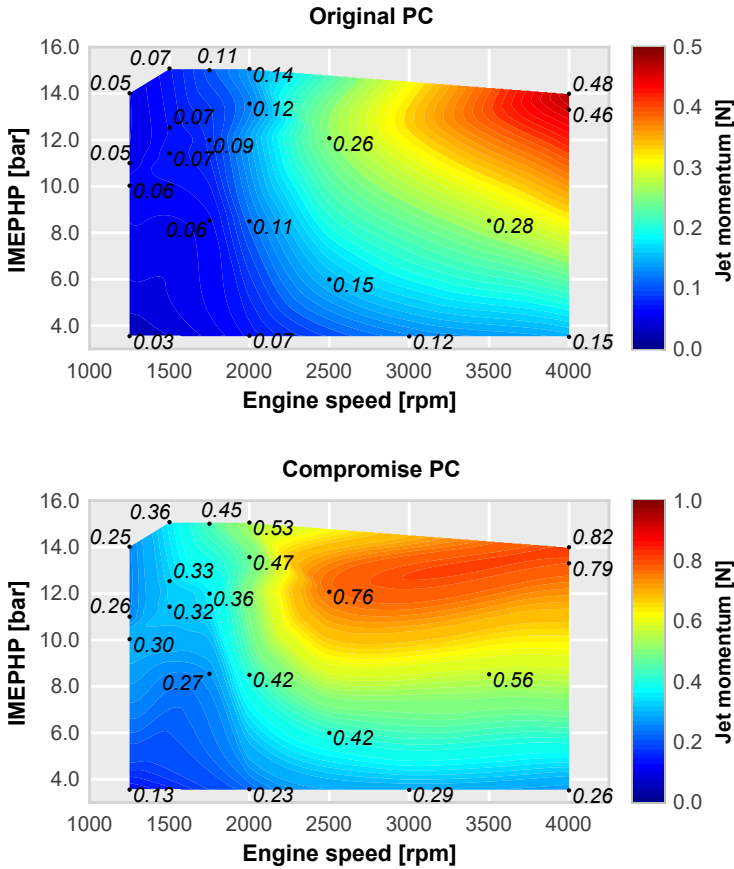


Figure 6.29: Maximum jet momentum peak maps for the passive pre-chamber ignition concept for pre-chamber (left) and compromise pre-chamber (right) at $\lambda = 1$ operating with CNG.

It is clear how there has been a reduction in the t^* , which results in a better sweep of main chamber and an increased concept performance. Higher reductions are located in the regions where the design focus has been set. Now, low-end torque t^* values are reduced from around 3 ms to 1.5-1.6 ms, while in the faster regions of the map t^* values are also reduced.

These t^* maps, with the confirmation of previous experimental results, highlight how choosing the most restrictive conditions for designing a suitable pre-chamber geometry is mandatory to increase performance of the concept. For better illustrating the decrease of t^* time obtained with this

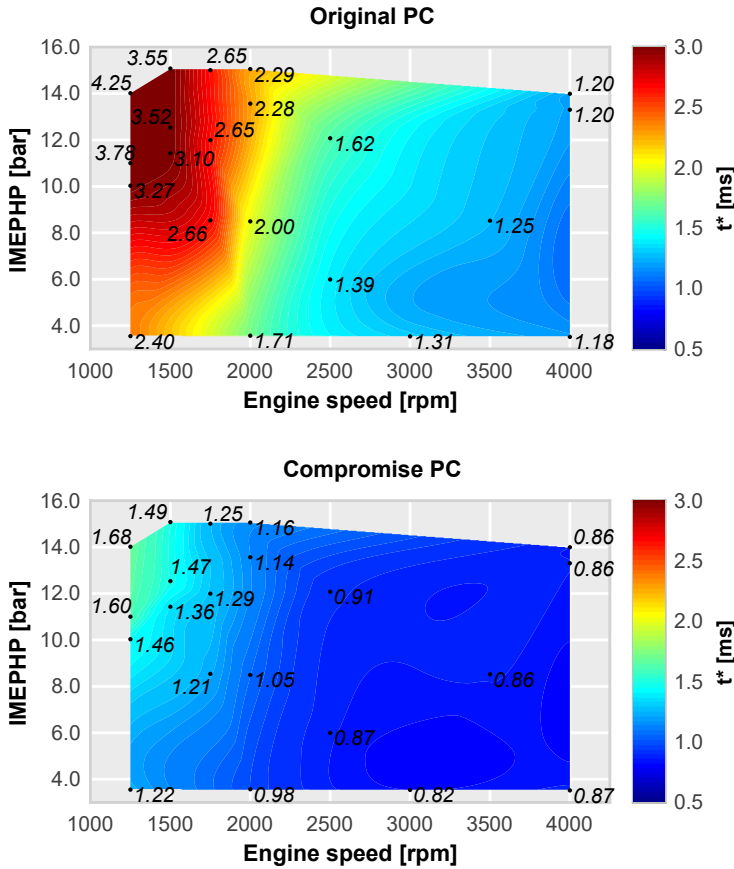


Figure 6.30: T^* value maps for the passive pre-chamber ignition concept for pre-chamber (left) and compromise pre-chamber (right) at $\lambda = 1$ operating with CNG.

compromise pre-chamber, Figure 6.31 presents the baseline (blue), compromise (orange) and optimum (yellow) t^* values for each extreme operating condition.

Yellow bars represent the minimum t^* achievable with an optimized geometry for each particular conditions, this is the best possible case among all combinations of pre-chamber volume and total hole area with a particular combustion process inside pre-chamber. Orange bars represent the obtained t^* values for the selected compromise pre-chamber geometry while blue bars are the t^* obtained with baseline pre-chamber geometry.

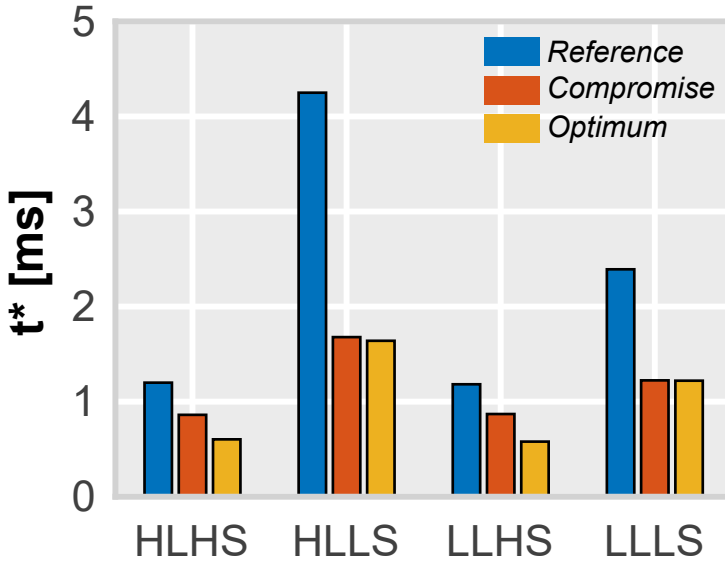


Figure 6.31: Comparison of t^* values at the most extreme operating conditions for baseline pre-chamber (blue), designed compromise pre-chamber (orange) and optimized pre-chamber geometry for each condition (yellow) at $\lambda = 1$ operating with CNG.

The design focus on lower engine speed conditions results in the greatest t^* reduction for HLLS (high engine load and low engine speed) and LLLS (low engine load and low engine speed) cases. As mentioned before in the t^* maps, the values are halved for these conditions. Also, for the conditions where the concept is not so compromised there is a reduction in the t^* , resulting in a global performance increase.

6.6. Conclusions

In this Chapter, different basic passive pre-chamber geometrical parameters, such volume, total hole area or nozzle orientation have been evaluated combining 1D simulation and experimental activities. A key parameter to benchmark different pre-chamber geometries and configurations, t^* , has been defined as the time needed for the jet to reach the furthest combustion chamber wall, and it has been proven to be a relevant parameter in pre-chamber evaluation. Furthermore, the insight generated by these evaluations led to the development of a preliminary design methodology and

the selection of a suitable compromise pre-chamber able to increase the performance of the passive pre-chamber ignition concept in the complete engine map.

Nozzle orientation evaluation showed different optimized values depending on operating conditions. For the low engine load and speed point, increasing the tangential angle resulted in a higher combustion stability and, thus, leading to an increased indicated efficiency. On the other hand, when operating at high engine load with EGR, an excessive increase of swirl level turned into a bad scavenging process near the spark plug location and reducing the efficiency.

Regarding pre-chamber internal volume, the combination of the two different 1D simulation tools proved that increasing pre-chamber volume benefits the generated jet momentum and thus, reduces t^* . This main result has been obtained with different combinations of engine load and speed. This result has been proven experimentally comparing a new bigger manufactured pre-chamber with baseline pre-chamber, obtaining faster and better phased combustion.

In terms of hole diameter, the optimal value to reduce t^* is related with the selected operating point. For low engine load region the hole area that reduces t^* is smaller than the hole area needed at high engine load region. When the selected hole diameter is low, the obtained pressure drop is elevated which compromises the pre-chamber fueling and scavenge. Contrarily, when the selected hole diameter is high the combustion process may not be suitable to pressurize pre-chamber and assure the ejection process, which will turn into the deterioration of the main chamber sweep and an increase of misfiring cycles.

Combustion process inside pre-chamber has been confirmed also as a key aspect for designing pre-chambers. Previous statements of geometrical parameters are dependent on pre-chamber combustion process, if this combustion changes enough, either by its duration or by its phasing, the obtained optimal geometry may change and the designing methodology must be repeated with the corrected combustion law. In this way, the optimum combustion process that enhances passive pre-chamber ignition system is an instantaneous combustion, which leads to a faster jet momentum profile.

Gathering all this knowledge a compromise optimum pre-chamber has been designed taking into account the operation of the engine at the most extreme conditions in terms of engine load and speed, specially focusing on the lower speed region since it has been proved the most restrictive

conditions for a proper concept operation. Result of the application of this methodology turns into a suitable geometry able to reduce the t^* value in all conditions.

However, the pre-chamber concept has very rigid boundaries (the pre-chamber geometry itself) that will prevent an optimal operation in the complete engine map as each region has its own necessities. To avoid this rigidity of passive pre-chamber, one solution is to change to an active system, with a dedicated fuel supply inside pre-chamber. This system can be more adaptive when improving the performance of the concept due to the ability to control the reactivity of the pre-chamber independently of the main chamber and the better scavenging process near the spark plug electrodes.

For further improvement of the concept, a deeper design process including more advanced tools, such as 3D Computer Fluid-Dynamics, can be implemented to better understand the pre-chamber internal configuration, allowing to design an even more sophisticated geometry taking into account the details of the pre-chamber internal aspects such as the shape of the surfaces or the position of the spark electrodes.

Conclusions and future investigation paths

7.1. Introduction

The objective of the present Chapter 7 is to gather and introduce the main conclusions and key aspects covered by this research work, and to list a series of future investigation paths that can provide a deeper knowledge of this passive pre-chamber ignition system. The conclusions reported at the end of each Chapter act as a quick view of the most important aspects.

Regarding the future investigation activities, a series of paths are presented, discussing their main benefits and the possible drawbacks that they may bring. Some of the activities are related to the continuation of the present work, and other activities are related with investigating new ideas that may have a good synergy with this passive pre-chamber ignition system.

7.2. Key aspects of the research work

In the first Chapter, a global introduction to the environmental issues that mankind is facing, especially in terms of greenhouse gases and nitrogen oxides emissions are presented, along with some of the actions that public institutions are performing to mitigate this problem. Furthermore, some potential solutions to reduce the contribution to this environmental issue from the transportation sector are also introduced, pointing main benefits and their respective drawbacks that avoid their direct implementation in the present passenger car engines.

Moreover, the passive pre-chamber ignition system has been marked as a potential solution to overcome these main drawbacks related to the thermal efficiency increase strategies. This ignition concept is able to provide a larger amount of energy during the ignition event, which turns into a more stable combustion process and therefore, an increased dilution tolerance.

On one hand lean burn or diluted combustion are two strategies that can increase the overall thermal efficiency by means of higher heat specific ratio and/or lower pumping losses. Nevertheless, this efficiency increase cannot be infinite being the dilution limit the maximum reachable condition while keeping a suitable combustion process. When reaching this limit, the stability of the process is compromised and the power output significantly reduces due to misfire cycles. While, on the other hand, Miller cycle is an effective strategy to increase the thermal efficiency by means of reducing pumping losses. However, this strategy has the main drawbacks of decreasing the turbulence level in the combustion chamber and limiting of the limited compression ratio.

Regarding the passive pre-chamber ignition concept itself, the key milestones of this system and a complete revision of how this concept affects to combustion process, including main combustion aspects, geometrical effects and pollutant formation are presented in the Literature Review Chapter.

In terms of combustion aspects, introducing a pre-chamber system requires to pay special attention to some processes such as the scavenging or the spark plug discharge timing in order to optimize the complete combustion process, among many others. Nevertheless, this ignition concept has been proven to be an excellent way to increase the combustion velocity and obtain those aforementioned thermal efficiency benefits.

Regarding pollutant emissions, the stoichiometric operation of the passive pre-chamber ignition concept requires the use of a three-way catalyst to achieve the restrictive emission regulations. Meanwhile, for an active pre-chamber application, if an ultra-lean operation ($\lambda > 2$) can be sustained, NO_x and CO emissions are significantly lowered compared with the stoichiometric operation, but an oxidation catalyst may be needed to reduce the HC emissions. Contrarily, if the ultra-lean operation is unattainable, raw NO_x and CO emissions must be reduced by means of a catalyst, even when operating with excess of air, which significantly increases the implementation costs, making the application of this concept unapproachable in these terms.

Methodology and the key tools, both experimental and numerical, selected for this research work are both presented in the Tools and Methodology Chapter. Main procedure in the experimental campaign was to keep constant

the energy provided by the fuel, modifying the amount of air, EGR or the ignition system. Furthermore, a design methodology from the experimental-numerical workflow was developed. This design methodology included a 1D Wave Action model used to obtain the characteristics of the combustion process within the pre-chamber and the main results of the jet momentum flux and gas exchange parameters through both chambers. Then, a 1D Jet model was used to calculate the jet penetration into the main chamber. By means of using the results of each tool as inputs for the next one in the workflow it was possible to create a design methodology, allowing to increase the pre-chamber performance by optimizing the benchmark t^* parameter.

In terms of direct application of the concept into the engine, the results revealed that the performance of the engine can be improved when switching to the passive pre-chamber ignition concept if the combustion phasing is strongly limited by knock. This is mainly caused because knock limits the performance of the conventional ignition system. It forces to push away the combustion from the TDC in order to assure a safe functioning. However, when switching to the passive pre-chamber ignition concept, the increase in combustion velocity allows to burn the charge quickly avoiding the end-gas knock, letting an advance in the combustion phasing and thus, increasing the efficiency.

However, this increase in efficiency is obtained only when the conventional system operates in knocking conditions. If the fuel is changed to a more knocking-resistant one, such as compressed natural gas, this main advantage of the passive pre-chamber system is lost. As there is no need to delay the combustion phasing, similar efficiency levels are obtained for both ignition systems. To obtain advantage of the new system, an increase in the maximum in-cylinder pressure must be feasible. A potential solution may be switching to Miller cycle and increase the volumetric compression ratio.

However, this operating cycle did not improve the obtained performance at the stoichiometric conditions while the compressed natural gas was kept as operating fuel. Results with this new architecture show similarities with the previous engine architecture, as the generated conditions were not generating knocking conditions when employing the conventional ignition system.

Analyzing the complete engine map in terms of engine load and speed at stoichiometric conditions it was revealed that low-end torque is a risky region to operate with the passive pre-chamber ignition system since the fast combustion and the instability avoids a proper combustion phasing, shifting

the combustion phasing before the TDC. Furthermore, it was shown that the operation at low engine speeds revealed that the increase of the heat losses worsens the efficiency of the engine.

Regarding the evaluation of the strategies to increase thermal efficiency, it was shown that air dilution increased the operating range of passive pre-chamber ignition compared with conventional spark ignition system when operating with gasoline. Also, the indicated gross efficiency was increased in the whole range until the dilution limit was reached due to the better combustion phasing of the passive pre-chamber system. In the limit, the obtained heat release rate profiles were quite similar between them, avoiding the advantage related to this alternative ignition system. Moreover it has been confirmed that combustion phasing is a prevalent parameter when seeking an increase in the indicated efficiency.

However, this increase of performance is no longer obtained when switching to compressed natural gas fuel since conventional spark system is able to achieve a proper combustion phasing, limiting and reducing the operative range and the efficiency gap between concepts, as it happened when directly implementing the concept.

Similar results are obtained by diluting with EGR. When conventional spark ignition is restricted by knocking, passive pre-chamber ignition system arises as a solution to advance combustion phasing and increase indicated efficiency. However, if the combustion phasing is not restricted, both by reducing engine load or by the higher ignition delay of the fuel, the gap between efficiencies decreases. Furthermore, another disadvantage related to the EGR operation is that the dilution limit is shorter for passive pre-chamber ignition system compared with conventional spark ignition system. This is caused by the difficulty of scavenging the pre-chamber, adding the external EGR to the IGR of previous cycle.

Regarding the operation at low engine load and speed, passive pre-chamber ignition system has shown difficulties to achieve a proper heat flow in the exhaust tailpipe. This is one of the most critical aspects of this ignition system, since compromises the its compatibility with the three-way catalyst required to control pollutant emissions. Two different strategies were evaluated to increase temperature in the exhaust line: increasing the intake temperature and adding external EGR. Both strategies were not able to raise the exhaust temperature to values able to activate the three-way catalyst. However, the addition of EGR showed a remarkable increase of temperature keeping similar efficiency as that without EGR.

When evaluating the EGR dilution strategy in a complete engine map clear benefits are obtained in the whole operating range, specially in the low-end torque region. In this area, a suitable combustion phasing is only achieved if passive pre-chamber is operated with EGR, otherwise the combustion phasing is set earlier than the TDC. This is caused by the longer combustion duration attained operating with EGR. Main drawbacks arise at low engine loads and high speed, when the cycle takes less time and the pre-chamber scavenging process is even more compromised.

From this investigation, the pre-chamber design arises as a key aspect to assure the proper performance of this concept. Optimized pre-chamber geometries are able to operate with higher dilution ratios, which turns into performance benefits in the different engine loads.

A complete design methodology was developed including different basic geometrical parameters of a pre-chamber, such as volume, total hole area or nozzle orientation. These parameters have been evaluated by means of 1D simulation tools and then, an experimental campaign to confirm the trends was carried out. From the numerical evaluation of the pre-chambers, a key parameter (t^*) was selected to benchmark different pre-chamber geometries and configurations. This parameter was defined as the time needed by the jet to reach the furthest combustion chamber wall, and it had been proven to be a relevant parameter in pre-chamber evaluation. A compromise pre-chamber geometry was selected following this design approach and an improvement in the main jet governing parameters was numerically observed.

Regarding the experimental evaluation of the nozzle holes orientation, it was found that optimum values depend on the operating conditions. For low engine load and speed, increasing the tangential angle resulted in a higher combustion stability and, thus, leading to an increased indicated efficiency. On the other hand, when operating at high engine load with EGR, an excessive increase of swirl level turned into a bad scavenging process near the spark plug location, decreasing the obtained efficiency.

In terms of pre-chamber internal volume, the combination of the two different 1D simulation tools proved that increasing pre-chamber volume benefits the generated jet momentum and thus, reduces the time needed to reach the further combustion chamber wall (t^*). This main result has been obtained at different combinations of engine load and speed. This result has been experimentally confirmed by comparing a new bigger manufactured pre-chamber with the baseline pre-chamber, obtaining faster and better phased combustion.

Similar trends were obtained for hole diameter. The optimal value to reduce t^* is related with the selected operating point. For low engine load region the hole area that reduces t^* is smaller than the hole area needed at high engine load region. When the selected hole diameter is low, the obtained pressure drop during the compression stroke increases, which compromises the pre-chamber fueling and scavenge. Contrarily, when the selected hole diameter is high the combustion process in the pre-chamber may not be suitable to pressurize it and assure a proper jet ejection process, which will turn into poor main chamber sweep and an increase of misfiring cycles.

And finally, combustion process inside pre-chamber was identified also as a very relevant aspect for designing pre-chambers. Previous statements of geometrical parameters are dependent on pre-chamber combustion process, if this combustion changes enough, either by its duration or by its phasing, the obtained optimal geometry may change and the design methodology must be iterated with the corrected combustion law. Following this reasoning, the optimum combustion process that enhances passive pre-chamber ignition system is an instantaneous combustion, which leads to a sharper jet momentum profile.

However, the passive pre-chamber concept has very rigid boundaries (the pre-chamber geometry itself) that will prevent an optimal operation in the complete engine map as each region has its own requirements. To avoid this rigidity of this concept, one solution is to change to an active system, with a dedicated fuel supply inside pre-chamber. This system can be more adaptive when improving the performance of the concept due to the ability to control the reactivity of the pre-chamber independently of the main chamber and the better scavenging process near the spark plug electrodes.

Moreover, the introduction of such passive pre-chamber ignition system into an internal combustion engine should take into account some aspects prior to its execution. One of these aspects is the change of the boost pressure. Changes in boost pressures resulting from improved combustion efficiency may require upgrading the turbocharger to handle increased demand for airflow or adjusting the wastegate for precise boost control. In terms of heat management, some considerations may involve enhancements to the intercooler or charge air cooling system in order to assure a proper operation. While, the alteration of exhaust gas flow could prompt evaluation and potential modifications to the exhaust system.

7.3. Future investigation activities

The application of the passive pre-chamber ignition system has been presented with describing its main benefits, especially in terms of combustion duration and stability, and a series of drawbacks associated to its operation.

However, there are some ways to continue this research work that may be interesting following activities. Moreover, a deeper knowledge of the concept will be obtained and some of the questions that remain unanswered may be solved. Among the possibilities to continue the investigation, the most promising ones are the following:

- The first and most obvious way to continue the research activities is to manufacture and experimentally evaluate the proposed compromise pre-chamber geometry. This pre-chamber geometry reported a substantial decrease of the benchmark t^* parameter in the most critical regions of the engine map, both at low engine loads and low-end torque conditions. By doing this not only will be possible to further extend the knowledge of basic phenomena of this concept but also to validate the design methodology with a brand new geometry designed by means of this procedure.
- Another possibility to continue with these activities is to include a complete advanced 3D CFD tool in the design methodology in order to take into account the phenomena that is not possible to simulate with basic 1D numerical tools. Some aspects related with the spatial advancement of combustion process, jet penetration process or the location of the spark plug within the pre-chamber have a strong impact on the performance of the concept and their analysis can only be performed in such advance numerical tools. For that reason, including this type of tool in the design loop will bring a higher increase of pre-chamber performance and a more optimized pre-chamber geometry.
- If a 3D CFD tool is included in the design methodology new definitions of pre-chamber geometries can be analyzed and manufactured if they report benefits in terms of t^* values. Advanced conical geometries that accelerate jet ejection may be a potential solution to even reduce the time to reach the cylinder inner wall and increase the combustion velocity. Moreover different and fancy geometries may be analyzed and evaluated, including shapes and/or number and position of holes.

- A potential path to continue with this research is to modify the ignition source directly. By changing the conventional spark plug to other more energetic concept the combustion process within the pre-chamber will become faster thus helping the jets to sweep better the main combustion chamber. One of these ignition concepts may be the nanosecond repetitive pulse (NRP) system. The key aspect of this concept is to provide small discharge pulses which finally transfer more energy to the mixture compared with the conventional spark plug. This effect increases combustion stability and thus, it is possible to further extend the dilution limit compared with the baseline ignition system and obtain a greater thermal efficiency.
- Finally, another possibility is to include an additional hydrogen supply to the pre-chamber in order to enhance its combustion within the pre-chamber. Investigation activities reported that an active pre-chamber system operating with hydrogen was able to achieve ultra-lean conditions. So in this way, a low to moderate hydrogen addition may be able to strengthen combustion process in the pre-chamber and lead to higher dilution tolerance limits.

As a final remark, the research activities reported in the present thesis improved significantly the understanding of the passive pre-chamber ignition concept, highlighting its strengths and weakness aspects.

This investigation describes the most relevant characteristics and the potential of this concept, setting the fundamentals for its future optimization and application in future SI engines.

Bibliography

- [1] J. Benajes, R. Novella, J. Gomez-Soriano, P. Martinez-Hernandiz, C. Libert, and M. Dabiri. “Evaluation of the passive pre-chamber ignition concept for future high compression ratio turbocharged spark-ignition engines”. *Applied Energy* 248, 2019, pp. 576–588 (cited in pp. 71, 87, 88, 121, 122).
- [2] J. Benajes, R. Novella, J. Gomez-Soriano, P. Martinez-Hernandiz, C. Libert, and M. Dabiri. “Performance of the passive pre-chamber ignition concept in a spark-ignition engine for passenger car applications”. In: *SIA Powertrain & Electronics*. 2019 (cited in pp. 71, 87, 88, 121).
- [3] J. López, R. Novella, J. Gomez-Soriano, P. Martínez-Hernández, et al. “Advantages of the unscavenged pre-chamber ignition system in turbocharged natural gas engines for automotive applications”. *Energy* 218, 2021, p. 119466 (cited in pp. 71, 87, 88, 96, 122).
- [4] R. Novella, J. Gomez-Soriano, P. Martinez-Hernandiz, C. Libert, and F. Rampanarivo. “Improving the performance of the passive pre-chamber ignition concept for spark-ignition engines fueled with natural gas”. *Fuel* 290, 2021, p. 119971 (cited in pp. 63, 71, 81, 121, 122, 159).
- [5] R. Novella, B. Pla, P. Bares, and P. J. Martinez-Hernandiz. “Closed-Loop Combustion Control by Extremum Seeking with the Passive-Chamber Ignition Concept in SI Engines”. In: *WCX SAE World Congress Experience*. SAE International, 2020.
- [6] J. García-Oliver, Y. Niki, R. Rajasegar, R. Novella, et al. “An experimental and one-dimensional modeling analysis of turbulent gas ejection in pre-chamber engines”. *Fuel* 299, 2021, p. 120861 (cited in pp. 71, 81, 82).
- [7] P. J. Martinez Hernandez, F. Di Sabatino, R. Novella, and I. Ekoto. “A Numerical and Experimental Investigation on Different Strategies to Evaluate Heat Release Rate and Performance of a Passive Pre-Chamber Ignition System”. In: *WCX SAE World Congress Experience*. SAE International, 2022.

- [8] F. D. Sabatino, P. J. Martinez-Hernandez, R. N. Rosa, and I. Ekoto. “Investigation of the effects of passive pre-chamber nozzle pattern and ignition system on engine performance and emissions”. *International Journal of Engine Research* 0 (0), 2022.
- [9] [Investigation on the Effects of Passive Pre-Chamber Ignition System and Geometry on Engine Knock Intensity](#). Vol. ASME 2022 ICE Forward Conference. Internal Combustion Engine Division Fall Technical Conference. 2022.
- [10] J. Lelieveld, J. S. Evans, M. Fnais, D. Giannadaki, and A. Pozzer. “The contribution of outdoor air pollution sources to premature mortality on a global scale”. *Nature* 525 (7569), 2015, p. 367 (cited in p. 1).
- [11] A. Malik, J. Lan, and M. Lenzen. “Trends in global greenhouse gas emissions from 1990 to 2010”. *Environmental science & technology* 50 (9), 2016, pp. 4722–4730 (cited in p. 1).
- [12] J. Hansen, M. Sato, R. Ruedy, K. Lo, D. W. Lea, and M. Medina-Elizade. “Global temperature change”. *Proceedings of the National Academy of Sciences* 103 (39), 2006, pp. 14288–14293 (cited in p. 1).
- [13] M. Ruiz-Medina and R. Espejo. “Integration of spatial functional interaction in the extrapolation of ocean surface temperature anomalies due to global warming”. *International Journal of Applied Earth Observation and Geoinformation* 22, 2013. *Spatial Statistics for Mapping the Environment*, pp. 27–39 (cited in p. 1).
- [14] T. Boningari and P. G. Smirniotis. “Impact of nitrogen oxides on the environment and human health: Mn-based materials for the NOx abatement”. *Current Opinion in Chemical Engineering* 13, 2016, pp. 133–141 (cited in p. 2).
- [15] M. Williams and R. Minjares. “A technical summary of Euro 6/VI vehicle emission standards”. International Council for Clean Transportation (ICCT), Washington, DC, accessed July 10, 2016, p. 2017 (cited in pp. 2, 3).
- [16] C. of European Union (2007). “Regulation (EC) No 715/2007 of the European Parliament and of the Council of 20 June 2007 on type approval of motor vehicles with respect to emissions from light passenger and commercial vehicles (Euro 5 and Euro 6) and on access to vehicle repair and maintenance information”. *OJ L* 171, 20-06-2007, pp. 1–16 (cited in p. 2).
- [17] M. Achtnicht. “German car buyers’ willingness to pay to reduce CO2 emissions”. *Climatic change* 113 (3), 2012, pp. 679–697 (cited in p. 2).
- [18] W. P. Attard, N. Fraser, P. Parsons, and E. Toulson. “A Turbulent Jet Ignition Pre-Chamber Combustion System for Large Fuel Economy Improvements in a Modern Vehicle Powertrain”. *SAE International Journal of Engines* 3 (2), 2010, pp. 20–37 (cited in pp. 5, 43–45, 48, 50, 58, 60).

- [19] A. Cooper, A. Harrington, M. Bassett, S. Reader, and M. Bunce. “Application of the Passive MAHLE Jet Ignition System and Synergies with Miller Cycle and Exhaust Gas Recirculation”. In: WCX SAE World Congress Experience. SAE International, 2020 (cited in pp. 5, 43, 46, 60, 61).
- [20] J. B. Heywood et al. Internal combustion engine fundamentals. Mcgraw-hill New York, 1988 (cited in pp. 12, 30, 48, 58, 60).
- [21] F. A. Ayala, M. D. Gerty, and J. B. Heywood. “Effects of Combustion Phasing, Relative Air-fuel Ratio, Compression Ratio, and Load on SI Engine Efficiency”. In: SAE 2006 World Congress & Exhibition. SAE International, 2006 (cited in p. 12).
- [22] F. Payri González and J. M. Desantes Fernández. “Motores de combustión interna alternativos”. Colección Académica. Editorial UPV, 2011 (cited in pp. 12, 48, 60).
- [23] W. P. Attard, S. Konidaris, F. Hamori, E. Toulson, and H. C. Watson. “Compression Ratio Effects on Performance, Efficiency, Emissions and Combustion in a Carbureted and PFI Small Engine”. In: Asia Pacific Automotive Engineering Conference. SAE International, 2007 (cited in p. 12).
- [24] W. P. Attard and H. Blaxill. “A Lean Burn Gasoline Fueled Pre-Chamber Jet Ignition Combustion System Achieving High Efficiency and Low NOx at Part Load”. In: SAE 2012 World Congress & Exhibition. SAE International, 2012 (cited in pp. 12, 43, 44, 65–67).
- [25] A. A. Quader. “Lean Combustion and the Misfire Limit in Spark Ignition Engines”. In: International Automobile Engineering and Manufacturing Meeting. SAE International, 1974 (cited in p. 13).
- [26] A. Stadler, M. Wessoly, S. Blochum, M. Härtl, and G. Wachtmeister. “Gasoline Fueled Pre-Chamber Ignition System for a Light-Duty Passenger Car Engine with Extended Lean Limit”. SAE International Journal of Engines 12 (3), 2019, pp. 323–339 (cited in p. 13).
- [27] E. Toulson, H. C. Watson, and W. P. Attard. “The Effects of Hot and Cool EGR with Hydrogen Assisted Jet Ignition”. In: Asia Pacific Automotive Engineering Conference. SAE International, 2007 (cited in pp. 13, 30, 51, 64).
- [28] H. Kuroda, Y. Nakajima, K. Sugihara, Y. Takagi, and S. Muranaka. “The Fast Burn with Heavy EGR, New Approach for Low NOx and Improved Fuel Economy”. In: 1978 Automotive Engineering Congress and Exposition. SAE International, 1978 (cited in p. 13).
- [29] G. Abd-Alla. “Using exhaust gas recirculation in internal combustion engines: a review”. Energy Conversion and Management 43 (8), 2002, pp. 1027–1042 (cited in p. 14).
- [30] R. H. Miller. “Supercharging and internal cooling cycle for high output”. Trans. ASME 69, 1947 (cited in p. 14).

- [31] M. Choi, Y.-H. Kwak, J. Song, V. Negandhi, and D. Gajowski. “Synergies of Cooled External EGR, Water Injection, Miller Valve Events and Cylinder Deactivation for the Improvement of Fuel Economy on a Turbocharged-GDI Engine; Part 1, Engine Simulation”. In: WCX SAE World Congress Experience. SAE International, 2019 (cited in p. 15).
- [32] M. Choi, Y.-H. Kwak, D. B. Roth, D. Jakiela, and J. Song. “Synergies of Cooled External EGR, Water Injection, Miller Valve Events and Cylinder Deactivation for the Improvement of Fuel Economy on a Turbocharged-GDI Engine; Part 2, Engine Testing”. In: WCX SAE World Congress Experience. SAE International, 2019 (cited in p. 15).
- [33] L. Cao, H. Teng, R. Miao, X. Luo, T. Hu, and X. Huang. “A Comparative Study on Influence of EIVC and LIVC on Fuel Economy of A TGDI Engine Part III: Experiments on Engine Fuel Consumption, Combustion, and EGR Tolerance”. In: International Powertrains, Fuels & Lubricants Meeting. SAE International, 2017 (cited in p. 15).
- [34] D. Cleary and G. Silvas. “Unthrottled Engine Operation with Variable Intake Valve Lift, Duration, and Timing”. In: SAE World Congress & Exhibition. SAE International, 2007 (cited in p. 15).
- [35] B. Patychuk, N. Wu, G. McTaggart-Cowan, P. Hill, and S. Munshi. “Intake and Exhaust Valve Timing Control on a Heavy-Duty, Direct-Injection Natural Gas Engine”. In: SAE 2015 World Congress & Exhibition. SAE International, 2015 (cited in p. 15).
- [36] E. Toulson, H. J. Schock, and W. P. Attard. “A Review of Pre-Chamber Initiated Jet Ignition Combustion Systems”. In: SAE 2010 Powertrains Fuels & Lubricants Meeting. SAE International, 2010 (cited in pp. 16, 17, 24, 31–33, 43).
- [37] C. E. C. Alvarez, G. E. Couto, V. R. Roso, A. B. Thiriet, and R. M. Valle. “A review of prechamber ignition systems as lean combustion technology for SI engines”. *Applied Thermal Engineering* 128, 2018, pp. 107–120 (cited in p. 16).
- [38] S. Zhu, S. Akehurst, A. Lewis, and H. Yuan. “A review of the pre-chamber ignition system applied on future low-carbon spark ignition engines”. *Renewable and Sustainable Energy Reviews* 154, 2022, p. 111872 (cited in pp. 16, 48, 68).
- [39] H. R. Ricardo. “Recent research work on the internal-combustion engine”. *SAE Transactions*, 1922, pp. 1–93 (cited in p. 18).
- [40] M. C. Turkish. “3 - Valve Stratified Charge Engines: Evolvement, Analysis and Progression”. In: International Stratified Charge Engine Conference. SAE International, 1974 (cited in pp. 18–22, 24, 50).
- [41] M. C. Turkish. “Prechamber and Valve Gear Design for 3-Valve Stratified Charge Engines”. In: 1975 Automotive Engineering Congress and Exposition. SAE International, 1975 (cited in pp. 18–22).

- [42] C. E. Summers. Internal Combustion Engine. U.S. Patent 1568638, Jan. 1926 (cited in p. 19).
- [43] M. Mallory. Internal Combustion Engine. U.S. Patent 2121920, Feb. 1938 (cited in pp. 19, 20).
- [44] A. Bagnulo. Engine with Stratified Mixture. U.S. Patent 2422610, Jun. 1947 (cited in p. 20).
- [45] W. B. Barnes. Improvements in or Relating to Internal Combustion Engines. British Patent No. 683162, Nov. 1952 (cited in pp. 20, 21).
- [46] N. O. Broderson. Method of operating internal-combustion engines. U.S. Patent 2615437, Oct. 1952 (cited in pp. 21, 22).
- [47] N. O. Broderson. Method of operating internal-combustion engines. U.S. Patent 2690741, Oct. 1954 (cited in p. 21).
- [48] K. S. Varde and M. J. Lubin. “The Roll of Connecting Nozzle and the Flame Initiation Point in the Performance of a Dual Chamber Stratified Charge Engine”. In: International Stratified Charge Engine Conference. SAE International, 1974 (cited in p. 21).
- [49] N. A. Nilov. Features of Carburetor Engines with Torch Ignition. *Automobilnaya Promyshlennost*, USSR, Nov. 8, 1958 (cited in pp. 21, 22).
- [50] P. H. Schweitzer and L. J. Grunder. “Hybrid Engines”. In: Pre-1964 SAE Technical Papers. SAE International, 1963 (cited in p. 21).
- [51] R. M. Heintz. Internal Combustion Engine. U.S. Patent 2884913, May 1959 (cited in pp. 21, 23).
- [52] A. L. London and K. J. Kadoch. “The RAM Straticharge Engine-Performance Characteristics”. ASME San Francisco Section, 1959 (cited in p. 21).
- [53] A. Barnard and C. D. Brewer. Improvements in or relating to internal combustion engines. British Patent No. 948686, Feb. 1964 (cited in pp. 22, 23).
- [54] H. K. Newhall and I. A. El-Messiri. “A combustion chamber concept for control of engine exhaust air pollutant emissions”, 1970 (cited in p. 24).
- [55] I. A. El-Messiri and H. K. Newhall. “The Role of Combustion Product Quenching in the Divided Chamber Engine”. In: Proc. Intersociety Energy Conversion Engineering Conference. 1971, p. 63 (cited in p. 24).
- [56] I. El-Messiri and H. Newhall. “Analytical characterization of the divided-chamber combustion process”. Symposium (International) on Combustion 14 (1), 1973. Fourteenth Symposium (International) on Combustion, pp. 843–850 (cited in p. 24).
- [57] H. K. Newhall and I. A. El Messiri. “A Combustion Chamber Designed for Minimum Engine Exhaust Emissions”. In: Mid-Year Meeting. SAE International, 1970 (cited in p. 24).

- [58] T. Date, S. Yagi, A. Ishizuya, and I. Fujii. “[Research and Development of the Honda CVCC Engine](#)”. In: National West Coast Meeting. SAE International, 1974 (cited in pp. 24, 25).
- [59] S. Yagi, T. Date, and K. Inoue. “[NOx Emission and Fuel Economy of the Honda CVCC Engine](#)”. In: International Stratified Charge Engine Conference. SAE International, 1974 (cited in p. 24).
- [60] T. Date and T. Nomura. “[Research and Development of the Carburetor for the CVCC Engine](#)”. In: 1980 Automotive Engineering Congress and Exposition. SAE International, 1980 (cited in p. 24).
- [61] S. Yagi, I. Fujii, M. Nishikawa, and H. Shirai. “[A Newly-Developed 1.5L CVCC Engine for Some 1980 Models](#)”. In: 1980 Automotive Engineering Congress and Exposition. SAE International, 1980 (cited in p. 24).
- [62] S. Yagi, I. Fujii, M. Watanabe, and S. Narasaka. “[On the Emission-Combustion Temperature Relationship in the CVCC Engine](#)”. In: 1976 Automotive Engineering Congress and Exposition. SAE International, 1976 (cited in p. 24).
- [63] T. Date. Viertakt-hubkolben-brennkraftmaschine. German Patent No. 2259286, Aug. 1973 (cited in p. 24).
- [64] W. R. Brandstetter, G. Decker, H. J. Schafer, and D. Steinke. “[The Volkswagen PCI Stratified Charge Concept-Results from the 1.6 Liter Air Cooled Engine](#)”. In: International Stratified Charge Engine Conference. SAE International, 1974 (cited in p. 25).
- [65] W. Brandstetter and G. Decker. “[Fundamental studies on the volkswagen stratified charge combustion process](#)”. *Combustion and Flame* 25, 1975, pp. 15–23 (cited in p. 25).
- [66] W. R. Brandstetter, G. Decker, and K. Reichel. “[The Water-Cooled Volkswagen PCI-Stratified Charge Engine](#)”. In: SAE Automobile Engineering and Manufacturing Meeting. SAE International, 1975 (cited in p. 25).
- [67] G. C. Davis, R. B. Krieger, and R. J. Tabaczynski. “[Analysis of the Flow and Combustion Processes of a Three-Valve Stratified Charge Engine with a Small Prechamber](#)”. In: International Stratified Charge Engine Conference. SAE International, 1974 (cited in p. 26).
- [68] F. A. Wyczalek, J. L. Harned, S. Maksymiuk, and J. R. Blevins. “[EFI Prechamber Torch Ignition of Lean Mixtures](#)”. In: 1975 Automotive Engineering Congress and Exposition. SAE International, 1975 (cited in p. 26).
- [69] D. L. Dimick, S. L. Genslak, R. E. Greib, and M. J. Malik. “[Emissions and Economy Potential of Prechamber Stratified Charge Engines](#)”. In: 1979 Automotive Engineering Congress and Exposition. SAE International, 1979 (cited in p. 26).

- [70] J. F. Sinnamon and D. E. Cole. “The Influence of Overall Equivalence Ratio and Degree of Stratification on the Fuel Consumption and Emissions of A Prechamber, Stratified-Charge Engine”. In: 1979 Automotive Engineering Congress and Exposition. SAE International, 1979 (cited in p. 26).
- [71] Y. Sakai, K. Kunii, S. Tsutsumi, and Y. Nakagawa. “Combustion Characteristics of the Torch Ignited Engine”. In: International Stratified Charge Engine Conference. SAE International, 1974 (cited in pp. 26, 50, 51, 56, 57).
- [72] D. Gruden. “Combustion and Exhaust Emission of an Engine Using the Porsche-Stratified-Charge-Chamber-System”. In: SAE Automobile Engineering and Manufacturing Meeting. SAE International, 1975 (cited in p. 26).
- [73] T. K. Garrett. “Porsche stratified charge engine”. *Environmental Science & Technology* 9 (9), 1975, pp. 826–830 (cited in p. 26).
- [74] A. Ekchian, J. B. Heywood, R. J. Tabaczynski, and J. C. Wall. “Performance and NOx Emissions Modeling of a Jet Ignition Prechamber Stratified Charge Engine”. In: 1976 Automotive Engineering Congress and Exposition. SAE International, 1976 (cited in p. 26).
- [75] A. Ekchian, J. B. Heywood, and J. M. Rife. “Time Resolved Measurements of the Exhaust from a Jet Ignition Prechamber Stratified Charge Engine”. In: 1977 International Automotive Engineering Congress and Exposition. SAE International, 1977 (cited in p. 26).
- [76] E. A. Purins. “Pre-Chamber Stratified Charge Engine Combustion Studies”. In: International Stratified Charge Engine Conference. SAE International, 1974 (cited in p. 26).
- [77] R. Krieger and G. Davis. “The influence of the degree of stratification on jet-ignition engine emissions and fuel consumption”. In: Conference on Stratified Charge Engines, Inst, of Mech. Engrs. 1976 (cited in p. 26).
- [78] L. Hideg and R. P. Ernest. Internal combustion engine control system. U.S. Patent 4077366, Mar. 1978 (cited in p. 26).
- [79] L. Hideg and R. P. Ernest. Internal combustion engine control system. U.S. Patent 4108136, Aug. 1978 (cited in p. 26).
- [80] L. Hideg and R. P. Ernest. Internal combustion engine control system. U.S. Patent 4259932, Apr. 1981 (cited in p. 26).
- [81] A. O. Simko. Fuel injection system for dual combustion chamber engine. U.S. Patent 4239023, Dec. 1980 (cited in p. 26).
- [82] A. O. Simko. Fuel flow control valve assembly. U.S. Patent 4301825, Nov. 1981 (cited in p. 26).
- [83] H. Huang and R. Hong. Air-assisted fuel injection applied in the two-stroke engine of flame-jet ignition type. U.S. Patent 5085189, Feb. 1992 (cited in p. 26).

- [84] J. D. Hiltner and M. L. Willi. Method and apparatus for providing a hydrogen enriched fuel to combustion prechamber. U.S. Patent 6739289, May 2004 (cited in p. 27).
- [85] B. Bailey, S. Fiveland, and W. Gong. Method to extend lean ignition limit within internal combustion engine. U.S. Patent 7100567, Sep. 2006 (cited in p. 27).
- [86] S. Fiveland. Compression ignition initiation device and internal combustion engine using same. U.S. Patent 7398743, Jul. 2008 (cited in p. 27).
- [87] N. Semenov. "Die Oxydation des Phosphordampfes bei niedrigen Drucken". *Zeitschrift für Physik* 46 (1), 1927, pp. 109–131 (cited in p. 27).
- [88] N. N. Semenov. "Chain reactions". Goskhimtekhnizdat, Leningrad 241, 1934, p. 285 (cited in pp. 27, 54).
- [89] N. Semenov. "On Types of Kinetic Curves in Chain Reactions". *Comptes Rendus (Doklady) de l'Academie des Sciences de l'URSS (I)* 43 (8), 1944, pp. 342–348 (cited in pp. 27, 54).
- [90] N. Semenov. "O nekotorykh problemakh khimicheskoi kinetiki i reaktivnoi sposobnosti (On Some Problems of Chemical Kinetics and Reactivity)", Moscow: Akad". Nauk SSSR, 1958, p. 42 (cited in p. 27).
- [91] V. Azatyan. "Role of Semenov's Theory of Chain Reactions in the Formation of Modern Concepts on the Processes of Combustion, Explosion, and Detonation of Gases". *Russian Journal of Physical Chemistry B* 15 (2), 2021, pp. 278–284 (cited in p. 27).
- [92] S. Biswas and L. Qiao. "Ignition of ultra-lean premixed hydrogen/air by an impinging hot jet". *Applied energy* 228, 2018, pp. 954–964 (cited in pp. 27, 42, 55).
- [93] L. Gussak, O. Ryabikov, G. Politenkova, and G. Furman. "Yield of atomic hydrogen during combustion of methane and hydrogen mixtures with air". *Bulletin of the Academy of Sciences of the USSR, Division of chemical science* 23 (2), 1974, pp. 451–452 (cited in p. 27).
- [94] L. Gussak, O. Ryabikov, G. Politenkova, and G. Furman. "Effect of adding individual combustion products on combustion of methane-Air mixture". *Russian Chemical Bulletin* 22 (9), 1974, pp. 2128–2128 (cited in pp. 27, 54).
- [95] L. Gussak, V. Karpov, V. Slutskii, and A. Spasskii. "Burning rate and stability in forechamber flame ignition in an internal-combustion engine". *Combustion, Explosion and Shock Waves* 19 (5), 1983, pp. 628–630 (cited in p. 27).

- [96] L. A. Gussak, M. C. Turkish, and D. C. Siegl. “High Chemical Activity of Incomplete Combustion Products and a Method of Prechamber Torch Ignition for Avalanche Activation of Combustion in Internal Combustion Engines”. In: SAE Automobile Engineering and Manufacturing Meeting. SAE International, 1975 (cited in p. 27).
- [97] L. A. Gussak, V. P. Karpov, and Y. V. Tikhonov. “The Application of Lag-Process in Prechamber Engines”. In: Passenger Car Meeting & Exposition. SAE International, 1979 (cited in pp. 27, 50, 54).
- [98] L. A. Gussak. “The Role of Chemical Activity and Turbulence Intensity in Prechamber-Torch Organization of Combustion of a Stationary Flow of a Fuel-Air Mixture”. In: SAE International Congress and Exposition. SAE International, 1983 (cited in p. 27).
- [99] L. Gussak and M. Turkish. “LAG-process of combustion and its application in automobile gasoline engines”. In: Proc. IMechE C. Vol. 257. 1976 (cited in pp. 27, 54).
- [100] L. A. Gussak, E. G. Voldemarovich, and A. R. D. Carburetor type internal combustion engine with prechamber. U.S. Patent 3092088, Jun. 1963 (cited in pp. 27, 28).
- [101] L. A. Gussak. Method of prechamber-torch ignition in internal combustion engines. U.S. Patent 3230939, Jan. 1966 (cited in p. 27).
- [102] L. A. Gussak and D. A. Gussak. Internal combustion engine with jet ignition of a non-uniformly distributed working mixture from a precombustion chamber cut-off by the piston. U.S. Patent 3283751, Nov. 1966 (cited in p. 27).
- [103] N. Semenov, L. A. Gussak, V. Boboley, E. Unxov, et al. Method and apparatus for producing a protective atmosphere in heating furnaces. U.S. Patent 3802827, May 1974 (cited in p. 27).
- [104] S. Biswas. Physics of turbulent jet ignition: mechanisms and dynamics of ultra-lean combustion. Springer, 2018 (cited in pp. 27, 42).
- [105] A. K. Oppenheim, K. Teichman, K. Hom, and H. E. Stewart. “Jet Ignition of an Ultra-Lean Mixture”. In: Passenger Car Meeting & Exposition. SAE International, 1978 (cited in p. 27).
- [106] A. K. Oppenheim, J. Beltramo, D. W. Faris, J. A. Maxson, K. Hom, and H. E. Stewart. “Combustion by Pulsed Jet Plumes - Key to Controlled Combustion Engines”. In: SAE International Congress and Exposition. SAE International, 1989 (cited in p. 27).
- [107] D. Hensinger, J. Maxson, K. Hom, and A. Oppenheim. “Jet Plume Injection and Combustion”. In: International Congress & Exposition. SAE International, 1992 (cited in pp. 27, 28).

- [108] E. Murase, S. Ono, K. Hanada, and A. K. Oppenheim. “Pulsed Combustion Jet Ignition in Lean Mixtures”. In: International Fuels & Lubricants Meeting & Exposition. SAE International, 1994 (cited in pp. 27, 29).
- [109] E. Murase, S. Ono, K. Hanada, J. H. Yun, and A. K. Oppenheim. “Performance of pulsed combustion jet at high pressures and temperatures”. JSAE review 17 (3), 1996, pp. 245–250 (cited in pp. 27, 29).
- [110] E. Murase and K. Hanada. “Enhancement of Combustion by Injection of Radicals”. In: SAE 2000 World Congress. SAE International, 2000 (cited in p. 27).
- [111] A. K. Oppenheim. “Prospects for Combustion in Piston Engines”. In: SAE 2002 World Congress & Exhibition. SAE International, 2002 (cited in p. 27).
- [112] A. K. Oppenheim. Combustion in piston engines: technology, evolution, diagnosis and control. Springer (cited in p. 27).
- [113] J. D. Dale and A. K. Oppenheim. “Enhanced Ignition for I. C. Engines with Premixed Gases”. In: SAE International Congress and Exposition. SAE International, 1981 (cited in p. 27).
- [114] J. D. Dale and A. K. Oppenheim. “A Rationale for Advances in the Technology of I. C. Engines”. In: SAE International Congress and Exposition. SAE International, 1982 (cited in p. 27).
- [115] J. Dale, M. Checkel, and P. Smy. “Application of high energy ignition systems to engines”. Progress in Energy and Combustion Science 23 (5), 1997, pp. 379–398 (cited in p. 27).
- [116] A. K. Hayashi, K. Matsuura, and S. Baba. “Performance of a Flame Jet Ignition System in a Two-Stroke Engine”. In: SAE 2000 World Congress. SAE International, 2000 (cited in p. 27).
- [117] R. Latsch. “The Swirl-Chamber Spark Plug: A Means of Faster, More Uniform Energy Conversion in the Spark-Ignition Engine”. In: SAE International Congress and Exposition. SAE International, 1984 (cited in pp. 27, 32, 37–39).
- [118] D. Y. Chen, A. F. Ghoniem, and A. K. Oppenheim. “Experimental and theoretical study of combustion jet ignition”, 1983 (cited in p. 28).
- [119] S. Yamaguchi, N. Ohiwa, and T. Hasegawa. “Ignition and burning process in a divided chamber bomb”. Combustion and Flame 59 (2), 1985, pp. 177–187 (cited in pp. 29, 55).
- [120] J. Maxson, D. Hensinger, K. Hom, and A. Oppenheim. “Performance of Multiple Stream Pulsed Jet Combustion Systems”. In: International Congress & Exposition. SAE International, 1991 (cited in p. 29).

- [121] J. Maxson and A. Oppenheim. “Pulsed jet combustion—Key to a refinement of the stratified charge concept”. Symposium (International) on Combustion 23 (1), 1991. Twenty-Third Symposium (International) on Combustion, pp. 1041–1046 (cited in p. 29).
- [122] E. Murase and K. Hanada. “Control of the Start of HCCI Combustion by Pulsed Flame Jet”. In: SAE Powertrain & Fluid Systems Conference & Exhibition. SAE International, 2002 (cited in p. 29).
- [123] E. Murase and K. Hanada. “Ignition timing control of homogeneous charge compression ignition engines by pulsed flame jets”. Combustion Science and Technology 174 (5-6), 2002, pp. 129–140 (cited in p. 29).
- [124] A. K. Oppenheim. “Quest for Controlled Combustion Engines”. In: SAE International Congress and Exposition. SAE International, 1988 (cited in p. 29).
- [125] H. C. Watson. Internal combustion engine ignition device. U.S. Patent 5611307, Mar. 1997 (cited in p. 29).
- [126] G. Lumsden and H. C. Watson. “Optimum Control of an S.I. Engine with a $\lambda=5$ Capability”. In: International Congress & Exposition. SAE International, 1995 (cited in pp. 29, 30, 59).
- [127] G. Lumsden and H. C. Watson. “HAJI Operation in a Hydrogen-Only Mode for Emission Control at Cold Start”. In: International Congress & Exposition. SAE International, 1995 (cited in pp. 29, 30).
- [128] N. Glasson, G. Lumsden, R. Dingli, and H. Watson. “Development of the HAJI System for a Multi-Cylinder Spark Ignition Engine”. In: International Fuels & Lubricants Meeting & Exposition. SAE International, 1996 (cited in pp. 29, 30).
- [129] G. A. Lumsden. “The phenomena of hydrogen assisted jet ignition”. University of Melbourne, 1995 (cited in pp. 29, 30).
- [130] J. Lawrence and H. C. Watson. “Hydrocarbon Emissions from a HAJI Equipped Ultra-lean Burn SI Engine”. In: International Congress & Exposition. SAE International, 1998 (cited in pp. 29, 30).
- [131] Z. H. Kyaw and H. C. Watson. “Hydrogen assisted jet ignition for near elimination of NO_x and cyclic variability in the S.I. Engine”. Symposium (International) on Combustion 24 (1), 1992. Twenty-Fourth Symposium on Combustion, pp. 1449–1455 (cited in pp. 29, 30).
- [132] E. Toulson, H. C. Watson, and W. P. Attard. “The Lean Limit and Emissions at Near-Idle for a Gasoline HAJI System with Alternative Pre-Chamber Fuels”. In: 8th International Conference on Engines for Automobiles. Consiglio Nazionale delle Ricerche, 2007 (cited in pp. 29, 30, 51, 59).

- [133] G. G. Dober and H. C. Watson. “[Quasi-Dimensional and CFD Modelling of Turbulent and Chemical Flame Enhancement in an Ultra Lean Burn S.I. Engine](#)”. In: SAE 2000 World Congress. SAE International, 2000 (cited in p. 29).
- [134] G. G. Dober. “Modelling the flame enhancement of a HAJI equipped spark ignition engine”. SAE No. 99091, 1999 (cited in pp. 29, 30).
- [135] E. Toulson. “Applying alternative fuels in place of hydrogen to the jet ignition process”. PhD thesis. 2008 (cited in p. 30).
- [136] E. Toulson, H. C. Watson, and W. P. Attard. “[Modeling Alternative Prechamber Fuels in Jet Assisted Ignition of Gasoline and LPG](#)”. In: SAE World Congress & Exhibition. SAE International, 2009 (cited in pp. 30, 130).
- [137] E. Toulson, H. C. Watson, and W. P. Attard. “[Gas Assisted Jet Ignition of Ultra-Lean LPG in a Spark Ignition Engine](#)”. In: SAE World Congress & Exhibition. SAE International, 2009 (cited in pp. 30, 59, 64).
- [138] F. Hamori and H. C. Watson. “Hydrogen assisted jet ignition for the hydrogen fuelled SI engine”. In: world hydrogen energy conference. 15. 2006 (cited in p. 30).
- [139] F. Hamori. “Exploring the limits of hydrogen assisted jet ignition”. 2006 (cited in p. 30).
- [140] K. Wakai, S. Kito, and I. Sumida. “[Effect of Small Hydrogen Jet Flame on Augmentation of Lean Combustion](#)”. In: International Pacific Conference On Automotive Engineering. SAE International, 1993 (cited in p. 31).
- [141] S. Kito, K. Wakai, S. Takahashi, N. Fukaya, and Y. Takada. “[Ignition limit of lean mixture by hydrogen flame jet ignition](#)”. JSAE Review 21 (3), 2000, pp. 373–378 (cited in p. 31).
- [142] M. Nagai. “Augmentation of Combustion in a Chamber by a Small Hydrogen-Air Jet Flame”. Dynamics of Heterogeneous Combustion and Reacting Systems 152, 1993, p. 319 (cited in p. 31).
- [143] T. Lezanski, M. Kesler, T. Rychter, A. Teodorczyk, and P. Wolanski. “[Performance of Pulsed Jet Combustion \(PJC\) System in a Research Engine](#)”. In: International Fuels & Lubricants Meeting & Exposition. SAE International, 1993 (cited in pp. 31, 32).
- [144] G. Gmurczyk, T. Leżański, M. Kesler, T. Chomiak, T. Rychter, and P. Wolański. “[Single compression machine study of a pulsed jet combustion \(PJC\)](#)”. Symposium (International) on Combustion 24 (1), 1992. Twenty-Fourth Symposium on Combustion, pp. 1441–1448 (cited in p. 31).
- [145] P. Wolanski and A. K. Oppenheim. “[Controlled Combustion Engines \(CCE\)](#)”. In: International Congress & Exposition. SAE International, 1999 (cited in p. 31).

- [146] C. Robinet, J. Andrzejewski, and P. Higelin. "Cycle-to-Cycle Variation Study of an SI Engine Fired by Spark Plug and a Non Conventional Device". In: International Fuels & Lubricants Meeting & Exposition. SAE International, 1997 (cited in p. 32).
- [147] H.-J. Koß, J. Thiemann, S. Pischinger, R. Böwing, and J. Geiger. "Ignition Systems for Highly Diluted Mixtures in SI-Engines". In: International Congress & Exposition. SAE International, 1999 (cited in pp. 32, 33).
- [148] C. Robinet, P. Higelin, B. Moreau, O. Pajot, and J. Andrzejewski. "A New Firing Concept for Internal Combustion Engines: "TAPIR"". In: International Congress & Exposition. SAE International, 1999 (cited in pp. 32, 50).
- [149] S. Couet, P. Higelin, and B. Moreau. "APIR: A New Firing Concept for the Internal Combustion Engines - sensitivity to knock and in-cylinder aerodynamics". In: International Spring Fuels & Lubricants Meeting. SAE International, 2001 (cited in pp. 32, 33).
- [150] P. M. Najt and D. E. Foster. "Compression-Ignited Homogeneous Charge Combustion". In: SAE International Congress and Exposition. SAE International, 1983 (cited in p. 32).
- [151] P. M. Najt, R. B. Rask, and D. L. Reuss. Dual mode engine combustion process. U.S. Patent 6595181, Jul. 2003 (cited in p. 32).
- [152] A. Kojic, J.-P. Hathout, D. Cook, and J. Ahmed. Control of auto-ignition timing for combustion in piston engines by prechamber compression ignition. U.S. Patent 6953020, Oct. 2005 (cited in p. 33).
- [153] A. Kojic, J.-P. Hathout, D. Cook, and J. Ahmed. Control of auto-ignition timing for homogeneous combustion jet ignition engines. U.S. Patent 7107964, Sep. 2006 (cited in pp. 33, 34).
- [154] H. E. Durling. Igniter for internal combustion engines operating over a wide range of air fuel ratios. U.S. Patent 7021275, Apr. 2006 (cited in pp. 33, 34).
- [155] D. Kuhnert, R. Latsch, J. Getzlaff, J. Pape, and C. Gruenig. "Investigations on Pre-Chamber Spark Plug with Pilot Injection". In: SAE World Congress & Exhibition. SAE International, 2007 (cited in pp. 33, 35).
- [156] D. A. Blank. "Lean Combustion Chemical-Kinetics Studies of an Ethanol Four-Stroke Radical-Ignition DI-Diesel Engine". In: SAE World Congress & Exhibition. SAE International, 2007 (cited in p. 35).
- [157] D. A. Blank. "Radical Controlled Autoignition in a HCRI Hydrogen DI Four-Stroke Diesel Engine with Reduced Heat Rejection". In: 2007 Fuels and Emissions Conference. SAE International, 2007 (cited in pp. 35, 50).
- [158] D. A. Blank. "Hydrogen Combustion in a Novel Rotary DI-HCRI Engine with Low Heat Rejection". In: SAE World Congress & Exhibition. SAE International, 2007 (cited in p. 35).

- [159] D. A. Blank. “Radical Ignition Combustion Studies with Hydrogen in a Two-Stroke DI-HCRI Diesel Engine”. In: SAE World Congress & Exhibition. SAE International, 2007 (cited in p. 35).
- [160] D. A. Blank. “CNG/Methane-Combustion in a Homogeneous-Combustion Radical-Ignition D.I. Diesel Engine”. In: 2007 Fuels and Emissions Conference. SAE International, 2007 (cited in p. 35).
- [161] D. A. Blank. Igniter for internal combustion engines operating over a wide range of air fuel ratios. U.S. Patent 7493886, Feb. 2009 (cited in p. 35).
- [162] J. G. C. Baeta, F. A. R. Filho, M. Pontoppidan, R. M. Valle, and T. R. V. da Silva. “Exploring the performance limits of a stratified torch ignition engine using numerical simulation and detailed experimental approaches”. *Energy Conversion and Management* 126, 2016, pp. 1093–1105 (cited in p. 35).
- [163] N. D. S. A. Santos, C. E. C. Alvarez, V. R. Roso, J. G. C. Baeta, and R. M. Valle. “Combustion analysis of a SI engine with stratified and homogeneous pre-chamber ignition system using ethanol and hydrogen”. *Applied Thermal Engineering* 160, 2019, p. 113985 (cited in pp. 35, 36, 40, 41).
- [164] C. E. C. Alvarez, V. R. Roso, N. D. S. A. Santos, A. T. Fernandes, and R. M. Valle. “Combustion analysis in a SI engine with homogeneous and stratified pre-chamber system”. In: 2018 SAE Brasil Congress & Exhibition. SAE International, 2018 (cited in pp. 35, 40).
- [165] V. R. Roso, C. E. C. Alvarez, N. D. S. A. Santos, J. G. C. Baeta, and R. M. Valle. “Combustion influence of a pre-chamber ignition system in a SI commercial engine”. In: 2018 SAE Brasil Congress & Exhibition. SAE International, 2018 (cited in pp. 35, 36).
- [166] F. A. R. Filho, T. A. A. Moreira, R. M. Valle, J. G. C. Baêta, M. Pontoppidan, and A. F. Teixeira. “E25 stratified torch ignition engine performance, CO2 emission and combustion analysis”. *Energy Conversion and Management* 115, 2016, pp. 299–307 (cited in pp. 35, 36).
- [167] F. A. R. Filho, J. G. C. Baêta, A. F. Teixeira, R. M. Valle, and J. L. F. de Souza. “E25 stratified torch ignition engine emissions and combustion analysis”. *Energy Conversion and Management* 121, 2016, pp. 251–271 (cited in p. 35).
- [168] M. Noguchi, S. Sanda, and N. Nakamura. “Development of Toyota Lean Burn Engine”. In: 1976 Automobile Engineering Meeting. SAE International, 1976 (cited in p. 36).
- [169] M. Konishi, N. Nakamura, E. Oono, and T. Baika. “Effects of a Prechamber on NOx Formation Process in the SI Engine”. In: 1979 Automotive Engineering Congress and Exposition. SAE International, 1979 (cited in p. 36).

- [170] S. Sanda and N. Nakamura. Internal combustion engine provided with pre-combustion chamber. U.S. Patent 4048973, Sep. 1977 (cited in pp. 36, 37).
- [171] T. G. Adams. “Theory and Evaluation of Auxiliary Combustion (Torch Chambers)”. In: Passenger Car Meeting & Exposition. SAE International, 1978 (cited in pp. 37, 60).
- [172] T. G. Adams. “Torch Ignition for Combustion Control of Lean Mixtures”. In: 1979 Automotive Engineering Congress and Exposition. SAE International, 1979 (cited in pp. 37, 38).
- [173] W. Brandstetter. “The Volkswagen Lean Burn PC-Engine Concept”. In: 1980 Automotive Engineering Congress and Exposition. SAE International, 1980 (cited in pp. 37, 38).
- [174] F. A. Wyczalek, D. L. Frank, and J. G. Neuman. “Plasma Jet Ignition of Lean Mixtures”. In: 1975 Automotive Engineering Congress and Exposition. SAE International, 1975 (cited in pp. 37, 38).
- [175] R. Latsch, H. Schlembach, and D. Scherenberg. Method for igniting lean fuel-air mixtures and an apparatus to perform the method. U.S. Patent 4442807, Apr. 1984 (cited in p. 37).
- [176] R. Latsch and H. Schlembach. Externally ignited internal combustion engine. U.S. Patent 4218992, Aug. 1980 (cited in p. 37).
- [177] W. Benedikt, R. Latsch, and H. Schlembach. Separately ignited internal combustion engine with at least one main combustion chamber and an ignition chamber. U.S. Patent 4416228, Nov. 1983 (cited in p. 37).
- [178] H. Ryu, A. Chitsu, and T. Asanuma. “Effect of Torch Jet Direction on Combustion and Performance of a Prechamber Spark-Ignition Engine”. In: SAE International Congress and Exposition. SAE International, 1987 (cited in pp. 37–39, 51).
- [179] H. Ryu and T. Asanuma. “Turbulent Flame Propagation in a Spark Ignition Engine with an Unscavenged Horizontal Prechamber”. In: 1988 SAE International Fall Fuels and Lubricants Meeting and Exhibition. SAE International, 1988 (cited in pp. 37, 50, 51).
- [180] H. Ryu and T. Asanuma. “Numerical Simulation of Two-Dimensional Combustion Process in a Spark Ignition Engine with a Prechamber using $k-\epsilon$ Turbulence Model”. In: SAE International Congress and Exposition. SAE International, 1989 (cited in p. 37).
- [181] S. Namekawa, H. Ryu, and T. Asanuma. “LDA Measurement of Turbulent Flow in a Motored and Firing Spark-Ignition Engine with a Horizontal Prechamber”. In: 1988 SAE International Fall Fuels and Lubricants Meeting and Exhibition. SAE International, 1988 (cited in p. 37).

- [182] S. Wojcicki and S. W. Beyerlein. “A Lean-Burn Catalytic Engine”. In: SAE International Congress and Exposition. SAE International, 1988 (cited in pp. 38, 39).
- [183] J. Jarosiński, R. Lapucha, and J. Mazurkiewicz. “Investigation of a Lean-Burn Piston Engine with Catalytic Prechamber”. In: International Congress & Exposition. SAE International, 1996 (cited in pp. 38, 39).
- [184] T. Rychter, R. Saragih, T. Lezański, and S. Wójcicki. “Catalytic activation of a charge in a prechamber of a SI lean-burn engine”. Symposium (International) on Combustion 18 (1), 1981. Eighteenth Symposium (International) on Combustion, pp. 1815–1824 (cited in pp. 38, 39).
- [185] S. W. Beyerlein. “Catalytic charge activation in a lean-burn internal combustion engine”. 1987 (cited in p. 38).
- [186] M. A. Cherry and C. L. Elmore. Timing chamber ignition method and apparatus. U.S. Patent 4977873, Dec. 1990 (cited in p. 39).
- [187] M. A. Cherry. Catalytic-compression timed ignition. U.S. Patent 5109817, May 1992 (cited in p. 39).
- [188] M. A. Cherry. Mass controlled compression timed ignition method and igniter. U.S. Patent 5297518, Mar. 1994 (cited in p. 39).
- [189] M. A. Cherry. Compression timed pre-chamber flame distributing igniter for internal combustion engines. U.S. Patent 5421299, Jun. 1995 (cited in p. 39).
- [190] R. D. Richardson. Ignition assisting device for internal combustion engines. U.S. Patent 5105780, Apr. 1992 (cited in p. 39).
- [191] A. P. Sabol and A. Sabol. Device to enhance combustion efficiency in an internal combustion engine. U.S. Patent 5245963, Sep. 1993 (cited in p. 39).
- [192] H. E. Durling, R. P. Johnston, and K. K. Polikarpus. Torch jet spark plug. U.S. Patent 5421300, Jun. 1995 (cited in p. 39).
- [193] R. Latsch, D. Kuhnert, V. Weng, J. Gindele, G. Töpfer, and U. Spicher. “Investigation of the Bowl-Prechamber-Ignition (BPI) Concept in a Direct Injection Gasoline Engine at Part Load”. In: International Fuels & Lubricants Meeting & Exposition. SAE International, 1999 (cited in pp. 39, 40).
- [194] D. Kuhnert, R. Latsch, M. Kettner, J. Fischer, et al. “The BPI Flame Jet Concept to Improve the Inflammation of Lean Burn Mixtures in Spark Ignited Engines”. In: SAE 2004 World Congress & Exhibition. SAE International, 2004 (cited in pp. 39, 40, 58).
- [195] M. Kettner, M. Rothe, A. Velji, U. Spicher, D. Kuhnert, and R. Latsch. “A new flame jet concept to improve the inflammation of lean burn mixtures in SI engines”. SAE transactions, 2005, pp. 1549–1557 (cited in pp. 39, 40, 52, 58).

- [196] H. E. Durling and J. G. Ralph. Directed jet spark plug. U.S. Patent 6213085, Apr. 2001 (cited in p. 40).
- [197] M. Kubo, T. Noda, and I. Hotta. Internal combustion engine with auxiliary combustion chamber. U.S. Patent 7204225, Apr. 2007 (cited in p. 40).
- [198] J. R. C. Gomes, R. M. Valle, F. J. P. Pujatti, and J. P. Pereira. Torch Ignition system analysis in an spark ignition engine. Tech. rep. SAE Technical Paper, 2005 (cited in p. 40).
- [199] I. W. S. L. Cruz, C. E. C. Alvarez, A. F. Teixeira, and R. M. Valle. “Zero-dimensional mathematical model of the torch ignited engine”. Applied Thermal Engineering 103, 2016, pp. 1237–1250 (cited in p. 40).
- [200] V. F. Duarte, C. E. Castilla Alvarez, F. T. Magalhães Avelar, M. A. Maia Pires, et al. “Exhaust Emission Analysis of a Spark Ignition Engine Operating with Hydrogen Injection in a Pre-Combustion Chamber”. In: 2019 SAE Brasil Congress & Exhibition. SAE International, 2020 (cited in pp. 40, 41).
- [201] V. R. Roso, N. D. S. A. Santos, R. M. Valle, C. E. C. Alvarez, J. Monsalve-Serrano, and A. García. “Evaluation of a stratified prechamber ignition concept for vehicular applications in real world and standardized driving cycles”. Applied Energy 254, 2019, p. 113691 (cited in p. 40).
- [202] A. Shah, P. Tunestal, and B. Johansson. “Investigation of Performance and Emission Characteristics of a Heavy Duty Natural Gas Engine Operated with Pre-Chamber Spark Plug and Dilution with Excess Air and EGR”. SAE International Journal of Engines 5 (4), 2012, pp. 1790–1801 (cited in p. 41).
- [203] A. Shah, P. Tunestal, and B. Johansson. “Applicability of Ionization Current Sensing Technique with Plasma Jet Ignition Using Pre-Chamber Spark Plug in a Heavy Duty Natural Gas Engine”. In: SAE 2012 International Powertrains, Fuels & Lubricants Meeting. SAE International, 2012 (cited in p. 41).
- [204] A. Shah, P. Tunestal, and B. Johansson. “Effect of Relative Mixture Strength on Performance of Divided Chamber ‘Avalanche Activated Combustion’ Ignition Technique in a Heavy Duty Natural Gas Engine”. In: SAE 2014 World Congress & Exhibition. SAE International, 2014 (cited in pp. 41, 42).
- [205] A. Shah, P. Tunestal, and B. Johansson. “Effect of Pre-Chamber Volume and Nozzle Diameter on Pre-Chamber Ignition in Heavy Duty Natural Gas Engines”. In: SAE 2015 World Congress & Exhibition. SAE International, 2015 (cited in pp. 41, 42).
- [206] A. Shah, P. Tunestål, and B. Johansson. “CFD Simulations of Pre-Chamber Jets’ Mixing Characteristics in a Heavy Duty Natural Gas Engine”. In: JSAE/SAE 2015 International Powertrains, Fuels & Lubricants Meeting. SAE International, 2015 (cited in p. 41).

- [207] A. Shah. Improving the efficiency of gas engines using pre-chamber ignition. Division of Combustion Engines, Department of Energy Sciences, Faculty of Lund, 2015 (cited in p. 41).
- [208] A. Shah, P. Tunestål, and B. Johansson. “CFD Simulations of Pre-Chamber Jets’ Mixing Characteristics in a Heavy Duty Natural Gas Engine”. In: JSAE/SAE 2015 International Powertrains, Fuels & Lubricants Meeting. SAE International, 2015 (cited in p. 41).
- [209] A. Shah, P. Tunestål, and B. Johansson. “Scalability Aspects of Pre-Chamber Ignition in Heavy Duty Natural Gas Engines”. In: SAE 2016 World Congress and Exhibition. SAE International, 2016 (cited in p. 41).
- [210] S. Biswas, S. Tanvir, H. Wang, and L. Qiao. “On ignition mechanisms of premixed CH₄/air and H₂/air using a hot turbulent jet generated by pre-chamber combustion”. Applied Thermal Engineering 106, 2016, pp. 925–937 (cited in pp. 42, 55, 130).
- [211] S. Biswas and L. Qiao. “Prechamber Hot Jet Ignition of Ultra-Lean H₂/Air Mixtures: Effect of Supersonic Jets and Combustion Instability”. SAE International Journal of Engines 9 (3), 2016, pp. 1584–1592 (cited in pp. 42, 55).
- [212] S. Biswas and L. Qiao. “Ignition of ultra-lean premixed H₂/air using multiple hot turbulent jets generated by pre-chamber combustion”. Applied Thermal Engineering 132, 2018, pp. 102–114 (cited in p. 42).
- [213] W. P. Attard, M. Bassett, P. Parsons, and H. Blaxill. “A New Combustion System Achieving High Drive Cycle Fuel Economy Improvements in a Modern Vehicle Powertrain”. In: SAE 2011 World Congress & Exhibition. SAE International, 2011 (cited in pp. 43, 44, 46, 58).
- [214] M. Sens and E. Binder. “Pre-Chamber Ignition as a Key Technology for Future Powertrain Fleets”. MTZ worldwide 80 (2), 2019, pp. 44–51 (cited in p. 43).
- [215] W. P. Attard and P. Parsons. “A Normally Aspirated Spark Initiated Combustion System Capable of High Load, High Efficiency and Near Zero NO_x Emissions in a Modern Vehicle Powertrain”. SAE International Journal of Engines 3 (2), 2010, pp. 269–287 (cited in pp. 43, 66).
- [216] W. P. Attard, H. Blaxill, E. K. Anderson, and P. Litke. “Knock Limit Extension with a Gasoline Fueled Pre-Chamber Jet Igniter in a Modern Vehicle Powertrain”. SAE International Journal of Engines 5 (3), 2012, pp. 1201–1215 (cited in pp. 44, 60).
- [217] W. P. Attard, J. Kohn, and P. Parsons. “Ignition Energy Development for a Spark Initiated Combustion System Capable of High Load, High Efficiency and Near Zero NO_x Emissions”. SAE International Journal of Engines 3 (2), 2010, pp. 481–496 (cited in pp. 44, 52, 64).

- [218] W. P. Attard and P. Parsons. “Flame Kernel Development for a Spark Initiated Pre-Chamber Combustion System Capable of High Load, High Efficiency and Near Zero NO_x Emissions”. SAE International Journal of Engines 3 (2), 2010, pp. 408–427 (cited in pp. 44, 64).
- [219] W. P. Attard and H. Blaxill. “A Single Fuel Pre-Chamber Jet Ignition Powertrain Achieving High Load, High Efficiency and Near Zero NO_x Emissions”. SAE International Journal of Engines 5 (3), 2011, pp. 734–746 (cited in pp. 44, 64, 66).
- [220] W. P. Attard and H. Blaxill. “A Gasoline Fueled Pre-Chamber Jet Ignition Combustion System at Unthrottled Conditions”. SAE International Journal of Engines 5 (2), 2012, pp. 315–329 (cited in pp. 44, 65).
- [221] W. P. Attard, E. Toulson, A. Huisjen, X. Chen, G. Zhu, and H. Schock. “Spark Ignition and Pre-Chamber Turbulent Jet Ignition Combustion Visualization”. In: SAE 2012 World Congress & Exhibition. SAE International, 2012 (cited in pp. 44, 47, 52, 59).
- [222] E. Toulson, A. Huisjen, X. Chen, C. Squibb, et al. “Visualization of Propane and Natural Gas Spark Ignition and Turbulent Jet Ignition Combustion”. SAE International Journal of Engines 5 (4), 2012, pp. 1821–1835 (cited in pp. 44, 45, 59).
- [223] G. Gentz, B. Thelen, P. Litke, J. Hoke, and E. Toulson. “Combustion Visualization, Performance, and CFD Modeling of a Pre-Chamber Turbulent Jet Ignition System in a Rapid Compression Machine”. SAE International Journal of Engines 8 (2), 2015, pp. 538–546 (cited in pp. 44, 52–54).
- [224] G. Gentz, B. Thelen, M. Gholamisheeri, P. Litke, et al. “A study of the influence of orifice diameter on a turbulent jet ignition system through combustion visualization and performance characterization in a rapid compression machine”. Applied Thermal Engineering 81, 2015, pp. 399–411 (cited in pp. 44, 46, 54).
- [225] G. R. Gentz and E. Toulson. “Experimental Studies of a Liquid Propane Auxiliary Fueled Turbulent Jet Igniter in a Rapid Compression Machine”. SAE International Journal of Engines 9 (2), 2016, pp. 777–785 (cited in p. 44).
- [226] G. Gentz, M. Gholamisheeri, and E. Toulson. “A study of a turbulent jet ignition system fueled with iso-octane: Pressure trace analysis and combustion visualization”. Applied Energy 189, 2017, pp. 385–394 (cited in pp. 44, 46, 52, 53).
- [227] A. Cooper, A. Harrington, M. Bassett, and D. Pates. “Knock Mitigation Benefits Achieved through the Application of Passive MAHLE Jet Ignition Enabling Increased Output under Stoichiometric Operation”. In: SAE WCX Digital Summit. SAE International, 2021 (cited in pp. 46, 60).

- [228] N. Peters, S. Krishna Pothuraju Subramanyam, M. Bunce, H. Blaxill, and A. Cooper. “[Optimization of Lambda across the Engine Map for the Purpose of Maximizing Thermal Efficiency of a Jet Ignition Engine](#)”. SAE International Journal of Advances and Current Practices in Mobility 2 (6), 2020, pp. 3140–3150 (cited in pp. 46, 47, 52, 53, 65).
- [229] J. Pihl, M. Moses-Debusk, D. Tew, G. Vishwanathan, et al. “Design and Development of a High-Efficiency Single Cylinder Natural Gas-Fueled Jet Ignition Engine”. In: Small Engine Technology Conference & Exposition. Society of Automotive Engineers of Japan, 2020 (cited in p. 47).
- [230] M. Silva, S. Sanal, P. Hlaing, E. Cenker, B. Johansson, and H. G. Im. “[Effects of Geometry on Passive Pre-Chamber Combustion Characteristics](#)”. In: WCX SAE World Congress Experience. SAE International, 2020 (cited in pp. 48, 52).
- [231] P. Hlaing, M. Echeverri Marquez, V. S. Bhavani Shankar, M. Ben Houidi, B. Johansson, and E. Cenker. “[A Study of Lean Burn Pre-Chamber Concept in a Heavy Duty Engine](#)”. In: 14th International Conference on Engines & Vehicles. SAE International, 2019 (cited in pp. 48, 61, 62).
- [232] B. C. Thelen, G. Gentz, and E. Toulson. “[Computational Study of a Turbulent Jet Ignition System for Lean Burn Operation in a Rapid Compression Machine](#)”. In: SAE 2015 World Congress & Exhibition. SAE International, 2015 (cited in pp. 48, 60, 130).
- [233] B. C. Thelen and E. Toulson. “[A Computational Study of the Effects of Spark Location on the Performance of a Turbulent Jet Ignition System](#)”. In: SAE 2016 World Congress and Exhibition. SAE International, 2016 (cited in pp. 48, 53, 60).
- [234] M. Blankmeister, M. Alp, and E. Shimizu. “Passive Pre-Chamber Spark Plug for Future Gasoline Combustion Systems with Direct Injection”. In: Ignition Systems for Gasoline Engines: 4th International Conference, December 6-7, 2018, Berlin, Germany. Ed.: M. Günther. 2018, p. 149 (cited in pp. 49, 50).
- [235] J. Benajes, R. Novella, J. Gomez-Soriano, I. Barbery, et al. “[Computational assessment towards understanding the energy conversion and combustion process of lean mixtures in passive pre-chamber ignited engines](#)”. Applied Thermal Engineering 178, 2020, p. 115501 (cited in pp. 49, 50, 56).
- [236] R. Novella, J. Pastor, J. Gomez-Soriano, I. Barbery, et al. “[Experimental and Numerical Analysis of Passive Pre-Chamber Ignition with EGR and Air Dilution for Future Generation Passenger Car Engines](#)”. In: WCX SAE World Congress Experience. SAE International, 2020 (cited in pp. 49, 56, 62, 174).

- [237] J. M. Desantes, R. Novella, J. De La Morena, et al. "Achieving Ultra-Lean Combustion Using a Pre-Chamber Spark Ignition System in a Rapid Compression-Expansion Machine". SAE Technical Paper, 2019 (cited in pp. 50, 130).
- [238] R. Roethlisberger and D. Favrat. "Comparison between direct and indirect (prechamber) spark ignition in the case of a cogeneration natural gas engine, part I: engine geometrical parameters". Applied Thermal Engineering 22 (11), 2002, pp. 1217–1229 (cited in p. 51).
- [239] F. F. Pischinger and K. J. Klöcker. "Single-Cylinder Study of Stratified Charge Process with Prechamber-Injection". In: International Stratified Charge Engine Conference. SAE International, 1974 (cited in p. 51).
- [240] K. Bardis, G. Xu, P. Kyrtatos, Y. M. Wright, and K. Boulouchos. "A Zero Dimensional Turbulence and Heat Transfer Phenomenological Model for Pre-Chamber Gas Engines". In: WCX World Congress Experience. SAE International, 2018 (cited in p. 51).
- [241] H. Ryu and T. Asanuma. "Combustion analysis with gas temperature diagrams measured in a prechamber spark ignition engine". Symposium (International) on Combustion 20 (1), 1985. Twentieth Symposium (International) on Combustion, pp. 195–200 (cited in p. 51).
- [242] E. Distaso, R. Amirante, E. Cassone, P. De Palma, et al. "Experimental and Numerical Analysis of a Pre-Chamber Turbulent Jet Ignition Combustion System". In: 14th International Conference on Engines & Vehicles. SAE International, 2019 (cited in pp. 52, 53).
- [243] E. Distaso, R. Amirante, E. Cassone, P. De Palma, et al. "Analysis of the combustion process in a lean-burning turbulent jet ignition engine fueled with methane". Energy Conversion and Management 223, 2020, p. 113257 (cited in p. 52).
- [244] P. Chinnathambi, M. Bunce, and L. Cruff. "RANS Based Multidimensional Modeling of an Ultra-Lean Burn Pre-Chamber Combustion System with Auxiliary Liquid Gasoline Injection". (April 2015), 2015 (cited in p. 53).
- [245] R. Rajasegar, Y. Niki, J. M. García-Oliver, Z. Li, and M. P. Musculus. "Fundamental insights on ignition and combustion of natural gas in an active fueled pre-chamber spark-ignition system". Combustion and Flame 232, 2021, p. 111561 (cited in p. 54).
- [246] M. Bunce, H. Blaxill, W. Kulatilaka, and N. Jiang. "The Effects of Turbulent Jet Characteristics on Engine Performance Using a Pre-Chamber Combustor". In: SAE 2014 World Congress & Exhibition. SAE International, 2014 (cited in pp. 54, 63).
- [247] M. Sens, E. Binder, P. Reinicke, M. Riess, T. Stappenbeck, and M. Woebke. "Pre-chamber ignition and promising complementary technologies". In: 27th Aachen Colloquium Automobile and Engine Technology. 2018 (cited in p. 54).

- [248] J. Hua, L. Zhou, Q. Gao, Z. Feng, and H. Wei. “Effects on Cycle-to-Cycle Variations and Knocking Combustion of Turbulent Jet Ignition (TJI) with a Small Volume Pre-Chamber”. In: WCX SAE World Congress Experience. SAE International, 2020 (cited in pp. 54, 65).
- [249] J. Hua, L. Zhou, Q. Gao, Z. Feng, and H. Wei. “Influence of pre-chamber structure and injection parameters on engine performance and combustion characteristics in a turbulent jet ignition (TJI) engine”. *Fuel* 283, 2021, p. 119236 (cited in p. 54).
- [250] P. Kyrtatos, K. Bardis, M. Bolla, A. Denisov, et al. “8.3 Transferability of insights from fundamental investigations into practical applications of prechamber combustion systems”. *Ignition Systems for Gasoline Engines Internationale Tagung Zündsysteme für Ottomotoren*, 2018, p. 442 (cited in p. 55).
- [251] B. Boust, J. Sotton, S. Labuda, and M. Bellenoue. “A thermal formulation for single-wall quenching of transient laminar flames”. *Combustion and Flame* 149 (3), 2007, pp. 286–294 (cited in p. 55).
- [252] B. Korb, K. Kuppa, H. D. Nguyen, F. Dinkelacker, and G. Wachtmeister. “Experimental and numerical investigations of charge motion and combustion in lean-burn natural gas engines”. *Combustion and Flame* 212, 2020, pp. 309–322 (cited in p. 56).
- [253] C. Zuo and K. Zhao. “A Study on the Combustion System of a Spark Ignition Natural Gas Engine”. In: *International Fuels & Lubricants Meeting & Exposition*. SAE International, 1998 (cited in p. 56).
- [254] M. Bunce, H. Blaxill, and A. Cooper. *28th Aachen Colloquium Automobile and Engine Technology*, 2019, pp. 907–942 (cited in pp. 57, 63, 65).
- [255] N. Peters, M. Bunce, and H. Blaxill. “The Impact of Engine Displacement on Efficiency Loss Pathways in a Highly Dilute Jet Ignition Engine”. In: *WCX SAE World Congress Experience*. SAE International, 2019 (cited in p. 58).
- [256] A. Yousefi and M. Birouk. “Numerical study of the performance and emissions characteristics of natural gas/diesel dual-fuel engine using direct and indirect injection systems”. In: *Proceedings of Combustion Institute–Canadian Section Spring Technical Meeting University of Waterloo* May. 2016, pp. 10–12 (cited in p. 60).
- [257] S. Wojcicki, J. Jarosinski, R. Lapucha, and J. Mazurkiewicz. “Combustion System of a Lean-Burn Piston Engine with Catalytic Prechamber”. In: *SAE 2001 World Congress*. SAE International, 2001 (cited in p. 60).
- [258] F. Almatrafi, P. Hlaing, M. Echeverri Marquez, M. Ben Houidi, and B. Johansson. “Narrow-Throat Pre-Chamber Combustion with Ethanol, a Comparison with Methane”. In: *SAE Powertrains, Fuels & Lubricants Meeting*. SAE International, 2020 (cited in p. 62).

- [259] M. Bolla, P. Kyrtatos, M. Kotzagianni, K. Boulouchos, E. Shapiro, and N. Tiney. “Numerical Study of Turbulence and Fuel-Air Mixing within a Scavenged Pre-Chamber Using RANS and LES”. In: WCX SAE World Congress Experience. SAE International, 2019 (cited in p. 63).
- [260] J. Wallesten and J. Chomiak. “Investigation of Spark Position Effects in a Small Pre-chamber on Ignition and Early Flame Propagation”. In: International Fuels & Lubricants Meeting & Exposition. SAE International, 2000 (cited in p. 64).
- [261] D. Serrano, J.-M. Zaccardi, C. Müller, C. Libert, and K. Habermann. “Ultra-Lean Pre-Chamber Gasoline Engine for Future Hybrid Powertrains”. SAE International Journal of Advances and Current Practices in Mobility 2 (2), 2019, pp. 607–622 (cited in p. 65).
- [262] P. Hlaing, M. Echeverri Marquez, E. Singh, F. Almatrafi, et al. “Effect of Pre-Chamber Enrichment on Lean Burn Pre-Chamber Spark Ignition Combustion Concept with a Narrow-Throat Geometry”. In: WCX SAE World Congress Experience. SAE International, 2020 (cited in p. 65).
- [263] C. Guido, D. Di Maio, P. Napolitano, and C. Beatrice. “Sub-23 particle control strategies towards Euro VII HD SI natural gas engines”. Transportation Engineering 10, 2022, p. 100132 (cited in p. 66).
- [264] D. Di Maio, P. Napolitano, C. Guido, D. Domenico, and S. Golini. “Ultra-Fine Particle Emissions Characterization and Reduction Technologies in a NG Heavy Duty Engine”. Atmosphere 13, 2022 (cited in p. 66).
- [265] P. Sementa, F. Catapano, S. Di Iorio, and B. M. Vaglieco. “Effects of Prechamber on Efficiency Improvement and Emissions Reduction of a SI Engine Fuelled with Gasoline”. In: Conference on Sustainable Mobility. SAE International, 2019 (cited in p. 66).
- [266] A. Stadler, H. Sauerland, M. Härtl, and G. Wachtmeister. “The Potential of Gasoline Fueled Pre Chamber Ignition Combined with Elevated Compression Ratio”. In: WCX SAE World Congress Experience. SAE International, 2020 (cited in pp. 67, 68).
- [267] C. Atis and H. Schock. “Comparison of Excess Air (Lean) vs EGR Diluted Operation in a Pre-Chamber Air/Fuel Scavenged Dual Mode, Turbulent Jet Ignition Engine at High Dilution Rate (40%)”. In: SAE WCX Digital Summit. SAE International, 2021 (cited in p. 67).
- [268] P. Sementa, F. Catapano, S. Di Iorio, M. Todino, and B. M. Vaglieco. “Turbulent Jet Ignition Effect on Exhaust Emission and Efficiency of a SI Small Engine Fueled with Methane and Gasoline”. In: Conference on Sustainable Mobility. SAE International, 2020 (cited in p. 68).
- [269] G. Onofrio, P. Napolitano, P. Tunestål, and C. Beatrice. “Combustion sensitivity to the nozzle hole size in an active pre-chamber ultra-lean heavy-duty natural gas engine”. Energy 235, 2021, p. 121298 (cited in p. 68).

- [270] M. Lapuerta, O. Armas, and J. Hernández. “[Diagnosis of DI Diesel combustion from in-cylinder pressure signal by estimation of mean thermodynamic properties of the gas](#)”. *Applied Thermal Engineering* 19 (5), 1999, pp. 513–529 (cited in pp. 79, 132).
- [271] F. Payri, S. Molina, J. Martín, and O. Armas. “[Influence of measurement errors and estimated parameters on combustion diagnosis](#)”. *Applied Thermal Engineering* 26 (2), 2006, pp. 226–236 (cited in pp. 79, 132).
- [272] J. V. Pastor, J. J. López, J. M. García, and J. M. Pastor. “[A 1D model for the description of mixing-controlled inert diesel sprays](#)”. *Fuel* 87 (13), 2008, pp. 2871–2885 (cited in p. 81).
- [273] J. Desantes, J. Pastor, J. García-Oliver, and J. Pastor. “[A 1D model for the description of mixing-controlled reacting diesel sprays](#)”. *Combustion and Flame* 156 (1), 2009, pp. 234–249 (cited in p. 81).
- [274] J. V. Pastor, J. M. Garcia-Oliver, J. M. Pastor, and W. Vera-Tudela. “[ONE-DIMENSIONAL DIESEL SPRAY MODELING OF MULTICOMPONENT FUELS](#)”. *Atomization and Sprays* 25 (6), 2015, pp. 485–517 (cited in p. 81).
- [275] CONVERGE 2.3 Theory Manual. CONVERGENT SCIENCE Inc. 2017 (cited in pp. 97, 141).
- [276] G. Vanhove, G. Petit, and R. Minetti. “[Experimental study of the kinetic interactions in the low-temperature autoignition of hydrocarbon binary mixtures and a surrogate fuel](#)”. *Combustion and Flame* 145 (3), 2006, pp. 521–532 (cited in p. 98).
- [277] R. Minetti, M. Carlier, M. Ribaucour, E. Therssen, and L. Sochet. “[Comparison of oxidation and autoignition of the two primary reference fuels by rapid compression](#)”. *Symposium (International) on Combustion* 26 (1), 1996, pp. 747–753 (cited in p. 98).
- [278] A. Burnham, M. Wang, and Y. Wu. Development and applications of GREET 2.7–The Transportation Vehicle-CycleModel. Tech. rep. Argonne National Lab.(ANL), Argonne, IL (United States), 2006 (cited in p. 98).
- [279] N. Scarlat, J.-F. Dallemand, and F. Fahl. “[Biogas: Developments and perspectives in Europe](#)”. *Renewable Energy* 129, 2018, pp. 457–472 (cited in p. 99).
- [280] S. Fuss, J. G. Canadell, G. P. Peters, M. Tavoni, et al. “[Betting on negative emissions](#)”. *Nature climate change* 4 (10), 2014, pp. 850–853 (cited in p. 100).
- [281] G. Xu, M. Kotzagianni, P. Kyratos, Y. M. Wright, and K. Boulouchos. “[Experimental and numerical investigations of the unscavenged prechamber combustion in a rapid compression and expansion machine under engine-like conditions](#)”. *Combustion and Flame* 204, 2019, pp. 68–84 (cited in p. 130).

- [282] M. Muller, C. Freeman, P. Zhao, and H. Ge. “Numerical Simulation of Ignition Mechanism in the Main Chamber of Turbulent Jet Ignition System”. ASME 2018 Internal Combustion Engine Division Fall Technical Conference, 2019 (cited in p. 130).
- [283] R. Borghi. “On the structure and morphology of turbulent premixed flames”. In: Recent advances in the Aerospace Sciences. Springer, 1985, pp. 117–138 (cited in p. 140).
- [284] N. Peters. “The turbulent burning velocity for large-scale and small-scale turbulence”. Journal of Fluid mechanics 384, 1999, pp. 107–132 (cited in p. 140).
- [285] C. Mounaïm-Rousselle, L. Landry, F. Halter, and F. Foucher. “Experimental characteristics of turbulent premixed flame in a boosted Spark-Ignition engine”. Proceedings of the Combustion Institute 34 (2), 2013, pp. 2941–2949 (cited in p. 140).
- [286] C. Iacovano, A. d’Adamo, and G. Cantore. “Analysis and Simulation of Non-Flamelet Turbulent Combustion in a Research Optical Engine”. Energy Procedia 148, 2018, pp. 463–470 (cited in p. 140).
- [287] N. Peters. Turbulent combustion. Cambridge university press, 2000 (cited in p. 141).

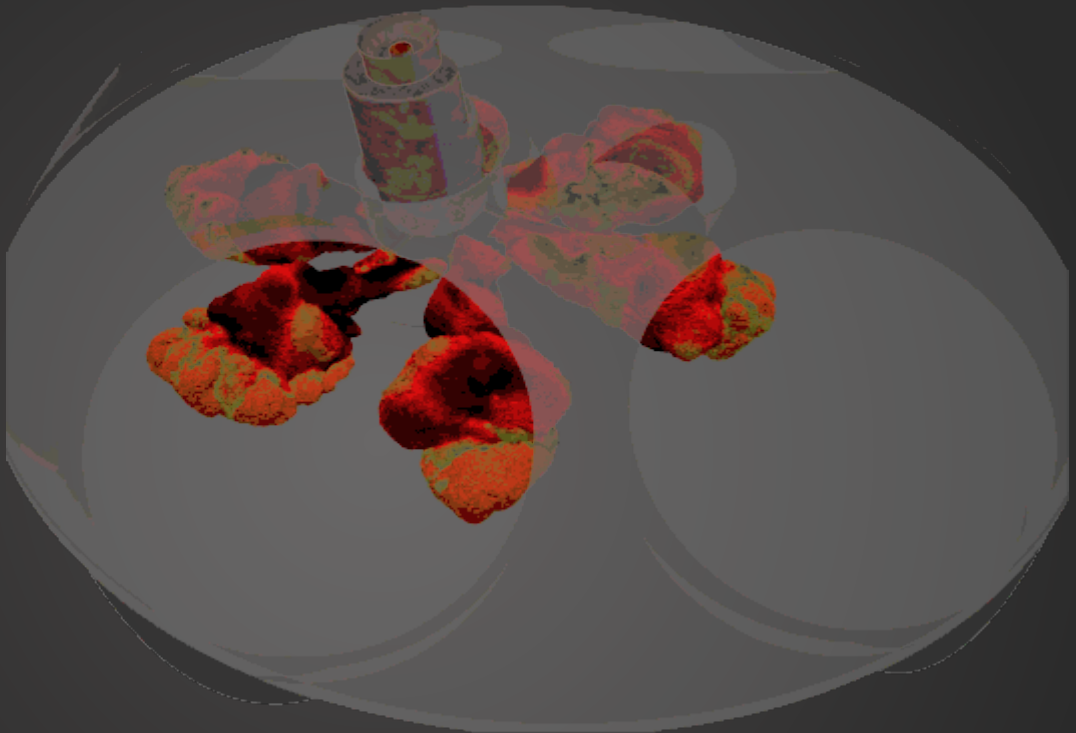


UNIVERSITAT
POLITÈCNICA
DE VALÈNCIA

DOCTORAL THESIS

**IMPLEMENTATION AND ANALYSIS OF THE PRE-CHAMBER IGNITION
CONCEPT IN A SI ENGINE FOR PASSENGER CAR APPLICATIONS**

Pablo José Martínez Hernández



November 2023

DEPARTAMENTO DE MÁQUINAS Y MOTORES TÉRMICOS